THÈSE

En vue de l'obtention du

DOCTORAT DE L'UNIVERSITÉ DE TOULOUSE

Délivré par : *l'Université Toulouse 3 Paul Sabatier (UT3 Paul Sabatier)*

Présentée et soutenue le *17/10/2016* **par :**

Weikai ZONG

Amplitude and frequency modulations of oscillation modes in hot B subdwarf and white dwarf stars from *Kepler* photometry

---

JURY

Dr. Marie-Jo Goupil	Astronome	Rapporteur
Dr. Roberto Silvotti	Chercheur	Rapporteur
Prof. Jianning FU	Professeur	Examinateur
Prof. Sylvie VAUCLAIR	Professeur d'Université	Président
Dr. Gérard VAUCLAIR	Directeur de Recherche	Co-Directeur de thèse
Dr. Stéphane CHARPINET	Chargé de Recherche	Directeur de thèse

---

École doctorale et spécialité :
SDU2E : Astrophysique, Sciences de l'Espace, Planétologie
Unité de Recherche :
Institut de Recherche en Astrophysique et Planétologie (UMR 5277)
Directeur de Thèse :
Dr. Stéphane CHARPINET et Dr. Gérard VAUCLAIR
Rapporteurs :
Dr. Marie-Jo GOUPIL et *Dr. Roberto SILVOTTI*

Acknowledgements

It is three years plus one month to fulfill the project aiming at searching for and characterizing amplitude and frequency modulations in oscillation modes in these fantasy stars that observed by the magnificent telescope KEPLER. I am very glad to see that our results may give a very tiny impetus on the way to see the nonlinear things in stellar pulsation theory. Now it is properly the time to thank many people who help me a lot during the last three years of being a Ph.d candidate in Toulouse, la Ville Rose.

First and foremost, my thanks are given to my supervisor, Stéphane Charpinet, for his patience, guidance, support, and inspiration that make this thesis possible. When I retrospect back the days, I am so grateful to be a student of Stéphane. He is a very special kind of supervisor, who always shows great passion on research. He is very knowledgable in our field and always answers my questions and inspires me with new ideas. I really learn quite a lot from him about how to become a good researcher. My great thanks are also given to Gérard Vauclair, my co-supervisor, who is a gracious person. He has many open minds on this field, or concretely, novel ideas on the nonlinear physics in stars. These knowledge brings me confidence on the way to firmly insist my research when I have to face to hard things. Both Stéphane and Gérard had never said any hard word on my works and always encourage me to progress in my study. I am very appreciate for this.

This thesis cannot be accomplished without the unprecedented high-quality and long-duration data from the KEPLER space telescope. It is funded by the NASA's Science Mission Directorate. I gratefully acknowledge the KEPLER Science Team and all those who have contributed to making the mission possible.

The works presented in the thesis are also contributed by two other collaborators, Noemi Giammichele and Valerie Van Grootel. I must thank their independent calculation of theoretical models on the white dwarf star that makes it comparing with the observed modulations possible. Noemi just joined our group as a postdoctoral around her defense in Montréal.

I thank my thesis and candidacy defense committee, which is composed of Marie-jo Goupil, Roberto Silvotti, Sylvie Vauclair, Jianning Fu, Gérard and Stéphane, for their valuable time on evaluating the work and for their important suggestions and comments to my future career. I thank the reporters, Marie-jo and Roberto, for their well-written reviews, for the positive view on the discovered mode modulations and the theoretical interpretations. Sylvie, she is the president of my examinations for three times continuously, who see my progresses during these three years, from a freshmen to a senior student. Jianning, he is my supervisor guiding me the master project, who is the guide leading me to enter the new domain of stellar physics—asteroseimology.

I must thank our team, PS2E, which consists of more than twenty researchers and about

ten students, for their embrace. We have four defenses this year, Mathieu Gaurat, Giovanni Mirouh, Morgan Deal and me. It is a great pleasure to work with you and be your friend. I owe you thanks for many helps and, especially, for being a translator. Rohit Kumar came to our lab not too long, while, you help me quite a lot to prepare for the defense. Thank you very much. I would like to thank our great young researchers, Sebastien Deheuvels, for whom organize the Journal Club and Workshop, and especially for the happy hour party, Clément Baruteau, for the vivid memory of the red wine from a chateau in the dark, Jérôme Ballot and Pascal Petit, for their charge of our group working well, ..., they are many. I also grateful to thank the excellent senior researchers, François Lignières, the director of PE2E team, for his discussion about the guideline to be a qualified student in the team, Michel Rieutord, for his discussion of physics and life, ..., they are many.

I also thank the administrative staffs in the lab and the doctoral school. They are Emillie Dupin and Josette Garcia, the secretary of the IRAP, Isabelle Moro, the accountant of the PS2E team, Martin Giard and Philippe Louarn, the previous and current director of the IRAP, Marie-Claude Cathala, the secretary of the doctoral school, Genevieve Soucail, the director of the doctoral school...

I would like to thank the China Government for providing the fund to support me living and study in France. Without it, I cannot pursue my study in Université de Toulouse and conduct my research in the lab IRAP (CNRS). I would also like to thank the funds from the Programme National de Physique Stellaire (PNPS, CNRS/INSU, France) and the Centre National d'Études Spatiales (CNES, France) that support me to attend many international conferences. Then it makes me learn many researchers in white dwarf stars and hot subdwarf stars possible. Gilles Fontaine is a kind of such people whom I first met in a white dwarf meeting even I heard his name before. Gille is very knowledgable in many research aspects, and more importantly, a gracious friend, for whom I thank the encouraging me to persist my research with confidence.

I cannot image that there is no friend for one living in an exotic country. I owe much from my dear friends, most of them are also Ph.d students in Toulouse. I share joys and sorrows with them, go skiing and hiking with them, have parties and communicate many different living skills with them.... They are Chen couple, Chen Chunxian, Gao Congzhang, Ke Diandian, Leng Faqiang, Lin Zifeng, Tian Feng, Wang Renjie, Zhao Xuefei... and many.

Finally, I am very grateful to my family, my father and mother, my younger brother and sister, for their supporting and understanding me that let me purchase my doctor degree in a foreign environment and culture, six or seven hours time lagging behind, many thousands miles away from them, almost across the entire continent, a long-haul trip of one transfer flight and one corresponding train to home.

Résumé

Les interactions non linéaires entre modes de pulsation, induisant des modulations d'amplitude et de fréquence, sont difficiles à mettre en évidence avec les télescopes au sol en raison des temps caractéristiques en jeu, de l'ordre de la semaine, du mois, ou même de l'année. L'avènement des télescopes spatiaux comme KEPLER (opéré par la NASA) a considérablement changé la donne en apportant de nouvelles données pour ce domaine de recherche. Dans cette thèse, nous analysons les données photométriques obtenues avec KEPLER pour 24 étoiles compactes pulsantes, incluant 18 étoiles sous-naines de type B (sdB) et 6 naines blanches. Nous établissons que les modulations d'amplitude et de fréquence des modes d'oscillation sont un phénomène courant dans ces étoiles. Nous étudions en particulier deux étoiles : KIC 0862602, une naine blanche pulsante de type DB, et KIC 10139564, une étoile sdB variable à courtes périodes. KIC 0862602 et KIC 10139564 ont été observées sans interruption par KEPLER en cadence rapide pendant deux années pour la première et plus de trois ans pour la seconde. En analysant en détail ces données photométriques de très haute précision, nous mettons en évidence différents types de comportements affectant les composantes de triplets induits par la rotation stellaire. Les fréquences et amplitudes de ces modes montrent des variations soi périodiques soi irrégulières, ou demeurent constantes. Ces comportements peuvent être connectés à ceux prédits par les équations d'amplitude dans le cas de couplages non linéaires résonants entre modes, en particulier pour les temps caractéristiques des modulations. De plus, nous montrons que les modes en résonance constituant les triplets peuvent également interagir avec des modes extérieurs par le biais d'autres formes de résonances telle que la résonance à trois modes $\nu_0 \sim \nu_1 + \nu_2$, une situation qui n'est pas prise en compte dans le cadre théorique existant. Ces études apportent pour la première fois une preuve claire de l'existence de mécanismes de couplages non linéaires entre modes d'oscillations dans les pulsateurs compacts. Cette découverte résonne comme un avertissement pour les projets visant à mesurer les taux de changement des périodes dus à l'évolution dans les étoiles compactes en général. Les modulations de fréquence d'origine non linéaire peuvent potentiellement empêcher toute mesure fiable de ces taux, à moins de corriger ces effets auparavant. Les modulations observées caractérisées dans cette thèse apportent un regard nouveau sur "l'astérosismologie non linéaire" et appellent à revisiter les méthodes d'analyse des courbes de lumière pour en extraire les modes d'amplitude et de fréquence variables. Dans un futur proche, nous anticipons davantage d'attention portée à ces phénomènes non linéaires dans différents types d'étoiles pulsantes observées depuis l'espace, ainsi qu'un regain d'intérêt pour la théorie non linéaire des oscillations stellaires en général.

Abstract

Nonlinear mode interactions, inducing amplitude and frequency modulations, are difficult to observe from ground-based telescopes as these typical timescales of the modulations are of the order of weeks, months, or even years. The launch of space telescopes such as *Kepler* (operated by NASA) has tremendously changed the situation by providing new data for this research field. In this thesis, we analyze the *Kepler* photometric data observed for 24 compact pulsators, including 18 hot B subdwarf (sdB) stars and six white dwarf stars. We find that it is a common phenomenon that oscillation modes in these pulsating stars show amplitude and/or frequency variations. We focus in particular on two stars, KIC 08626021, a DB white dwarf, and KIC 10139564, a short period sdB star. KIC 08626021 and KIC 10139564 have been monitored by *Kepler* in short-cadence mode for nearly two years and more than three years without interruption, respectively. By analyzing in depth these high-quality photometric data, we find that the modes within triplets induced by rotation clearly reveal different types of behaviors : their frequency and amplitude may exhibit either periodic or irregular modulations, or remain constant. These various behaviors can be linked to those predicted within the amplitude equation formalism in the case of the nonlinear resonant mode coupling mechanism, particularly for the modulation timescales. Furthermore, we find that the triplet resonance modes can also interact with outside modes through other types of resonances such as the three-mode resonance $\nu_0 \sim \nu_1 + \nu_2$, which is not considered within the current nonlinear theoretical frameworks. These findings constitute the first clear evidence of nonlinear resonant mode couplings occurring in compact pulsators. This should resonate as a warning to projects aiming at measuring the evolutionary change rate of pulsation periods in compact stars in general. Nonlinear modulations of the frequencies can potentially jeopardize any attempt to measure reliably such rates, unless they can be corrected beforehand. The observed modulations characterized in this thesis provide new insights to "nonlinear asteroseismology" and call for new methods to process the signals of variable modes from the observed light curves. We foresee that increasing attention will focus on these nonlinear phenomena in various types of pulsating stars observed from space in the near future, thus reviving interest in the nonlinear oscillation theory in general.

Table of contents

Table of figures

List of tables

Introduction générale

L'astérosismologie est une technique puissante pour sonder l'intérieur des étoiles pulsantes. Elle offre l'opportunité de connaitre la composition et la structure des étoiles à partir de leur spectre d'oscillation. Les pulsations observées ont généralement de très faibles amplitudes et peuvent être décrites dans l'approximation des pertubations linéaires dans le cadre de la théorie de l'hydrodynamique stellaire. Dans l'approximation linéaire, les oscillations prédites sont stables, leurs amplitudes et leurs fréquences demeurant constantes. Pourtant, les observations au sol montrent que pour certaines étoiles les oscillations peuvent avoir des variations d'amplitude et de féquence au cours du temps, comme par exemple pour l'étoile variable de type GW Virginis PG 0122+200 (Vauclair et al. 2011) ou encore la naine blanche de type DB GD 358 (Winget et al. 1994). La théorie linéaire des pulsations stellaires ne peut pas rendre compte de ces modulations et c'est vers une approche non linéaire que l'on doit se tourner pour interpréter ces comportements.

Ces modes variables, comme le révèlent les observations, présentent des modulations sur des temps caractéristiques se comptant en semaines, en mois, voire meme en années, soit bien plus que les périodes d'oscillation typiques. En conséquence, il est très difficile avec les réseaux de telescopes terrestres de suivre de façon continue ces phénomènes sur des bases de temps aussi longues. La situation a cependant changé avec le lancement de telescopes spatiaux comme *CoRoT* (Baglin et al. 2006) et *Kepler* (Borucki et al. 2010), permettant un suivi photométrique des étoiles sur plusieurs mois, voire années, sans interruption. La qualité sans précédent des données issues de ces missions permet un regard nouveau sur le mystère des modulations des modes d'oscillation dans les étoiles pulsantes.

Dans cette thèse, je me focalise principalement sur les pulsateurs compacts, incluant les étoiles sous-naines de type B (sdB) et les naines blanches (WD), observées par le satellite *Kepler*. Les étoiles sdB et les naines blanches sont associées aux stades ultimes de l'évolution stellaire pour les étoiles de masse initiale inférieure à huit masses solaires. Les étoiles sdB appartiennent à la branche horizontale extrême (EHB) et sont les restes d'anciennes étoiles géantes rouges ayant perdu la quasi totalité de leur enveloppe riche en hydrogène, laissant une étoile chaude de masse $\sim 0.47\ M_\odot$ et de rayon $\sim 0.10 - 0.25 R_\odot$, brûlant de l'hélium dans le coeur. Les naines blanches sont les restes en cours de refroidissement des étoiles dont le carburant nucléaire est épuisé. La plupart d'entre elles ont une masse autour de $0.6\ M_\odot$ et un rayon comparable à celui de la Terre.

Les étoiles sdB et les naines blanches sont connues pour développer des oscillations non-radiales multi-périodiques. Depuis 1997, deux groupes de pulsateurs sdB ont été identifiés : les étoiles de type *V361 Hya* oscillent rapidement en ondes acoustiques (modes p) à des périodes de l'ordre de quelques minutes et les étoiles de type *V1093 Her* montrent des oscillations plus lentes associées à des modes de gravité (modes g) avec des périodes de $\sim 1 - 4$ heures. Quelques étoiles hybrides oscillant à la fois en modes p et en modes g sont également connues. Les naines blanches comptent quatre bandes d'instabilité le long de leur séquence de refroidissement : les étoiles de type *GW Vir*, très chaudes, ainsi que, par ordre de température effective décroissante,

les DBVs, les DQ chaudes, et les DAVs. Toutes les pulsations observées jusqu'à présent dans les naines blanches sont associées à des modes g et leurs périodes s'échelonnent typiquement de quelques minutes à une heure.

Le satellite *Kepler* a observé 18 sdB et 6 naines blanches pulsantes avant la perte de la seconde roue inertielle en Mai 2013. La plupart d'entre elles, observées pendant approximativement 3 ans, montrent des spectres d'oscillation dont les amplitudes des modes varient au cours du temps. C'est la première fois que nous avons l'opportunité, grâce à *Kepler*, de caractériser les comportements nonlinéaires des modes d'oscillation dans ces étoiles. Ces observations pourraient notamment encourager de nouveaux développements sur le front des théories nonlinéaires des oscillations stellaires. Cette thèse est organisée comme suit :

Chapitre 1 — La théorie des oscillations stellaires est la théorie fondamentale pour étudier les variations de luminosité intrinsèques dans les étoiles. Nous décrirons dans un premier temps la théorie de perturbation linéaire et ses conditions limites permettant d'obtenir les valeurs propres caractérisant les modes d'oscillation. La rotation stellaire et le magnétisme peuvent également affecter ces modes propres, levant les dégénérescences et créant des multiplets symétriques ou asymétriques. Toutefois, des nonlinéarités dans le comportement des modes sont généralement à l'origine de combinaisons de fréquences régulièrement observées dans les spectres de Fourier. Nous aborderons donc également dans ce contexte les théories nonlinéaires des oscillations stellaires ou les modes peuvent aussi avoir un comportement variable au cours du temps, dépendant des conditions de résonance et des coefficients de couplage tel que décrits par les équations d'amplitude.

Chapitre 2 — L'astérosismologie des pulsateurs compacts est l'un des champs les plus actifs de la recherche en physique stellaire. Les oscillations dans les étoiles sdB et naines blanches sont respectivement générées par le mécanisme κ et la convection. L'astérosismologie permet d'obtenir des contraintes précises sur les paramètres fondamentaux de ces étoiles, par exemple leur masse, température effective, et gravité de surface. Les observations de naines blanches pulsantes sur des décennies permettent également de mesurer des taux de changement des périodes associés à l'évolution séculaire (refroidissement) de l'étoile. Toutefois, un grand nombre de ces étoiles montrent des variations d'amplitude sur des échelles de temps allant de quelques jours, semaines, mois à quelques années, i.e., bien plus courtes que les temps évolutifs. La photométrie spatiale, par sa qualité propre et les longues bases de temps d'observation, apparait alors très prometteuse pour identifier les mécanismes derrière ces variations.

Chapitre 3 — Dans ce chapitre, nous introduisons les méthodes utilisées pour exploiter les données photométriques. La plupart des 24 pulsateurs compacts découverts dans le champ *Kepler* ont été observées pendant plus de deux ans sans interruption. Ces données spatiales diffèrent considérablement des données photométriques obtenues au sol en terme de précision et de durée. Aussi, avant d'extraire les fréquences des courbes de lumière *Kepler*, nous effectuons une série de tests statistiques avec le logiciel FELIX pour nous assurer de la fiabilité des mesures d'incertitude sur les paramètres des modes (fréquences et amplitudes) et pour établir les seuils de détection en évaluant les probabilités de "fausse alarme". Les étoiles les plus intéressantes sont ensuite identifiées après une première analyse du spectre de fréquence de tous les pulsateurs de l'échantillon selon des critères comprenant la durée des observations, la détection ou non de multiplets, et la période de rotation des étoiles. L'utilisation de périodogrammes de Lomb-Scargle glissants facilite grandement la recherche de modulations d'amplitude et de fréquence dans les étoiles prioritaires. Nous nous concentrons en particulier sur le comportement des modes dans les multiplets générés par la rotation, ainsi que sur les combinaisons linéaires qui présentent les conditions pour différents types de résonances. Les comportements observés dans les données sont alors comparés avec les prédictions théoriques décrivant les mécanismes de couplages résonants nonlinéaires.

Chapitre 4 — La naine blanche pulsante de type DB KIC 08626021 est la seule DBV suivie par *Kepler*. Après l'analyse d'environ 2 années de données, nous présentons la preuve de l'existance de modulations de fréquence et d'amplitude dans 3 triplets et nous identifions 3 combinaisons de fréquence dans cette étoile. Deux triplets se trouvent être dans le régime intermédiaire de la résonance entre leurs composantes et montrent des variations d'amplitude et de fréquence manifestement périodiques, avec un temps caractéristique compatible avec la théorie. Un troisième triplet présente un comportement différent, avec un verrouillage des fréquences et des amplitudes modulées, associé à un régime transitoire de la résonance. Ces résultats montrent ainsi que deux triplets peuvent se trouver dans deux régimes différents. Il s'agit de la première signature claire d'interactions nonlinéaires identifiée dans une étoile naine blanche pulsante.

Chapitre 5 – L'étoile sdB pulsante KIC 10139564 est la seule étoile hybride dominée par des modes p observée par *Kepler*. Après avoir analysé sa courbe de lumière couvrant 38 mois, nous présentons la découverte intriguante de comportements variés au niveau des modes constituant plusieurs multiplets et combinaisons linéaires de fréquences. Trois multiplets montrent clairement des modulations d'amplitude et de fréquence typiques du régime intermédiaire de la résonance. Deux triplets montrent des modulations d'amplitude mais avec verrouillage des fréquences correspondant au régime transitoire. Un autre triplet est quant à lui complètement verrouillé, avec amplitudes et fréquences constantes sur la durée des observations. De plus, trois fréquences à travers une relation de combinaison linéaire sont probablement dans une résonance directe à trois modes. Il s'agit du premier cas clairement établi révélant des signatures d'interactions non linéaires entre modes dans une étoile sdB, et le second cas identifié parmi les pulsateurs compacts.

En conclusion, nous résumons brièvement les résultats et discutons les perspectives de ce travail. Les interactions nonlinéaires entre modes peuvent se produire dans toutes les étoiles pulsantes et les modulations observées sont parfois plus complexes que les prédictions théoriques.

Introduction

Asteroseismology is a powerful technique to probe the interior of pulsating stars. It offers us the opportunity to know the compositions and the structure of the stars, revealed by their oscillation spectra. The observed oscillations typically have very small amplitudes and can be described by the approximation of linear perturbations within the framework of stellar hydrodynamics theory. In the linear theory domain, the predicted oscillations are stable over time, i.e., having constant amplitudes and frequencies. However, some stars observed by ground-based telescopes show that oscillation modes may have temporal amplitude and/or frequency variations, e.g., the GW Virginis variable star PG 0122+200 (Vauclair et al. 2011) and the DB white dwarf star GD 358 (Winget et al. 1994). The linear theory of stellar pulsation can not account for those mode modulations and one may need to consider the second order—nonlinear terms—of perturbation theory to interpret the behaviors of mode modulations over time.

Those variable modes, as revealed by the observations, have modulations on timescales of weeks, months, and even years, that is much longer than the period of pulsations. Therefore, it is difficult for the ground-based telescopes to continuously monitor these phenomena as a result of the difficulty in organizing network observations to cover such a long time. The situation has tremendously changed with the launch of space telescopes like *CoRoT* (Baglin et al. 2006) and *Kepler* (Borucki et al. 2010), which had the ability to observe stars for months and years without interruption. The unprecedented high-quality photometric data gathered by these spacecrafts shred new light on the mystery behind the behaviors of mode modulations in pulsating stars.

In this dissertation, I mainly focus on the compact pulsators, including hot B subdwarf (sdB) and white dwarf (WD) stars, observed by the *Kepler* spacecraft. White dwarf and sdB stars are related to the ultimate stages of evolution of stars which have an initial mass less than eight solar masses. The sdB stars belong to the so-called Extreme Horizontal Branch (EHB) and are the remnants of former red giants that have lost essentially all of their H-rich envelop, leaving a hot star with mass $\sim 0.47\ M_{\odot}$ and of radius $\sim 0.10 - 0.25 R_{\odot}$, burning helium in the core. The WD stars are the cooling remnants of stars after the nuclear reactions have fade out and most of them have a mass around $0.6\,M_{\odot}$ with a radius comparable to the radius of the Earth.

Both sdB and WD stars are well known to develop nonradial multi-periodic oscillations. There are two groups of identified sdB pulsators since 1997 : the *V361 Hya* stars that oscillate rapidlly in acoustic modes (p-modes) with periods of a few minutes and the *V1093 Her* stars that show slower oscillations due to gravity modes (g-modes) with periods of $\sim 1 - 4$ hours, as well as a few hybrid pulsators that show oscillations both in p- and g-modes. The WD stars count four instability strips along their cooling sequence, i.e., the very hot *GW Vir* stars, as well as, by order of decreasing effective temperature, the DBV, hot-DQ and DAV pulsating stars. All the pulsations observed so far in white dwarf stars are associated with g-modes and their periods typically range from a few minutes to one hour.

Kepler has observed eighteen pulsating sdB stars and six pulsating white dwarf stars before it lost the second reaction wheel in May 2013. Most of them show varying amplitudes in their

oscillation spectra and had been observed for around three years. This is the first time that we have the opportunity, offered by *Kepler*, to characterize the nonlinear behaviors of the oscillating modes excited in these stars. These observed nonlinear mode modulations would particularly encourage new development on the front of nonlinear theory of stellar pulsations. The dissertation is organized as follows :

Chapter 1 — Stellar oscillation theory is the fundamental theory to study the intrinsic luminosity variations in stars. We will firstly describe the linear perturbation theory within which the eigenvalues of oscillation modes can be obtained with the boundary conditions. Stellar rotation and magnetism can affect the eigenvalues, lifting the degeneracy modes into symmetric or asymmetric multiplets. However, strong nonlinearities of eigenmodes are at the origin of some observed linear combination frequencies appearing in the Fourier spectra. We will then present the nonlinear perturbation theory where the involved modes may have temporal behaviors, depending on the resonance conditions and their coupling coefficients, predicted by numerical explorations of the amplitude equations.

Chapter 2 — Asteroseismology of compact pulsators is one of the most intensive research fields in stellar physics. The oscillations in hot B subdwarfs and white dwarfs are driven by κ-mechanisms and convection, respectively. The technique of asteroseismology can provide accurate constraints on the fundamental parameters for those stars : e.g., mass, effective temperature and surface gravity. Observations monitoring some white dwarf stars from decades can also measure the rates of period change of pulsations, which is associated with evolutionary (cooling) effects. Nevertheless, many of those stars exhibit amplitude variations on timescales of days, weeks, months even years, that is much shorter than the evolution timescales. Promisingly, the spaceborne photometry could uncover the mechanisms for the short timescale variations due to its merits of high-quality and long-duration.

Chapter 3 — In this chapter, we provide the methods used to exploit the photometric data. Most of the 24 compact pulsators discovered in the *Kepler* field have been observed continuously for more than two years. The spaceborne data differs significantly from the ground-based photometric data in terms of precision and duration. Before we proceed to extract frequencies from the *Kepler* light curves, we thus do statistical procedures, operated by the software FELIX, to test error confidence and probability of false alarm signals with artificial data with a duration and precision similar to those of *Kepler* photometry. The most interesting targets are sorted out after obtaining the frequency contents of all the compact pulsators, based on their observational durations, richness of multiplets and periods of rotation. The use of sliding Lomb-Scargle periodograms greatly accelerates our search of amplitude and frequency variations of oscillation modes in those priority targets. We concentrate on the mode behaviors of multiplet frequencies as well as some linear combination frequencies because they are in the conditions of different types of resonance. The observed mode behaviors are compared with the theoretical predictions of nonlinear resonant coupling mechanisms.

Chapter 4 — The pulsating DB white dwarf star KIC 08626021 is the unique DBV star monitored by *Kepler*. After analyzing the nearly two years of data, we present evidence of amplitude and frequency modulations in three triplets as well as three linear combination frequencies in that star. The two triplets, that are in the so-called intermediate regimes of triplet resonance, show clearly periodic amplitude and frequency variations, with modulating timescales consistent with the theoretical expectations. Another triplet show a different behavior, locked frequencies and modulated amplitudes, linked to the narrow transitory regime. The results indicate that two neighbor triplets can belong to different resonant regimes. This is the first clear signatures of nonlinear mode interactions identified so far in a white dwarf star.

Chapter 5 — The pulsating hot B subdwarf star KIC 10139564 is the unique p-mode dominated hybrid star from *Kepler* photometry. After analyzing the contiguous 38-month data,

we present the intriguing findings that various mode behaviors occur in different components of multiplets and several linear combination frequencies. Three multiplets show clear amplitude and frequency variations that are typically of the intermediate regime. Two triplets exhibit amplitude modulations but have locked frequencies suggesting that they are in the transitory regime. Another triplet appears in the frequency locked regime in which both amplitude and frequency constant. Three frequencies through linear combination relationship are likely in a three-mode direct resonance. This is the first clear signatures of nonlinear mode interactions identified so far in a hot B subdwarf star and the second case in compact pulsators.

Finally, we summarize the results briefly and propose prospective for the further work. Nonlinear mode interactions can occur in pulsating stars independent of their types. The observed mode modulations sometimes look more complex than the theoretical expectations.

Chapter 1

Stellar oscillation theory

1.1 Linear stellar oscillation theory

The linear stellar oscillation theory is the current theory to investigate the intrinsic luminosity variations of stars. In the very early times of the developing stellar oscillation theory, the radial pulsation one was the chief attention to understand the stellar pulsations in Cepheids (Eddington 1926). It is realized that more complicated pulsations should be considered in some other types of pulsating stars, the nonradial pulsations, which may have been started from the work of Ledoux (1951). Later observations revealed that nonradial pulsations are responsible for the variations in some of the pulsating stars, including the epoch-making discovery of five-minute oscillations in the Sun (Leighton et al. 1962) and the first white dwarf pulsators (Landolt 1968). Along with those observational developments, much progress had been done on the theoretical aspect of nonradial oscillations in the Sun and stars, e.g., the solutions to the equations of linear nonradial oscillations for realistic stellar models (Osaki 1975; Saio & Cox 1980). A comprehensive review of linear stellar theory can be found in Unno et al. (1989), Cox (1980) and Aerts et al. (2010).

In the section, we first introduce the basic equations to depict the equilibrium state of stars, then the linear perturbations will be imposed on the equilibrium state to describe the stellar oscillations. The boundary conditions for the adiabatic oscillations and nonadiabatic oscillations are discussed in Section 1.1.3 and 1.1.4.

1.1.1 Basic hydrodynamics equations

Equations of hydrodynamics, that involves the physical quantities as functions of position $\mathbf{r}$ and time t, are the basic equations to describe oscillations of a star. We begin with the ideal model that the star is self-gravitationally, with physical properties, e.g., the local pressure $p(\mathbf{r}, t)$, the local temperature $T(\mathbf{r}, t)$, the local density $\rho(\mathbf{r}, t)$, and the local velocity of fluid $\mathbf{v}(\mathbf{r}, t)$, without hydrodynamical treatment of convection in the stellar interior, and without presence of magnetism on the surface. The first of these equations is the *conservation of mass*, which is expressed by :

$$\frac{\partial \rho}{\partial t} + \nabla \cdot (\rho \mathbf{v}) = 0. \tag{1.1}$$

In the stellar interior, the viscosity in the gas is generally small and could be neglected. Then equation of the *conservation of momentum* (a.k.a. the Euler equation) can be written as

$$\rho\Big(\frac{\partial}{\partial t} + \mathbf{v} \cdot \nabla\Big)\mathbf{v} = -\nabla p - \rho \nabla \Phi. \tag{1.2}$$

Here the gradient of the gravitational potential Φ satisfies the Poisson equation and it is written as

$$\nabla^2\Phi = 4\pi G\rho, \tag{1.3}$$

where G is the gravitational constant. Again, ignoring the small heat generation induced by viscosity in stellar interior, the final equation is the *conservation of energy*, which can be written as

$$\rho T\Big(\frac{\partial}{\partial t} + \mathbf{v}\cdot\nabla\Big)S = \rho\varepsilon - \nabla\cdot\mathbf{F}, \tag{1.4}$$

where $S(\rho, T)$ is the entropy and $\varepsilon(\rho, T)$ is the energy generation rate. The radiative flux is given by the radiative diffusion equation

$$\mathbf{F} = -K\nabla T = -\frac{4ac}{3\kappa_c\rho}T^3\nabla T, \tag{1.5}$$

where a is the radiation density constant, c is light velocity, and κ_c denotes the opacity.

The small perturbations of oscillations are superimposed on the equilibrium state of a star. In the case of the equilibrium state of a non-rotating, non-magnetic star without convection, the basic equations (1.1)–(1.5) can be written in the spherical polar coordinates as the standard form equations of stellar structure :

$$\frac{dp}{dr} = -\rho g, \text{ with } g \equiv \frac{GM_r}{r^2}, \tag{1.6}$$

$$\frac{dM_r}{dr} = 4\pi r^2\rho \tag{1.7}$$

$$\frac{dL_r}{dr} = 4\pi r^2\rho\varepsilon \tag{1.8}$$

and

$$\frac{dT}{dr} = -\frac{3\kappa\rho}{4ac}\frac{1}{T^3}\frac{L_r}{4\pi r^2} \tag{1.9}$$

where the radiative luminosity $L_r = 4\pi r^2 F$ (may also contains the flux of convective energy F_C) is the energy flow per unit time and M_r is the mass through and within the sphere of radius r, respectively.

1.1.2 The linear perturbation theory

The oscillations in pulsating stars are typically small and can be treated as a system that the "small" perturbations is superimposed upon the equilibrium state of a star. In the domain of the linear pulsation theory, all perturbations are sufficiently small so that only the first-order terms in perturbations are taken into consideration and the second and higher order term in perturbations are neglected. However, the second and third order terms—nonlinear term—that will be considered in the nonlinear amplitude equation formalism in Section 1.4.

A physical quantity x is expressed by either the Eulerian form of

$$x(\mathbf{r}, t) = x_0(\mathbf{r}) + x'(\mathbf{r}, t) \tag{1.10}$$

or the Lagrangian form of

$$x(\mathbf{r}, t) = x_0(\mathbf{r}_0) + \delta x(\mathbf{r}_0, t). \tag{1.11}$$

The above two forms of perturbations are related to each other as

$$\delta x(\mathbf{r}, t) = x'(\mathbf{r}, t) + \boldsymbol{\xi}\cdot\nabla x_0(\mathbf{r}), \text{ with } \boldsymbol{\xi} \equiv \mathbf{r} - \mathbf{r}_0. \tag{1.12}$$

Neglecting the high order terms, the linear perturbed version of the basic equations (1.1)–(1.5), the *conservation of mass, momentum* and *energy* that are derived in the Eulerian forms, are as follows :

$$\frac{\partial \rho'}{\partial t} + \nabla \cdot (\rho_0 \mathbf{v}') = 0, \text{ with } \mathbf{v}' = \frac{\partial \boldsymbol{\xi}}{\partial t}, \tag{1.13}$$

$$\rho_0 \frac{\partial \mathbf{v}'}{\partial t} + \nabla p' + \rho_0 \nabla \Phi' + \rho' \nabla \Phi_0 = 0, \tag{1.14}$$

$$\rho_0 T_0 \frac{\partial}{\partial t}(S' + \boldsymbol{\xi} \cdot \nabla S_0) = (\rho \varepsilon)' - \nabla \cdot \mathbf{F}', \tag{1.15}$$

$$\nabla^2 \Phi' = 4\pi G \rho', \tag{1.16}$$

and

$$\mathbf{F}' = -K_0 \nabla T' - K' \nabla T_0. \tag{1.17}$$

Now we separate the time t from the physical variables (e.g., ρ', T', Φ', $\mathbf{v}'$, ...) and also separate them into radial and angular parts, with the help of the time dependence factor $\exp(i\omega t)$ and the spherical harmonics function $Y(\theta, \phi)$ (see Appendix A.1 for the low-order ones). For equilibrium quantities, the subscript 0 is omitted if there is no confusion.

With this separation of variables, a physical perturbation can be taken as the following form :

$$p'(r, \theta, \phi, t) = p'(r) Y_\ell^m(\theta, \phi) e^{i\omega t}. \tag{1.18}$$

The corresponding expression for the displacement vector $\boldsymbol{\xi}$ is written as

$$\boldsymbol{\xi} = \boldsymbol{\xi}_r + \boldsymbol{\xi}_h = \Big[\xi_r(r),\, \xi_h(r) \frac{\partial}{\partial \theta},\, \xi_h(r) \frac{\partial}{\sin\theta \partial \phi}\Big] Y_\ell^m(\theta, \phi) e^{i\omega t}, \tag{1.19}$$

where $\boldsymbol{\xi}_r$ and $\boldsymbol{\xi}_h$ is the radial and the tangential component of the displacement, respectively, and ξ_h is given (see equation 13.38 in Unno et al. 1989) as,

$$\xi_h = \frac{1}{\omega^2 r}\Big(\frac{p'}{\rho} + \Phi'\Big). \tag{1.20}$$

Figure 1.1 shows some examples of oscillation modes at the stellar surface. The colors represent the temperature of the modes. Modes with azimuthal $m = 0$ are called zonal modes and lines of latitude are the nodal lines of the spherical harmonics. While for the modes with $m = \ell$, i.e., sectoral modes, are separated by the nodal lines of longitude. Other modes are called tesseral modes and their nodal lines are both latitude and longitude.

With the given separation for physical quantities $\{\xi_r,\, p',\, \Phi',\, \delta S,\, T',\, F_r'\}$, a set of ordinary differential equations from equations (1.13)–(1.17) can be obtained as follows :

$$\frac{1}{\rho}\frac{dp'}{dr} + \frac{g}{\rho c^2} p' + (N^2 - \omega^2)\xi_r + \frac{d\Phi'}{dt} = g \nabla_{ad} \frac{\rho T}{p} \delta S, \tag{1.21}$$

$$\frac{1}{r^2}\frac{d}{dr}(r^2 \xi_r) + \frac{1}{\Gamma_1}\frac{d \ln p}{dr}\xi_r + \Big(1 - \frac{L_\ell^2}{\omega^2}\Big)\frac{p'}{\rho c^2} - \frac{\ell(\ell+1)}{\omega^2 r^2}\Phi' = \nabla_{ad}\frac{\rho T}{p}\delta S, \tag{1.22}$$

$$\frac{1}{r^2}\frac{d}{dr}\Big(r^2 \frac{d\Phi'}{dr}\Big) - \frac{\ell(\ell+1)}{r^2}\Phi' - 4\pi G\rho\Big(\frac{p'}{\rho c^2} + \frac{N^2}{g}\xi_r\Big) = -4\pi G \nabla_{ad}\frac{\rho^2 T}{p}\delta S, \tag{1.23}$$

$$K\frac{dT'}{dr} = -F_r' - K'\frac{dT}{dr}, \tag{1.24}$$

and

$$i\omega\rho T \delta S = (\rho\varepsilon)' - \frac{1}{r^2}\frac{d(r^2 F_r')}{dr} + \frac{\ell(\ell+1)}{r^2} K T', \tag{1.25}$$

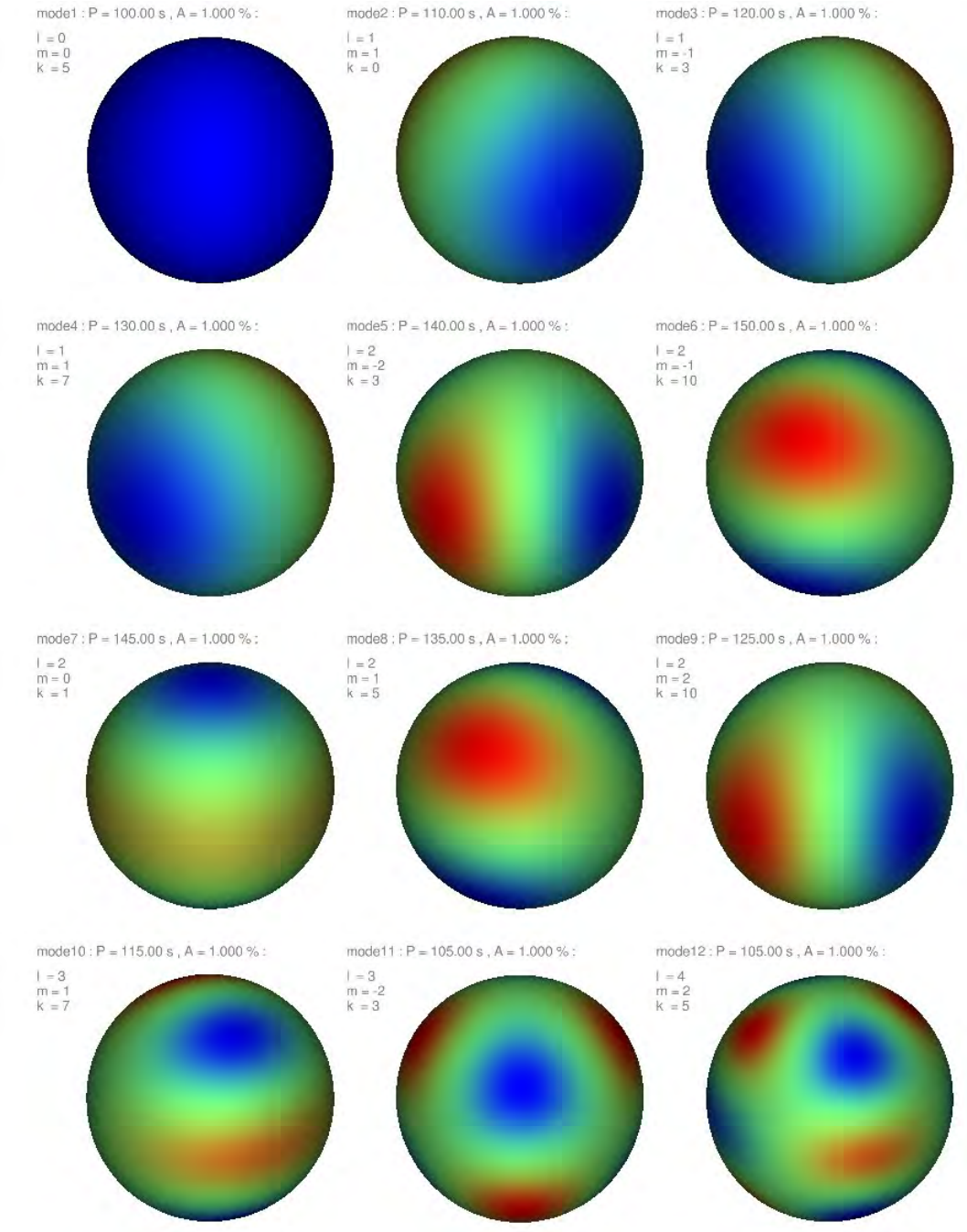

FIGURE 1.1 – Examples of oscillation modes at the stellar surface, label by the radial order k, degree ℓ and azimuthal order m (plotted by the software GLPulse3D).

where $c = \sqrt{\Gamma_1 p/\rho}$ is the sound velocity, Γ_1 and ∇_{ad} are the thermodynamic gradients defined as

$$\Gamma_1 \equiv \Big(\frac{\partial \ln p}{\partial \ln \rho}\Big)_S \text{ and } \nabla_{ad} \equiv \Big(\frac{\partial \ln T}{\partial \ln p}\Big)_S. \tag{1.26}$$

L_ℓ and N are the Lamb frequency and Brunt-Väisälä frequency, respectively, and defined by

$$L_\ell^2 = \frac{\ell(\ell+1)c^2}{r^2}, \tag{1.27}$$

and

$$N^2 = g\Big(\frac{1}{\Gamma_1}\frac{d\ln p}{dr} - \frac{d\ln \rho}{dr}\Big). \tag{1.28}$$

Equations (1.21)–(1.25) are basic equations of linear nonadiabatic nonradial oscillations. With neglecting the right-hand side terms, equations (1.21)–(1.23) are reduced to be those of linear adiabatic nonradial oscillations.

1.1.3 Adiabatic oscillations

In the adiabatic approximation of stellar oscillations, the thermal relaxation time is much longer than the pulsation periods so that the specific entropy is conserved during the oscillations, for such case, $\delta S = 0$. Then the reduced equations (1.21)–(1.23), with terms at right side set to zero, for adiabatic approximation with proper boundary conditions give an eigenvalue problem with an eigenvalue ω^2. We consider the boundary conditions at the center ($r = 0$) and the surface ($p = 0$) where the equations are singular. With the properties of the involving physical quantities near the center (see, Section 14.1 of Unno et al. 1989 and Section 17.6 of Cox 1980, for details), i.e., $r \sim 0$, the reduced equations (1.21)–(1.23) at the center can be expressed by

$$\frac{d\Phi'}{dr} - \frac{\ell\Phi'}{r} = 0 \tag{1.29}$$

and

$$\xi_r - \frac{\ell}{\omega^2 r}\Big(\frac{p'}{\rho} + \Phi'\Big) = 0. \tag{1.30}$$

Since the reduced equations (1.21)–(1.23) are equivalent to a 4th-order differential equation with a single variable, there are two other boundary conditions at the surface. Assuming that the pressure p and the density ρ are zero at the surface $r = R$, we therefore have the zero-boundary conditions,

$$\delta p = 0 \tag{1.31}$$

and

$$\frac{d\Phi'}{dr} + \frac{\ell+1}{r}\Phi' = 0. \tag{1.32}$$

The reduced equations (1.21)–(1.23) and the boundary conditions (1.29) –(1.32) pose an eigenvalue problem which has the solution for the eigenvalue ω^2, independent on index m of the spherical surface harmonics. The degeneracy in index m is lifted by rotation or magnetism (see Section 1.2.1).

For the properties of oscillation eigenmodes in the case of adiabatic approximation and some treatment of mode analysis, e.g., the Cowling (1941) approximation, the asymptotic method, and the numerical method analysis, we suggest you to read books of Unno et al. (1989); Cox (1980); Aerts et al. (2010) and a review of Helioseismology (adiabatic approximation for oscillations in the Sun) by Christensen-Dalsgaard (2002) for details.

1.1.4 Nonadiabatic oscillations

In most stars, the adiabatic approximation treatment can well describe oscillations. However, oscillations in nature are inevitably nonadiabatic that means energy exchange among mass elements during stellar oscillation. In mathematical term, the eigenfrequencies ω of oscillations are complex in description of linear nonadiabatic oscillations. The real part of ω is the frequency of oscillation mode and the imaginary part of ω is the linear growth rate of the mode. The amplitude of oscillation mode grows if the imaginary part of ω is negative, i.e., excited mode. While, if the imaginary part of ω is positive, oscillation mode is vibrationally stable and its amplitude decreases, i.e., damped mode.

The energy conservation equation and the flux equation (1.24) and (1.25) have to be incorporated to solve the linear nonadiabatic oscillations. We note that it is more convenient to use the Lagrangian perturbations of nuclear energy generation rate ε and radiative flux F although they are in the Eulerian perturbation form in equations (1.24) and (1.25), without necessary to consider the dependence of the physical quantities ε and the opacity κ on the chemical composition. The Lagrangian perturbations of these equations (1.24) and (1.25) can be seen in Unno et al. (1989, equation 21.14 and 21.15). In addition to these equations, the thermodynamic relation between δT and δS is also needed,

$$\delta S = c_p\Big(\frac{\delta T}{T} - \nabla_{ad}\frac{\delta p}{p}\Big), \text{ with } c_p \equiv T\Big(\frac{\partial S}{\partial T}\Big)_p. \tag{1.33}$$

The nonadiabatic oscillation involves sixth-order differential equations and six boundary conditions which pose an eigenvalue problem with a complex eigenvalue ω. Four of the six boundary conditions, two at the center $r \sim 0$ and two at the surface $r = R$, are the same to the adiabatic oscillations as discussed in last section, see equations (1.29)–(1.32), with assumptions of the simple reflective boundary conditions in which the pressure and the density near the stellar surface decreases rapidly outward. Another boundary condition at the center may be chosen as

$$\delta S = 0. \tag{1.34}$$

Another surface boundary condition could be the fact that there is no inward radiative flux at the surface, i.e.,

$$\frac{\delta F}{F} = \frac{\delta f_E}{f_E} + 4\frac{\delta T}{T}, \tag{1.35}$$

where f_E is the Eddington factor. For simplicity, the perturbation of the Eddington factor $\delta f_E$is a really difficult problem and is usually not considered (Christensen-Dalsgaard & Frandsen 1983).

1.2 Stellar rotation effects

Some of real stars, in fact, rotate at certain speed, e.g., observation on the DB white dwarf GD 358 (Winget et al. 1994). Therefore, the influence of stellar rotation should be taken into consideration to obtain the eigenvalues of oscillation modes. As the theory of rapid rotation is very complicated, only is the effects of slow rotation considered in this thesis.

Assuming a star that is uniformly rotating with an angular velocity $\mathbf{\Omega}$, the linear perturbations of equation (1.14), in the frame rotating with the star, must be replaced by

$$\frac{\partial \mathbf{v}'}{\partial t} + (\mathbf{v}\cdot\nabla)\mathbf{v}' + (\mathbf{v}'\cdot\nabla)\mathbf{v} + 2\mathbf{\Omega}\times\mathbf{v}' = -\frac{1}{\rho}\nabla p' - \nabla\Phi' - \frac{\rho'}{\rho}\nabla\Phi, \tag{1.36}$$

where the fourth term in the left side represents the linear perturbations of the Coriolis force.

Assuming that velocity fields affect the equilibrium state as small perturbations, equilibrium quantity such as ρ, eigenfunctions $\boldsymbol{\xi}$, and eigenfrequencies ω, are expanded up to second orders as

$$\rho = \rho_0 + \rho_1'(\Omega) + \rho_2''(\Omega^2) + \mathcal{O}(\Omega^3), \tag{1.37}$$

$$\boldsymbol{\xi} = \boldsymbol{\xi}_0 + \boldsymbol{\xi}_1'(\Omega) + \boldsymbol{\xi}_2''(\Omega^2) + \mathcal{O}(\Omega^3), \tag{1.38}$$

and

$$\omega = \omega_0 + \omega_1'(\Omega) + \omega_2''(\Omega^2) + \mathcal{O}(\Omega^3). \tag{1.39}$$

To obtain the corrections of the first and second order terms of rotation to eigenfrequencies, we firstly introduce a linearized operator that represents for the linear adiabatic nonradial oscillations (Lynden-Bell & Ostriker 1967; Cox 1980; Unno et al. 1989),

$$\mathscr{L}(\boldsymbol{\xi}) = \omega^2 \boldsymbol{\xi}, \tag{1.40}$$

where the full expression of $\mathscr{L}(\boldsymbol{\xi})$ can be found in Appendix A.2.

1.2.1 The first order effect of stellar rotation on eigenfrequencies

With the help of this linear operator $\mathscr{L}$, the first order effect of rotation on eigenfrequency of oscillations can be given by (see details in Hansen et al. 1977; Unno et al. 1989),

$$\Delta\omega_{n\ell m} \equiv \omega_1' = m \int_0^R \int_0^\pi K_{n\ell m}(r,\theta)\Omega(r,\theta) r dr d\theta, \tag{1.41}$$

where the rotational kernel function $K_{n\ell m}(r,\theta)$ is very complicated and can be found in Appendix A.3. The kernel $K_{n\ell m}(r,\theta)$ can be calculated from the eigenfunctions for the nonrotating stellar model and only depends on m^2 (Hansen et al. 1977; Cuypers 1980). Now we could see that the $(2\ell+1)$-degeneracy of eigenfrequency of each mode is lifted by stellar rotation, a similar effect as Zeeman splitting in magnetic field. Therefore the eigenfrequencies depend on not only the degree ℓ of but also the azimuthal index m of the spherical harmonics $Y_\ell^m(\theta,\phi)$.

In the simple case of a star with uniform rotation, with Ω constant, the frequency corrections induced by rotation is simple as

$$\Delta\omega_{n\ell m} = -m(1 - C_{n\ell})\Omega, \tag{1.42}$$

where $C_{n\ell}$ is the Ledoux constant (Ledoux 1951) which is expressed by

$$C_{n\ell} = \frac{\int_0^R [2\xi_r\xi_h + \xi_h^2]\rho r^2 dr}{\int_0^R [\xi_r^2 + \ell(\ell+1)\xi_h^2]\rho r^2 dr}. \tag{1.43}$$

The rotation effect on frequency is proportional to the azimuthal order m and to the rotational velocity Ω. For p-modes, as radial order n increases the radial displacement ξ_r dominates over the horizontal displacement ξ_h and the quantity $C_{n\ell}$ approaches to zero. While in the case of g-modes, the horizontal displacement ξ_h becomes the dominant term as n increases in the outer part of the star and $C_{n\ell}$ trends to $1/\ell(\ell+1)$. We could easily see that the $(2\ell+1)$ components in an ℓ-multiplet are well equally spaced from equation (1.42). It indicates that the components in such as a triplet are in the exact resonance $2\omega_0 = \omega_+ + \omega_-$ where the ω_+ and ω_- are the frequencies of the prograde and retrograde modes in the triplet, respectively, and ω_0 is the frequency of the central component, unperturbed eigenfrequency. These symmetrically spaced components may be distorted, such as, by the second order perturbation of rotation effect (e.g., Dziembowski & Goode 1992), and will be discussed in next section.

1.2.2 Frequency mismatch in multiplets induced by stellar rotation

The higher order terms of stellar rotation can distort the symmetrical components in a multiplet. The second order corrections to eigenfrequencies due to slow rigid rotation is in a more complicated form than in that of the first order and has a general expression as (see, e.g., Saio 1981; Soufi et al. 1998),

$$\delta\omega_{n\ell m} \equiv \omega_2'' = D_{n\ell}\,\omega_0\Big(\frac{\Omega}{\omega_0}\Big)^2, \tag{1.44}$$

where $D_{n\ell}$ contains the corrections both from the Coriolis force and the distortion of spherical symmetry of the star. The expression of $D_{n\ell}$ is very complicated and will be not given here (see details in, e.g., Saio 1981; Gough & Thompson 1990; Dziembowski & Goode 1992; Soufi et al. 1998). In the case of g-modes, the quantity $D_{n\ell}$ is typically on the same order of $C_{n\ell}$, e.g., $D_{n\ell} \sim 4C_{n\ell}$ in Goupil et al. (1998). However, $D_{n\ell}$ varies in a large range for p-modes, e.g., see values of $D_{n\ell}$ in Saio (1981) and Dziembowski & Goode (1992). We note that the second order corrections, $\delta\omega$, distort the symmetrically spaced components in a multiplet since $\delta\omega$ is always positive, i.e., all the eigenfrequencies will be shifted to the same direction in Fourier amplitude spectra, a similar effect to the magnetism which will be discussed in the following. This frequency mismatch could govern which kind of regime of the nonlinear mode resonance the multiplet in, exhibiting amplitude and frequency variations or remaining stable, which will be discussed in Section 1.4.3.

The third order term due to stellar rotation may be considered in the case of fast rotating stars. However, in most sdB stars and white dwarfs, the rotation periods are far longer than that of oscillations, $\omega \gg \Omega$. Therefore the contributions from the third order perturbations of rotation can generally be ignored in our context (see, e.g., equation 61 in Soufi et al. 1998).

Magnetism effects

In this short section we will discuss the effect of magnetism on the eigenfrequencies of oscillation modes, although the magnetic perturbations on eigenfrequencies are smaller than that from rotation in most white dwarfs and almost all sdB stars. The correction induced by magnetic effects $\delta\omega_{mag}$ could be deduced by the similar perturbation method of stellar rotation, and the result shows that it is proportional to the square of the magnetic strength $|\mathbf{B}|^2$ as (Jones et al. 1989),

$$\delta\omega_{mag} \simeq D_{mag} m^2 |\mathbf{B}|^2, \tag{1.45}$$

where D_{mag} is a constant and depends on stellar models. Equation (1.45) shows that $\delta\omega_{mag}$ depends on m^2 instead of m and the degeneracy frequency will be lifted by the magnetism into $\ell + 1$ modes instead of $2\ell + 1$ by stellar rotation. The magnetic effect on correction of eigenfrequencies also lead the frequencies to shift in the same direction, a similar effect of second order rotational perturbations, and could contribute to the frequency mismatch in a multiplet.

1.3 Combination frequencies in the Fourier spectra induced by strong nonlinearities

We have discussed the self-excited nonradial modes (eigenmodes) within the domain of linear stellar oscillation theory in Section 1.1 before. However, the observable amplitude of $\ell \geq 3$ mode is reduced by geometric cancellation effects because we cannot resolve the stellar disk spatially (Dziembowski 1977). We are only limited to observe the luminosity variations of

low-degree ($\ell = 1, 2$) modes from the ground-based observations. Observations on some stars present a richness of signals that are too numerous to be real self-excited eigenmodes, e.g., GD 358 (Winget et al. 1994). Some of the signals in Fourier spectra have relationships with other oscillation modes through linear combinations, e.g., sum or difference frequencies.

Linear combination frequencies are observed in the Fourier spectra of many white dwarf and sdB pulsating stars, e.g., multi-site observation on sdB star PG 1325+101 (Silvotti et al. 2006), the Whole Earth Telescope (WET hereafter) observations on sdB star PG 0014+067 (Vučković et al. 2006), ZZ Ceti star HL Tau 76 (Dolez et al. 2006), DB white dwarf GD 358 (Winget et al. 1994), and hot pre-white dwarf RXJ 2117+3412 (Vauclair et al. 2002). They are too numerous to be eigenmodes themselves and their amplitudes may have correlations with their principal parent modes. There are two proposals that the origin of linear combination frequencies involves strong nonlinear mixing of sinusoidal signals that are associated with eigenfrequencies of oscillation modes : 1. The depth of convection zone at stellar surface varies when the star undergo oscillations (Wu 2001) ; 2. The emergent flux changes due to the second order of temperature perturbations at the stellar surface (Brassard et al. 1995). Both of those two interpretations on the origin of linear combination frequencies predict that the amplitudes of the combination frequencies depend somewhat on the inclination angle between the stellar rotation axis and the observing sight and the amplitudes of those resulting frequencies are typically very small, compared to the amplitudes of their principal parent modes.

We note that linear combination frequencies are also in the conditions of being resonant with their principal parent modes, e.g., $\omega_1 \sim \omega_2 + \omega_3$, where ω_1, ω_2 and ω_3 are the frequencies of the three involved modes. If the linear combination frequencies are indeed in a resonance, their amplitudes could be substantial large, even larger than the amplitudes of their principal parents (see, e.g., Breger & Montgomery 2014). The resonance of $\omega_1 \sim \omega_2 + \omega_3$ will be discussed in Section 1.4.4 in which the nonlinear perturbation theory should be addressed for stellar oscillations.

1.3.1 The depth-varying surface convection zone

Brickhill firstly proposed that the linear combination frequencies result from nonlinear mixing of eigenmodes in context of the surface convection in pulsating DA variable white dwarfs (Brickhill 1992). The depth of the convection zone varies instantaneously during stellar pulsations and affect the photospheric flux variations. This process distorts the shape of the light curve at the stellar photosphere and brings about the presence of the combination frequencies in the Fourier power spectra. Based on this proposal, Wu (2001) developed the analytical expressions for the amplitudes and phases of the combination frequencies with three assumptions : (1) perturbations along neighboring angular directions do not affect each other ; (2) the radiative interior cause little nonlinearity in the pulsation signals ; (3) equilibrium models adjacent in effective temperature quantify the time-dependent nature of the convective zone.

The dimensionless amplitude ratio, R_c, between the observed amplitude of a combination frequency and its principal modes is defined as (van Kerkwijk et al. 2000),

$$R_c \equiv \frac{A_{i\pm j}}{n_{ij} A_i A_j}, \tag{1.46}$$

where $A_{i\pm j}$ is the amplitude of the combination frequency, A_i and A_j are the amplitudes of the principal parent modes, and n_{ij} denotes the number of possible permutations : $n_{ij} = 1$ if $i = j$, and $n_{ij} = 2$ if $i \neq j$. The theoretically expression for the observable R_c to be as (Wu 2001),

$$R_c = \frac{|2\beta + \gamma|(\omega_i \pm \omega_j)\tau_{c_0}}{4\alpha_V \sqrt{1 + [(\omega_i \pm \omega_j)\tau_{c_0}]^2}} \frac{G_{\ell_i \ell_j}^{m_i \pm m_j}}{g_{\ell_i}^{m_i} g_{\ell_j}^{m_j}}, \tag{1.47}$$

where $\alpha_V \sim 0.4$ for a ZZ Ceti star in the optical band, ω_i and ω_j are the frequencies of the principal parent modes. The value of the convection zone thermal time constant, τ_{c_0}, ranges from 20 s to 1300 s between the blue and red edge of the ZZ Ceti instability strip (Wu 2001). The two dimensionless numbers, β and γ, quantify the deepening of the convection zone when a white dwarf cools and $|2\beta + \gamma| \sim 12$ for the pulsating white dwarfs. The expression for the geometric factors that associate with the inclination angle, $g_{\ell_i}^{m_i}$, $g_{\ell_j}^{m_j}$ and $G_{\ell_i\ell_j}^{m_i \pm m_j}$, can be found in Appendix A.5.

These formalism had been applied to two types of white dwarf variables, i.e., DB star GD 358 (Winget et al. 1994) and a cool ZZ Ceti G29-38 (Kleinman et al. 1998). In general, theoretical considerations could reproduced most ($\sim 90\,\%$ for GD 358) linear combination frequencies in both stars, with a few discrepancies which needs further discussion. In this formalism, the amplitude ratio R_c between linear combinations frequencies and their parents modes are typically less than 10 for the $(\ell = 1, \ell = 1)$ and $(\ell = 1, \ell = 2)$ modes (see Eqn. 1.47). There are also some open problems for this formalism that some types of variables do not present convection zone in their surface, e.g., DO white dwarfs and hot B subdwarfs. In some of these types of stars, linear combination frequencies also exit, e.g., pre-white dwarf star PG 1707+427 (Fontaine et al. 1991) and sdB star Balloon 090100001 (Baran et al. 2008).

1.3.2 The temperature variations at stellar surface

Brassard et al. (1995) proposed that linear combination frequencies in ZZ Ceti stars can be reproduced by the second order of local temperature perturbations at the stellar surface induced by oscillations, based on the work by Robinson et al. (1982) in which the authors proposed that the luminosity or color variations of the white dwarf stars are caused by the temperature variations instead of geometry or gravity variations. These strong nonlinearities can be explained in terms of the nonlinear response of the emergent flux to change of the local temperature at stellar surface. In this formalism, the amplitude of an oscillation mode with frequency ω_i (in percentage in filter x) is expressed by

$$A_i = A_{\ell_i}^x \epsilon_i T_0 \overline{Y}_\ell^m(\theta), \tag{1.48}$$

where ϵ_i is the dimensionless amplitude of the temperature perturbation due to the oscillations of mode i, T_0 is the unperturbed effective temperature of the star, $A_{\ell_i}^x$ is the frequency-integrated quantity, and the real spherical harmonics function $\overline{Y}_\ell^m(\theta) \equiv Y_\ell^m(\theta, \phi)e^{-im\phi}$ and θ is the inclination angle (see Appendix A.5). The amplitude of the linear combination frequencies (in percentage) , e.g., $\omega_k = \omega_i + \omega_j$, is given by

$$A_{i+j} = \epsilon_i \epsilon_j T_0^2 \sum_{k=|\ell_i - \ell_j|}^{\ell_i + \ell_j} [\ell_i, m_i; \ell_j, m_j]_k \overline{Y}_k^{m_i+m_j}(\theta) B_k^x. \tag{1.49}$$

Here subscript i, j denote two different mode i and j, B_k^x is a physical quantity in filter x that depends on stellar model, and $[\ell_i, m_i; \ell_j, m_j]$ is a rewritten form of the Clebsch-Gorden coefficients between quantum numbers (Cohen-Tannoudji et al. 1977), which is defined as,

$$Y_{\ell_i}^{m_i}(\theta, \phi) Y_{\ell_j}^{m_j}(\theta, \phi) \equiv \sum_{k=|\ell_i - \ell_j|}^{\ell_i + \ell_j} [\ell_i, m_i; \ell_j, m_j]_k \overline{Y}_k^{m_i+m_j}(\theta). \tag{1.50}$$

Therefore the dimensionless amplitude ratio, R_c, in this formalism is given by

$$R_c = \frac{\sum_{k=|\ell_i - \ell_j|}^{\ell_i + \ell_j} [\ell_i, m_i; \ell_j, m_j]_k \overline{Y}_k^{m_i+m_j}(\theta) B_k^x}{n_{ij} A_{\ell_i}^x A_{\ell_j}^x \overline{Y}_{\ell_i}^m(\theta) \overline{Y}_{\ell_j}^m(\theta)} \times 100. \tag{1.51}$$

From this equation (1.51) we note that R_c is independent on the temperature and its perturbation term ϵ_i. It only depends on the spherical harmonics function Y_ℓ^m and the physical quantities A^x, B^x in filter x. Table 1–8 in Brassard et al. (1995) provide the calculated values of quantities $A^x_{\ell_i}$ and B^x_k for a series of stellar models in different filters. They also provide the specific expressions of the low degree ($\ell \leq 4$) of the real spherical harmonics functions $\overline{Y}^m_\ell(\theta)$ and their relationships of equation (1.50) for low degree modes $\ell = 1$ or $\ell = 2$, in Appendix (Brassard et al. 1995).

Now we apply this formalism to some real modes in a ZZ Ceti star, by adopting the values provided by Brassard et al. (1995). Here we only give an example to the combination frequencies of modes $[\ell = 1, m = 0; \ell = 1, m = \pm 1]$ in white filter that is the most similar filter in Brassard et al. (1995) to the color of *Kepler* photometric data. In such case, R_c is reduced to $50B^x_2/A^x_1A^x_1$. In the white filter, A^x_1 is $\sim 10^{-2}$ and B^x_2 is $\sim 10^{-7}$ to 10^{-6}, and $R_c < 1$. That means the amplitudes of the linear combination frequencies between an $(\ell = 1, m = 0)$ and $(\ell = 1, m = \pm 1)$ modes in white filter should be very small, comparing to amplitudes of their principal parent modes. We note that the formalism of temperature perturbations are independent on the presence of convection zone in stellar surface and could be applied to any kind of pulsating stars.

1.4 Nonlinear resonant mode coupling mechanism

Linear stellar pulsation theory is in a fairly satisfactory state with the observations of oscillations in pulsating stars, where the eigenfrequencies are stable over time. However, observations show that eigenmodes may have temporal variations in amplitude and frequency on timescales much longer than oscillation periods themselves, which is beyond the scope of the linear theory and lies in the domain of nonlinear pulsation theory. There are basically two approaches to nonlinear stellar pulsations that are complementary in some ways, numerical hydrodynamics and the amplitude equation formalism. The later one gained much attention since it reduces the problem of involved modes from a partial differential equation system in time and space to a simpler case, a system of ordinary differential equation only in time. The amplitude equations formalism (hereafter AEs) is the only tool with which we can understand nonlinear nonradial pulsations, in particular for mode interactions and resonance (Buchler 1993). Essentially, AEs is limited to weakly nonadiabatic pulsators, e.g., white dwarf and hot B subdwarf stars (Buchler 1993, 1998).

In context of stellar physics, the theoretical derivation of AEs began around 1980's. Dziembowski (1982) applied AEs to the case of resonant mode coupling $\omega_1 \sim \omega_2 + \omega_3$ or $\sim 2\omega_2$, followed by which parametric resonance of an unstable p-mode with g-mode pairs was investigated to explain the low-amplitude modes in δ Scuti stars (Dziembowski & Krolikowska 1985). In their investigations, the nonadiabatic effects were only taken into account in the linear perturbation terms and the nonlinear mode coupling was calculated in an adiabatic approximation. This type of resonant mode coupling predicts periodic amplitude modulations under certain conditions in pulsating stars (Moskalik 1985; Wu & Goldreich 2001) and the amplitude saturation of gravity modes in ZZ Ceti stars (Wu & Goldreich 2001). We note that the most recent investigations of AEs of this type was extended to give prediction on saturation of poloidal mode instability in neutron star (Pnigouras & Kokkotas 2015), which could determine the amplitude of gravitational wave signals (see the first direct detection in Abbott et al. 2016) emitted by that neutron star.

Parallel to the adiabatic ones, the nonadiabatic treatment included by nonlinear AEs was originally developed for the most simple case, radial pulsations in pulsating stars (Buchler & Goupil 1984). It is remarkable that the solutions of AE agree pretty well with the exact nonlinear

models for the classical Cepheids models (Buchler & Kovacs 1986). Then the radial AEs was extended to the nonradial pulsations in the Eulerian form and also in the Lagrangian form (Goupil & Buchler 1994; Van Hoolst 1994a). Buchler et al. (1995) applied AEs to a specific case, i.e., nonradial modes in an $\ell = 1$ triplet induced by slow stellar rotation. The results of the solution to AEs of such case show that amplitudes and frequencies of the modes in the considered triplet may exhibit periodic behaviors, constant or even chaotic modulations. It must be stressed that resonant couplings exist only between certain nonradial modes that is imposed by the selection rules of angular momentum constraints. The consequences of nonlinear resonant couplings of nonradial modes and possible evidences of observations in several stars are discussed by Buchler et al. (1997) and Goupil et al. (1998).

Nonlinear AEs predict that temporal behaviors of amplitude and frequency of oscillation modes modulate on timescales of weeks, months even years, much longer than the pulsation periods. This is difficult with ground-based observations to monitor continuously one cycle of such modulations. Nevertheless, there are some possible hints from ground-based observations, e.g., in white dwarfs (see examples in Vauclair 2013), that amplitude and frequency variations are significantly larger than the detection errors. To uncover clear evidences of nonlinear mode interactions, launch of satellite telescopes are particularly needed (e.g., Dziembowski 1993). With spaceborne data, nonlinear AEs may be better constrained by extracting nonlinear coefficients from the observed modulations. Moreover, nonlinear stellar pulsation theory can provide new tools for diagnostic of a more precise stellar interior.

This section is organized as follows : We first introduce the nonlinear nonadiabatic perturbations theory of stellar oscillations ; then nonlinear AEs is applied to specific cases, particularly for resonant mode couplings within an $\ell = 1$ triplet, aligning to the first proposal of this thesis, i.e., searching for the first evidences of triplet resonances ; following that, resonant mode coupling of three modes $\omega_1 \sim \omega_2 + \omega_3$ or $\sim 2\omega_2$ is given but in an adiabatic approximation ; we end up this section with the particular explorations on this three mode couplings.

1.4.1 Nonlinear perturbations

In this section, we extend the small linear perturbations to higher nonlinear perturbations as involves higher orders terms in the Eulerian form which is mainly investigated by Goupil & Buchler (1994), and see Van Hoolst (1994a,b) for the perturbations in the Lagrangian and Hamiltonian formalism. We do neither introduce the equilibrium state of hydrodynamics equations for a nonrotating and non-magnetic star again nor the linear perturbations (see Section 1.1.2 for details). As the nuclear time scale of the evolution of chemical composition is much longer than that of dynamical and thermal process, the treatment of the chemical composition in a star is constant during oscillations, i.e., $\partial\mu_i/\partial t = 0$, thus the change of chemical composition will not be involved in the linear and nonlinear perturbation operators, $\mathcal{L}$ and $\mathcal{N}$.

The perturbation of physical quantities, $\{p, T, \mathbf{F}, ...\}$, can be expressed as,

$$\begin{aligned} x'(\mathbf{r}, t) =& x(\mathbf{r}, t) - x_0(\mathbf{r}) \\ =& x'_1(\mathbf{r}, t) + x''_2(\mathbf{r}, t) + x^{(3)}_3(\mathbf{r}, t) + ... , \end{aligned} \tag{1.52}$$

where $x_i^{(i)}$ is the Eulerian perturbation of the ith order of $x(\mathbf{r}, t)$, and it also can be expressed in terms of the independent variable $\mathbf{z}$. For a independent physical quantity $x(\mu)$ where $\mu = (\mu_1, \mu_2, ..., \mu_n)$, the perturbations in the Eulerian formalism are written as

$$x'_1 = \sum_i \frac{\partial x}{\partial u_i} u'_i, \tag{1.53}$$

$$x_2'' = \frac{1}{2!}\sum_{i,j}\frac{\partial^2 x}{\partial u_i \partial u_j}u_i' u_j', \tag{1.54}$$

and

$$x_3^{(3)} = \frac{1}{3!}\sum_{i,j,k}\frac{\partial^3 x}{\partial u_i \partial u_j \partial u_k}u_i' u_j' u_k'. \tag{1.55}$$

With inserting the nonlinear perturbations (equation 1.52), we derived the nonlinear equations into the general form as,

$$\frac{\partial \mathbf{z}}{\partial t} - \mathcal{L}\mathbf{z} = \mathcal{N}\mathbf{z} = \mathcal{N}_2\mathbf{z} + \mathcal{N}_3\mathbf{z} + \dots, \tag{1.56}$$

where $\mathbf{z} = (\rho', \mathbf{v}', S')^t$. The component of the linear operator $\mathcal{L}$ can be easily obtained by rewritting the equations (1.13)–(1.17). Setting the partial differential with time t on the left side, the rest terms on the right side are the linear operator $\mathcal{L}$ for density ρ, velocity $\mathbf{v}$, and entropy S, respectively. Now we consider the quadratic contributions $\mathcal{N}_2$ which are obtained for density ρ, velocity $\mathbf{v}$, and entropy S, respectively, as

$$\mathcal{N}_2^{\rho}(\mathbf{z}, \mathbf{z}) = -\nabla \cdot (\rho \mathbf{v}'), \tag{1.57}$$

$$\mathcal{N}_2^{\mathbf{v}}(\mathbf{z}, \mathbf{z}) = -(\mathbf{v}' \cdot \nabla)\mathbf{v}' - -\frac{1}{\rho}\Big(\nabla p_2'' - \rho' \nabla p_1' - \rho \rho'^2 \nabla \Phi\Big), \tag{1.58}$$

$$\mathcal{N}_2^{S}(\mathbf{z}, \mathbf{z}) = -\mathbf{v}' \cdot \nabla S' - \frac{1}{\rho T}\Big(\nabla \cdot \mathbf{F}_2'' - (\frac{T_1'}{T} + \rho')\nabla \cdot \mathbf{F}_1'\Big). \tag{1.59}$$

and the cubic operator $\mathcal{N}_3$ that are expressed by

$$\mathcal{N}_3^{\rho}(\mathbf{z}, \mathbf{z}, \mathbf{z}) = 0, \tag{1.60}$$

$$\mathcal{N}_3^{\mathbf{v}}(\mathbf{z}, \mathbf{z}, \mathbf{z}) = -\frac{1}{\rho}\Big(\nabla p_3^{(3)} - \rho' \nabla p_2'' + (\rho')^2 \nabla p_1' + \rho(\rho')^3 \nabla \Phi\Big), \tag{1.61}$$

$$\mathcal{N}_3^{S}(\mathbf{z}, \mathbf{z}, \mathbf{z}) = -\frac{1}{\rho T}\Big[\nabla \cdot \mathbf{F}_3^{(3)} - (\frac{T_1'}{T} + \rho')\nabla \cdot \mathbf{F}_2'' + \Big((\frac{T_1'}{T})^2 - \frac{T_2''}{T} + (\rho')^2 + \rho' \frac{T_1'}{T}\Big)\nabla \cdot \mathbf{F_1'}\Big]. \tag{1.62}$$

Equations (1.13)–(1.17) and (1.56) are the backbone for the derivation of the amplitude equations of various types of resonance. The linear operator provides the solutions of the eigenvectors (see Section 1.1 for details) that form the vector-basis in which the nonlinear AEs formalism could proceed.

1.4.2 Amplitude equations of nonlinear nonadiabatic nonradial resonance

In context of nonlinear system (see equation 1.56), amplitude equation formalism takes advantage that only the dominant modes are considered since the vast majority of the oscillation modes are strongly damped and could be eliminated as much as possible (Goupil & Buchler 1994). Therefore AEs are possible to describe the general behaviors of dominant modes by their temporal amplitudes. These amplitudes are ordinary differential equations that solely depends on the resonance conditions occurring among the dominant modes of the considered system. A number of equivalent approaches of deriving such AEs can be found in, e.g., Guckenheimer et al. (1984), Nayfeh (1973) and Buchler & Goupil (1984).

The stellar oscillations can be represented by temporal amplitudes as

$$\mathbf{z} = \sum_j \frac{1}{2} A_j(t) e^{i\omega_j t}\mathbf{e}_j + \mathcal{C} + \mathcal{O}, \tag{1.63}$$

where $\mathbf{e}_j$, ω_j, and $A_j(t)$ denote the linear nonadiabatic eigenvectors, eigenfrequency and the temporal amplitude of mode j, respectively, $\mathcal{C}$ denotes complex conjugation and $\mathcal{O}$ represents 'higher order terms'. With the help of known $A_j(t)$, that needs to solve the amplitude equations *a priori*, the temporal behaviors of all the physical quantities such as density ρ and entropy S can be finally determined.

Amplitude equations are applied in a few cases of special interest in stellar oscillations. The first case concerns the no-existing resonance situation where the modes does not satisfy any resonance conditions of the form $\sum_j k_j\omega_j \approx 0$, with k_j is small integer. For each mode j, AEs is expressed by

$$\frac{dA_j}{dt} = (i\omega_j + \kappa_j)A_j + Q_{jj}|A_j|^2A_j + \sum_k Q_{jk}|A_k|^2A_j, \tag{1.64}$$

where the nonlinear coupling coefficients Q_{jk} are very complicated and will be not given here (see Appendix B in Goupil & Buchler 1994, for the full expression of Q_{jk} and the coupling coefficients in the subsequent equations 1.65 and 1.66). It is note that there is no quadratic terms in the nonresonant case and the cubic ones, which is at least and sufficient (Kovacs & Buchler 1989), has to be considered to describe amplitude saturation by nonlinear effects. Now taking AEs in the case of resonances where the nonlinear quadratic terms will arise, for example, a resonant condition in which the two involved modes whose frequencies have the relationship $2\omega_1 \approx \omega_2$, the $2:1$ resonance AEs are obtained as

$$\frac{dA_j}{dt} = (i\omega_j + \kappa_j)A_j + P_jA_{n_{j2}}A_1^* + \sum_k Q'_{jk}|A_k|^2A_j, \tag{1.65}$$

where $j,k = 1,2$, the asterisk represents complex conjugation, P_j is the nonlinear quadratic terms, and Q'_{jk} differ from Q_{jk} through the absence of the terms that became divgergent caused by resonance. Finally, nonradial modes in the condition of $1:1:1$ resonance within an $\ell = 1$ triplet, i.e., $\omega_1 \approx \omega_2 \approx \omega_3$, or a general case $\omega_1 + \omega_2 \approx 2\omega_3$, are particularly interesting. This AEs saturates at cubic order as

$$\frac{dA_j}{dt} = (i\omega_j + \kappa_j)A_j + \sum R_{jlqk}A_lA_qA_k^* + \sum_k Q''_{jk}|A_k|^2A_j \tag{1.66}$$

which has $q,l,j,k = 1,2,3$. Nonlinear coefficients Q''_{jk} again differ from Q_{jk} in which the appropriate terms have been removed. The sum in the nonlinear coefficients R is over all those cubic terms which do not already appear as Q terms.

It is noted that AEs do not depend on the details of the stellar structure under linear or nonlinear treatment. The general forms of nonradial AEs are indeed the same to the radial ones, only differing in the number of coupling coefficients (Buchler & Goupil 1984; Goupil & Buchler 1994). The coupling coefficients, on the other hand, depend on the star and on the type of considered modes. The number of couplings can be substantially reduced by angular momentum selection rules, particularly for the triplet $(1:1:1)$ resonance. The nonlinear coupling coefficients all are constructed on the basis of the building blocks of $\langle \mathbf{e}_q|\mathcal{N}_2(\mathbf{e}_j,\mathbf{e}_k)\rangle$ and $\langle \mathbf{e}_q|\mathcal{N}_3(\mathbf{e}_l,\mathbf{e}_j,\mathbf{e}_k)\rangle$ that represent the components of the spatial nonlinearities in the basis of eigenfunctions of the star. Nonzero quadratic coefficients should obey the angular selection rule that are simply $|\ell_k + \ell_k| \le \ell_q \le \ell_k + \ell_j$, $\ell_q + \ell_k + \ell_j$ even, and $m_q + m_k + m_j = 0$. For the cubic terms one has the constraints $m_q + m_l + m_k + m_j = 0$, $\ell_q + \ell_l + \ell_k + \ell_j$ even, and $max(|\ell_k - \ell_j|, |\ell_q - \ell + l|) \le min(\ell_q + \ell_l, \ell_k + \ell_j)$. The specific explorations of AEs for the above resonances will be discussed next.

1.4.3 Temporal amplitude behaviors of modes in an $\ell = 1$ triplet

To derive the AEs for three components in an $\ell = 1$ triplet, with amplitudes of A_-, A_0, A_+ and frequencies $\omega_-, \omega_0, \omega_+$, some basic assumptions should be made (Buchler et al. 1995) :

a) the linear growth rates κ_m of modes are much smaller than their frequencies ω_m, thus the amplitudes $A_m(t)$ vary slowly compared to the phase $\omega_m t$;

b) the nonlinear couplings are weak so that AEs can be truncated at the cubic terms ;

c) the triplet is considered as an isolated system so that the behaviors of the triplet modes are not affected by other modes outside the triplet in the star.

In general, the first two assumptions are fundamental to derive AEs and are satisfied for most nonradial pulsators. However, assumptions (c) is more difficult and needs observational testification. The amplitude equations for an $\ell = 1$ triplet are obtained as (equation 1.66 is the general form),

$$\frac{dA_-}{dt} = (\kappa_- + i\Delta\omega_-)A_- + \gamma_- A_+^* A_0^2 - \beta_{--}A_-|A_-|^2 - \beta_{-0}A_-|A_0|^2 - \beta_{-+}A_-|A_+|^2, \quad (1.67a)$$

$$\frac{dA_0}{dt} = \kappa_0 A_0 + \gamma_0 A_0^* A_+ A_- - \beta_{0-}A_0|A_-|^2 - \beta_{00}A_0|A_0|^2 - \beta_{0+}A_0|A_+|^2, \quad (1.67b)$$

$$\frac{dA_+}{dt} = (\kappa_+ + i\Delta\omega_+)A_+ + \gamma_+ A_-^* A_0^2 - \beta_{+-}A_+|A_-|^2 - \beta_{+0}A_+|A_0|^2 - \beta_{++}A_+|A_+|^2, \quad (1.67c)$$

where $\Delta\omega_\pm$ are the linear corrections induced by rotation (see equation 1.42), the nonlinear coefficients $\beta_{mm'}$ and γ_m can be seen in Buchler et al. (1995).

Slow stellar rotation does not affect the symmetrical spatial structure of the star, while, the linear eigenvalues and eigenvectors are affected slightly. Neglecting of all effects of rotation on the cubic couplings and assuming that the eigenvectors $\mathbf{e}_m$ are all same, the AEs for an $\ell = 1$ triplet modes simplify to, with the help of symmetry among the coefficients $\beta_{mm'}$,

$$\frac{dA_-}{dt} = (\kappa_- + i\Delta\omega_-)A_- + C_1 A_+^* A_0^2 - 2C_3 A_-|A_-|^2 - 2C_3 A_-|A_0|^2 - 4C_2 A_-|A_+|^2, \quad (1.68a)$$

$$\frac{dA_0}{dt} = \kappa_0 A_0 + 2C_1 A_0^* A_+ A_- - 2C_3 A_0|A_-|^2 - 3C_0 A_0|A_0|^2 - 2C_2 A_0|A_+|^2, \quad (1.68b)$$

$$\frac{dA_+}{dt} = (\kappa_+ + i\Delta\omega_+)A_+ + C_1 A_-^* A_0^2 - 4C_2 A_+|A_-|^2 - 2C_3 A_+|A_0|^2 - 2C_3 A_+|A_+|^2, \quad (1.68c)$$

where the full expressions of the nonlinear complex coupling coefficients C are discussed in Buchler et al. (1995). Before moving forward to searching the solutions to the above AEs (1.67) and (1.68), the notation E_m is introduced to represent the "kinetic energy" of mode m in the triplet, i.e.,

$$E_m = |A_m|^2, \text{ and } A_m(t) = |A_m|e^{i\phi_m}.$$

Here $|A_m|$ denotes the real amplitude and ϕ_m is the phase of the nonlinear effect on mode m.

The fixed-point solutions are the simplest solutions to the AEs (1.67) or (1.68). These solutions are characterized by constant amplitudes, and they can be single-mode, double-mode, or triple-mode. In the three-mode fixed solutions, the nonlinear mode couplings will cause the nonlinear phase-lock in which the amplitudes are constant and the frequencies are forced to be equally spaced that, linearly, may not be the case due to stellar rotation involving higher order terms ($\Delta\omega_- \neq \Delta\omega_+$, see Section 1.2). It is also noted from the nonlinear AEs explorations that the amplitude asymmetries in the triplet have an intrinsic nonlinear origin, contrary to geometric effects which can also produce amplitude asymmetries in split triplet but the side components maintain symmetry with respect to the central one (see, e.g., Pesnell 1985).

Mathematically, the first and simple case is the fixed-point single-mode solutions in an $\ell = 1$ triplet, i.e., e.g., $E_- \neq 0, E_+ = E_0 = 0$, although it will not be encountered in the context of observations. For the single-mode fixed-point solutions, e.g., $d|A_-|/dt = 0$, the AEs then reduce to

$$0 = (\kappa_- + i\Delta\omega_-)A_- - \beta_{--}A_-|A_-|^2, \tag{1.69}$$

which could be separated by real part and imaginary part. The integration of the latter one introduce the nonlinear frequency correction $\Delta\widetilde{\omega}_-$. The stability of the solution is explored and see details in Buchler et al. (1995).

Equations (1.67) or (1.68) suggests that a double-mode fixed-point with the case of either $E_- = 0$ or $E_+ = 0$ is not possible, and the only possible case that one has a double-mode fixed-point is with $E_0 = 0$. For this double-mode fixed-point such as of equation (1.68) one finds

$$E_- = \frac{2C_3^R\kappa_- - 4C_2^R\kappa_+}{-12C_0^RC_1^R}, \tag{1.70a}$$

$$E_+ = \frac{2C_3^R\kappa_+ - 4C_2^R\kappa_-}{-12C_0^RC_1^R}. \tag{1.70b}$$

The necessary stability conditions of the above solutions are

$$C_0^RC_1^R < 0 \text{ and } C_3^R > 0.$$

Futher conditions must be set here for stability with respect to a perturbation with the central mode (see Appendix B of Buchler et al. 1995).

Particular interest is paid on the three-mode fixed-point solutions in triplet resonance where only the phase combination $\Phi = \phi_+ + \phi_- - 2\phi_0$ appears in the AEs rather than the phases ϕ_m themselves. The three-mode fixed-point solutions are complicated to obtain and must be calculated numerically, except for some extremely simple cases. The numerical explorations of fixed-point solutions will be discussed next. However, it should be firstly noted that once the fixed-point solutions are obtained, the nonlinear effects will force the central component exactly at the half-way between the two side-components in the Fourier amplitude spectra, whether the triplet is linearly symmetric or not. In the case of triplet-mode fixed-points, the amplitudes are constant in time and one has $d\Phi/dt = 0$, therefore

$$\widetilde{\omega}_0 = (\widetilde{\omega}_- + \widetilde{\omega}_+)/2, \tag{1.71}$$

where $\widetilde{\omega}_m$ are the frequencies of mode m after nonlinear corrections.

The frequency-locked solutions can not only exist around the resonance center but also far from the resonance. We here first summarize the condition for frequency locking in real stars proposed by Buchler et al. (1997) : the locked frequencies eventually vanish as the rotation become fast. When the frequency locked regime occurs in the triplet in stars with slow rotation, the nonlinear effects are strong enough to force the triplet to be equally spaced, $\Delta\omega_- = \Delta\omega_+$, which is not a condition that happens in the linear context due to the high order rotation effects, $\delta\omega \propto \Omega^2/\omega_0$. With rapid enough rotation, the nonlinear frequency lock can be broken as the modes move far away from the resonance center. One first expects modulated amplitudes and frequencies and the amplitude modulations become shallower and negligible as modes move very far away from the resonance center. Finally, at extremely large Ω, one recovers the regime of nonresonant pulsations in which nonlinear frequencies from the nonresonant AEs differ from the linear predicted frequencies only in slight (fairly small) nonlinear corrections.

Quite generally, a resonant frequency locked solution can exist in the vicinity of the resonance center, as

$$|\delta\omega|/\omega \lesssim \mathcal{O}(\kappa/\omega). \tag{1.72}$$

This is a rough order-of-magnitude estimate with factors of ten possible on either side (Buchler et al. 1997). However, the real value of the solutions of AEs depends obviously on the numerical values of the linear and nonlinear coefficients. We note that equation (1.72) is also valid for the case that the frequency mismatch is caused by the magnetism (see equation (1.45)). The numerical explorations suggest that there are mainly three regimes when the considered modes move away from the resonance center, i.e., when $\delta\omega/\kappa$ increases : the frequency locked regime, the intermediate regime and the nonresonant one. The specific properties of these three distinct regimes will be given later.

In real stars, e.g., for δ Scuti stars, the rotational asymmetry splitting is in the range of $\delta\omega/\omega_0 \sim 10^{-3} - 10^{-2}$ and the linear growth rates for most of the observed unstable modes are $\kappa/\omega \sim 10^{-7} - 10^{-4}$, thus the range of $\delta\omega/\kappa$ is $10 - 10^5$ (Dziembowski 1993). On the aspect of white dwarf variables, they are slow rotators with $\delta\omega/\omega_0 \sim 10^{-8} - 10^{-6}$ and $\kappa/\omega \sim 10^{-10} - 10^{-5}$ (see, e.g., Dolez & Vauclair 1981). Therefore the range of $\delta\omega/\kappa$ is $10^{-3} - 10^4$. Take an order of magnitude, the condition of frequency lock is satisfied and it can occur for the unstable modes in stars with slow rotation. The frequency lock regime also may occur in several of the multiplets because the condition of the frequency lock depends on the linear growth rates of the modes which may differ from mode to mode. These order of magnitude indicates that the frequency lock is more likely to occur in white dwarfs, and possibly in slow δ Scuti stars, although the linear growth rates of pulsation modes remain very uncertain in pulsating stars.

Theoretical extent of frequency locking in the case of 2 :1 resonance

Now we turn to the discussion on the theoretical explorations of what will happen to the frequency lock solutions of AEs when the resonant modes move away from the resonance center, i.e., technically, in terms of numerical calculation. We first introduce the numerical explorations on the two modes resonance 2 : 1 which shows similar results to the triplet resonance but in a easier way to explore (Buchler et al. 1997). All the nonlinear coefficients are set artificially and not aim at to compare with their real values for a specific star. For convenience, the time in AEs are rescaled by setting one of the unknown linear growth rates to be one, e.g., $\kappa_1 = 1$, which does not impact the generality of the numerical results (e.g., Buchler et al. 1997).

The appropriate AEs for the case of 2 : 1 resonance can be expressed as,

$$\frac{dA_1}{dt} = \kappa_1 A_1 - \tilde{q}_{11}^R A_1^3 - \tilde{q}_{12}^R A_1 A_2^2 + R_1 A_1 A_2 \sqrt{1 - S_1^2}, \tag{1.73a}$$

$$\frac{dA_2}{dt} = \kappa_2 A_2 - \tilde{q}_{12}^R A_2 A_1^2 - \tilde{q}_{22}^R A_2^3 + R_2 A_1^2 \sqrt{1 - S_2^2}, \tag{1.73b}$$

$$\frac{d\Phi}{dt} = \delta\omega - (\tilde{q}_{12}^I A_1^2 - \tilde{q}_{22}^I A_2^2) + 2(\tilde{q}_{11}^I A_1^2 + \tilde{q}_{12}^I A_2^2) + R_2 S_2 \frac{A_1^2}{A_2} - 2R_1 S_1 A_1. \tag{1.73c}$$

where $S_1 = \sin(\Phi - \delta_1)$ and $S_2 = \sin(\Phi + \delta_2)$, respectively, the superscripts R and I denote the real and imaginary parts, respectively, $\Phi = \phi_2 - 2\phi_1$, and where $r_k = R_k e^{i\delta_k}$, $k = 1, 2$.

The resonant AEs (1.73) cannot be analytically solved and the result of the numerical explorations by Buchler et al. (1997) are given here. The parameters e.g., coupling coefficients, whose values are set artificially and can be seen in Section 3.1 of Buchler et al. (1997). They found that the stable fixed-point solutions exist only in the range of $|\delta\omega| < \delta\omega_{bif} \approx 18.24$. In the domain $12.64 < \delta\omega < 18.24$, four fixed-solutions could be found but three of them are unstable. The numerical integration of the differential AEs leads to an oscillatory solutions in the domain $\delta\omega > 18.24$ where no stable fixed-point exist any more.

Figure 1.2 shows the amplitude modulations of oscillation modes for several values of $\delta\omega$. As the frequency mismatch $\delta\omega$ increasing, the amplitude modulations firstly become sinusoidal and then the amplitude modulations become evanescent. The amplitude modulations on the

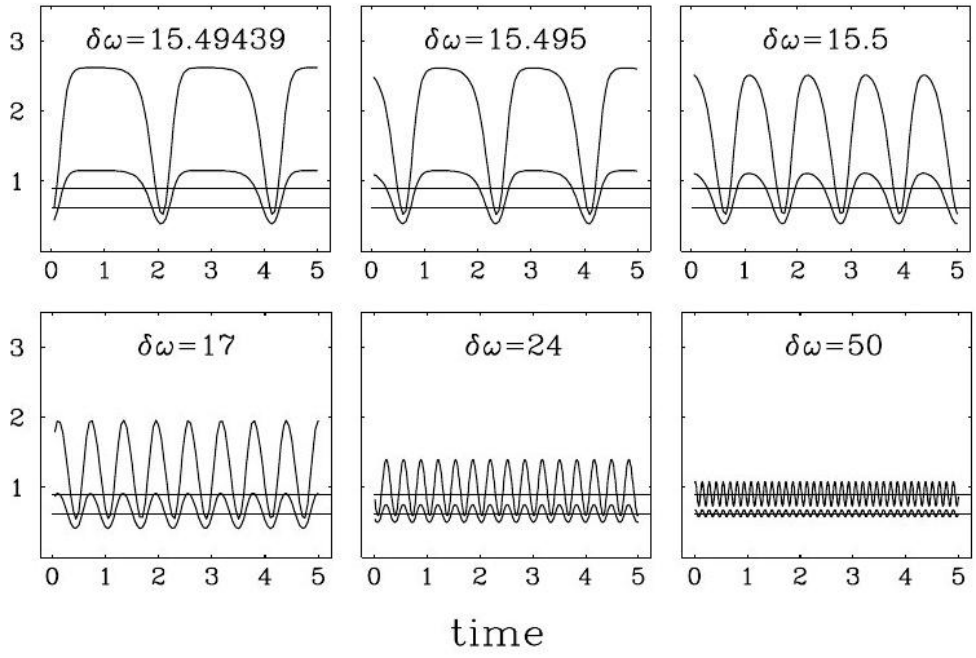

FIGURE 1.2 – The result of numerical explorations on the 2 : 1 resonance from Buchler et al. (1997). Amplitude modulations are as a function of the related to the frequency mismatch $\delta\omega$ and the growth rate of κ_1. The large and small amplitudes denotes mode 1 and 2, respectively. Time is in unit of $1/\delta\omega$. The two horizontal lines denote the amplitude of mode 1 and 2 of one fixed-point solution.

$\delta\omega \sim 15.5$ domain becomes very large and with a modulating time scale around $1/\delta\omega$. It is noted that the oscillatory solution coexists with the stable fixed-point solutions in the region $15.495 \lesssim \delta\omega \lesssim 18.24$ which indicates that in a real star the resonant modes could have modulating amplitudes and stable frequencies.

The extent of frequency locking for 1 :1 :1 resonance

For an $\ell = 1$ triplet, the nonlinear complex AEs (e.g., equation 1.68) of the three modes are rewritten as an equivalent lower set,

$$\frac{dA_-}{dt} = \kappa_- A_- + R_- A_0^2 A_+ \cos(\Phi - \delta_-) - A_-(q_{11}A_-^2 + q_{12}A_0^2 + q_{13}A_+^2), \quad (1.74a)$$

$$\frac{dA_0}{dt} = \kappa_0 A_0 + R_0 A_0 A_+ A_- \cos(\Phi + \delta_0) - A_0(q_{21}A_-^2 + q_{22}A_0^2 + q_{23}A_+^2), \quad (1.74b)$$

$$\frac{dA_+}{dt} = \kappa_+ A_+ + R_+ A_0^2 A_- \cos(\Phi - \delta_+) - A_+(q_{31}A_-^2 + q_{32}A_0^2 + q_{33}A_+^2), \quad (1.74c)$$

$$\frac{d\Phi}{dt} = \delta\omega - 2R_0 A_- A_+ \sin(\Phi + \delta_0) + A_0(R_- \frac{A_+}{A_-}\sin(\Phi - \delta_-) + R_+ \frac{A_-}{A_+}\sin(\Phi - \delta_+)), \quad (1.74d)$$

where $\Phi = \phi_+ + \phi_- - 2\phi_0$.

Examples of numerical searching for fixed-point solutions for the case of triplet 1 : 1 : 1 resonance can be found in Buchler et al. (1997) where their results are very similar to the 2 : 1 resonance. In the resonance center, the resonant AEs have three-mode fixed-points, i.e.,

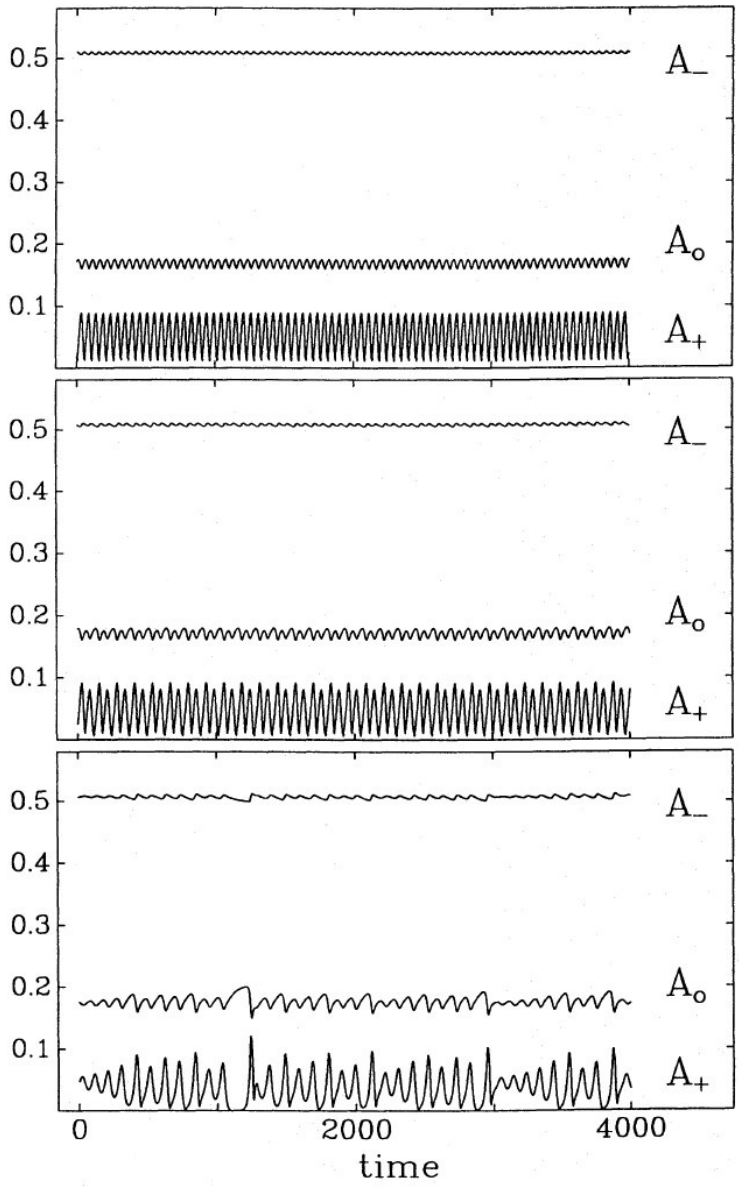

FIGURE 1.3 – Examples of different types of behaviors of amplitude modulations of resonant modes in Buchler et al. (1995). *Top panel* : periodic modulations ; *Middle panel* : 2-periodic modulations ; *Bottom panel* : chaotic cycles. Time is in unit of $\kappa_0 t$.

frequency lock. The amplitude modulations occurs at first with large excursions that later scale as $1/\delta\omega$ and the timescale of the modulating periods is also about $1/\delta\omega$. There also exists a narrow transitory regime, as the above $2:1$ resonance showing, in which the frequency locked and the amplitude modulated solutions can coexist.

The fixed-point frequency lock is the easiest solutions to obtain for the nonlinear resonance AEs, while, the particular interesting nonlinear phenomenon on observations of real stars must be paid on the temporal modulations of amplitude of the resonant modes, which gives a different prediction to the linear stellar pulsation theory. We thus introduce the example of numerical explorations of this intermediate regime of nonlinear resonant mode couplings, i.e., modulating amplitudes of oscillation modes, in which the modulations can be periodic (limit cycles),

irregular, or even chaotic, that depends mainly on the coupling coefficients.

Figure 1.3 shows the typical examples of time-dependent solutions of nonlinear resonant AEs in Buchler et al. (1995), i.e., periodic, double-periodic, and chaotic modulations. The timescale of the amplitude modulations is governed by the linear growth rates of the resonant modes, or specifically, central mode in the triplet, κ_0, assuming that the slow stellar rotation cause the growth rates of side components differ not too much from that of the central one (Carroll & Hansen 1982). For the modulations in white dwarf stars, one expects that the modulating timescale is ranging from weeks, months, even years, considering by the order of magnitude of linear growth rates (Dolez & Vauclair 1981). The different characters of amplitude modulations are sensitive to the parameters one chooses in searching for numerical solutions. For the above examples as shown in Fig. 1.3, the parameters can be found in Section 4.2 of Buchler et al. (1995). It is note that the frequencies should also have modulating behaviors in the intermediate regime where amplitude have periodic or irregular modulations since the phase equation, e.g., equation (1.74d), depends on the amplitudes. Therefore the frequencies must be corrected all the time by the nonlinear coupling effects from the temporal amplitudes.

In conclusion of the above numerical explorations of the frequency lock solutions, one can distinguish roughly three nonlinear regimes of amplitude and frequency modulations when one moves away from the resonance center (Buchler et al. 1995, 1997; Goupil et al. 1998) :

R1) the first regime is the nonlinear frequency lock. It often happens near the resonance center ($\delta\omega = 0$) where a stable fixed-point solution can be found, i.e., frequency lock. Therefore the nonlinear couplings between the involved modes force the frequencies of the modes to be well equally spaced, i.e., the central component is at the exactly half way of the two side components, whether they are linearly symmetric ($2\omega_0 = \omega_- + \omega_+$, very slow rotation, with $\delta\omega \approx 0$) or not ($2\omega_0 \sim \omega_- + \omega_+$). In this regime, the amplitudes are all constant since the nonlinear effects are strong enough to lock them. Even if the involved modes are constant in amplitude and frequency, they somewhat differ from the linear predictions, due to effects of nonlinear corrections.

R2) the second one is the intermediate regime. The fixed-point solutions eventually becomes unstable or disappear as the modes move away from the resonance center, or in an order of magnitude way, $\delta\omega/\kappa$ increases. In this second regime, one find an oscillatory nature of the numerical solutions, and giving rise to amplitude and frequency modulations of the resonant modes. These modulations could be periodic, multi-periodic, irregular, or even chaotic, which depends on the chosen parameters of the star. If the parameters (linear and nonlinear coefficients) were found to be for the periodic amplitude modulations, the period of the modulations is about the inverse of the linear frequency mismatch $1/\delta\omega$, which also has a link with several times of the inverse of the linear growth rate $1/\kappa$. These amplitude and frequency modulations cause the peaks in Fourier amplitude spectra to form a more complex structure or closed side-lobes around the main peaks due to the modulations.

R3) the nonresonant one is the third regime. Once the modes in the resonance move far away from the resonance center, the nonlinear coupling effects are very slight and the nonlinear correction on frequencies are very small. Therefore the modes recover steady pulsations and their nonresonant values are very closed to the linear ones.

In addition to the above three main regimes, there exists a narrow transitory regime which is between the first frequency lock and the intermediate regimes. In that regime, the frequency locked and oscillatory solutions coexists, arising stable frequencies and modulating amplitudes in the observed resonant modes.

Although the nonlinear effects are very slight on the stellar pulsations, there are still some observational hints that are possible connections to the nonlinear predictions of AEs. Those observational results will be introduced in next chapter. In the next section, we will focus on another nonlinear treatment within the formalism of AEs, i.e., the adiabatic approximation of resonant mode coupling of the type $\omega_1 \approx \omega_2 + \omega_3$ or $2\omega_3$.

1.4.4 Nonlinear resonant mode coupling in the adiabatic approximation

In this section, the nonlinear adiabatic treatment on the resonant mode couplings within the amplitude equations formalism is introduced, which was first investigated by Dziembowski (1982). With the ignorance of nonadiabatic effects during the stellar oscillations, the nonlinear equation for adiabatic pulsations is written in the form of

$$\frac{\partial^2 \mathbf{v}}{\partial t^2} + \mathscr{L}\mathbf{v} + \mathscr{N}\mathbf{v} = \mathbf{0}, \tag{1.75}$$

where the linear operator of adiabatic oscillations $\mathscr{L}$ and the nonlinear operator $\mathscr{N}$ are provided in Appendix A.2.

In the case of the three modes in the resonance condition $\omega_1 \approx \omega_2 + \omega_3$, the final formal solution of equation (1.75) can be obtained with amplitude equation forms as,

$$\frac{dA_1}{dt} = \kappa_1 A_1 + \frac{iq}{\omega_1 I_1} A_2 A_3 e^{-i\delta\omega t}, \tag{1.76a}$$

$$\frac{dA_2}{dt} = \kappa_2 A_2 + \frac{iq}{\omega_2 I_2} A_1 A_3^* e^{-i\delta\omega t}, \tag{1.76b}$$

$$\frac{dA_3}{dt} = \kappa_2 A_3 + \frac{iq}{\omega_3 I_3} A_1 A_2^* e^{-i\delta\omega t}. \tag{1.76c}$$

where the frequency mismatch is $\delta\omega = \omega_1 - \omega_2 - \omega_3$, term I_j are the mode inertia, the nonlinear coupling coefficient q is very complicated and will be not given here (see, e.g., Dziembowski 1982, for its full expression). The derivation of the above AEs is also based on the same assumption to the nonadiabatic AEs (Section 1.4.3). For the two-mode resonance $\omega_1 \approx 2\omega_2$, equation (1.76) will reduce to a set of two amplitude equations (Dziembowski 1982).

The three modes in the resonance condition $\omega_1 \approx \omega_2 + \omega_3$ could involve two types of resonance, the parametric resonance and the direct resonance. Parametric instability involves an overstable parent mode that grows with the growth rate $\kappa_1 > 0$ and two daughter modes that linearly damped with $\kappa_{2,3} < 0$. While the direct resonance involves two unstable parent modes with lower frequencies, with $\kappa_{2,3} > 0$, and the linearly damped daughter mode, with $\kappa_1 < 0$.

To investigate behaviors of the resonant modes, equation (1.76) must be solved in various initial conditions. Again, the same as the triplet resonance (Section 1.4.3), equilibrium solutions are the easiest solutions to obtain for both the parametric and direct resonances. Then the equilibrium solutions of AEs (1.76) could be easily obtained with $dA_j/dt = 0$, and the solutions are given by

$$|A_1|^2 = \frac{I_2 I_3 \omega_2 \omega_3}{q^2} \kappa_2 \kappa_3 \Big[1 + \Big(\frac{\delta\omega}{\kappa_1 + \kappa_2 + \kappa_3}\Big)^2\Big], \tag{1.77a}$$

$$|A_2|^2 = -\frac{I_1 I_3 \omega_1 \omega_3}{q^2} \kappa_1 \kappa_3 \Big[1 + \Big(\frac{\delta\omega}{\kappa_1 + \kappa_2 + \kappa_3}\Big)^2\Big], \tag{1.77b}$$

$$|A_3|^2 = -\frac{I_1 I_2 \omega_1 \omega_2}{q^2} \kappa_1 \kappa_2 \Big[1 + \Big(\frac{\delta\omega}{\kappa_1 + \kappa_2 + \kappa_3}\Big)^2\Big], \tag{1.77c}$$

and with

$$\cot(\varphi_1 - \varphi_2 - \varphi_3 + \delta\omega t) = \frac{\delta\omega}{\kappa_1 + \kappa_2 + \kappa_3}, \tag{1.78}$$

where the complex amplitude A_j may be written as the form of $A_j = |A_j|e^{i\varphi_j}$.

We now turn to analyze the stability of equilibrium solutions in the case of three modes couplings. The coefficients of the linear perturbations around the equilibrium solutions (see, e.g., Dziembowski 1982, for details) are,

$$a_1 = -2\overline{\kappa}, \quad a_2 = \overline{\kappa}^2[1 + (\delta\omega/\overline{\kappa})^2] - 4(\delta\omega/\overline{\kappa})^2(\kappa_1\kappa_2 + \kappa_2\kappa_3 + \kappa_3\kappa_1),$$

$$a_3 = 4\prod_j \kappa_j[1 + 3(\delta\omega/\overline{\kappa})^2], \qquad a_4 = -4[1 + (\delta\omega/\overline{\kappa})^2]\overline{\kappa}\prod_j \kappa_j,$$

where $\overline{\kappa} = \sum_j \kappa_j$. The Routh-Hurwitz stability criteria are used for the case, which are given by

$$W_1 \equiv a_1 > 0, \qquad W_2 \equiv a_1 a_2 - a_3 > 0,$$

$$W_3 \equiv a_3 W_2 - a_1^2 a_4 > 0, \quad W_4 \equiv a_4 W_3 > 0.$$

From the above criteria, one would see that at least one of the first three conditions must be less than zero in the case of direct resonance since the growth rate $\kappa_1 < 0$. In the case of parametric instability, the second and fourth criteria are redundant and follow from the remaining ones. Therefore it is easy to find that the three-mode equilibrium is always unstable in the direct resonance. While in the case of parametric resonance it is stable if the modes satisfy the condition,

$$\mathscr{D} > 0, \tag{1.79}$$

where the expression of $\mathscr{D}$ that involves the frequency mismatch and the linear growth (damping) rates of the mode can be found in Appendix A.4. The conditions imposed by the stability are not difficult to meet in stellar pulsations where the damping rates of higher order modes are much larger than the growth rate of the linearly unstable modes. In the next section we would introduce the modulating behaviors of the resonant modes in some certain conditions, i.e., limit cycles in parametric resonance.

1.4.5 Temporal amplitude behaviors induced by the adiabatic AEs

This section is dedicated to the amplitude modulations of parametric resonance modes, which was investigated by Moskalik (1985), Wu & Goldreich (2001) and Pnigouras & Kokkotas (2015). The three coupling modes would lead periodic modulations under certain conditions which are related to the linear growth (damping) rates κ_j and the frequency mismatch $\delta\omega$. Note that when $\kappa_2 = \kappa_3$ the three mode resonance would reduce to a simpler case, i.e., $\omega_1 \approx 2\omega_2$. Provided $\kappa_1 \ll -(\kappa_2 + \kappa_3)/2$, the equilibrium state would be a stable system with $\delta\omega > -(\kappa_2 + \kappa_3)/2$, otherwise unstable (refer to the criteria of equation 1.79).

Figure 1.4 shows examples of two different characters of mode behaviors in the parametric resonance, stable amplitude and limit cycles (Wu & Goldreich 2001). The stable one is with the parameters of $\delta\omega = 2 \times 10^{-5}$ s^{-1}, $\kappa_1 = 10^{-7}$ s^{-1} and $\kappa_2 = \kappa_3 = 10^{-6}$ s^{-1}. While the parameters for the case of limit cycle modulations are $\delta\omega = \times 10^{-6}$ s^{-1}, $\kappa_1 = 10^{-7}$ s^{-1} and $\kappa_2 = \kappa_3 = 10^{-5}$ s^{-1}. In the case of limit cycles, the amplitude of the parent mode firstly grows on timescale κ_1^{-1}, after it reaches the maximum the amplitude drops rapidly on timescale $\kappa_{2,3}^{-1}$. The daughter mode whose amplitudes stay far below the equilibrium ones for most of the cycle but the amplitudes grows to comparable to the amplitude of the parent mode for a short interval κ_1^{-1} since the amplitude of the parent mode drops very rapidly after it reaches the maximum value. During this brief interval, the accumulated energy by parent mode is transferred to and

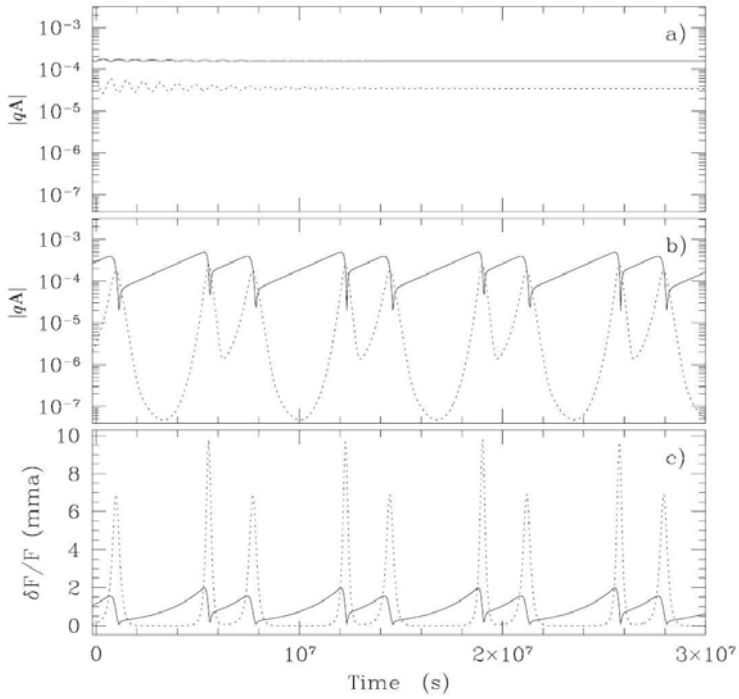

FIGURE 1.4 – Examples of different types of behaviors of amplitude modulations of parametric resonance in Wu & Goldreich (2001). *Top panel* : steady state ; *Middle panel* : periodic modulations ; *Bottom panel* : flux variations associated with the case of periodic modulations. The solid lines denote the parent growing mode and the dashed lines denote the damping daughter modes, assuming two identical daughter modes.

dissipated by the daughter modes. Therefore the equilibrium state defines the amplitude of the parent mode.

The interval of the increasing and decreasing amplitude of the parent mode depends obviously on the linear growth and damping rates of the involved modes, as shown in Fig. 1.4. The shapes of amplitude modulations of these involved modes also depend on the quantity, the value of the frequency mismatch $\delta\omega$. Given certain linear growth and damping rates that leads to the unstable equilibrium state, the larger value of $\delta\omega$ is, the shallower the amplitude modulations appear (Moskalik 1985). As the amplitude of the involved mode modulating, the nonlinear phases φ_j should also be affected by the nonlinear interactions between modes, thus the frequencies ω_j of the involved should have the nonlinear corrections, as

$$\widetilde{\omega}_j = \omega_j + \frac{d\varphi_j}{dt}. \tag{1.80}$$

Note that the variations of frequencies are in a more complicated ways, and in some extreme conditions, the corresponding variations of the periods can be in the order of 10^{-2} ss^{-1} for ZZ Ceti stars and 10^{-3} ss^{-1} for the δ Scuti stars (Moskalik 1985). Of course, there will be some closed side-frequencies around the main peaks in the Fourier amplitude spectra due to the amplitude and frequency modulations of the involved modes, which is very similar to the triplet resonant modes discussed in Section 1.4.3.

To conclude Section 1.4, we introduce the nonlinear perturbations of the stellar oscillation theory which can only be investigated by the amplitude equation formalism. In this formalism

the amplitudes and frequencies of the oscillation modes may not be in a stable state any more. Although in certain conditions the oscillation modes are stable, the nonlinear corrections on frequencies should be taken into consideration. If the periodic amplitude modulations of the resonant modes were found as predicted by the nonlinear AE formalism, this would be an very important test of the nonlinear resonant mode coupling theory. It is interesting that the observational periodic amplitude and frequency modulations may give the first determination of the linear growth rates of the nonlinear interacting modes, as the predictions of the timescale of these modulations have very closed relationship with the growth rates. This would lead new diagnostic tools of the stellar interior.

The nonlinear AEs can only be solved numerically as a result of the complex nonlinear equations. Only nonlinear coefficients of Cepheids are currently obtained. Nonlinear coefficients of other types of pulsating stars may be extracted from the observed mode modulations. The observed (amplitude) modulations from ground indeed suggest that the modulated timescale is much longer than that of the periods of pulsations, as well as do the results in this thesis

1.5 Conclusion

In this Chapter, we first introduced the linear perturbation theory of stellar oscillations for the nonrotating, non-magnetic stars with which one would obtain the eigenvalues of the oscillation modes with the boundary conditions for both the adiabatic and nonadiabatic cases. However, stellar rotation and magnetism lift the degeneracy modes to multiplets of $2\ell + 1$ and $\ell + 1$ components with respect to azimuthal number m, respectively. These multiplets should be equally spaced in frequency by the effect of the first order of stellar rotation. However, these equidistant multiplets may be distorted by the higher order effects of rotation or by stellar magnetism. The presence of a richness of frequencies from observations suggests that some observed frequencies may not be eigenfrequencies because we are limited to observe the low-degree ($\ell = 1, 2$) modes from ground due to the geometric cancellation effect. Two formalisms that involves nonlinearities of linear eigenmodes may explain some observed frequencies that are exact sums or differences of other frequencies, the variations of the depth of convection zone and the variations of the temperature at stellar surface.

A particular attention has been paid on the nonlinear perturbation theory of stellar oscillations in which the amplitude and frequency of the oscillation mode may have temporal behavior. The mode behaviors depend on the condition of resonance, and also depend on the nonlinear coefficients of the interacting modes.

In the next chapter, we recall the background around the specific types of stars on which this thesis will focus, white dwarf and hot B subdwarf stars. These stars are well studied by asteroseismology based on the current linear oscillation theory. Some hints linked to nonlinear AEs predictions in these two types of pulsating stars will also be described, which are all observed from ground-based telescope networks. If these nonlinear phenomena of mode behaviors were confirmed, that will pose new questions of the measurement of frequency changing of stellar oscillations which may relate to stellar evolutionary effects.

Chapter 2

Pulsating evolved compact stars and Asteroseismology

Stellar pulsations are found through the entire H-R diagram, as shown in Figure 2.1 (a detailed description of all kinds of pulsating stars can be found in Chapter 2 of Aerts et al. 2010). The stellar oscillation theory can well predict the behavior of a star when it pulsates, swelling and contracting, heating and cooling. The driving mechanisms for a star to pulsate are mainly of three different types : the κ-mechanism, stochastic driving, and the ϵ-mechanism. The κ-mechanism is connected with the opacity of the gas inside the star and works for most of pulsating stars seen in Figure 2.1. Most pulsations driven by the κ-mechanism are associated with hydrogen and helium, e.g., in RR Lyrae stars, δ Scuti stars. Some are associated with the ionization of Fe-group element, e.g., β Cephei stars, hot B subdwarf stars (see details later). The stochastic driving is the mechanism that operates in the Sun and solar-like stars, as well as in pulsating red giant stars, in which the heat-engine mechanism is not sufficient to drive the oscillations. The ϵ-mechanism is the third identified mechanism that may drive pulsations in some evolved massive stars.

Well below the main sequence are the evolved compact pulsating stars, regrouping pulsating the white dwarf and hot subdwarf stars. The pulsating white dwarf stars have been one of the earliest studied variables among all types of pulsating stars. Pulsating hot B subdwarf (hereafter sdB) stars have also been well investigated using the technique of asteroseismology although they were discovered more recently than white dwarf pulsators in general (Kilkenny et al. 1997). Both white dwarf and sdB stars are compact stars, i.e., with surface gravity larger than $10^5\,\mathrm{cm\,s^{-2}}$. Figure 2.2 shows a portion of the surface gravity–effective temperature plane where the compact pulsators are found. There are nine different classes of compact pulsators, six of those belong to pulsating white dwarf stars and the remaining three are hot subdwarf stars. Those compact pulsators are formed through four typically evolutionary tracks followed by four distinct post-phase stars, with masses from $0.200\,M_\odot$ to $0.593\,M_\odot$ and with rich or deficient hydrogen. One group of pulsating hot subdwarf stars, the hot O subdwarfs (sdO), are very rare (Woudt et al. 2006; Randall et al. 2011). Additionally, no pulsating sdO star was found from *Kepler* photometry. Therefore we will not give further details about this family of pulsators. The neutron stars, that cannot be observed by spectroscopy or photometry, are not concerned in this thesis although they are very compact stars (Aerts et al. 2010). We will focus on the different types of pulsating white dwarf stars, as well as sdB variables, in this thesis, as a consequence of those pulsators benefit a lot from the long and continuous *Kepler* observations.

The detailed structure of this chapter is as follows : the detailed description of pulsating white dwarf stars will be given in Section 2.1, followed by an introduction of the asteroseismology progress in the pulsating sdB stars in Section 2.2. Progresses in compact pulsators from

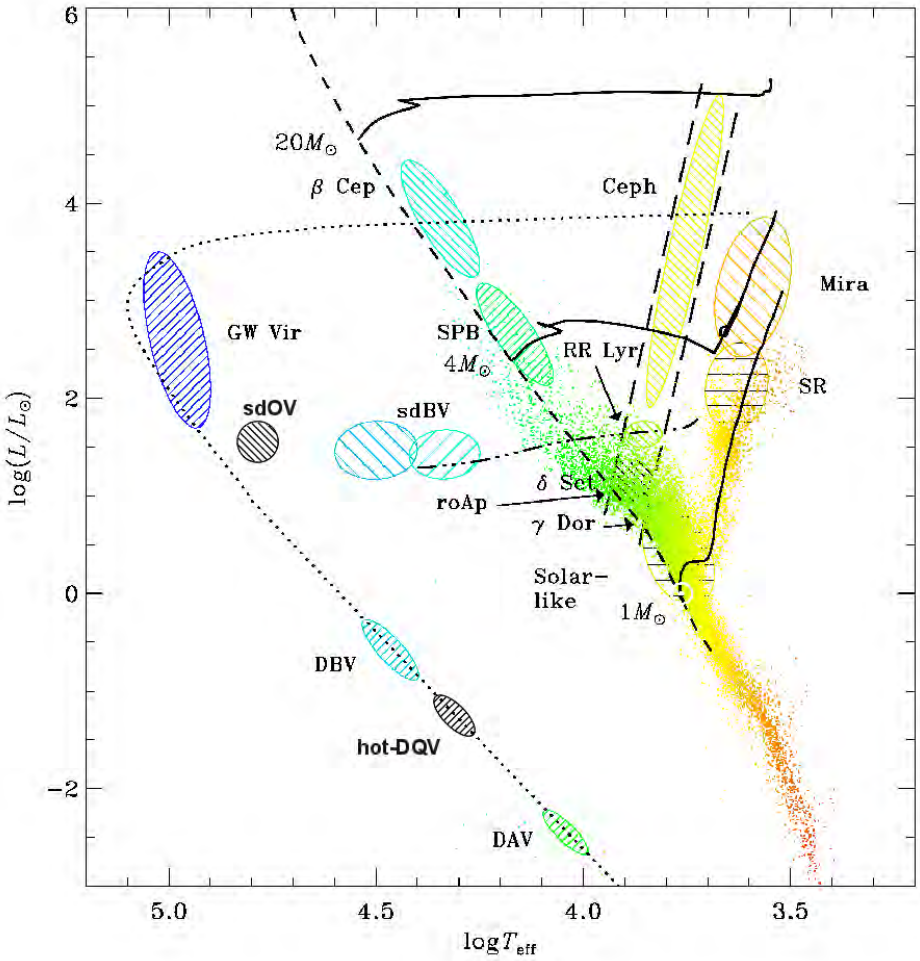

FIGURE 2.1 – A pulsation H–R diagram for pulsating stars for which the technique of asteroseismology could be applied. Each type of pulsators is labeled by its official IAU name in the diagram. Three typically evolutionary tracks from zero-age main-sequence stars are plotted with different masses, $1\,M_\odot$, $4\,M_\odot$ and $20\,M_\odot$, represented by the three solid curves. The dotted curve infers the cooling track of pulsating white dwarf stars, the dashed curve the zero-age main-sequence, and the two parallel dashed lines the classical instability strip.

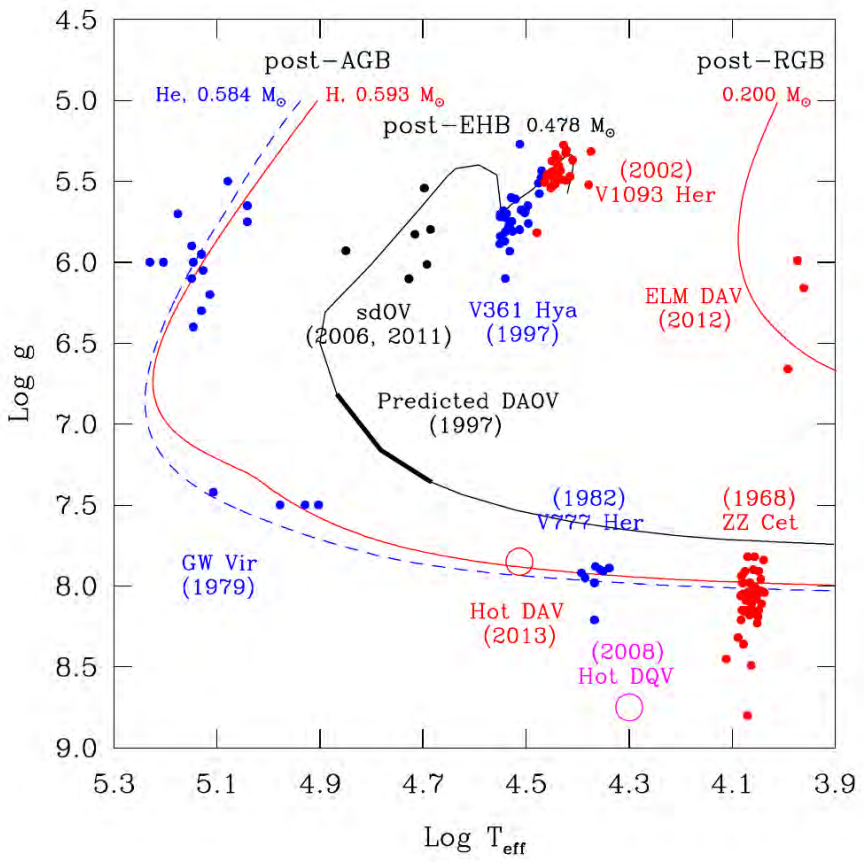

FIGURE 2.2 – The compact pulsators in the $\log g - \log T_{\rm eff}$ diagram. Both the official name and the discovery year of each families of the compact pulsators are indicated. Four typically evolutionary tracks are plotted that show (1) the cooling track of a H-atmosphere white dwarf (red solid curve at the left side) followed by a $0.593\,M_{\odot}$ post-AGB, H-rich star, (2) the track followed by a $0.584\,M_{\odot}$ post AGB, H-deficient star, which becomes a He-atmosphere white dwarf star (dashed blue curve), (3) the cooling track of a low-mass H-atmosphere white dwarf (black curve) followed by a $0.478\,M_{\odot}$ post-EHB star, and (4) the path followed by a $0.200\,M_{\odot}$ post-RGB star, which forms the extreme low-mass white dwarf star (red solid curve at the right side).

space photometry will be discussed in Section 2.3, including some observational results of mode behavior showing amplitude and frequency variations which are connected with the nonlinear stellar pulsation theory (see Chapter 1). Finally, a brief conclusion of Chapter 2 will be given in Section 2.4.

2.1 Pulsating white dwarf stars

White dwarf stars can provide a wide range of extreme conditions to test elementary physics, which are far beyond the capability of the best terrestrial laboratory, such as extreme high temperature and pressure. They are the end fates of stellar evolution for 98% of the stars in our Galaxy and can be chronometers for measuring the age of the various stellar populations (Fontaine et al. 2001). They are also the progenitors of type Ia supernovae which are the evidence

for an accelerating universe. Asteroseismology can provide accurate masses and luminosities for white dwarf pulsators, which could give a better understanding on stellar evolution. For a detailed description of the pulsating white dwarf stars and precise asteroseismology of such pulsators, see the reviews of Fontaine & Brassard (2008) and Winget & Kepler (2008).

The story of pulsating white dwarf asteroseismology really begins with the discovery of low-amplitude variations of luminosity in the DA white dwarf star HL Tau 76 (Landolt 1968). Up till now there are at least six sub-types of pulsating white dwarf stars, see their cooling tracks and the distributions on the H-R diagram in Figure 2.1 and on the surface gravity–effective temperature diagram of Figure 2.2. They are mainly in three major families : DOV, DBV and DAV white dwarf stars, as the effective temperature descends. The other three families are new comers into this field recently, discovered with the names of hot DQV, ELM and hot DAV stars. These new coming pulsating white dwarf stars are rather rare in general and they will be regarded as a whole in our consideration. In the following section we will discuss the details of those different types of white dwarf families.

We mention there is a theoretical prediction oscillations driven in low-mass DAO white dwarfs by Charpinet et al. (1997b), see the heavy part of the black cooling tracks in Figure 2.2, although variable DAOVs have yet to be found. We also mention that the acoustic p-mode oscillations had been predicted for quite a long time and Vauclair (1971) gave the first theoretical studies of white dwarf stars and show that some of the acoustic modes should be excited on a timescale of several seconds and the amplitude is very small, typically less than one percent magnitude. Therefore the acoustic oscillations are very difficult to observe and we must use very fast photometric device to detect them. Currently, the p-mode pulsation has still not been found yet even through there are some attempts (e.g., Silvotti et al. 2011).

2.1.1 Classification of white dwarf pulsators

All white dwarf (hereafter WD) pulsators are found to pulsate in nonradial g-modes and typically with multiperiodic pulsations on timescale of several minutes. Figure 2.3 shows representative light curves of four distinct WD families, one each for each class of pulsator. White dwarf pulsators are intrinsically faint objects and photon starvation should be an inescapable observational constraint in this field. The brightest known pulsating WD star is the ZZ Ceti star G226–29 with a magnitude in V band of 12.24, which is one of the lowest amplitude variables in the whole group of pulsating stars. We will discuss these WD pulsators separately, almost along the line with the time of the discovery year of the first pulsator in each family.

The **DAV** (or **ZZ Ceti**) is the first class of WD pulsators to be observed, with hydrogen atmosphere, in a very narrow instability strip in the lower right corner of the H-R diagram (see Figure 2.2). The first DAV pulsator is HL Tau 76 (mentioned above ; Landolt 1968), soon afterward, followed by that oscillations in G44-32 and R 548 were found by Lasker & Hesser (1969, 1971). We note that ZZ Ceti is the variable name of Ross 548 and the DA pulsator class was not named after the prototype HL Tau 76. AT present there are around 200 DAV stars, which constitutes $\sim 80\%$ of all WD pulsators. The pulsations detected in DAV stars correspond to low- to mid-order, low-degree g-modes. Dolez & Vauclair (1981) first found that nonradial g-mode pulsations in DAV models are driven by the κ-mechanism in the helium partial ionization zone, indicated by observations for some ZZ Ceti stars in different Stromgren colors (McGraw 1979). The exact mode excitation is sometimes referred to as convective driving, a mechanism proposed by Brickhill (1991), while the culprit is the recombination of hydrogen in the envelope as a cooling DAV star enters and then transits across a narrow strip (Fontaine et al. 2014).

The **DBV** (or **V 777 Her**) stars is the closely related family to the DAV stars, but with He-atmosphere and higher effective temperature located at $T_{\rm eff} \simeq 29\,000$ K to $22\,000$ K. The DB stars are the cooling descendants of 20% post-asymptotic giant branch (AGB) stars which

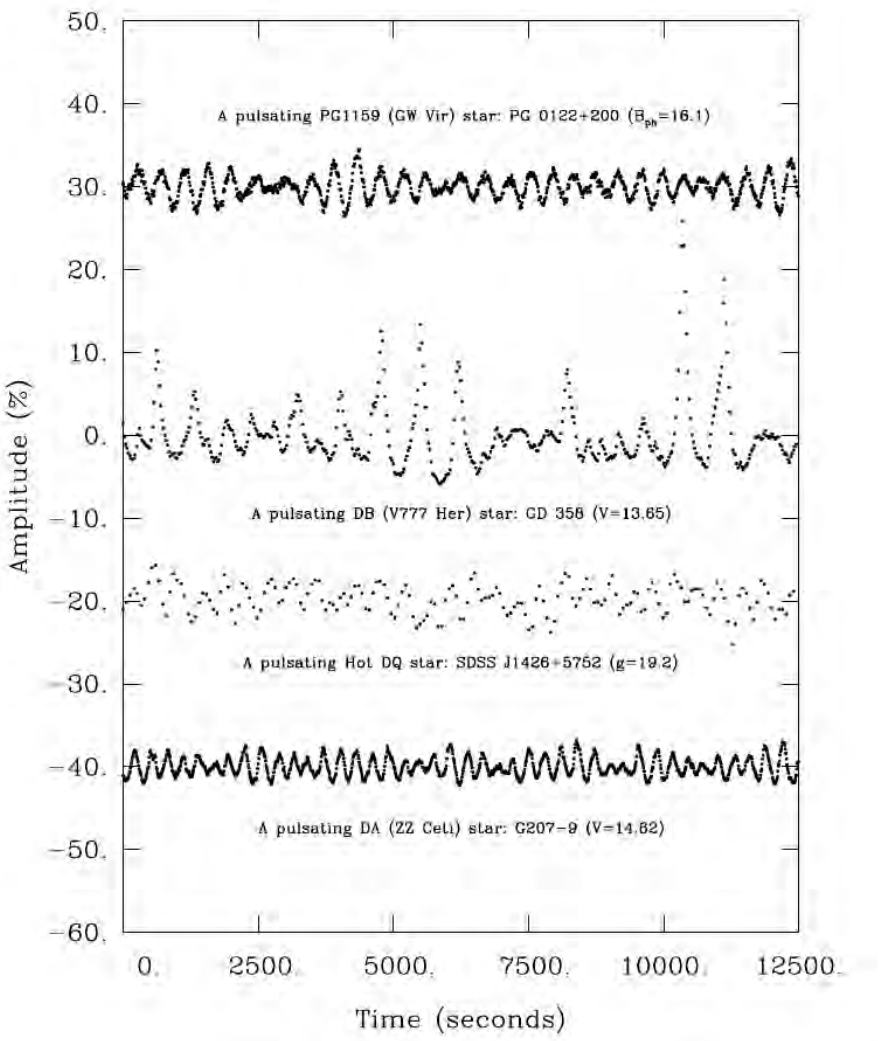

FIGURE 2.3 – Optical light curves for four representative families of pulsating white dwarf stars. Those light light curves were obtained from the 3.6-m CFHT telescope (see details in Fontaine & Brassard 2008).

had experienced a very late He flash in the stellar evolution. The pulsations in DBV stars was first investigated theoretically by Winget et al. (1982b) who found that He-driving could contribute the excitation of nonradial g-mode pulsations in the narrow instability strip at effective temperature around 19 000 K corresponding to the DB white dwarf stars. The soon survey of DB white dwarfs showed that the brightest DB star with the broadest He-I lines, GD 358 = V 777 Her (the prototype of the DBV star), did indeed pulsate in nonradial g-modes, similar to the large-amplitude DAV stars (Winget et al. 1982a, and see a part of light curve for that star in Figure 2.3). We note that the DBVs comprise the first class of variable stars that is predicted theoretically before the observations. The pulsations spectra in DBV in general show a great amount of harmonics and combination frequencies, resulting either from a thick convection zone distorting the eigenmodes at its base or from higher order temperature perturbation terms at the stellar surface (see details in Section 1.3).

The **DOV** (a.k.a. **PG 1159** stars, or **GW Vir**) pulsating stars are the hottest hot white dwarfs which are found on the left side of Figure 2.2. They span a huge region in effective

temperature and surface gravity, from $\sim 170\,000$ K to $75\,000$ K and $\log g = 5.7 - 7.5$. The first DOV star was the prototype star PG 1159-035 discovered by McGraw et al. (1979), three year earlier than the discovery of the first DBV star. Their atmosphere are mainly composed of He, C and O, and may also have strong lines of N. The PG 1159 stars are the evolutionary remnants of stars that has experienced a late He flash at their post-AGB phase (Althaus et al. 2007). During the PG 1159 stars evolution into cooler white dwarfs, gravitational settling of C and O produces almost pure He atmosphere, a DB spectral type, see the cooling tracks in Figure 2.2. The pulsations in GW Vir stars are low- to mid-order, low degree g-modes. As the convection is negligible in these very hot stars, the classical κ-mechanism associated with the C and O partial ionization in the envelope is the excitation mechanism, which was originally proposed by Starrfield et al. (1983) and confirmed by Bradley & Dziembowski (1996) and Quirion et al. (2004).

Oscillations in the hot **DQV**, **ELM** (extremely low-mass) DA and **hot DAV** white dwarfs are the most recent discoveries among pulsating stars in general. The hot DQV stars, around $20\,000$ K in effective temperature, are composed of C-atmosphere and with relatively high surface gravities. The DQ white dwarf stars had been discovered by Dufour et al. (2007), and its exact origin is uncertain and need to be classified. The pulsations observed in hot DQV correspond to mid- to low-order low-degree g-modes. Convective driving that is associated with the recombination of C in the envelope is the excitation mechanism for the oscillations in the hot DQV stars (Fontaine et al. 2008). G-mode pulsations have been first detected in an ELM DA white dwarf by Hermes et al. (2012). These relatively rare objects are post-red giant branch (RGB) remnants and are composed with a relatively thick H-envelope. The detected pulsations in ELM DAVs correspond again to the low- to mid-order low degree g-modes and the periods are much longer compared to the other pulsating WD stars as a result of lower surface gravity. The last class of pulsating white dwarf stars is the discovery of oscillations in DA white dwarfs clustering around $30\,000$ K (Kurtz et al. 2013), which should be referred to as hot DAV white dwarfs. The tentative explanation for the mode excitation is that these stars have very thin H out layers based on a He mantle in which the driving region resides.

2.1.2 Progresses in white dwarf asteroseismology

To extract information from pulsating white dwarf stars, one obviously need to disclose the amplitude power spectra of the oscillations. Therefore it is necessary to collect the photometric data covering as long as thousands of period cycles. The Whole Earth Telescope (WET) network came into astronomer's vision with which the regular gaps caused by the diurnal cycle can be avoided (Nather et al. 1990). The WET gathered very important photometric data and made great progresses in white dwarf asteroseismology. More than 100 pulsations have been detected in the prototype of DOV stars, PG 1159-035, by the WET observations (Winget et al. 1991). With those data many fundamental parameters of PG 1159-035 are constrained, the precise rotation period, the rotational inclination, the inner stratification and an upper limit of the strength of magnetic field. Another example of the WET observations is the DBV prototype GD 358 which had been observed many times by this network (e.g. Winget et al. 1994). The frequency spectrum of GD 358 is very complex, the amplitudes exhibit temporal variations on timescales of weeks while the frequencies turn out to be stable, further discussed in Section 2.1.4.

The investigation of pulsating white dwarfs inevitably depends on the accuracy of the determination of effective temperature and surface gravity from spectroscopy. The number of white dwarf stars had increased to at least double as a result of data release from Sloan Digital Sky Survey (SDSS, York et al. 2000). Kepler et al. (2007) made a detailed analysis of the distribution of mass and effective temperature for DA and DB stars from SDSS data.

With the high signal-to-noise (S/N) spectra for the bright WD stars, a pure instability strip

of DAVs are found (e.g., Bergeron et al. 2004; Gianninas et al. 2005)—all the stars within this instability strip, with effective temperature from 12 270 K to 10 850 K, are observed to pulsate. On the theoretical front to explain this pure instability strip, the time-dependent convection (TDC) into nonadiabatic calculations was introduced to DAV pulsators (Van Grootel et al. 2012). Convective driving with TDC well predicts the blue edge of the instability strip, but it fails at explaining the red edge. A semi-analytic criterion based on the comparison between the thermal timescale at the base of the convection zone and the cutoff g-mode period was proposed (Van Grootel et al. 2013b), which gives a good description of the red edge of DAV instability strip. This is the first time that the theory agrees well on the observations on the instability strip problem. We note that the three new discovered ELM DAVs fall within the extension of the theoretical strip into the low-gravity region.

A coherent picture of the GW Vir instability strip problem was made recently by Quirion et al. (2012) based on the examination that the existence of the GW Vir pulsators invokes the competing actions of a residual stellar wind against the gravitational settling of carbon and oxygen elements. Some hot PG 1159 WD pulsators rotate very slowly at the stellar surface, which may indicate that most of the angular momentum may be stored beneath the surface. Recent seismology analysis have successfully penetrated $\sim 99\,\%$ of the mass of PG 1159-035 and a few other GW Vir stars. The seismic results reveal that the inner parts of PG 1159 stars rotate at slow speed, thus cannot hide most of the angular momentum, which means that these stars lost almost all their angular momentum (Charpinet et al. 2009c). This is a very important clue to theories of angular momentum transfer between the radiative core and the convective envelope in red giant phases which ultimately leads to the white dwarf phase in stellar evolution.

Up to present, it is hard to give a precise number of these various classes of white dwarf pulsators as new discoveries of WD pulsators change very rapidly with the development of the capability of facilities to obtain mass data on white dwarf stars both in photometry and spectroscopy. The number of WD pulsator families becomes larger and larger, the discovery of an ultra-massive one may be followed quickly by an extreme low mass one (Hermes et al. 2013a,b), or see the newest pulsator joining the WD pulsating family very recently (e.g., Kilkenny 2016). The launch of space missions, e.g., *Kepler*, provide a great opportunity to obtain exquisite photometric data for white dwarf asteroseismology. For this specific WD pulsators from space photometry, the discussion on it will be reserved for Section 2.3.

2.1.3 Change of pulsation period

As a white dwarf cools along the evolutionary track, the periods of oscillation modes change as a result of the change of the internal structure of the star. Therefore the observations of the period change of pulsations in WD pulsators could provide a direct measurement of the evolutionary timescale of white dwarf stars. The pulsation periods of nonradial g-modes, P, changes are related to changes in the radius and temperature of the star, with the relation of,

$$\frac{\dot{P}}{P} = -a\frac{\dot{T}}{T} + b\frac{\dot{R}}{R}, \tag{2.1}$$

where a and b are constants of order unity (Winget et al. 1983). To measure a sufficient accuracy in the periods of pulsations, all observational data must be on a uniform time-base, the Barycentric Julian Coordinated Date scale, because the effect from the Earth's motion must be corrected since the effect often have a very long timescale, many years or even decades.

The rate of period change is typically small, we thus may expand the time of maximum light of a pulsation, T_{max}, in a Tylor series, dismissing terms higher than the quadratic, then

$$T_{max} = T_0 + P_0 E + \frac{1}{2}\dot{P}\overline{P}E^2, \tag{2.2}$$

where E is the integer number of cycles after $t = 0$, P_0 is the period of the mode at time $t = 0$ and $\overline{P}$ is the average period over the whole time interval. The observed times of maxima O minus the calculated times of maxima C is

$$O - C = \frac{1}{2}\dot{P}\overline{P}E^2. \tag{2.3}$$

We could use a parabolic fit to the $O - C$ diagram, and finally obtain the rate of period change for the pulsations, $\dot{P}$. Equation (2.2) applies to the period change with slow rate, or specifically, a period change with linear rate which may be caused by stellar evolution. The presence of an orbital companion such as a Jupiter-like planet could contribute to the period change of pulsation. This contribution repeats in the $O - C$ diagram and is often fitted by sinusoidal signals as,

$$T_{max} = T_0 + P_0 E + \frac{1}{2}\dot{P}\overline{P}E^2 + A\sin(\frac{2\pi}{\Pi}E + \phi), \tag{2.4}$$

where A is the amplitude, Π the period and ϕ the phase of the sinusoidal variations.

The rate of period change $\dot{P}$ is extremely important to constraint the core composition of a white dwarf pulsator because the composition determines the cooling rate of a white dwarf evolution, e.g., calculations for DAVs stars (e.g., Brassard et al. 1992a), for DBV stars (e.g., Kim et al. 2006) and DOVs (e.g., Althaus et al. 2008). The total rate of period change may contain the contribution of the contraction rate, the cooling rate and the rate of reflex motion (see equation 2.1, and, e.g., Winget & Kepler 2008). The cooling rate is the dominating term in the period change of pulsation in a WD pulsator during its evolution, e.g., for a hot DOV, PG 1159-35, the cooling rate $\dot{T}/T = -7.61 \times 10^{-11}\,\mathrm{s}^{-1}$ which is much greater than the contraction rate $\dot{R}/R = -0.89 \times 10^{-11}\,\mathrm{s}^{-1}$ (Costa & Kepler 2008), and for cool ZZ Ceti stars which cool at nearly constant radius, $\dot{R}/R \ll \dot{T}/T$. In white dwarf evolution, the plasmon neutrinos are the dominant form of energy loss. Thus measuring the cooling rate of WD evolution could constrain the neutrino emission rate in hot white dwarfs, which may give us an unique way to test the fundamental physics of weak interactions of elementary particles. The cooling rate of white dwarf evolution depends sensitively on the effective temperature of that star. For the hottest WD pulsators, DOVs, the rate of period change may be on the order of $\dot{P} = 10^{-10} - 10^{-12}\,\mathrm{ss}^{-1}$, see, e.g., the mode of 516.0 s in PG 1159-35 (Costa & Kepler 2008). The theoretical calculations on DB white dwarf models obtain that the rate of period change due to the cooling effect are on the order of $\dot{P} = 10^{-13}\,\mathrm{ss}^{-1}$ down to the effective temperature of 25 000 K (Winget et al. 2004). The cool DAV stars have the slowest cooling rate as they have the lowest effective temperature in all WD stars. The rate of period change in a ZZ Ceti star, G 117-B15A, can be used as the most stable optical clock currently known, with $\dot{P} = 3.57 \pm 0.82 \times 10^{-15}\,\mathrm{ss}^{-1}$ for the 215.2 s mode (Kepler et al. 2005). These above values of the rate of period change suggest that the pulsation period has a variation in the range of 10^{-2} s over a time baseline of ten years even for the hottest WD pulsators.

Another great advantage of the $O - C$ diagram it that it can reveal the eventual presence of a planet orbiting around the pulsators when we measure the rate of period change over a long timescale, as indicated by equation (2.4). If the sinusoidal signals were found in WD pulsators, one can obtain the exact period of the companions. Planetary objects or asteroids indeed are believed to exist around white dwarf stars ; see the most recent report on white dwarf WD 1145+017 (Vanderburg et al. 2015). The presence of planetary objects around a pulsating white dwarf star has yet to be discovered by the technique of $O - C$ diagram.

2.1.4 Hints of resonant mode couplings

In this section we discuss a phenomenon affecting oscillation modes in white dwarf pulsators, amplitude and period variations on a much larger range than the slow secular rate of period

change caused by stellar evolution as discussed in the last section. This phenomenon of amplitude and period variations of pulsations also differs from the period change induced by the presence of orbiting objects around white dwarfs in which all the modes have the same systematic trend. This phenomenon are related to the nonlinear perturbations theory (see Section 1.4.1) which predicts various behaviors of oscillation modes. We call the below examples as "hints" of such nonlinear mechanism because the observed results from ground-based telescopes are inevitably affected by the gaps in the data, thus there is no clear evidence that covers several continuous modulating cycles of the inferred nonlinear phenomenon which is on the timescale of weeks, months or even years. There are definitely some hints in other type of pulsating stars, we here merely introduce several examples in the domain of pulsating white dwarf stars.

The first example is the ZZ Ceti star, GD 385, observed by Fontaine et al. (1980) and Vauclair & Bonazzola (1981). Both their results show that the dominant mode of 256 s may change abruptly on a timescale of days, with a behavior that the mode disappear on several occasions during the observations. The role of simple beating phenomena was ruled out with the complex abrupt amplitude variation. It is proposed that nonlinear couplings between nonradial modes may account for such modulations occurring in GD 385. It is almost at the same epoch that the nonlinear resonant mode couplings between oscillation modes was put forward and developed (see, e.g., Dziembowski 1982; Buchler & Goupil 1984). Another case is the ZZ Ceti star, G 191-16, whose frequencies are regularly spaced in the power spectrum (Vauclair et al. 1989). The presence of subharmonics of the primary frequency in G 191-16 is difficult to explain by a linear theory and suggest that a nonlinear mechanism may be needed to interpret it. The observations on G 191-16 show that the amplitude increased in the second observational run.

Such nonlinear phenomena in DB pulsators may have been revealed by the WET observations on the DBV star, GD 358 (Winget et al. 1994). The interesting features are that there are large differences in amplitudes between consecutive triplets and between the components within the same triplets, asymmetric amplitudes and frequencies within the same triplets, and variations occurring in some of the triplet modes. Numerical explorations for those modes can depict the interesting features in GD 358 in general, based on nonlinear amplitude equations (Goupil et al. 1998). The amplitude differences between consecutive triplets mainly reflect the behaviors of linear growth rates of the modes which may vary in a very large range from mode to mode. While the differences in amplitude within the triplet depend somewhat on the precise values of the nonlinear coupling coefficients. Some triplets have amplitude (frequency) modulations because the neighboring triplets may belong to different nonlinear regimes (frequency locked, time dependent or nonresonant) that are related on how far the triplets are away from their resonance center, see Section 1.4.3. We note that GD 358 were not continuously observed by the WET network, thus the nonlinear AE explorations could not describe the exact behaviors of the modes in that star.

In the case of DOV stars, PG 0122+200, the coolest GW Vir variable, amplitude and frequency variations have been obtained for the first seven largest amplitude modes over a time baseline of $\sim$22 years (Vauclair et al. 2011). Their results show that the frequencies of the considered modes change in a much larger amplitude and in a much shorter timescale than the theoretical predictions by the stellar models in which the frequency variations are mainly induced by the cooling effect of neutrino emissions, as discussed in the last section. The frequency variation of the largest amplitude 240 s mode can be well fitted by a combination of two terms : a long-term one with a timescale of 5.4×10^4 years (the evolutionary cooling timescale is $\sim 8 \times 10^6$ year) and a short one with a timescale of $\sim$200 days. The short-term variations is probably a hint of a nonlinear mode coupling in the $1:1:1$ resonance in which the modes may have modulations with a timescale on weeks, months or years, depending on the nonlinear parameters the involved modes have (Section 1.4.3).

There are also amplitude variations in some white dwarf pulsators, see Vauclair (2013) and reference therein. From the theory of nonlinear AEs, the amplitude variations may have nonlinear corrections on the frequencies of the modes, thus the observed frequencies had been corrected by these nonlinear effects, which can jeopardize the attempt to measure the rates of period change to constrain the evolutionary cooling that are mainly induced by neutrino emission. In order to getting a secure measurement of those cooling rates, one needs to correct the nonlinear effects beforehand. In the next section we will discuss another type of compact pulsators, hot B subdwarf pulsating stars.

2.2 Pulsating hot B subdwarf stars

Hot subdwarf stars belong to the extreme horizontal branch (EHB) in H-R diagram, including the O (sdO) and B (sdB) types, according to their colors on the relatively simple classification. They are stars with helium buring in the core, a tiny hydrogen envelope, and with a mass typically around $\sim 0.47\,M_{\odot}$. Their nature and fates are relatively well understood, while the origin of EHB stars is wrapped in mystery. A significant fraction of sdB stars are found in binary systems. Some of sdB stars are found having pulsations and are good candidates for asteroseismology. For more details about such kind of stars we refer the very complete reviews by Heber (2009, 2016).

2.2.1 Hot B subdwarf stars

Hot subdwarfs are the subluminous blue stars that were first discovered at high Galactic latitudes in the late 1940s (Humason & Zwicky 1947). Their nature and evolution remained unknown for decades until the first determination of effective temperature and surface gravity for these faint blue stars, an attempt to place them in the Hertzsprung-Russell diagram (Greenstein & Sargent 1974). The large samples of hot subdwarfs were first provided by the photometric and objective prime surveys in 1980s (e.g., the Palomar-Green survey, Green et al. 1986).

Atmospheric parameters and abundances of subdwarf stars can be derived from spectroscopic measurements by using appropriate model atmosphere. They typically fell into several groups on the spectroscopic classification. The dominant and simplest nomenclature is to distinguish between the hot subdwarfs of B and O type, sdB and sdO stars. SdB stars are characterized by spectroscopy with the abnormally broad Balmer lines, weak He I lines, and form a homogeneous class. While sdO stars, rarer in number compared with sdB, show more variety in their spectral properties (see more details about sdO stars in Heber 2009, sdB stars as well). From now on we focus in particular on sdB stars as the representative of hot subdwarfs in this thesis. Significant efforts on the investigation of the properties for sdB stars were led by the computation of local thermodynamic equilibrium (LTE) or non-LTE atmosphere models, with or without metals. LTE is a good approximation for sdB stars with high gravity and low temperature, while non-LTE model is more appropriate for the hot ones as effective temperature higher than $\sim 35\,000$ K (e.g., Napiwotzki 1997). The analysis of 207 sdB stars whose atmospheric parameters are derived from non-LTE H/He models shows that they cluster between 22 000 K to 40 000 K in temperature and between 5.2 to 6.4 in $\log g$ (see, Fig. 1 in Charpinet et al. 2009a). Helium is highly deficient in the atmosphere of sdB stars. Many heavy elements of the iron group and beyond have large overabundance, in particular for the hottest ones, based on the Ultraviolet spectroscopy from HST and FUSE (O'Toole & Heber 2006; Blanchette et al. 2008). These overabundance of heavier elements are believed to be the signature of diffusive effects including gravitational settling and radiative levitation which can affect the selectively on the chemical element distribution on the stellar envelope.

A significant fraction of sdB stars are in binaries, as revealed by spectral observations (e.g., Maxted et al. 2001). The cool companions can be detected by the combination of optical and infrared photometry since the sdB stars dominate the blue parts while the cool companions dominate the infrared part of the spectrum. Many single sdB stars show variations of radial velocity on short periods, which suggest the presence of invisible companions (e.g., Napiwotzki et al. 2004). These invisible companions are expected to be either white dwarfs or low-mass main-sequence stars. The sdB+WD binary can be a good candidate for SN Ia progenitor through the double-degenerate formation channel, because total mass of the binary system can exceed the Chandrasekhar limit (e.g., KPD 1930+2752 ; Maxted et al. 2000). SdB stars in eclipsing binaries provide an accurate determination of the stellar masses. HW Vir stars consist of eclipsing binaries of sdB+dM in short-period orbits (Wood et al. 1993). An example of one HW Vir system, HS 0705+6700, shows that the mass derived from the radial velocity is very close to that from the evolutionary model (Drechsel et al. 2001). We note that the NW Vir itself is very important because it is one of the only two eclipsing binary with a pulsating sdB companion (see Section 2.2.3).

Several scenarios have been developed to explain the evolution of sdB stars. Canonical EHB models are characterized by a $\sim 0.5\,M_{\odot}$ core mass and a tiny inert hydrogen rich envelope (Dorman et al. 1993). In such scenario, the core mass is fixed at the onset of the helium core flash at the tip of the RGB and descends slightly on metallicity and helium abundance, thus the core mass is restricted to a very narrow range around $\sim 0.47\,M_{\odot}$. The mass of the envelope is too low to let an EHB star ascend the AGB. The post-EHB stars then evolve toward higher temperatures until they reach the cooling sequences of low-mass white dwarfs. Quantitative spectroscopic investigations obviously demonstrated that sdB stars can naturally be associated with EHB and post-EHB models, sdB stars forming a very homogeneous group in the H-R diagram that fits with EHB models in the phase of core helium burning (e.g., Heber et al. 1984; Heber 1986).

Although the nature and fate of sdB stars is relatively well understood, the formation channel may still be uncertain. The long standing difficulty for a single star formation of sdB star has been to understand how a star can lose all except a very tiny fraction of its H-rich envelope before or during the He-flash for the star to settle down as an EHB and not as a typical HB star. The formation through binary channels may play an important role for the origin of sdB stars, as the observed high fraction of short period sdB binaries. Three channels for forming sdB stars were proposed by Han et al. (2002, 2003) : the common-envelope (CE) ejection channel, the stable Roche lobe overflow channel, and the double helium white dwarfs merger channel. The population-synthesis of binary models give a prediction of a broader mass distribution in the range of $0.3 - 0.8\,M_{\odot}$ peaking near at the canonical $0.47\,M_{\odot}$ due to masses of the mergers.

2.2.2 Classification of hot B subdwarf pulsators

The discovery of nonradial oscillations in hot subdwarf stars provide new opportunities to probe their interior structure with the technique of asteroseismology. There are two classes of nonradial pulsators identified among sdB stars, officially named the V 361 Hya and V 1093 Her stars. Figure 2.4 shows a global view of the location of these two groups of sdB pulsators in the $\log g - T_{\rm eff}$ diagram.

The first discovery of low-amplitude multiperiodic luminosity variations with periods of a few minutes was in the sdB star EC 14026 (or **V 361 Hya**) by Kilkenny et al. (1997) at almost the same time when the theoretical prediction that nonradial pulsations should exist in sdB stars (Charpinet et al. 1996). This type of pulsators show rapid multiperiodic pulsations with periods in the range from 80 s to 600 s generally, identified to low-order, low degree acoustic (p-) modes. The amplitude of these oscillations are typically very low (less than a percent of the mean

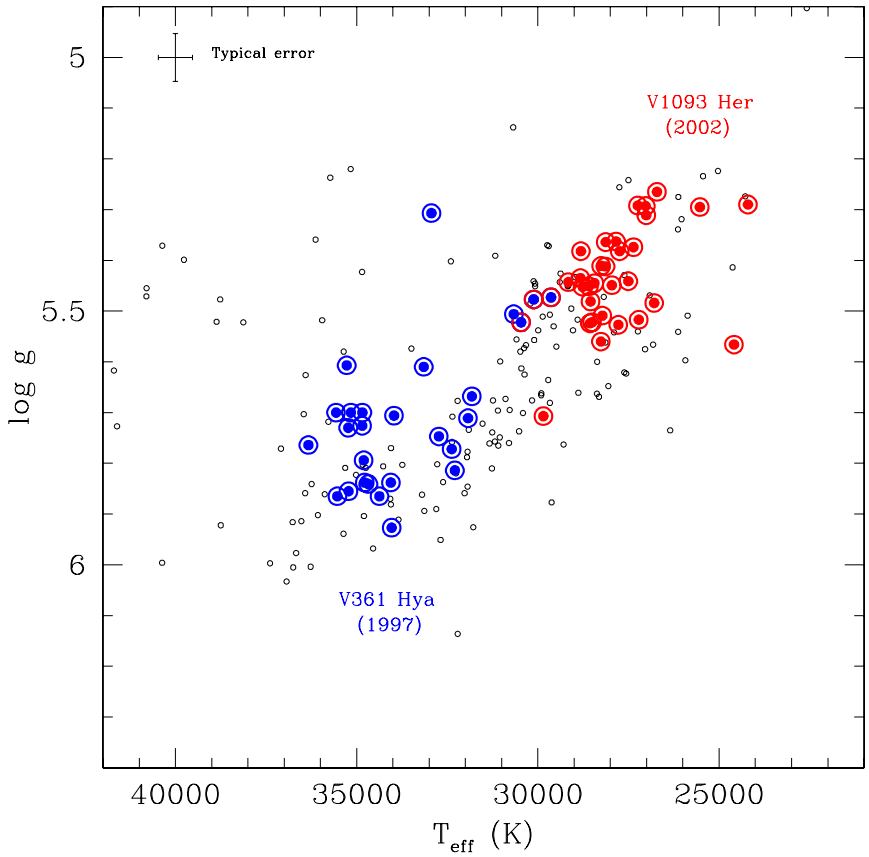

FIGURE 2.4 – The instability strip of the two known families of sdB pulsators in $\log g - T_{\rm eff}$ diagram. A sample of 28 short-period sdB pulsators (officially, V 361 Hya type) and 33 long-period ones (officially, V 1093 Her) are shown in blue and red, respectively. Three stars are hybrid pulsators with oscillations both in long- and short-period (blue filled circles within red annuli). The typical 1σ error of the determination of the atmospheric parameters for the sdB stars are shifted to the top left corner. The black open circles represent the constant sdB stars.

brightness of the star), while, occasionally, relatively large amplitude modes (a few percents of the mean brightness) were found. Examples of several representative light curves of V 361 Hya stars are shown in the upper part of Figure 2.5 (in blue). Such short period pulsations are only detected among the hotter sdB stars (with a very low fraction) with effective temperature, $28\,000 < T_{\rm eff} < 36\,000$ K, and surface gravity, $5.2 < \log g < 6.1$, typically, indicated by blue symbols in Figure 2.4. The driving mechanism for the pulsations in V 361 Hya stars turns out to be the opacity bump associated with iron ionization (Charpinet et al. 1996, 1997a). Radiative levitation is particularly important to produces iron overabundances in the driving region. Once this overabundance is sufficient locally in the Z-bump region zone of iron, low order p-mode oscillations are excited (Charpinet et al. 1997a).

Green et al. (2003) discovered the second type of pulsating sdB stars, **V 1093 Her**, which are cooler than the V 361 Hya stars, with effective temperatures in the range $22\,000 < T_{\rm eff} < 30\,000$ K (red symbols in Figure 2.4). The pulsations in the V 1093 Her stars have much longer periods than those in the V 361 Hya stars, typically in the range of $45 - 120$ minutes, corresponding to mid-order gravity (g-) modes. Examples of several representative light curves of

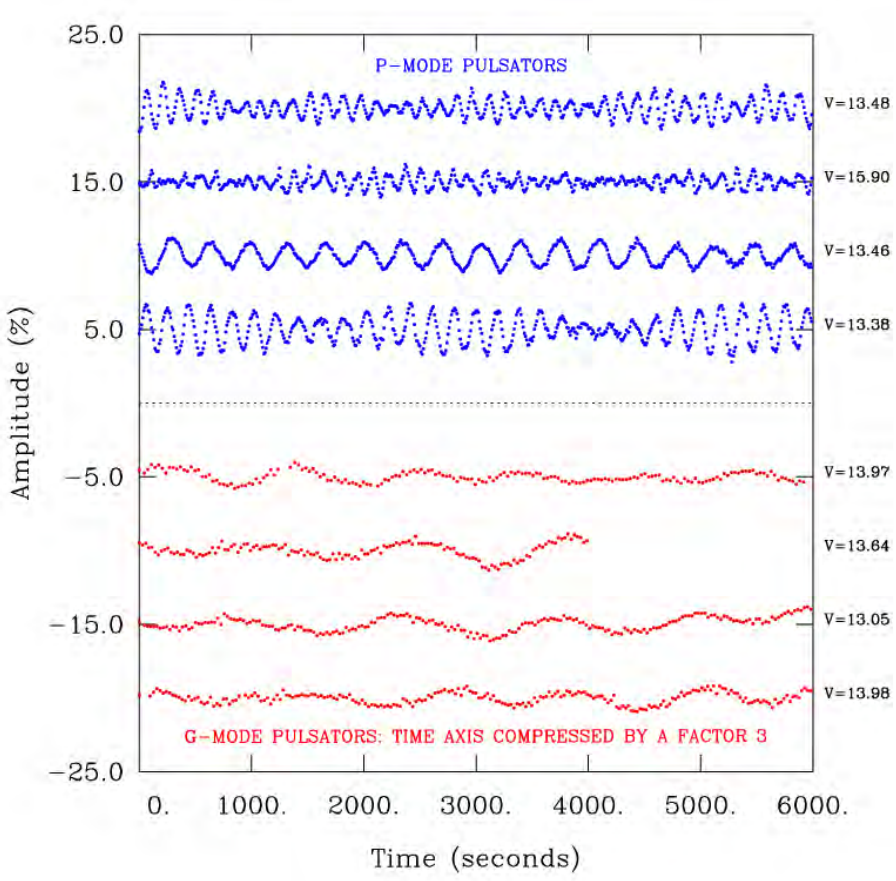

FIGURE 2.5 – Representive light curves of two different types of sdB pulsators. The upper blue ones are the segments of light curves for four rapid p-mode sdB pulsators with sampling of 10 s. The lower red ones are for four slow g-mode sdB pulsators with sampling of ~ 80 s. See details in Charpinet et al. (2009a)

V 1093 Her stars are shown in the lower part of Figure 2.5 (in red). The g-mode oscillations have noticeably lower amplitudes—less than one percent of the mean brightness. Thus the V 1093 Her stars are much more challenging to observe with ground-based campaigns. However, asteroseismic studies of the V 1093 Her stars have benefited from a lot of observations by space telescopes (see Section 2.3). The same driving mechanism (κ-mechanism) as for the p-modes oscillations is responsible for the excitation of g-mode pulsations in V 1093 Her stars (Fontaine et al. 2003). Beyond iron, the enhancement of nickel on the opacity profile, as well as the opacity sources themselves, also play a role (Jeffery & Saio 2006), in particular to explain all the excited modes observed in g-mode sdB pulsators. Finally note that Figure 2.4 also shows the distribution of three hybrid pulsating sdB stars with pulsations both in short period p-mode and long period g-modes (blue filled circles within red annuli). The first hybrid stars was first found by Schuh et al. (2006). They are found near the red edge of the V 361 Hya instability strip and the blue edge of the V 1093 Her instability.

2.2.3 Asteroseismology of hot B subdwarfs

The pioneering work on the potential of sdB stars for asteroseismology comes from Brassard et al. (2001) whose results agree well on the parameters determined from spectroscopy for the

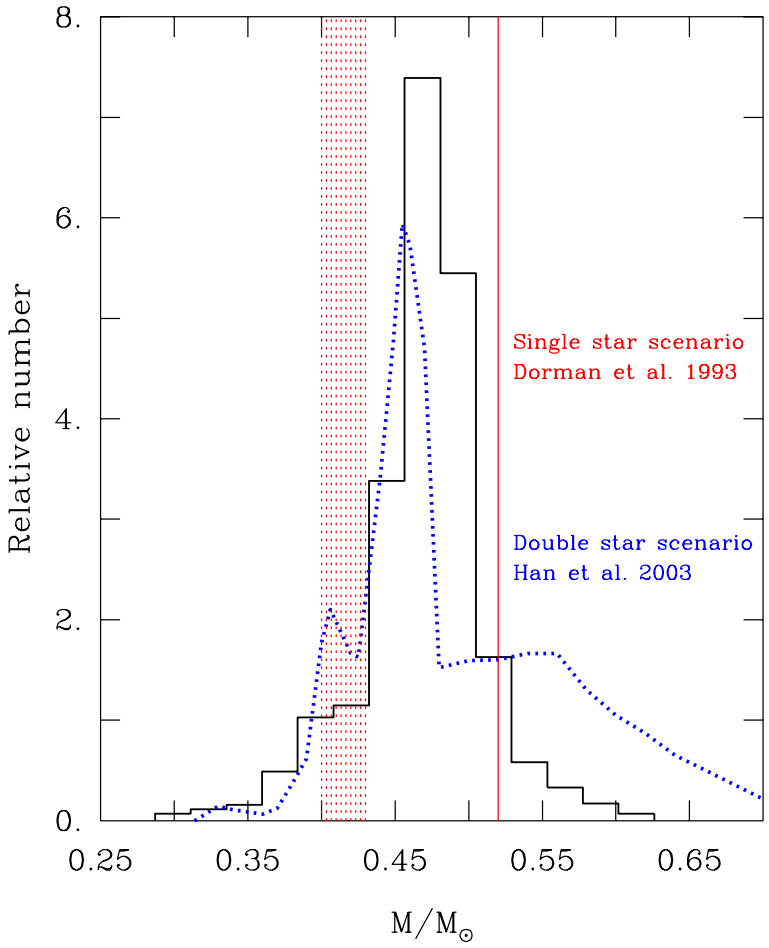

FIGURE 2.6 – The empirical mass distribution of 22 sdB stars in comparison with two theoretical predictions. Histograms represent the mass of 15 sdB stars are derived from asteroseismology and the others from binary determinations (Fontaine et al. 2012). The red lines are the (sharp) upper and (fuzzy) lower boundaries of mass range from single star evolution (Dorman et al. 1993). The blue curve denotes the mass distribution from binary evolution models (Han et al. 2003) which is normalized here.

EC 14026 pulsator PG 0014+067. This seismic probing relied on stellar envelope models of the so-called second generation (2G) for sdB stars. The 2G sdB models incorporate a nonuniform abundance profile of iron that is predicted by equilibrium between radiative levitation and gravitational settling (e.g., Charpinet et al. 2002a). These models are appropriate for the seismic exploration of pure *p*-mode sdB pulsators whose pulsations are only sensitive to the details of the outmost regions of the star. Third generation (3G) models have been developed to apply the seismic investigation of *g*-mode pulsators (Brassard & Fontaine 2008). The 3G models are complete stellar structures that incorporate a detailed description of the core region, and the nonuniform abundance profiles of iron in the envelope (a detailed description can be found in Van Grootel et al. 2013a).

Asteroseismology of sdB stars is based on the "forward modeling method" whose basic principle is to simultaneously fit all of the observed pulsation periods with the theoretical ones calculated from stellar models, in order to find the best match in the parameter space. The

quality of a period match is evaluated through a merit function defined as

$$S^2(x_1, x_2, ..., x_n) = \sum_{i=1}^{n} \Big(\frac{P_o^i - P_t^i}{\sigma^i} \Big)^2, \tag{2.5}$$

where n is the number of observed pulsation periods, $\{x_1, x_2, ..., x_n\}$ is the parameter set, P_o^i is the observed period and P_t^i the calculated one (Charpinet et al. 2009a).

After about a decade of efforts, 16 pulsating sdB stars have been analyzed by the foward modeling method with 2G and 3G sdB models (Fontaine et al. 2012). In all cases, the solution of a best-fit model match well with the atmospheric parameters of the star derived from spectroscopy, and, furthermore, all the observed periods are matched to driven modes according to nonadiabatic calculations. For the *p*-mode pulsators, the typical average dispersion between the observed and computed periods is $\overline{\Delta P/P} \sim 0.5\%$ (e.g., PG 1325+101 ; Charpinet et al. 2006). The optimal model for the long period *g*-mode pulsators can also reach such high precision, e.g., the 3G model for KPD 1943+4058 have an average period dispersion of about 0.22% (Van Grootel et al. 2010b). An important aspect of sdB asteroseismology is that the optimal seismic models can provide an accurate mass for sdB pulsator. Figure 2.6 shows the empirical mass distribution of 22 sdB stars—15 of the 16 sdB pulsators with seismic solutions and 7 sdB stars in binary systems from light curve modeling and spectroscopy—compared with two theoretical distributions (Fontaine et al. 2012). The empirical mass distribution determined by Fontaine et al. (2012) is consistent with the expectations from the two different stellar evolutionary theories of single star channel (Dorman et al. 1993) and double star channels (Han et al. 2003). For example, about 86% of the stars in the 22 star sample have masses falling right within the mass range $0.40 - 0.52\,M_\odot$ predicted by Dorman et al. (1993). However, the presence of low- and high-mass wings in the mass distribution in Figure 2.6 are expected from the binary evolutionary channels (Han et al. 2003). We also note that the average mass of the sample in Fontaine et al. (2012) is $0.470\,M_\odot$ which differ slightly from that of binary evolution of $0.499\,M_\odot$. At this stage, however, the result is only suggestive because the sample is still small.

In exploiting asteroseismology for sdB stars, the case of NY Vir (=PG 1336+018) is particularly important. It is one of the only two eclipsing binary system (sdB+M) with the sdB component displaying short-period oscillations (Kilkenny et al. 1998). It offers the opportunity to determine the stellar parameters of the sdB component from independent methods, modeling from the light curve of the binary system and modeling solution from the seismic exploration (Charpinet et al. 2008). Based on the 25 detected pulsations in NY Vir, the best-fitting solution of the foward modeling by Charpinet et al. (2008) agrees remarkably with one of the best-fitting solutions from the eclipsing binary light curve by Vučković et al. (2007). Furthermore, NY Vir can be the test bed for the new generation seismic models. The test of 3G seismic model obtains the stellar parameters, mass M, radius R and surface gravity $\log g$, within 1σ error of the solution independently obtained from spectroscopy and light curve modeling (Van Grootel et al. 2013a), respectively.

The forward modeling method allows one to determine the basic stellar parameters with high precision. However, there are some room left for improving further detailed description of the stars in the models. In particular nonadiabatic asteroseismology (Charpinet et al. 2009b) may help constrain the microscopic diffusive processes and their competitors, e.g., turbulent mixing, stellar winds, thermohaline convection (e.g., Théado et al. 2009).

2.2.4 Frequency and amplitude variations in sdB pulsators

Like white dwarf pulsators, pulsating sdB stars may have sufficiently stable pulsation periods to measure secular changes based on long time baseline observations. On the theoretical front,

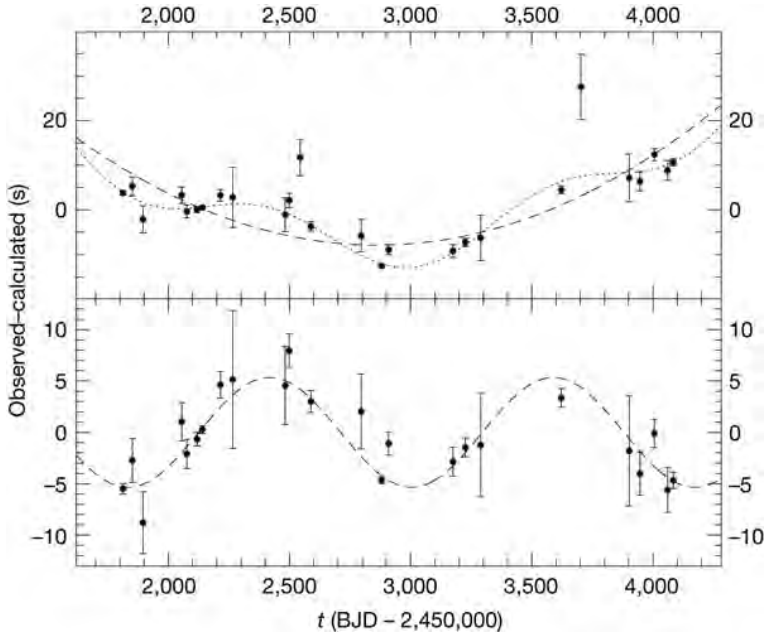

FIGURE 2.7 – The $O-C$ diagram of the frequency f_1 of sdB star V 391 Peg based on the observational time-length of seven years (Silvotti et al. 2007). The upper panel shows the parabolic fit of the long-term trend (dashed) and an improved fit with an additional sinusoidal fitting (dotted). The alone sinusoidal fitting component is shown in the lower panel.

the effects of stellar evolution on the oscillation eigenmodes of sdB models have been calculated by Charpinet et al. (2002b). On the observational side, the observed rates of pulsation period change can be derived from the $O-C$ diagram for an sdB star (see details in Section 2.1.3). However, such $O-C$ determinations need well resolved and constant frequencies in the amplitude spectrum of oscillation modes. But some pulsations in sdB stars are found with amplitude variations.

The pulsation periods P and the rates of period change $\dot{P}$ are related to the adjustments of stellar structures that EHB stars undergo during evolution. The secular variations of the surface gravity are the main factor to affect the acoustic modes (Charpinet et al. 2002b). The average relative rate of period change for acoustic modes is $\overline{\dot{P}/P} \sim 5 \times 10^{-3}\,\mathrm{Myr}^{-1}$. During the evolution of EHB stars, the sign of $\overline{\dot{P}/P}$ changes between ~ 87 and 92 Myr depending on the exact sequence of a star. The gravity modes, however, whose periods change are related to three main factors : the evolutionary effects on the surface gravity and effective temperature, the onset and growth of a chemical discontinuity between the C-O-enriched nucleus and the He-enriched mantle (Charpinet et al. 2002b). The average relative rate of period change for gravity modes is $\overline{\dot{P}/P} \sim \times 10^{-3}$ to $10^{-2}\,\mathrm{Myr}^{-1}$ and its sign changes at ~ 60 Myr, ~ 25 Myr earlier than that of the acoustic modes. These theoretical explorations of the pulsation periods and their changing rates, in principle, could be determined by observations over a time baseline of decades, using the $O-C$ diagram.

The EHB star, V 391 Pegasi, is an example of the $O-C$ method applied to determine the rate of period change in sdB stars (Silvotti et al. 2007). Figure 2.7 shows the building $O-C$ diagram for the main frequency f_1 of V 391 Peg spanning over a time baseline of about seven years. As sdB pulsators have been discovered more recently than pulsating white dwarfs, the time baseline of observations for one single sdB star is several times shorter than that of WD

stars, about 7 years comparing to 20–30 years. The parabolic fit of the $O-C$ measurements infers that the main frequency whose period changes at a rate of $\dot{P} = 1.46 \pm 0.07 \times 10^{-12}\,\mathrm{ss}^{-1}$, corresponding to 1 s in 22 000 years, which is rather consistent with theoretical expectations from stellar model as discussed above. However, as shown in the upper and lower panels of Figure 2.7, an additional sinusoidal fitting to the residuals significantly improves the fitting of the $O-C$ measurements. This cyclical signal is interpreted as the signature of the presence of stellar and/or planetary companions around the pulsating star (see equation 2.4). Indeed, this cyclical signal also occurs in the $O-C$ diagram for the frequency f_2, with the same period of about three years. Silvotti et al. (2007) found that the best interpretation for such sinusoidal signals in the $O-C$ diagram is the presence of a Jupiter-like planet orbiting V 391 Pegasi, with $M \sin i = 3.2 M_{\mathrm{jupiter}}$, distant of 1.7 astronomical unit (AU) with an orbital period of 3.2 years. This discovery demonstrates that planets within an orbit of 2 AU can survive after their parent stars expanding at the red-giant phase, which has important implication to understand the evolution of sdB star progenitors and their planets. Very closed orbiting planets can also survive after the late phase of expansion of red giant stars, e.g., two earth-size planets have been found around a *Kepler* sdB star (Charpinet et al. 2011a), which will be discussed in Section 2.3.1.

Kilkenny (2010) reported a number of sdB pulsating stars with amplitude variations over seasons of observations, e.g., the prototype EC 14026, EC 09582 and V 384 Pegasi. From their results, it seems that amplitude modulations of the pulsation modes are a common phenomenon in sdB pulsators. The timescales of the amplitude variations appear to be from a day to several years (Kilkenny 2010). However, whether the frequencies of the oscillation modes are constant or also change with time could not be resolved by Kilkenny (2010) because the observation coverage was still not long enough for that measuring. Much longer time-coverage observations are particularly needed to measure accurate frequency variations (see, e.g., frequency variations in the pre-white dwarf PG 0122+200 from multi-site observations Vauclair et al. 2011). The origin of these mode variations is still an open question, which we address in this thesis (see Chapter 4 and 5).

2.3 Asteroseismology from space photometry

Observation from space has been a long awaited dream for who is particular eager of asteroseismology, providing high-quality long consecutive photometric data. The pioneering observations by space-based telescope for asteroseismology began with the contribution from the Canadian space project *MOST* (The Microvariablity and Oscillations of Stars ; Walker et al. 2003). This small-aperture telescope however was designed to detect oscillations in bright stars ($V < 10$, compact pulsators are typically fainter than this). Nevertheless, three independent modes were detected in the long-period g-mode sdB star PG 0101+039 from the continuous observations by MOST (Randall et al. 2005). A revolutionary situation in asteroseismology has happened with the launch of the French-led space telescope *CoRoT* (Convection, Rotation, and Planetary Transits ; Baglin et al. 2006). This 27-cm telescope, *CoRoT*, opened a new era in sdB asteroseismology, in particular for the long-period g-mode V 1093 Her stars (Charpinet et al. 2010). *Kepler*, the big cousin of *CoRoT*, was launched by NASA in 2009 to discover Earth-size planets (Borucki et al. 2010), as well as providing extremely high-quality data for asteroseismology (Gilliland et al. 2010). *Kepler* then turned into a new called mission *K2* (the second light of *Kepler* ; Howell et al. 2014) after losing the second reaction wheel in May 2013. A more detailed description of the *Kepler* satellite will be given in Chapter 3. Future space missions are planned, e.g., TESS (The Transiting Exoplanet Survey Satellite ; Ricker et al. 2014) and PLATO (Rauer et al. 2014), which will continuous to provide high-quality photometric data for asteroseismology in years to come.

In this section, we will present the advancement of asteroseismology in compact pulsators exploiting the emergent space-based observations. The photometric data from space gives a sharper resolution for frequencies in Fourier amplitude spectra than ever before and lower the detection threshold to a few ppm (parts per million), thus allowing one to detect much more modes than ground-based observations. This is useful to obtain better seismic constraint for stellar models. The space photometry definitely provide a new window to the study of temporal behaviors of pulsating modes due to its long and uninterrupted observations.

2.3.1 Advancements in compact pulsators

Space missions finally overcome the aliasing problem that is inevitable from ground-based observations, as a result of monitoring one specific observational field for a very long time, months or even years. Therefore these long, uninterrupted, high-precision photometric data have a heavy impetus on the understanding of long-period, low-amplitude pulsating stars, particularly for the *g*-mode V 1093 Her stars. Figure 2.8 shows comparison of amplitude spectra for three different stars observed from the ground and from space with *CoRoT* and *Kepler*. Figure 2.8(a) shows a portion of the LSP (*p*-mode dominated region) for the hybrid pulsating sdB star Feige 48 observed with the 1.54 m Kuiper Telescope on Mount Bigelow, Arizona, in 2009. The daily aliases are clearly seen and the noise level is about one tenth ppt from the LSP. Figure 2.8(b) shows that the 24 days of high-quality, uninterrupted photometric data from *CoRoT* permitted the detection of 17 independent modes in the long-period sdB star KPD 0629-0016, with a noise level about a few dozen ppm (Charpinet et al. 2010). This gave the first opportunity to probe the deep internal structure of the *g*-mode sdB pulsators with great success by asteroseismology (Van Grootel et al. 2010b). Figure 2.8(c) shows an example of amplitude spectrum of the long-period sdB star KIC 02697388, obtained by *Kepler* with a duty time of $\sim$ one month (Charpinet et al. 2011b). The frequency resolution, oscillation amplitudes and noise level are very similar in both two cases, except 47 pulsation modes are found in the *Kepler* target KIC 02697388. We note that the amplitude spectrum for *Kepler* target provided here is only for one-month observation. A much sharper and larger number of low-amplitude modes can be found with *Kepler* since some of the compact pulsators in its FOV (field of view) have been observed for as long as ~ 4 years.

The long observations (of the order of years) offered by *Kepler* are particularly important to determine the rotational periods of these stars, because rotation in compact pulsators needs sharp enough frequency structures to resolve the rotational splitting of affecting nonradial modes (see Section 1.2). Most of *Kepler* sdB stars have slow rotation with a period from about one month to several months. For example, KIC 10670103 has a slow rotation period of 88 ± 8 days derived from the rotational splitting multiplets (Reed et al. 2014). The presence of splitting multiplets also provide direct way to identify modes in compact pulsators, e.g., KIC 2991403 (Baran & Winans 2012). The *g*-mode periods turn out to be evenly spaced in sdB stars from *Kepler* photometry (e.g, Reed et al. 2011), which indeed is a prediction of the asymptotic pulsation theory. The high precision *Kepler* data also permits us to explore the low-amplitude Doppler beaming effect which is an alternative and independent method to establish the binarity of the stars (Rybicki & Lightman 1979). This method was applied to sdB stars and the results are consistent with measurements of radial velocities (e.g., KIC 11558725 ; Telting et al. 2012). We note that at least 8 of the 18 ($\sim 45\%$) sdB stars continuously observed by *Kepler* are found in binaries.

Two Earth-size planets have been discovered in very tight orbits around the isolated EHB star KIC 05807616 monitored by the *Kepler* spacecraft (Charpinet et al. 2011a). These two planets complete one orbit in 5.7625 and 8.2293 hours ($2:3$ resonance), respectively, placing them at a distance of 0.0060 and 0.0076 AU, as revealed by two weak (but clearly significant)

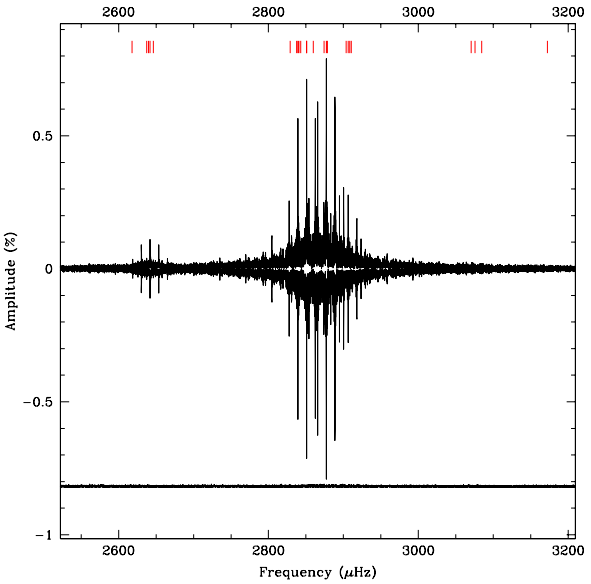

(a) Ground

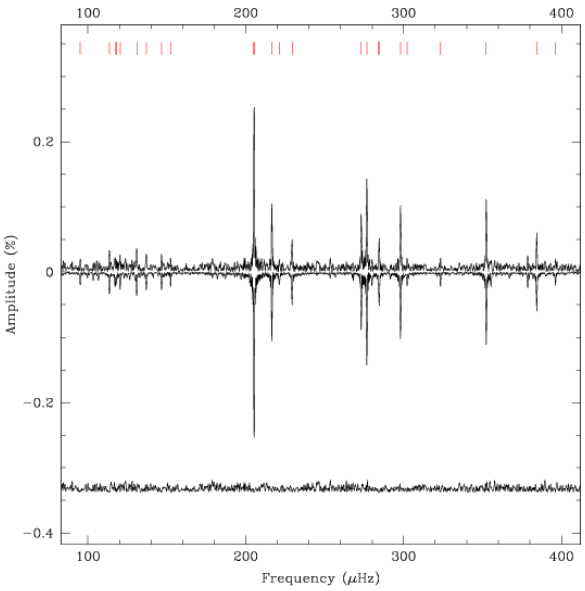

(b) *CoRoT*

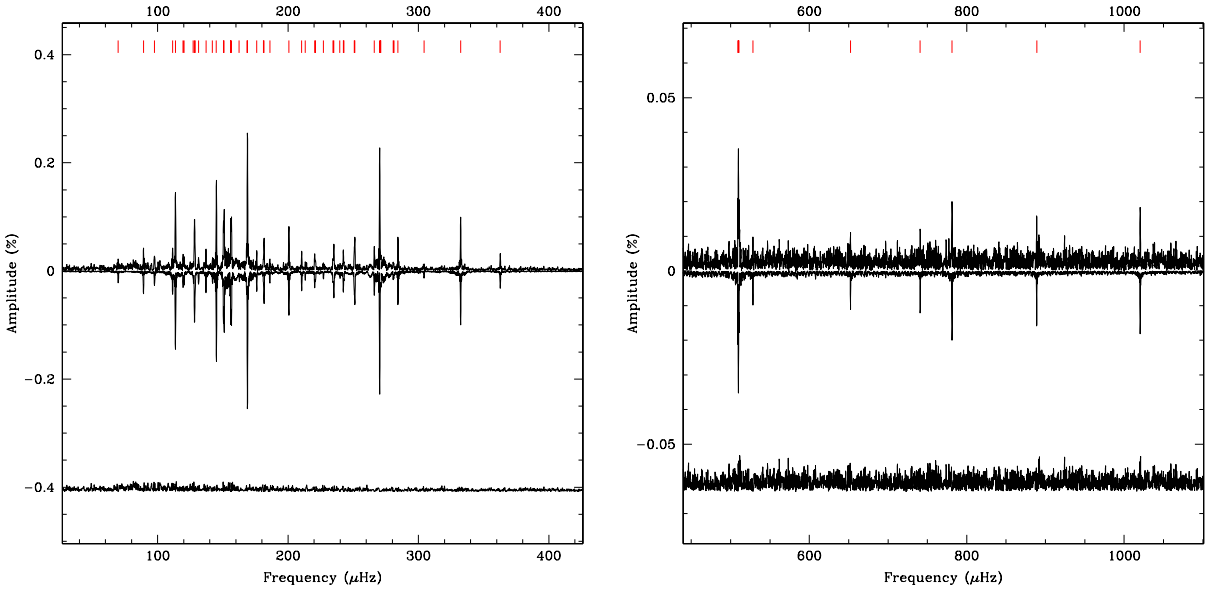

(c) *Kepler*

FIGURE 2.8 – Amplitude spectrum companion between ground-based observations, *CoRoT*, and *Kepler* for three pulsating stars : (a) *p*-mode region in the hybrid pulsating sdB star Feige 48 from ground-based observations ; (b) long-period sdB star KPD 0629-0016 from *CoRoT* (Charpinet et al. 2010) ; (c) long-period sdB star KIC 02697388 from *Kepler* (Charpinet et al. 2011b). The red vertical segment denotes the position where the signal is above the detection threshold, 4σ typically.

signals in the amplitude spectrum, that are longer than the period of the cutoff frequency. Silvotti et al. (2014a) discovered a second case suggesting that presence of small planets around a post-red-giant EHB star from *Kepler* photometry. The star is KIC 10001893, whose Fourier spectrum shows three weak peaks at very low frequencies similar to KIC 05807616, with orbital

periods of $P_1 = 5.273$, $P_2 = 7.807$, and $P_3 = 19.48$ h which are near the $2:3$ and $2:5$ resonance. These interpretations, associating the low frequencies in these sdB pulsators with the presence of companions, are the most plausible among known alternatives, but they particularly need to be confirmed by other independent methods, e.g., radial velocity measurements or transit detection (e.g., Silvotti et al. 2014b). These planetary candidates raise important questions that planets could survive during the engulfment in their host stars at the red giant phase, and this is a crucial implication to the formation of sdB stars.

Kepler also monitored several white dwarf pulsators, one hot DBV star, KIC 08626021 (see, Østensen et al. 2011a, which will be discussed in later chapters), and six ZZ Ceti stars (e.g., Greiss et al. 2016). A few pulsations have been detected in these WD pulsators from the long-term *Kepler* photometry, although all of them are very faint, typically $Kp \sim 18$ (*Kepler* magnitude), which is not suitable for ground-based observations. The high-quality, long-term photometry offers a window to investigate the mode behaviors in WD pulsators and sdB stars.

2.3.2 Amplitude and frequency modulations related to nonlinear resonance

Some achievements to characterized the mode behaviors in some pulsating stars have been reported recently (e.g., Breger & Montgomery 2014), by exploiting the long-term high-quality photometric data from *CoRoT* and *Kepler*. Degroote et al. (2009) tentatively applied the nonlinear resonant mode couplings to interpret the high-quality photometric data obtained on the β Cephei star HD 180642, as mode interactions may occur between 11 independent modes and their 33 linear combination frequencies. *Kepler* is a more powerful instrument to study such nonlinear behaviors of pulsation modes, compared to *CoRoT*, with bigger aperture in diameter, longer observational duty. An example of the exploitation of *Kepler* photometry is the mode behaviors in the δ Scuti star, KIC 5892969, which had been continuously observed by *Kepler* for four years (Barceló Forteza et al. 2015). The three highest modes in that star accumulate energy (amplitude growing) slowly then dissipate it (amplitude decreasing) rapidly, a phenomenon similar to the modes in parametric resonance (illustrated in Figure 1.4). Furthermore, as more than one thousand signals appear above the detection threshold, there are several different kinds of linear combinations which have a relationship with those three highest amplitude frequencies, e.g., $\omega_1 \sim \omega_2 + \omega_3$. There are several other modes with amplitude high enough to investigate using the same method to the three highest amplitude modes in that star. This could be the signature of the parametric resonance $\omega_1 \sim \omega_2 + \omega_3$ where the parent mode transfer energy into the child modes (see, e.g., Moskalik 1985). The direct resonance of $\omega_1 \sim \omega_2 + \omega_3$ was reported in the fast rotating δ Scuti star KIC 8054146 with about 928 days *Kepler* data (Breger & Montgomery 2014). They found that the amplitudes of some linear combination frequencies are at least three order higher of magnitude than the "normal" ones, which may need nonlinear resonant mode coupling to interpret such large amplitude ratios between the parent and child modes. With the variations in amplitude and phase, they also distinguish which modes are parent and child. All the above examples are related to the three modes resonance $\omega_1 \sim \omega_2 + \omega_3$, adiabatic resonant mode couplings (e.g., Dziembowski 1982).

The amplitude variations of pulsation modes also attracted the interest of the compact pulsator community (KASC working group 11) [1]. A prevailing method of sliding Fourier transformation for the photometric light curves has been adopted, a method to illustrate amplitude stability of oscillation mode in general, see, e.g., Figure 1 in Zong et al. (2015). Østensen et al. (2014a) report irregular amplitude and phase variations in a short period sdB star KIC 2991276, as shown in Figure 2.9. The near continuous light curves of ~ 1000 days was divided into pieces with time intervals of 20 days. The amplitudes sometimes increase up to 1.4 % for a short time

1. KASC : *Kepler* Asteroseismic Science Consortium. Link : http ://astro.phys.au.dk/KASC

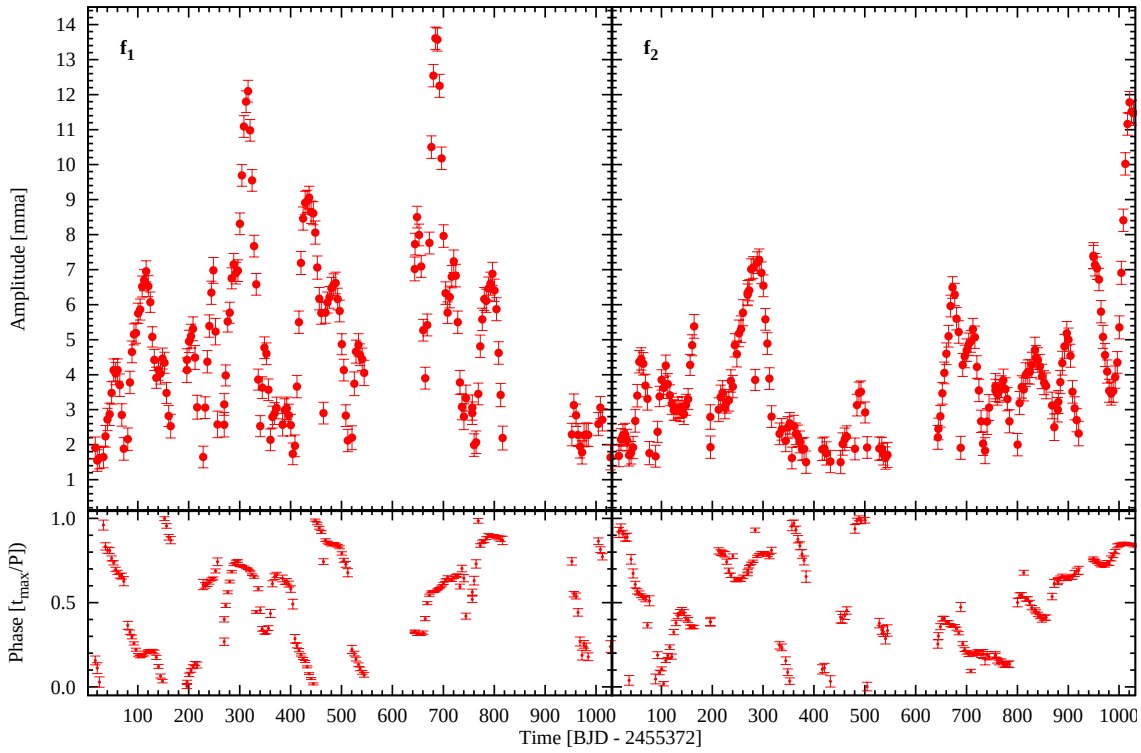

FIGURE 2.9 – Example of continuous amplitude (upper) and phase (lower panels) variations of two modes with highest amplitude in the sdB star KIC 2991276 with an time interval of 20 days (Østensen et al. 2014a).

($\sim$ 1 month) but they are below 0.7 % for most of the observations. We note that the (seeming) random phase variations may be less secure since the frequency resolution from 20 days of data cannot be sharp enough to prove that the frequencies are stable during the observations, thus, even a very tiny frequency variation could contaminate final measurements of phases over a large number of period cycles. The long period sdB star KIC 10670103 also shows amplitude variations for many significant modes, as revealed by the sliding Fourier transformation (Reed et al. 2014). Photometric data from space indeed offers the opportunity to study the amplitude variations of pulsation modes. However, the mechanisms for such amplitude variations are not clear from the above studies.

2.4 Conclusion

Compact pulsators are one of the most intensively investigated type of pulsating stars with the linear stellar oscillation theory. The κ-mechanisms drive the oscillations in both white dwarf and hot B subdwarf stars. They can be well probed by the technique of asteroseismology, providing accurate fundamental parameters, e.g., mass, effective temperature and surface gravity. Measuring rate of period change of pulsations could provide a chance to obtain the cooling rate in white dwarf stars associated with neutrino emissions, based on observations over a time baseline of decades. This method can also be applied to the sdB stars. However, many sdB and WD stars seem to have amplitude variations on timescale of days, months, or even years. The nonlinear resonant mode couplings may be the cause for such amplitude modulations, and indeed it was proposed almost at the time when the nonlinear theories began and developed.

Those amplitude modulations in oscillation modes may also have nonlinear contributions on the frequencies of the modes, thus, a varying frequency could jeopardize any attempt to measure the true rate of period change in compact pulsators. The problem whit testing the nonlinear theories from the observations on compact pulsators is that the photometry from ground-based telescopes can not cover a long enough time baseline due to time allocation, constraint from weather conditions, and daily aliasing. The space missions fortunately offer new opportunities for such research, as revealed by the merits of space-based observations, i.e., long and uninterrupted unprecedent high-precision. Some compact pulsators from *Kepler* photometry show obvious amplitude variations.

In the next chapter, we will present details on the methods we use to analyze the *Kepler* photometry. The attention will focus the compact pulsators, in particular some of them observed by *Kepler* spacecraft for more than one year. Compact pulsators with rotation are our priority, in searching for the periodic amplitude and frequency modulations within triplets, a phenomenon predicted by the nonlinear nonadiabatic amplitude equation formalism. We, of course, also consider the amplitude and frequency variations in oscillation modes with the linear relationship near other type of resonance, e.g., $\omega_1 \sim \omega_2 + \omega_3$.

Chapter 3

Analysis of *Kepler* photometry : Methods and Tools

3.1 The *Kepler* space telescope

The *Kepler* spacecraft was launched by NASA on March 7, 2009, with the primary goal to discover Earth-size planets around other stars (Borucki et al. 2010). It also provides unprecedented high-quality photometric data that are well suitable for asteroseismology (Gilliland et al. 2010). *Kepler* was initially planned for 3.5 years, and extended with another 4 years, thanks to the great success from its photometry. However, it lost a second reaction wheel on May 11, 2013, which abruptly stopped its operation. Fortunately, a new operating mode named *K2* (*Kepler*'s Second Light) has been approved by NASA, using the two reaction wheels left on the telescope with the help of light pressure to point the field of view (Howell et al. 2014).

Kepler mounts a Schmidt camera with a 0.95-meter lens feeding a 1.4-meter primary mirror. Its focal plane is covered by an array of 42 CCDs each having 2200×1024 pixels, 95 megapixels in total. The photometer use one broad bandpass, from 420 to 900 nm, containing most of the optical spectrum. For a Sun-like star with $m_V = 12$ (magnitude in V band), the photometric precision is 20 ppm with a 6.5-hour integration for *Kepler*, aiming at stars with brightness in the range of 9–16th magnitude. The spacecraft orbits the Sun in order to avoid the effects from Earth such as Earth occultation, stray light and gravitational perturbations.

Kepler continuously pointed its field of view (FOV) fixed at a region in the Cygnus constellation, centered on R.A. = 19h 22m 40s and Dec. = $+44° 30' 00''$, except when the satellite downlinked data to the ground-based control center. Figure 3.1 shows the *Kepler* FOV of each of the 21 CCD modules (each with two 2200×1024 pixel CCDs) [1]. Each module is 5 square degrees, 105 square degrees in total. In this region, the number of stars is large and the effects from the Sun can be avoided, thus it allowed *Kepler* to continuously monitor more than 100 000 stars simultaneously. Furthermore, this region can also be well studied with ground-based follow-up observations. Note that about half of the 15 stars in the FOV brighter than $m_V = 6$ fall in the aligned gaps between the CCD modules.

There are two exposure modes for the *Kepler* photometric data, the short-cadence (SC) mode, with exposure time of ~ 1 minute, and the long-cadence (LC) mode, with exposure time of ~ 30 minutes. The data from the *Kepler* spacecraft are archived and publicly accessible in the Multimission Archive at STScI (MAST) [2]. These data are divided by quarters (Q_n, or seasons) because the spacecraft needed to roll on its pointing axis four times every *Kepler* year (372.5 days) to maintain its orientation. During the *Kepler* lifetime, it almost completed 17 quarters

1. http ://kepler.nasa.gov/Science/about/targetFieldOfView/
2. http ://archive.stsci.edu/kepler/

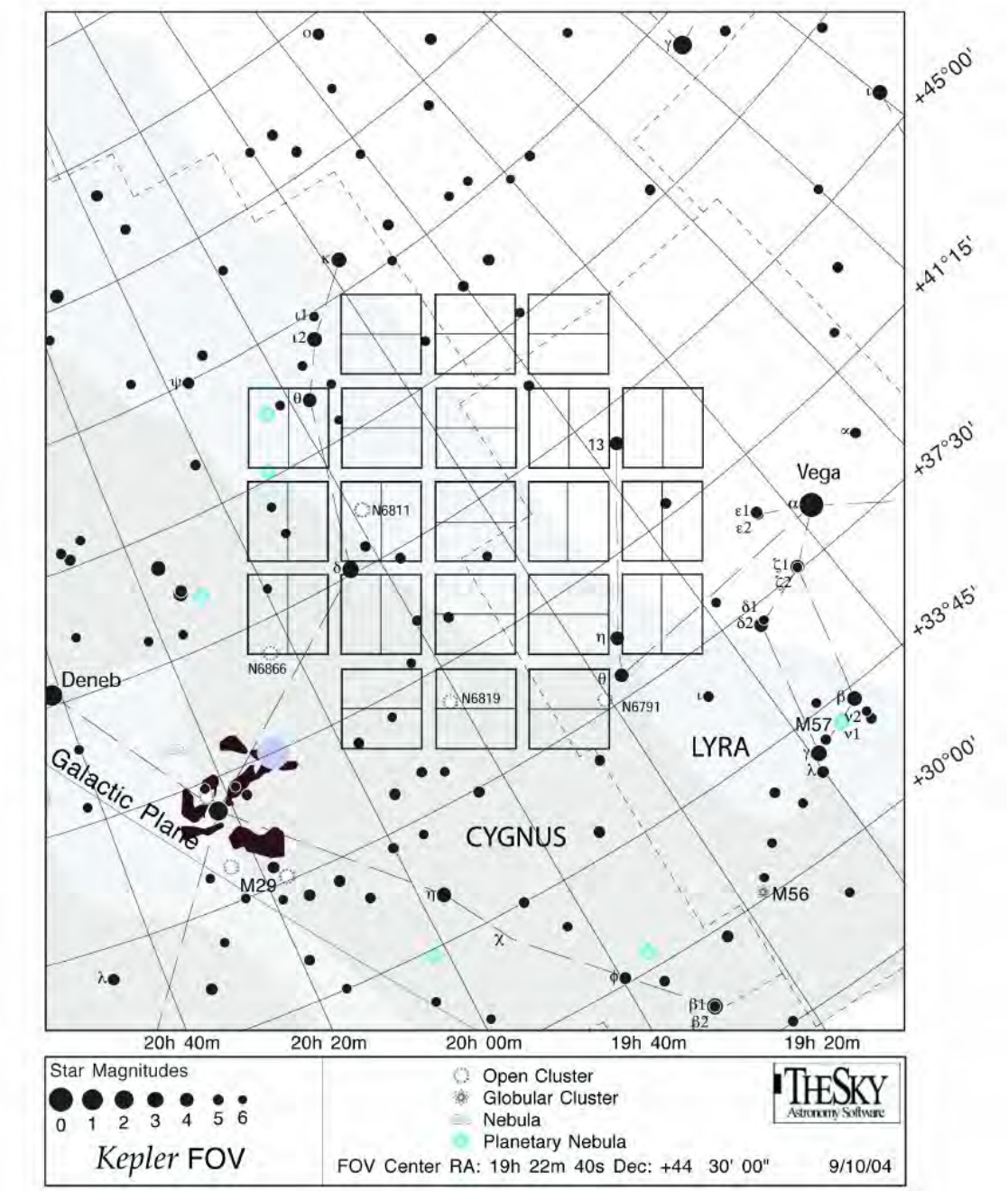

FIGURE 3.1 – The *Kepler* FOV consists of 21 CCD modules with each module of 5 square degrees, 105 square degrees in total. Credit : NASA/*Kepler* Mission.

of observations, and each quarter has a time length of about 90 days. The SC mode data are also divided by sub-quarters (or month) as $Q_{n.m}$ where the subscript $n \in (1, 2, ..., 17)$ and $m \in (1, 2, 3)$. The *Kepler* Input Catalog (KIC) is the premary source of objects observed by the spacecraft, containing photometric and physical information for the stars (Brown et al. 2011). The "*Kepler* magnitude" (*Kp*) is used for the brightness of KIC stars through the wide *Kepler* bandpass, which can be computed through the transformation of *SDSS* g and r band if these values are available (e.g., Brown et al. 2011).

TABLE 3.1 – Fundemetal informations of the *Kepler* compact pulsators.

KIC #	Name	R.A. (J2000)	Dec. (J2000)	*Kp*	Quarter	Type♣
02697388	J19091+3756	19h 09m 7.14s	+37 56′ 14.36″	15.391	Q2.3, Q5.1–Q17.2	V 1093 Her
02991276	J19271+3810	19h 27m 9.14s	+38 10′ 26.40″	17.423	Q2.1, Q6.1–Q11.3, Q13.1–Q17.2	V 361 Hya
02991403	J19272+3808	19h 27m 15.88s	+38 08′ 08.24″	17.136	Q1, Q5.1–Q17.2	V 1093 Her
03527751	2M1903+3836	19h 03m 37.02s	+38 36′ 12.64″	14.859	Q2.3, Q5.1–Q17.2	V 1093 Her
05807616	KPD 1943+4058	19h 45m 25.48s	+41 05′ 33.85″	15.019	Q2.3, Q5.1–Q17.2	V 1093 Her
07664467	J18561+4319	18h 56m 07.07s	+43 19′ 19.26″	16.446	Q2.3, Q5.1–Q11.3, Q13.1–Q17.2	V 1093 Her
07668647	J19051+4318	19h 05m 6.38s	+43 18′ 31.1″	15.402	Q3.1, Q6.1–Q17.2	V 1093 Her
08302197	J19310+4413	19h 31m 3.37s	+44 13′ 26.12″	16.432	Q3.3, Q5.1–Q11.3, Q13.1–Q17.2	V 1093 Her
09472174	2M1938+4603	19h 38m 32.61s	+46 03′ 59.15″	12.264	Q0, Q5.1–Q17.2	sdBV+dM⋆
10001893	2M1909+4659	19h 09m 33.41s	+46 59′ 04.16″	15.846	Q3.2, Q6.1–Q17.2	V 1093 Her
10139564	J19249+4707	19h 24m 58.2s	+47 07′ 54″	16.126	Q2.1, Q5.1–Q17.2	V 361 Hya
10553698	2M1953+4743	19h 53m 8.39s	+47 43′ 00.22″	15.134	Q4.1, Q8.1–Q10.3, Q12.1–Q14.3, Q16.1–Q17.2	V 1093 Her
10670103	2M1934+4758	19h 34m 39.94s	+47 58′ 11.7″	16.526	Q2.3, Q5.1–Q17.2	V 1093 Her
11179657	J19023+4850	19h 02m 21.95s	+48 50′ 52.59″	17.065	Q2.3, Q5.1–Q7.3, Q9.1–Q11.3, Q13.1–Q15.3, Q17.1–17.2	V 1093 Her
11558725	J19265+4930	19h 26m 34.11s	+49 30′ 29.68″	14.947	Q3.3, Q6.1–Q17.2	V 1093 Her
02437937	B5(NGC 6791)	19h 21m 02.46s	+37 47′ 09.2″	13.94	Q11.1	V 1093 Her
02438324	B4(NGC 6791)	19h 21m 12.91s	+37 45′ 51.3″	18.267	Q6.1–Q17.2	V 1093 Her
02569576	B3(NGC 6791)	19h 20m 45.19s	+37 49′ 31.54″	18.076	Q11.3, Q14.1–Q17.2	V 1093 Her
01718290	J19230+3715	19h 23m 00.68s	+37 15′ 04.48″	15.486	†Q1–Q17	BHB
04552982	WD J1916+3938	19h 16m 43.83s	+39 38′ 49.69″	17.853	Q11.1–Q17.2	DAV
04357037	J19171+3927	19h 17m 19.19s	+39 27′ 18.82″	17.979	Q16.2	DAV
07594781	J19083+4316	19h 08m 35.88s	+43 16′ 42.4″	18.21	Q16.3	DAV
08626021	WD J1929+4447	19h 29m 04.6s	+44 47′ 08″	18.46	Q7.2, Q10.1–Q17.2	DBV
10132702	J19134+4709	19h 13m 40.89s	+47 09′ 31.3″	18.759	Q15.1–15.3	DAV
11911480	J19202+5017	19h 20m 24.90s	+50 17′ 22.4″	17.631	Q12.1–12.3, Q16.1–Q17.2	DAV

Note. (♣)Dominating frequencies. (⋆)Eclipsing binary star with a long-period pulsating sdB star. (†)Only long-cadence data available.

3.2 *Kepler* compact pulsators

During the survey phase for pulsating stars, a total of 113 compact pulsator candidates were monitored by *Kepler* in order to search for oscillations in those stars (Østensen et al. 2010b, 2011b). From the survey results, one sdB candidate shows short-period, V 361 Hya type pulsations, and a total of fourteen sdB stars show long-period, V 1093 Her type oscillations, including an eclipsing binary (sdB+dM) with the hot component showing rich pulsations (Østensen et al. 2010a). Three more long-period sdB pulsators have been identified in the open cluster NGC 6791 (Reed et al. 2012; Pablo et al. 2011). Short-period oscillations haven been detected in another sdB star which was formerly identified as a short-period transient (Østensen et al. 2010b). Therefore the total number of sdB pulsators reaches up to 18, at last. Quite notably, there was no pulsating white dwarfs among these 113 compact candidates from the first survey phase of *Kepler*. The first pulsating WD star, a DBV star, was discovered about two years after *Kepler* launch (Østensen et al. 2011a). Additionally, a total of five DAV stars have been monitored by *Kepler* afterward (see, Greiss et al. 2016, and references therein). Table 3.1 gives the full list of compact pulsating stars observed by *Kepler*, including one blue horizontal branch (BHB) star. The list provides the basic information about these compact pulsators : their KIC number, name, right ascension (R.A.) and declination (Dec.) at the epoch of 2000, brightness in *Kepler* band (*Kp*), observational runs (in quarter), and their variable type.

3.2.1 Eighteen sdB pulsating stars

Most of the 18 sdB pulsators have been continuously monitored by *Kepler* for more than two years, except KIC 02437937 (one month) and KIC 02569576 (12 months). [3] In this section we provide some the details for each star, except the three sdB stars in the open cluster NGC 6791.

KIC 02697388, or *SDSS* J190907.14+375614.2, with R.A. (J2000) = 19h 09m 7.14s and Dec. (J2000) = +37 56′ 14.36″, has a mean brightness $Kp = 15.391$. It was found as a V 1093 Her star by the *Kepler* survey phase of Q2.3 (Østensen et al. 2010b), with near 40 significant frequencies. The properties from spectroscopy suggest that KIC 02697388 is a cool sdB star, with effective temperature $T_{\rm eff} = 23\,900 \pm 300$ K and low gravity $\log g = 5.32 \pm 0.03$ dex. It is one of the two sdB stars investigated with seismic models (Charpinet et al. 2011b). The optimal seismic solutions for KIC 02697388 are very similar to the atmospheric parameters derived by non-LTE models. Baran (2012) detected 148 pulsations with the extension of Q5.1–Q7.3 photometry for this star, among the pulsations a rotation period of about 45 days was obtained. KIC 02697388 has been consecutively observed by *Kepler* since Q5.1, about 39 months in total (including the survey phase Q2.3).

KIC 02991276, or *SDSS* J192709.14+381026.3, with R.A. (J2000) = 19h 27m 9.14s and Dec. (J2000) = +38 10′ 26.40″, has a mean brightness $Kp = 17.423$, effective temperature $T_{\rm eff} = 33\,900 \pm 200$ K and surface gravity $\log g = 5.82 \pm 0.04$ dex. Only one single pulsation mode at 122 s was detected in KIC 02991276 over one month (Q2.1) data (Østensen et al. 2010b). It has been further monitored by *Kepler* throughout Q6.1–Q11.3 and Q13.1–Q17.2, about 33 months in total. The entire data for this target was exploited by Østensen et al. (2014a) whose results show that two pulsation modes with the largest amplitudes display abrupt amplitude variations on a timescale of about one month, increasing up to 1.4% and sometimes decreasing completely in the noise.

KIC 02991403, or *SDSS* J192715.88+380808.2, with R.A. (J2000)=19h 27m 15.88s and Dec. (J2000) = +38 08′ 08.24″, has a mean brightness $Kp = 17.136$. The spectroscopic para-

3. Here we only denote the observations of short-cadence mode for the compact pulsators. The Nyquist frequency for the long-cadence (30 min) mode data is about 280 μHz which is lower than most pulsations detected in compact pulsators, particularly in the V 361 Hya star and white dwarf pulsators.

meters for this stars are $T_{\rm eff} = 27\,300 \pm 200$ K and $\log g = 5.43 \pm 0.03$ dex (Østensen et al. 2010b). The *Kepler* Q1 data for this star show 16 significant (g-mode) peaks and two peaks with about 10 h period which is related to the irradiation effect generated by the hot sdB star heating up the cool M-dwarf (Kawaler et al. 2010). With the extended 12-month data, Pablo et al. (2012) found evidence of non-synchronization in KIC 02991403 whose rotation period is 10.3 d, much slower than the orbiting period of about 0.4 d. This star has been continuously observed by *Kepler* from Q5.1 to Q17.2, 39 months in total.

KIC 03527751, or 2MASS J19033701+3836126, with R.A. (J2000)=19h 03m 37.02s and Dec. (J2000) = $+38\,36'\,12.64''$, has a mean brightness $Kp = 14.859$. This star was regarded as a hybrid sdB pulsators with detection of 41 g- and 3 p-mode pulsations from the one month *Kepler* survey data (Q2.3 ; Reed et al. 2010). The atmospheric parameters determined by Foster et al. (2015) are : $T_{\rm eff} = 27\,818 \pm 163$ K and $\log g = 5.35 \pm 0.03$ dex. The full data set (~ 1148 days) was studied and 251 periodicities were detected by Foster et al. (2015). From the detected multiplets, KIC 03527751 implies a differential radial rotation with 15.3 days at surface and 42.6 days in the deep interior.

KIC 05807616, or KPD 1943+4058, with R.A. (J2000)=19h 45m 25.48s and Dec. (J2000) = $+41\,05'\,33.85''$, has a mean brightness $Kp = 15.019$. It was found as an V 1093 Her star from the one month survey data (Q2.3) and 18 observed periodicities were identified with theoretical model (Van Grootel et al. 2010a). The seismic solutions provide effective temperature $T_{\rm eff} = 28\,050 \pm 470$ K and $\log g = 5.52 \pm 0.03$ dex which are similar to that from spectroscopy, $T_{\rm eff} = 27\,730 \pm 270$ K and $\log g = 5.552 \pm 0.04$. Interestingly, with the Q5.1–Q8.3 data, two small Earth-size planets are revealed from two low frequencies (Charpinet et al. 2011a). The entire data set, Q5.1–Q17.2, was exploited very recently by Krzesinski (2015) who suggested a precise rotation period of 44.9 ± 1.1 days.

KIC 07664467, or 2MASS J18560707+4319192, with R.A. (J2000)=18h 56m 07.07s and Dec. (J2000) = $+43\,19'\,19.26''$, has a mean brightness $Kp = 16.446$. Baran et al. (2016) recently derived the updated atmospheric parameters for this star, with $T_{\rm eff} = 27\,440 \pm 120$ K and $\log g = 5.382 \pm 0.019$ dex by non-LTE models. From the survey (Q2.3) data, a total of 11 g-mode frequencies were detected in KIC 07664467 (Østensen et al. 2010b). It has been observed with the spacecraft during Q5.1–Q11.3 and Q13.1–17.2. Baran et al. (2016) exploited the entire data and found that it was in a binary with orbital period of ~ 1.6 d. They also found a rotation period of 35.1 ± 0.6 d from the well resolved multiplets, which suggests that the rotation in KIC 07664467 is not synchronous with the orbit.

KIC 07668647, or 2MASS J19050638+4318310, with R.A. (J2000)=19h 05m 06.39s and Dec. (J2000) = $+43\,18'\,31.1''$, has a mean brightness $Kp = 15.402$. Spectroscopic observations for this star provide : (1) effective temperature $T_{\rm eff} = 27\,700 \pm 300$ K and $\log g = 5.50 \pm 0.03$ dex by LTE method ; and (2) an orbital period of 14.1742 ± 0.0042 d with a probably unseen white dwarf companion (Telting et al. 2014). The long-period g-mode oscillations in KIC 07668647 were discovered by Østensen et al. (2011b) with the survey (Q3.1) data. It has been continuously observed by *Kepler* from Q6.1–Q17.2, about 2.88 years in total. The entire photometric data confirmed the binarity with a orbital period 14.1666 ± 0.0019 d (Telting et al. 2014). They also derived a rotational period of about 47 d from the splitting multiplets.

KIC 08302197, or 2MASS J19310336+4413261, with R.A. (J2000)=19h 31m 03.37s and Dec. (J2000) = $+44\,13'\,26.12''$, has a mean brightness $Kp = 16.432$. Atmospheric parameters form spectroscopy provide effective temperature $T_{\rm eff} = 27\,450 \pm 200$ K and surface gravity $\log g = 5.438 \pm 0.033$ dex for this star (Baran et al. 2015a). It was identified as a V 1093 Her star from the second half survey (Q3.3) data by Østensen et al. (2011b). KIC 08302197 has been monitored by *Kepler* from Q5.1 to Q17.2, without data in Q12. The whole data set was investigated recently by Baran et al. (2015a) to search for rotation and period distribution of

pulsations. However, KIC 08302197 does not show any multiplet that may be due to either a near pole on orientation of the pulsating axis or an extremely low rotation period (probably longer than 1 000 d).

KIC 09472174, or 2MASS J19383260+4603591, with R.A. (J2000)=19h 38m 32.61s and Dec. (J2000) = +46 03′ 59.15″, has a mean brightness $Kp = 12.264$. It was recognized as the second eclipsing binary sdB+dM system (orbital period of 0.126 d) with the hot component showing oscillations from the first month (Q0) data (Østensen et al. 2010b). Spectroscopic determination of the sdB component provides $T_{\rm eff} = 29\,564 \pm 106$ K and $\log g = 5.425 \pm 0.009$ dex with the LTE models (Østensen et al. 2010b). This star has been continuously monitored by *Kepler* from Q5.1 to Q17.2, about 39 months in total. The entire data were studied by Baran et al. (2015b) who found a strong signature of the presence of a third body which is probably a Jupiter-mass planet with a period of 416 days at a 0.92 AU distance. They did not uncover any splitting multiplets in the Fourier spectrum, due to the complicated frequency structures or to a very long rotation period.

KIC 10001893, or 2MASS J19093340+4659041, with R.A. (J2000)=19h 09m 33.41s and Dec. (J2000) = +46 59′ 04.16″, has a mean brightness $Kp = 15.846$. The best estimation of atmospheric properties of KIC 10001893 is $T_{\rm eff} = 27\,500 \pm 500$ K and $\log g = 5.35 \pm 0.05$ dex (Silvotti et al. 2014a). The long period g-mode pulsations were found in this star from the *Kepler* survey (Q3.2) data (Østensen et al. 2011b). It has been continuously observed from Q6.1 to Q17.2, when *Kepler* lost its second reaction wheel. The entire data were exploited thoroughly by Silvotti et al. (2014a) who found probably three small planets orbiting the sdB star, indicated by the low frequency signals in the Fourier spectrum, which is similar to KIC 05807616. There is no multiplet detected in KIC 10001893 that may be due to a very low inclination or to an extremely long rotation period.

KIC 10139564, or J19245816+4707536, with R.A. (J2000)=19h 24m 58.16s and Dec. (J2000) = +47 07′ 53.6″, has a mean brightness $Kp = 16.126$. It was discovered as a short-period V 361 Hya star from one month Q2.1 data. One low-amplitude g-mode oscillation was also detected in its Fourier spectrum. The atmospheric parameters derived by Baran et al. (2012) are $T_{\rm eff} = 31\,859 \pm 126$ K and $\log g = 5.673 \pm 0.026$ dex, and did not find any radial-velocity variations, indicating KIC 10139564 is an isolate star. With extended observations of *Kepler*, a total of 57 periodicities were detected by Baran et al. (2012) with the 15 month photometric data (Q5.1–Q9.3), including many of multiplets. A rotation period of 25.6 ± 1.8 d was found in KIC 10139564 from the common spacing both in g- and p-mode multiplets. This target has been continuously observed from Q5.1 to Q17.2, about 39 months in total.

KIC 10553698, or 2MASS J19530839+4743002, with R.A. (J2000)=19h 53m 08.39s and Dec. (J2000) = +47 43′ 00.22″, has a mean brightness $Kp = 15.134$. It was identified as a g-mode pulsator in the survey phase (Q4.1) by Østensen et al. (2011b), and further monitored by *Kepler* throughout Q8.1–Q17.2, but without data during Q11 and Q15 when the target fell on CCD Module #3 which was dead in January 2010. Spectroscopy demonstrates that KIC 10553698 is a sdB+WD binary with orbital period of 3.6 d, and the best fit atmospheric parameters are $T_{\rm eff} = 27\,750 \pm 130$ K and $\log g = 5.452 \pm 0.020$ dex (Østensen et al. 2014b). They confirmed the binarity and found a 3.387 ± 0.014 d period with the entire photometric data. From the detected multiplets, a rotation with a 41 ± 3 d period was determined by Østensen et al. (2014b).

KIC 10670103, or 2MASS J19343993+4758117, with R.A. (J2000)=19h 34m 39.94s and Dec. (J2000) = +47 58′ 11.73″, has a mean brightness $Kp = 16.526$. A total of 28 g-mode pulsations were found in KIC 10670103 with the survey (Q2.3) data (Østensen et al. 2010b). Reed et al. (2014) determined atmospheric parameters $T_{\rm eff} = 21\,485 \pm 540$ K and $\log g = 5.14 \pm 0.05$ dex for KIC 10670103. With the 2.75 years *Kepler* (Q5.1–Q15.3) data, a very slow rotation period of

88±8 d was derived from the multiplet modes (Reed et al. 2014). This star has been continuously observed until *Kepler* lost the second reaction wheel.

KIC 11179657, or USNO-A2.0 1350-10140904, with R.A. (J2000)=19h 02m 21.95s and Dec. (J2000) = +48 50′ 52.59″, has a mean brightness $Kp = 17.065$. Spectroscopic determination for this star provides effective temperature $T_{\rm eff} = 26\,000 \pm 800$ K and $\log g = 5.14 \pm 0.13$ dex. The one month (Q2.3) data of KIC 11179657 show a similar result to KIC 02991403, ~ 10 h luminosity variations in light curves (Kawaler et al. 2010). Non-synchronization was also discovered in KIC 11179657 by Pablo et al. (2012) with 9 month extended *Kepler* data (Q5.1–Q7.3), 7.4 d rotation and 0.4 d orbit. It has been observed by *Kepler* with several segments, Q2.3, Q5.1–Q7.3, Q9.1–Q11.3, Q13.1–Q15.3 and Q17.1–17.2, 30 months in total.

KIC 11558725, or 2MASS J19263411+4930296, with R.A. (J2000)=19h 26m 34.11s and Dec. (J2000) = +49 30′ 29.68″, has a mean brightness $Kp = 14.947$. This star was classified as V 1093 Her star from the one month survey *Kepler* (Q3.3) data (Østensen et al. 2011b). Its atmospheric parameters are effective temperature $T_{\rm eff} = 27\,910 \pm 210$ K and $\log g = 5.41 \pm 0.15$ dex (Telting et al. 2012). These spectroscopic data suggest that KIC 11558725 is a binary (sdB+WD) with period of 10.05 d and confirmed by 15 month *Kepler* data, Q6.1–Q10.3 (Telting et al. 2012). They also derived a probable rotation period of ~ 45 days for KIC 11558725. This target has been continuously observed by *Kepler* since Q6.1 until the loss of its second reaction wheel.

Three pulsating sdB stars have been detected in the open cluster NGC 6791 (Pablo et al. 2011; Reed et al. 2012) . They are **KIC 02437937** (**B5**), **KIC 02438324** (**B4**) and **KIC 02569576** (**B3**) which are all long-period V 1093 Her type pulsators. **B5**, with R.A. (J2000)=19h 21m 02.46s and Dec. (J2000) = +37 47′ 09.2″, has a mean brightness $Kp = 13.94$ and was just observed for one month by *Kepler*, Q11.1. **B4**, with R.A. (J2000)=19h 21m 12.91s and Dec. (J2000) = +37 45′ 51.3″, has a mean brightness $Kp = 18.267$, which was identified as a binary, while, no pulsations has been detected in B4 until the realization of *Kepler* photometry (Pablo et al. 2011). With the six month *Kepler* data (Q6.1–Q7.3), Pablo et al. (2011) found an orbital period of 0.3984944(35) d and a rotational period of ~ 9.63 d, which means that tidal synchronization has not been reached yet in this system. B4 has been consecutively observed by *Kepler* since Q6.1 until Q17.2, 39 month in total. **B3**, with R.A. (J2000)=19h 20m 45.19s and Dec. (J2000) = +37 49′ 31.5″, has a mean brightness $Kp = 18.076$. It was observed by *Kepler* during 12 months, Q11.3, Q14.1–Q17.2. Reed et al. (2012) derived the spectroscopic properties for the three stars : B3 with $T_{\rm eff} = 24\,250 \pm 459$ K and $\log g = 5.17 \pm 0.05$ dex, B4 with $T_{\rm eff} = 24\,786 \pm 665$ K and $\log g = 5.30 \pm 0.09$ dex, and B5 with $T_{\rm eff} = 23\,844 \pm 676$ K and $\log g = 5.31 \pm 0.09$ dex

3.2.2 Six white dwarf pulsators

A total of six white dwarf pulsating stars have been observed by *Kepler*, including one DBV and five DAV stars. Only two of them have the data longer than one year, KIC 04552982 (20 months) and KIC 08626021 (~ 2 years).

KIC 04552982, or WD J1916+3938, with R.A. (J2000)=19h 16m 43.83s and Dec. (J2000) = +39 38′ 49.69″, has a mean brightness $Kp = 17.853$. KIC 04552982 was first identified as a ZZ Ceti from ground-based photometry and the follow-up spectroscopy confirmed that it was exactly in the ZZ Ceti instability strip, with $T_{\rm eff} = 11\,129 \pm 115$ K and $\log g = 8.34 \pm 0.06$ dex (Hermes et al. 2011). With the one month (Q11.1) data, seven pulsations between 800 and 1450 s were detected in KIC 04552982 (Hermes et al. 2011). It was continuously observed by *Kepler* from Q11.1 to Q17.2, 20 months in total. Bell et al. (2015) investigated the entire data set and suggests that this star probably has a rotation period of 17.47 ± 0.04 hr. They also found outbursts in the *Kepler* light curves of KIC 04552982, with significant brightness increases on a timescale of hours to a day.

TABLE 3.2 – Atmospheric parameters of the *Kepler* compact pulsators[†].

KIC #	$\log g$ (dex)	$T_{\rm eff}$ (1 000 K)	KIC #	$\log g$ (dex)	$T_{\rm eff}$ (1 000 K)
02697388	5.32(3)	23.9(3)	11179657	5.14(13)	26.0(8)
02991276	5.82(4)	33.9(2)	11558725	5.41(15)	27.91(21)
02991403	5.43(3)	27.3(2)	02437937	5.31(9)	23.844(676)
03527751	5.35(3)	27.818(163)	02438324	5.30(9)	24.786(665)
⋆05807616	5.52(3)	28.05(47)	02569576	5.17(5)	24.250(459)
07664467	5.382(19)	27.44(12)	04552982	8.34(6)	11.129(115)
07668647	5.50(3)	27.7(3)	08626021	7.91(7)	24.90(75)
08302197	5.438(33)	27.45(20)	11911480	7.94(10)	12.16(25)
09472174	5.425(9)	29.564(106)	04357037	8.11(4)	10.95(13)
10001893	5.35(5)	27.5(5)	07594781	8.11(4)	11.73(14)
10139564	5.673(26)	31.859(126)	10132702	8.12(4)	11.94(38)
10553698	5.452(20)	27.75(13)	[a]01718290	4.72(4)	22.100(344)
10670103	5.14(5)	21.485(540)			

Note. [⋆]Seismic solutions. [†]See ref. in the context. [a]Østensen et al. (2012).

KIC 08626021, or WD J1929+4447, with R.A. (J2000)=19h 26m 34.11s and Dec. (J2000) = +49 30′ 29.68″, has a mean brightness $Kp = 18.46$. The best fit of the spectrum of KIC 08626021 determines the parameters with $T_{\rm eff} = 24\,900 \pm 750$ K and $\log g = 7.91 \pm 0.07$ dex (Østensen et al. 2011a). It is the first white dwarf pulsator discovered from the *Kepler* photometry, based on one month (Q7.2) data (Østensen et al. 2011a). This star has been continuously observed by *Kepler* from Q10.1–Q17.2, nearly two years in total. As a unique object, KIC 08626021 attracted much attention by many groups (e.g., Bischoff-Kim et al. 2014). Two independent seismic models obtained two different masses for the target, a mass about $0.55\,M_{\odot}$ in Bischoff-Kim et al. (2014) and a stellar mass in the range $0.6 \lesssim M \lesssim 0.87\,M_{\odot}$ in Córsico et al. (2012). However, both the two models suggest a hotter temperature determined from models than that from spectroscopy, $\sim$ 27 300 and $\sim$ 29 550 K, comparing to the spectroscopic one $T_{\rm eff} = 24\,900 \pm 750$ K. With the nearly two year data, Bischoff-Kim et al. (2014) found a rotation period of 1.8 ± 0.4 days. They also suggest that KIC 08626021 might be a very good candidate for measuring the rate of period change of pulsations.

KIC 11911480, or KIS J19202+5017, with R.A. (J2000)=19h 20m 24.90s and Dec. (J2000) = +50 17′ 22.4″, has a mean brightness $Kp = 17.631$. The atmospheric parameters determined from the best fit of spectrum of KIC 11911480 are : $T_{\rm eff} = 12\,160 \pm 250$ K and $\log g = 7.94 \pm 0.10$ dex (Greiss et al. 2014). It was the second ZZ Ceti star in the *Kepler* field which was found by (Greiss et al. 2014) with the two quarters SC-mode data Q12 and Q16. They also detected a rotation period of 3.5 ± 0.5 days from the amplitude power spectra. An extended observations of about 50 days was conducted by *Kepler* on KIC 11911480, Q17.1 and 17.2.

Greiss et al. (2016) recently reported the discovery of three new ZZ Ceti stars in the *Kepler* FOV, which are KIC 04357037, KIC 07594781 and KIC 10132702. **KIC 04357037**, or *SDSS* J191719.16+392718.8, with R.A. (J2000)=19h 17m 19.167s and Dec. (J2000) = +39 27′ 18.82″, has a mean brightness $Kp = 17.979$. It was only observed by *Kepler* for one month Q16.2. The atmospheric parameters for KIC 04357037 are : $T_{\rm eff} = 10\,950 \pm 130$ K and $\log g = 8.11 \pm 0.04$ dex (Greiss et al. 2016). **KIC 07594781**, or KIS J1908+4316, with R.A. (J2000)=19h 08m 35.91s and Dec. (J2000) = +43 16′ 42.3″, has a mean brightness $Kp = 18.21$. It was only observed by *Kepler* for one month Q16.3. Greiss et al. (2016) determined the atmospheric parameters for KIC 07594781, that are effective temperature $T_{\rm eff} = 11\,730 \pm 140$ K and surface gravity

$\log g = 8.11 \pm 0.04$ dex. **KIC 10132702**, or KIS J1913+4709, with R.A. (J2000)=19h 13m 40.89s and Dec. (J2000) = $+47\,09'\,31.3''$, has a mean brightness $Kp = 18.759$. It was only observed by *Kepler* for three month Q15.1–15.3. The best fit of spectroscopy of KIC 10132702 obtained atmospheric parameters with $T_{\rm eff} = 11\,940 \pm 130$ K and $\log g = 8.12 \pm 0.04$ dex (Greiss et al. 2016).

Table 3.2 lists the full set of atmospheric parameters of 24 compact pulsators from *Kepler* photometry, including two short-period V 361 Hya, 16 long-period V 1093 Her, one DB and 5 DA pulsating white dwarf stars, and additionally one BHB star. All the parameters are provided by the latest spectroscopic determinations, except KIC 05807616 whose are provided by the seismic solutions. In the next section, we describe the methods and tools to exploit these photometric data, aiming at studying the mode behaviors in these stars.

3.3 Analysis of photometric data

Periodic functions, mathematically, can be written as a sum of infinite simple sinusoidal waves, which is known as Fourier transform (FT). The definition of FT for an integrable function $f(t)$ is :

$$F(\omega) = \int_{-\infty}^{\infty} f(t) e^{-2\pi i \omega t} dt, \tag{3.1}$$

where transform variable ω is the frequency, and function F is the inverse transform. However, technically, time-series photometric data cannot be obtained for an infinite time and only at a discrete time. The Discrete Fourier Transform (DFT) developed by Deeming (1975) is a straightforward method to calculate the periodogram of unequally spaced photometric data, which is widely used in asteroseismology where the stellar oscillations cause periodic luminosity variations in the light curves of pulsating stars. The DFT $F_N(\omega)$ is defined as,

$$F_N(\omega_j) = \sum_{k=1}^{N} X_k(t) e^{i 2\pi \omega_j t_k}, \tag{3.2}$$

where $X_k(t)$ in asteroseismology represents the magnitudes (or intensities) measured at the times t_k. With slight modification of periodogram as represented by equation (3.2), Scargle (1982) report that the modified periodogram is equivalent to the least-squares fitting of sine waves to the data. This new periodogram, now known as Lomb-Scargle (LS [4]) periodogram, is written as,

$$P_X(\omega) = \frac{1}{2}\Big\{ \frac{[\sum_k X_k \cos\omega(t_k - \tau)]^2}{\sum_k \cos^2\omega(t_k - \tau)} + \frac{[\sum_k X_k \sin\omega(t_k - \tau)]^2}{\sum_k \sin^2\omega(t_k - \tau)} \Big\}, \tag{3.3}$$

where the time delay term τ is defined by

$$\tan(2\pi\tau) = \frac{\sum_k \sin 2\omega t_k}{\sum_k \cos 2\omega t_k}. \tag{3.4}$$

A dedicated software, FELIX [5], was used to extract frequency content of the light curves of *Kepler* compact pulsators. The code FELIX is based on the standard prewhitening and nonlinear least squares fitting methods as indicated by equation (3.2) and (3.3). FELIX greatly ease and accelerate the application of this procedure for the spaceborne time-series photometry, see examples of the application for this software on *CoRoT* and *Kepler* data (Charpinet et al. 2010,

4. Named after Lomb, N. R. and Scargle, J. F., for their independent contributions of developing this method, see the references of Lomb (1976) and Scargle (1982).

5. Frequency Extraction for LIghtcurve eXploitation which was developed by Stéphane Charpinet.

2011b). However, before proceeding with the extraction of the frequencies, statistical tests should be done first, since the data used here have a particularly large number of measurements and long time baseline than data from ground-based photometry. The tests are mainly focused on : (1) the criterion of frequency detection threshold for the long consecutive *Kepler* photometric data, and (2) the real errors in amplitude, frequency and phase when one extracts frequencies from the light curves of these compact pulsators.

3.3.1 Defining a secure detection threshold

The ground-based observations of pulsating stars typically span over on a few days to weeks in one observational season, consisting of data sets with $\sim 10^4$ measurements (e.g., Vauclair et al. 2002). With such data sets, a prevailing rule of thumb was to consider the 4σ limit (4 times the average local noise in the power spectrum or Fourier transform) as the detection threshold above which a signal could safely be considered as real (see, e.g., Breger et al. 1993). However, with observations from space, in particular with the *Kepler* telescope, it became increasingly clear that this 4σ rule underestimates the risks of false detections resulting from statistical noise fluctuations. The reason lies probably in the very large number of data points collected during months (or years) of *Kepler* observations with a sampling time of 58.85 s in SC mode. To be specific, more than half a million frequency bins are necessary to represent the Lomb-Scargle Periodogram (LSP) of a *Kepler* SC light curve of about 2-year length. Some of the compact targets are indeed monitored by *Kepler* with a observational duration much longer than two years, e.g., KIC 10139564, 38 months, which has near a million frequency bins in its LSP. Therefore, for the *Kepler* compact stars, noise fluctuations are very likely to occur at least one time (and more) above a standard 4σ threshold in their LSPs. For this reason, the trend has been to increase the threshold to higher S/N values in somewhat arbitrary ways to avoid false detections for the *Kepler* photometry (e.g., the acceptable limit of 5σ was assumed by Bischoff-Kim et al. 2014).

Instead of adopting an arbitrary value, we quantitatively estimate what should be an acceptable detection threshold with the following procedure. Adopting the same time sampling as the observations of *Kepler* short-cadence, we randomly build 10 000 artificial light curves just containing white gaussian noise (a random normal deviate is calculated at each time point) for a representative light curves with a time length of about two years (specifically for KIC 08626021, 684 d). We then calculate the LS Periodograms of these artificial light curves, and the median values of the noise in each resulting LSPs. Here, we define $x\sigma$ as x times the median noise level. For any given S/N threshold, we then find the number of times that at least n peaks in the LSP (which by definition are just noise peaks) happen to be above the chosen limit. Then, dividing by the number of tests (10 000 here), we obtain the false alarm probability $P_n(x)$ that at least n peaks above a given S/N threshold of $x\sigma$ is due to noise fluctuations.

The results of this procedure for the probabilities P_1 to P_5 as functions of the S/N threshold are shown in Figure 3.2 where the most interesting case is P_1 (the probability that at least 1 peak due to noise is above the threshold). We clearly see that at the widely used 4σ limit, the probability to have at least one false detection P_1 is close to 1 (and ~ 0.5 to have at least 5 false detections according to P_5), confirming that the 4σ threshold is particularly unsafe in the *Kepler* case. Nevertheless, with increasing S/N, P_1 eventually decreases down to reach 0.1 (10% chance) at S/N ~ 4.58, 0.01 (1% chance) at S/N ~ 4.92 (approximately the detection threshold chosen by Bischoff-Kim et al. 2014), and less than 1 chance out of 10 000 at S/N $= 5.56$ that is the limit above which not a single peak due to noise has been found among the 10 000 random artificial light curves.

As the 24 compact pulsators have different data length, the same test was also performed again on the white noise light curve, but this time with a time baseline of three years (repre-

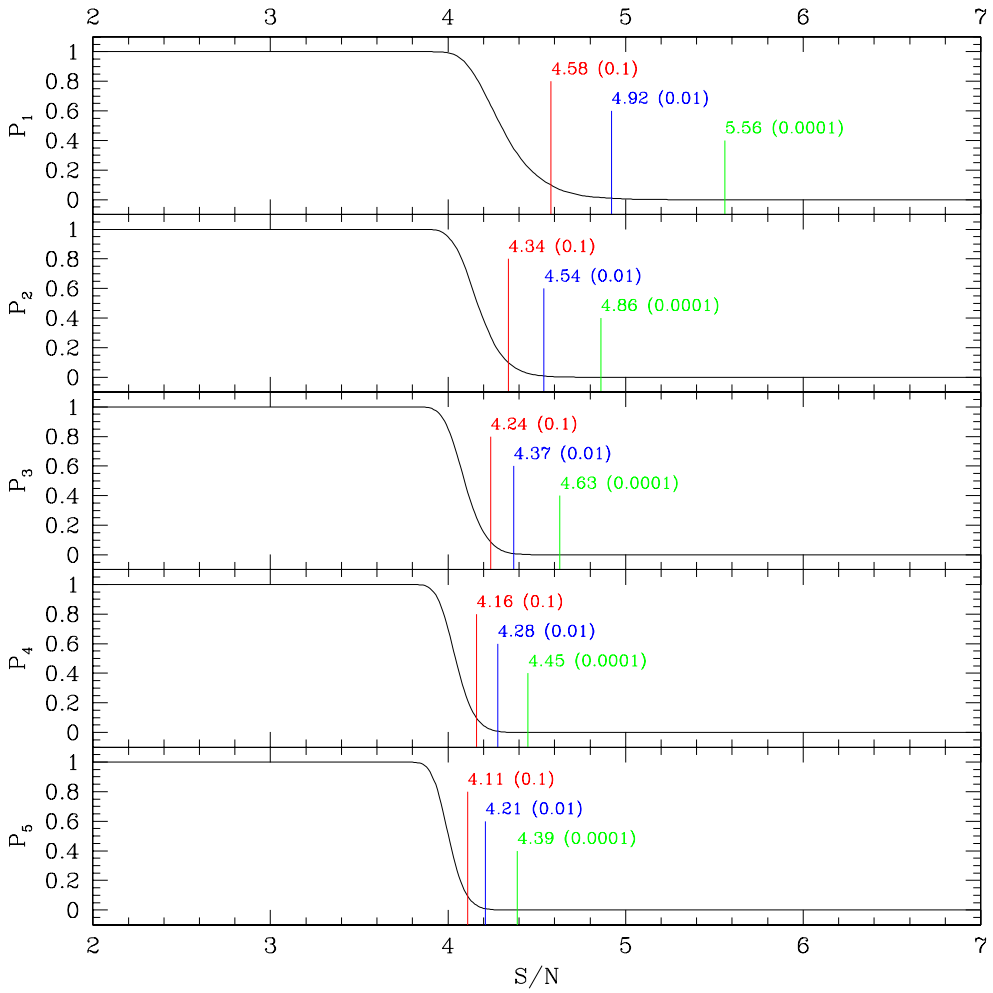

FIGURE 3.2 – False alarm probability P_n of having at least n peaks caused by noise above a given signal-to-noise ratio (S/N) threshold in the Lomb-Scargle periodogram of a $\sim$ 2-year light curve. In each of the five panels, the three vertical lines indicate, from left to right, color in red, blue and green, the S/N value corresponding to $P_n = 0.1$, 0.01, and 0.0001, respectively. The limit $P_1 = 0.0001$, meaning that the risk of having a false detection above that threshold is reduced to less than 1 event over 10 000, defines our adopted criterion which corresponds to the limit of 5.6σ.

sentative of KIC 10139564 monitored during $\sim$ 1150 d). The results are very similar to that of Figure 3.2, although the number of measurements has almost doubled. We have not done the same tests for light curve of a few months only, since they are not our priority targets in this thesis (see the details in Section 3.4). The normal 4σ limit is still valid for those stars monitored in a few months. Based on these calculations, we adopt the conservative 5.6σ threshold as the new detection criterion.

3.3.2 Testing error estimates from our prewhitening procedure

In this section, we give a brief discussion on the quantitative evaluations of the robustness of the measured uncertainties in frequency and amplitude that are provided by the standard prewhithening and nonlinear least squares fitting techniques. Montgomery & Odonoghue (1999) proposed a formalism for error estimation on frequency, amplitude and phase for least squares fitting to time series photometric data, which is widely used nowadays. However, the errors, particularly in frequency, calculated with this formalism may sometimes be underestimated for ground-based data (Montgomery & Odonoghue 1999). Since error measurements are fundamental for our analysis, this propels us to test the difference between the measured errors and real errors for the *Kepler* photometry. We have performed two types of Monte Carlo experiments : the first one is injection of 1 000 peaks with constant amplitude and another one with random amplitudes in artificial light curves including white gaussian noise.

In the tests, we first construct an artificial light curve with white gaussian noise, spanning over 200 days with a sampling of 58.85 s (exposure time of the *Kepler* short-cadence mode), which is chosen to be comparable to *Kepler* observations of about seven-month duration. This 200-d time length compromise between time resolution, frequency resolution and S/N for the sliding LS periodograms (see, e.g., the case of KIC 08626021 in Zong et al. 2016, and next chapter). Then we inject 1 000 sinusoidal signals, with constant amplitude (S/N $\sim$ 160), but with increasing frequency separated by $\sim 8.2\,\mu$Hz from one another (in order to reduce the number of harmonics and linear combinations, a few tenth μHz of random frequency shift is performed around the $8.2\,\mu$Hz seeding step), into the artificial light curve. We then perform automatically the prewhitening process of the artificial light curves with the software FELIX to obtain the measured frequencies and their amplitudes. Now we have both the injected values and the prewhitened values of the 1 000 injected signals. The normalized deviations in amplitude and frequency are defined as

$$\Delta A = \frac{A_{\rm pre} - A_{\rm in}}{\sigma_A}, \tag{3.5a}$$

$$\Delta f = \frac{f_{\rm pre} - f_{\rm in}}{\sigma_f}, \tag{3.5b}$$

where σ are the measured errors, the subscript represent the prewhitened value and the injected one, respectively. A window around each frequency is chosen and the median value of the amplitudes in that frequency range defines σ_A. The formalism given in Montgomery & Odonoghue (1999) is then used to compute the other errors, in particular σ_f. A variant of this test is also conducted by again injecting 1000 sinusoidal signals, but this time with random amplitudes (not a constant one) in the range of S/N $\in (5, 60)$. This second test allow us to check the reliability of error estimates as a function of amplitude since σ_f increases when S/N decreases.

Figure 3.3 shows the results of test for the constant amplitude case. We found that the 2-D distribution of frequency and amplitude deviations are well confined in the areas of 3σ. The separated 1-D frequency and amplitude deviations are also consistent with the Normal Distribution, $\mathcal{N} \sim (0, 1)$, as indicated by the red solid curves in Fig. 3.3 where only one or two data points are outside the $[-3\sigma, +3\sigma]$ range (the normal distribution, $\mathcal{N} \sim (0, 1)$, gives 99.73% within the $[-3\sigma, +3\sigma]$ domain). The results of the test with random amplitudes are very similar, as shown in Figure 3.4. The deviations are divided into three groups, according to their amplitudes, specifically, S/N $\in (5, 15], (15, 25]$ and $(25, 60)$, respectively. We have not found any tendency that the deviations depends on their amplitudes.

These tests suggest that the real errors are consistent with the values determined by least squares fitting method for the near consecutive photometric data provided by *Kepler*, which, therefore, can be considered robust.

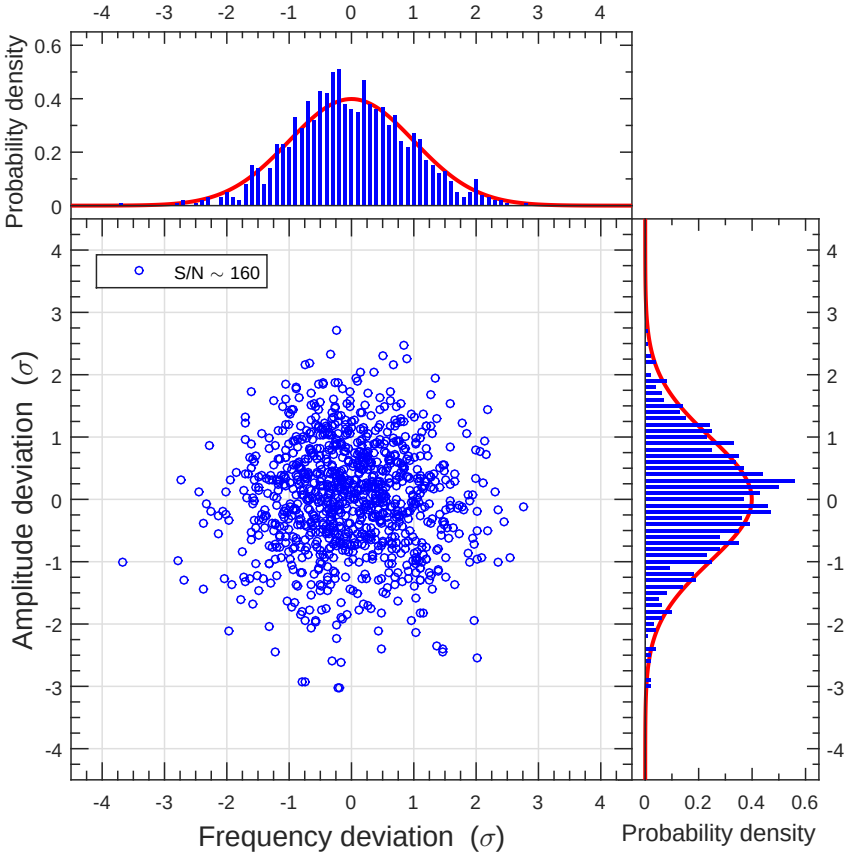

FIGURE 3.3 – The 2-D distribution of frequency and amplitude deviations between the prewhitened and the injected ones of 1 000 constant artificial signals. The deviation has been normalized by its 1σ error both in frequency and amplitude (see context for details). The 2-D distribution is projected into 1-D (frequency and amplitude) distribution in the top and right panels, respectively, to be compared with the Normal Distribution, $\mathcal{N} \sim (0, 1)$ (red solid curves).

3.3.3 Frequency contents

We obtained the light curves from either MAST or KASC, the latter archive the photometric data of pulsating stars from *Kepler* observations. As is standard, these data were reduced through the *Kepler* Science Processing Pipeline (Jenkins et al. 2010). In practice, we only concentrate on the continuous data and leave the data in discovery phase alone for most stars since those one month data usually present a large time gap in the assembled light curves. There are three types of data available in the archive, the raw fluxes, the corrected fluxes and the fluxes in pixels. The raw fluxes are just calibrated for instrumental effects, bias, flat field and cosmic rays, the corrected fluxes also consider the on-board systematics and flux excesses (contamination from nearby stars), and the pixel fluxes can be used to check for where the flux modulations comes from, either from the target itself or from a nearby stars, when the field is crowded (e.g., Charpinet et al. 2011a). Here we mainly consider the corrected data (and the raw and pixel data if/when they are needed), which are sufficient for investigating the amplitude and frequency variations of the pulsations. Tests show that the main difference between these raw data and corrected data occur in the measured amplitudes, but has no noticeable incidence on

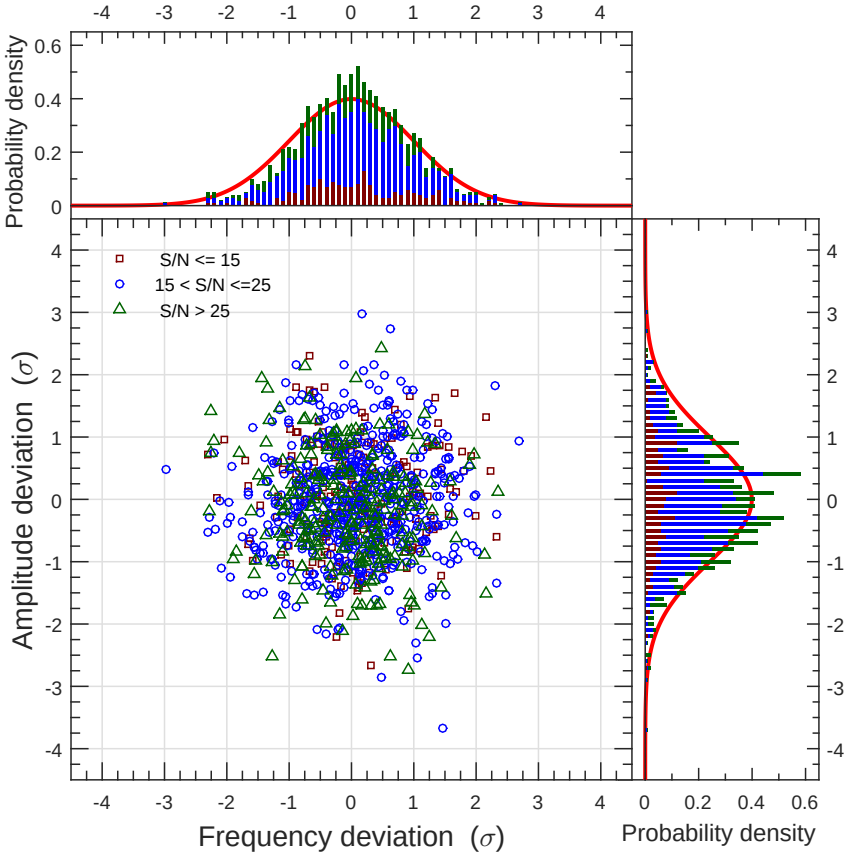

FIGURE 3.4 – Same as Figure 3.3 but for 1000 modes with random amplitude. These injected modes are divided into three groups of S/N in the ranges $\in (5, 15], (15, 25]$ and $(25, 60)$, respectively (represented by three different symbols and colors, the latter are also adopted in the 1-D distribution).

the extracted frequencies and the general trends of the amplitude modulations (the modulations are variations relative to the mean amplitude).

Before we extract frequencies from the Fourier transform (prewhitening) on the obtained light curves, we perform a six-order polynomial fit on each quarter light curve individually to remove residual long-term trends whose effects may appear as very low frequencies (typically $< 1.5\mu$Hz) in the amplitude spectrum. We, of course, inspect every polynomial fits to avoid removing the periodic signals such as that caused by beaming effects in binaries (an orbital period of ~ 10 d induces a stable $\sim 1\mu$Hz peak). These intrinsic physical signals are persistent through different quarters, while, long-term trends by instrumental effects have various behaviors. Consequently, they are easily identified. Then a running 3σ clipping filter is applied to the light curves in order to remove data points that differ significantly from the local standard deviation. It is assumed that these few data points are caused by noise fluctuations. This later operation decreases the overall noise level very slightly and affect only a few $(\sim 10-100)$ points among the $\sim 44\,000$ ones (for 30 d observations in short-cadence mode). After these procedures are done, we perform frequency prewhitening on the obtained light curves.

The Lomb-Scargle Periodogram of KIC 07664467 is taken as representative example, as shown in Figure 3.5. The $\sim$ 3-year observations give a resolution in frequency as sharp as

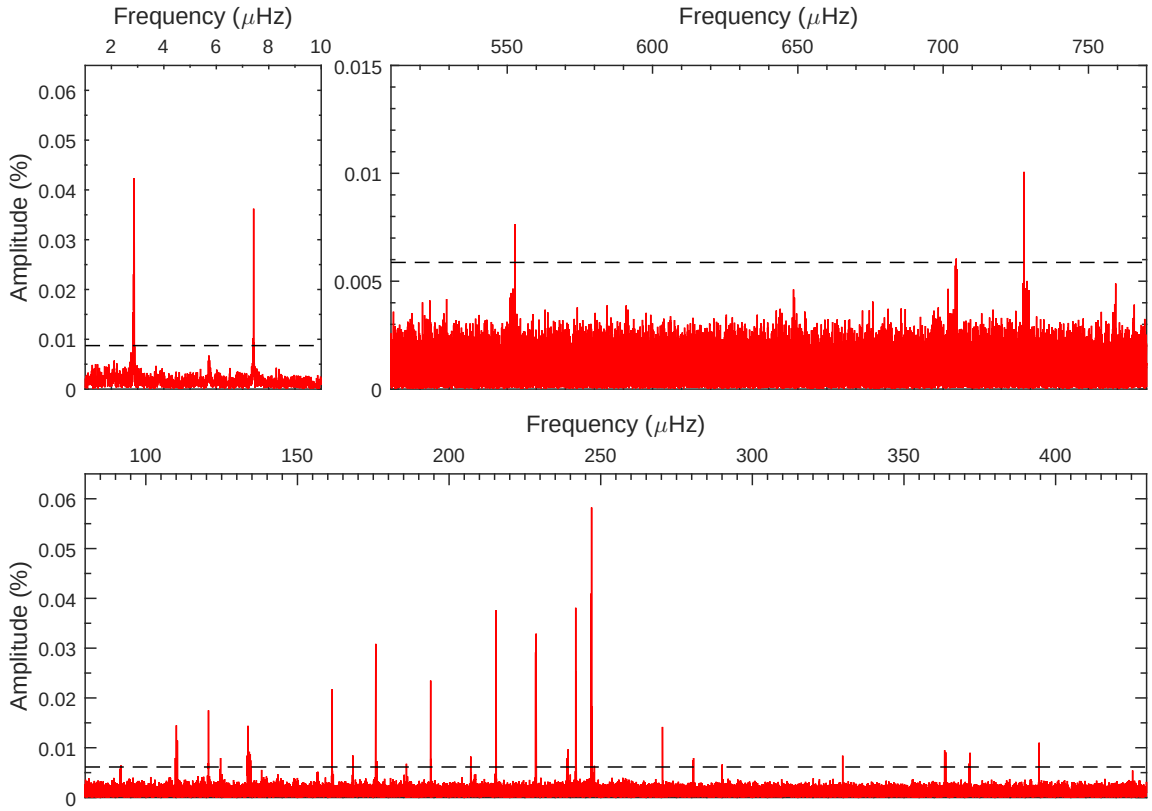

FIGURE 3.5 – Lomb-Scargle Periodogram (Amplitude in percent of the residual of the mean brightness v.s. frequency in μHz) of the *Kepler* light curve obtained on KIC 07664467. *Top-left panel* : Two low frequencies. *Top-right panel* : The frequency region of 500–770 μHz where several pulsations are found. *Bottom panel* : The represented range where main peaks were detected. The dashed horizontal lines denote our 5.6σ threshold.

0.01 μHz and a noise level of $\sim$ 11 ppm (parts per million) on this *Kp*=16.45 star, that is far beyond the ability of ground-based observations. We note that most *Kepler* sdB stars can reach such a high precision and sharp resolution. The pulsations are all found in the *g*-mode region 80–780 μHz, corresponding to pulsation periods of hours. The main frequencies are found in the frequency region of 100–400 μHz (see bottom panel of Figure 3.5), where the highest peak has a very low amplitude of $\sim$ 0.6 ppt. Additional two low frequencies are found in the frequency region of 2–8 μHz, where the peak at $\sim$ 7.4 μHz clearly represents the flux variations caused by binarity, corresponding to a 1.56 d orbiting period. The signal near 2.84 μHz shows a broad structure and amplitude variations that can not be associated with the binarity effects. Baran et al. (2016) suggest that this low frequency might be induced by instrumental effects.

During the prewhitening process, we adopt the 5.6σ detection threshold to extract frequencies. In practice, we push the limit down to 5σ to include also suspected frequencies in the list. Figure 3.6 shows 32 identified frequencies with amplitudes above 5.6σ noise from the 38-month light curve of KIC 02991403. All the frequencies are found in the 80–400 μHz frequency range, which agrees well with the result of Pablo et al. (2012), except 4 low-amplitude frequencies that were not detected in their analysis. We note that the data used here are about three times larger than theirs. Five of their (low amplitude) peaks are not detected in our results. This slight difference suggests that some the different frequencies migth be noise fluctuations instead of intrinsic signals of the star. From the residual LSP curve in Figure 3.6, it is clear

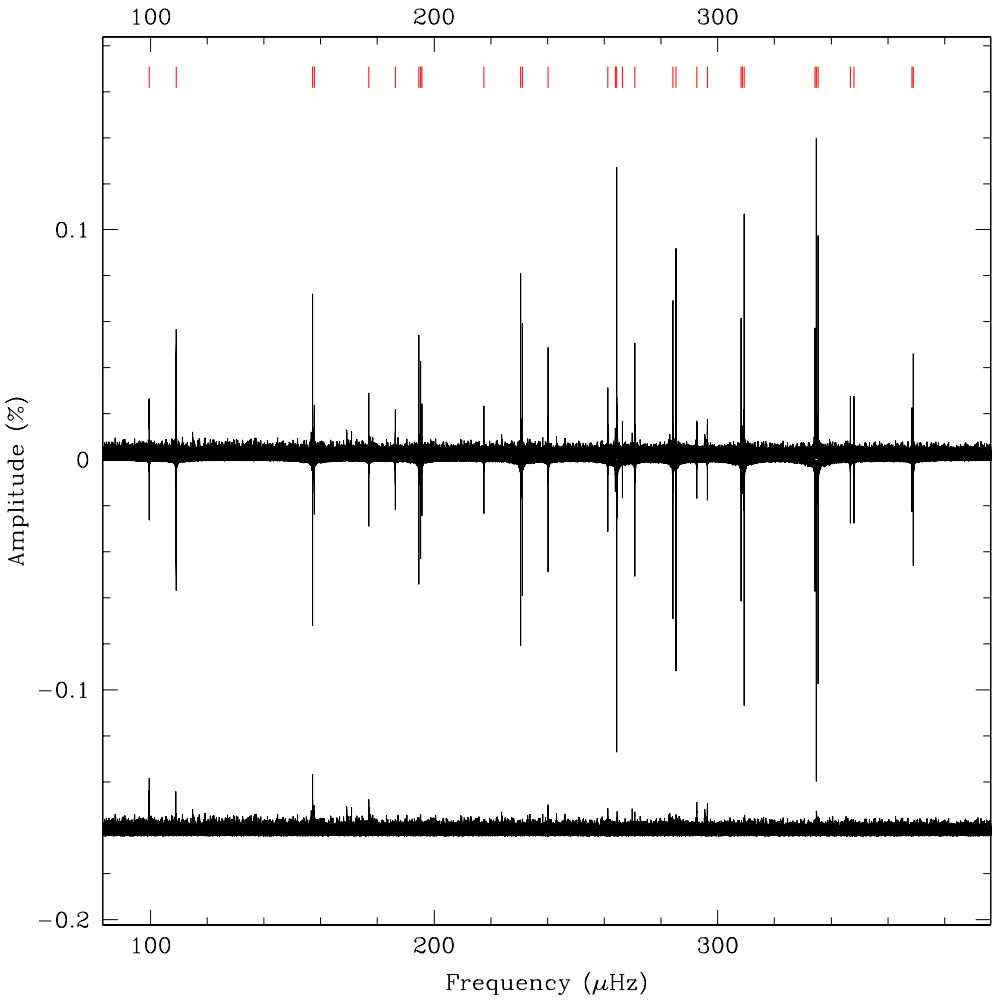

FIGURE 3.6 – Lomb-Scargle periodogram in the frequency range of 80–400 μHz where the pulsations are found in KIC 02991403. The constructed LSP based on the 32 frequencies (indicated by the red solid vertical segments) is shown upside down. The downward curve is the residual LSP (so-called noise) after substracting all the 32 frequencies. Note that there are still several peaks (outstanding in the noise) whose position are very close (on the order of the frequency resolution 0.01 μHz) to the substracted frequencies.

that there are still several outstanding peaks in the noise after frequency prewhitening. These outstanding peaks are very near to the around substracted frequencies, with frequency spacing of $\sim$ 0.01 μHz. This suggests that some signals in the light curve can not be prewhitened by pure sinusoidal waves, indicating their frequencies and amplitudes are varying. These side peaks around the main prewhitened ones may contain important information on variations associated with the main peaks. However, the frequencies, completely removed by one sinusoidal fitting, have a stable behavior : constant amplitude and frequency. We finally mention that there are some instrumental artefacts in the entire LSP (0–8500 μHz), which are well documented and can easily be recognized.

3.3.4 Stellar rotation

Equally spaced frequencies are expected as a consequence of slow stellar rotation in a pulsating star. Rotation will lift an ℓ nonradial mode into $2\ell + 1$ components (see Section 1.2 for details). The multiplet frequencies themselves are in condition of resonance, e.g., triplet modes being the $2\omega_0 \sim \omega_1 + \omega_2$ resonance. Therefore, we naturally focus on the detection of the rotational multiplets in these compact stars. Thanks to the high-quality and long-duration observations offered by *Kepler*, the sharp frequency resolution and low-noise level in Fourier transform make it possible to detect many multiplets in the *Kepler* compact stars. Figure 3.7 shows an example of rotational multiplets in KIC 11179657. We have detected four well formed triplets with frequency spacing of $\sim 0.8\,\mu$Hz, indicating a rotation period of 7.4 days. They are near 195.725, 284.629, 308.657 and 337.174 μHz, and the retrograde component in the last triplet has a 4.6σ amplitude (the prewhitened frequencies at the exactly right position). All the triplets have been shifted to the position relative to the central components. The window aliases in the LSP come from the fact that KIC 11179657 was observed by *Kepler* with a break time of one quarter every three quarters, see the observation log in Table 3.1. Pablo et al. (2012) detected only two complete triplets with 9 months data, while, ours are based on about 2.25 years data, with a lower noise level and sharper resolution. It is interesting that all the four triplets show the same frequency mismatch, $\sim 0.02\,\mu$Hz ($\delta\omega = 2\omega_0 - \omega_- - \omega_+$), which is possibly the effect induced by the second order of stellar rotation (e.g., Charpinet et al. 2008).

Table 3.3 lists the currently available information on stellar rotation and orbital periods in *Kepler* compact pulsators. Rotational periods and orbital periods are derived based on the entire *Kepler* photometry, typically from Q5.1 to Q17.2 (see exact observational duty for each case in Table 3.1). Note that we take the rotational and orbital periods in the literature for the stars formerly studied based on the (near) entire *Kepler* data set because those values are not significantly different from ours. For most sdB stars, they rotate with periods of the order of days to months, from ~ 6 (KIC 02991403, the shortest) to ~ 90 days (KIC 10670103, the longest). Nine of them are rotating at periods of about one months, indicating that they are typically slow rotators. Three of them, KIC 08302197, KIC 09472174 and KIC 10001893, are not detected with multiplets in their LSPs, which indicates that these targets may have a very low inclination angle or an extremely long rotation period ($P_{\rm rot} \gtrsim 1000$ d). We have not found any multiplet in B5 in NGC 6791 resulting that this star was monitored just with one month duration. We have detected several "multiplets" in B3 but the frequency spacing $\sim 0.1\,\mu$Hz is just about twice of the frequency resolution $\sim 0.04\,\mu$Hz, suggesting a possible rotation period of ~ 110 days. We found that the rotation in white dwarfs are a bit faster than that in sdB stars, with period on timescale of a day. Rotation has not been detected in the three newest WD pulsators, KIC 04357037, KIC 07594781 and KIC 10132702, due to, possibly, the short observational time baseline. Eight of 18 sdB stars are found in binary systems which is consistent with the high binary fraction (e.g., Maxted et al. 2001). It is interesting that the orbital periods are all much faster than the rotating period in these sdB stars if they are found in the binary system.

3.3.5 Sliding Lomb-Scargle periodogram method

This section discusses a prevailing method to analyze the *Kepler* photometry, sliding Fourier transform (sFT, or time frequency dynamic diagram). One can analyze the time variability of modes with the sliding periodogram, aiming at characterizing the amplitude and frequency modulations. Our software FELIX can compute sliding Lomb-Scargle periodograms (sLSP, no significant difference from sFT) of the entire *Kepler* photometry (e.g., Zong et al. 2016). This technique consists of constructing time-frequency diagrams by filtering in only parts of the entire light curve as a function of time. The sLSP shows the time-averaged values of any given

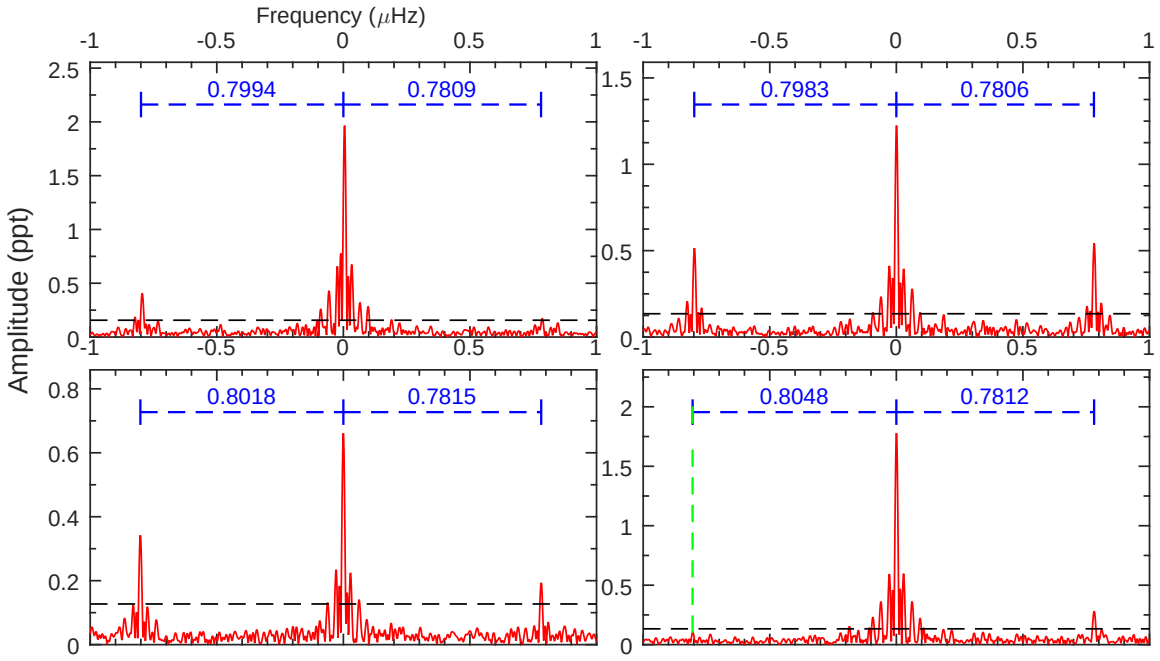

FIGURE 3.7 – Rotationally splitting triplets in KIC 11179657. All the triplets are shifted to the positions of central components and they are equally spaced with $\sim 0.8\,\mu$Hz. The dashed horizontal (black) line represents the 5.6σ threshold. The vertical segments (blue) indicate the prewhitened frequencies. The green vertical segment and dashed line denotes the component with S/N of 4.6 (at the exactly right position).

TABLE 3.3 – Rotation and binarity of compact pulsators from *Kepler* photometry.

KIC #	$P_{\rm rot}$ (d)	$P_{\rm orb}$ (d)	KIC #	$P_{\rm rot}$ (d)	$P_{\rm orb}$ (d)
02697388	~ 45	···	11179657	7.37	0.394
02991276	6.3	···	11558725	~ 45	10.04
02991403	10.54	0.44	02437937	···	···
03527751	15.3–42.6*	···	02438324	~ 9.63	0.4
05807616	44.9(1.1)	···	02569576	···	···
07664467	35.1(0.6)	~ 1.6	04552982	0.73	···
07668647	~ 47	14.17	08626021	1.75	···
08302197	···	···	11911480	3.5(5)	···
09472174	···	0.126	04357037	···	···
10001893	···	···	07594781	···	···
10139564	25.6	···	10132702	···	···
10553698	41(3)	3.387(14)	†01718290	~ 100	···
10670103	88(8)	···			

Note. $^{(\star)}$Differntial rotation. $^{(\dagger)}$Østensen et al. (2012).

mode and gives an overall view of the amplitude and frequency variability. Therefore, the sLSP greatly accelerates our search for some interesting mode behaviors in amplitude and frequency, in particular for periodic mode modulations. In practice, for each given star, we choose a good compromise between the width of filtering window and the length of time steps when the

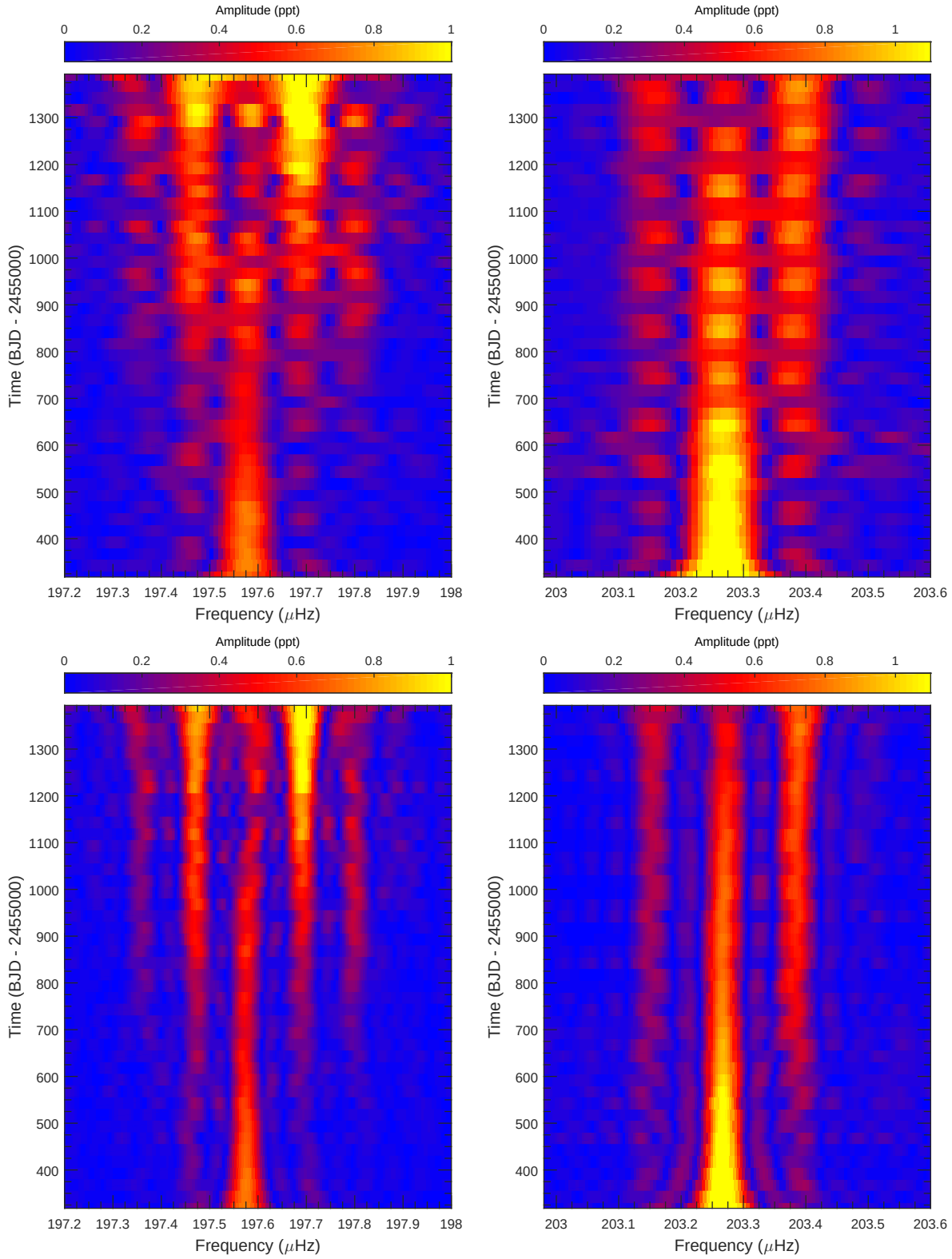

FIGURE 3.8 – Sliding LSPs of the 197.6 μHz quintuplet and the 203.3 μHz incomplete quintuplet with different filtering windows in KIC 10670103. The color scale represents the amplitude and the colorbar is shifted to the up side of each panels. As a comparison, the two top panels are built with window width of 150 d and the two bottom panels are built with a wider window, 300 d, which, obviously, gives a different frequency resolution.

filtering window is sled along the entire light curve, ensuring a good time resolution (to obtain continuous amplitude and frequency modulations), frequency resolution (to resolve the close peaks in each calculated LSP), and enough signal-to-noise (to insure a good detection of signals). Once the interesting modulations have been spotted, we extract the frequencies (using the standard techniques) in various parts of the light curve with a similar time length of the width of the filtering window and time steps of one month. This latter approach provides a measurement of the frequencies and amplitudes at a given time, along with the associated errors.

Figure 3.8 shows an example of sliding Lomb-Scargle periodogram that illustrates the resolution difference when the window width changing. The sLSP are concentrated on two multiplets, the quintuplet at $\sim 197.55\,\mu$Hz and the incomplete quintuplet at $\sim 203.26\,\mu$Hz, in KIC 10670103. To resolve correctly the splitting quintuplets with frequency spacing $\Delta\omega \sim 0.11\,\mu$Hz, we need a frequency resolution at least as sharp as $\Delta\omega/1.5$ corresponding to a time length of about 130 days. Therefore we choose the filtering window with the width of 150 d and time steps of 25 d, as a first step, and the results are shown in the two top panels of Figure 3.8. We clearly see the amplitude modulations in the components of the two quintuplets, while, at this frequency resolution, the frequency modulations (typically very small, less than a few percent μHz) can not be distinguished. Again, the amplitude modulations show long-term variations that are longer than 1 000 days since the amplitude of different modes increase or decrease during most of the observations. Thus, there is no confusion if we apply a wider filtering window on the entire light curve to acquire a higher frequency resolution (the sLSP gives an averaged LSP at a given time and the short timescale amplitude and frequency modulations may have an cancellation effect in a very wide window). The two bottom panels of Figure 3.8 show the results of sLSP on the same two quintuplets but with a window width of 300 d. This window definitely gives a shaper resolution and now we clearly see how the amplitude grows and withers in the components.

3.4 The priority targets and some preliminary results

We have presented the procedures to analyze the *Kepler* data in the last section, now we discuss our criteria to select the priority targets among the 18 sdB stars and 6 white dwarf stars. Then, we provide several examples of amplitude and frequency variations in rotational multiplet modes in three sdB stars. Various types of mode behaviors suggest that some modes are stable and some are not, which is associated with the prediction of nonlinear mode coupling mechanisms where the involving modes have three main regimes (see Section 1.4.2 for details).

3.4.1 Target classification

The 24 compact pulsators constitute a rather massive data set, in which one assembled light curve may contain up to one million points for a star continuously monitored with a duration of ~ 2 years in short-cadence. A blind investigation of the 24 stars would cost a huge amount of time. Thus, we first built a list to categorize three different groups of targets after extracting the frequency contents from the assembled light curves : class A, the first priority targets ; class B, targets with medium priority ; and class C, the least interesting stars. This categorization is based on the length of continuous observations (enough time resolution), the number of multiplets (to maximize chance to see various mode behaviors) and the rotation period (enough frequency resolution).

Table 3.4 lists the three categories of *Kepler* compact stars, where there are eight pulsators in each category. We first concentrate on the 8 class A stars in which 7 targets have been observed more than two years, except KIC 08626021 (24 month). The 8 stars typically rotate

TABLE 3.4 – The privilege of *Kepler* compact pulsators.

Class	KIC #				
A	02991403	03527751	07664467	07668647	10139564
		11179657	02438324	08626021	
B	02697388	05807616	10553698	10670103	11558725
		02991276	04552982	01718290[†]	
C	08302197	09472174	10001893	02437937	02569576
		04357037	07594781	10132702	

Note. [(†)]BHB, Østensen et al. (2012).

at a period on the order of days and present at least three multiplets. These properties and observational conditions meet our criteria to be good candidates for the search of evidence of nonlinear mode interactions occurring between multiplet modes. We also pay attention to the modes with a relationship of linear combinations, that may indicate nonlinear resonance with three mode coupling of $\omega_1 \sim \omega_2 + \omega_3$. We provide examples of preliminary results for three stars whose multiplet modes show amplitude and frequency modulations in the next section, KIC 02438324, KIC 03527751 and KIC 07668647. Among these 8 class A stars, two stars are particularly interesting after we have a general view on all the mode behaviors in these stars, which are KIC 08626021 and KIC 10139564. The unique *Kepler* DBV star, KIC 08626021, will be discussed in detail in Chapter 4. This star is also the longest observed white dwarf star so far with a duration of about two years. Chapter 5 will be dedicated the interesting results of KIC 10139564, a short-period pulsating star, which is also the longest observed *p*-mode dominating pulsating sdB star so far with a duration of more than three years. Stars in class B are found for the second priority targets since their rotation is either very slow (need for a wide filtering window to resolve the splitting frequencies and this reduce the time resolution in general), or they show only a few multiplets in their frequency spectra, or they have already been studied by others, e.g., KIC 10670103 (Reed et al. 2014). The class C stars typically show no rotational splitting multiplets, e.g., KIC 08302197, KIC 09472174, and KIC 10001893, or have only short duration observations : KIC 02437937, KIC 02569576, KIC 04357037, KIC 07594781 and KIC 10132702. However, these may become important targets if their modes show short timescale mode interactions, e.g., on a timescale of about a day. However, as time is limited, we follow the order of the list in general.

3.4.2 Examples of some preliminary results

We provide some preliminary results for three stars whose multiplet modes show amplitude and frequency modulations from the sliding LSP. These sLSPs only give us an overall view of the behaviors occurring for a given mode. More precise amplitude and frequency variations can be obtained with the technique of prewhitening parts of light curves (see, e.g., Chapter 4), which has not been applied to these three stars yet. With these amplitude and frequency variations, we can characterize the mode behaviors and associate them with the predicted regimes from the nonlinear stellar pulsation theory : exhibit either periodic or irregular modulations, or remain constant.

Figure 3.9 shows the amplitude and frequency modulations observed in two incomplete quintuplets and three triplets in KIC 07668647. The sLSPs around each multiplets are provided

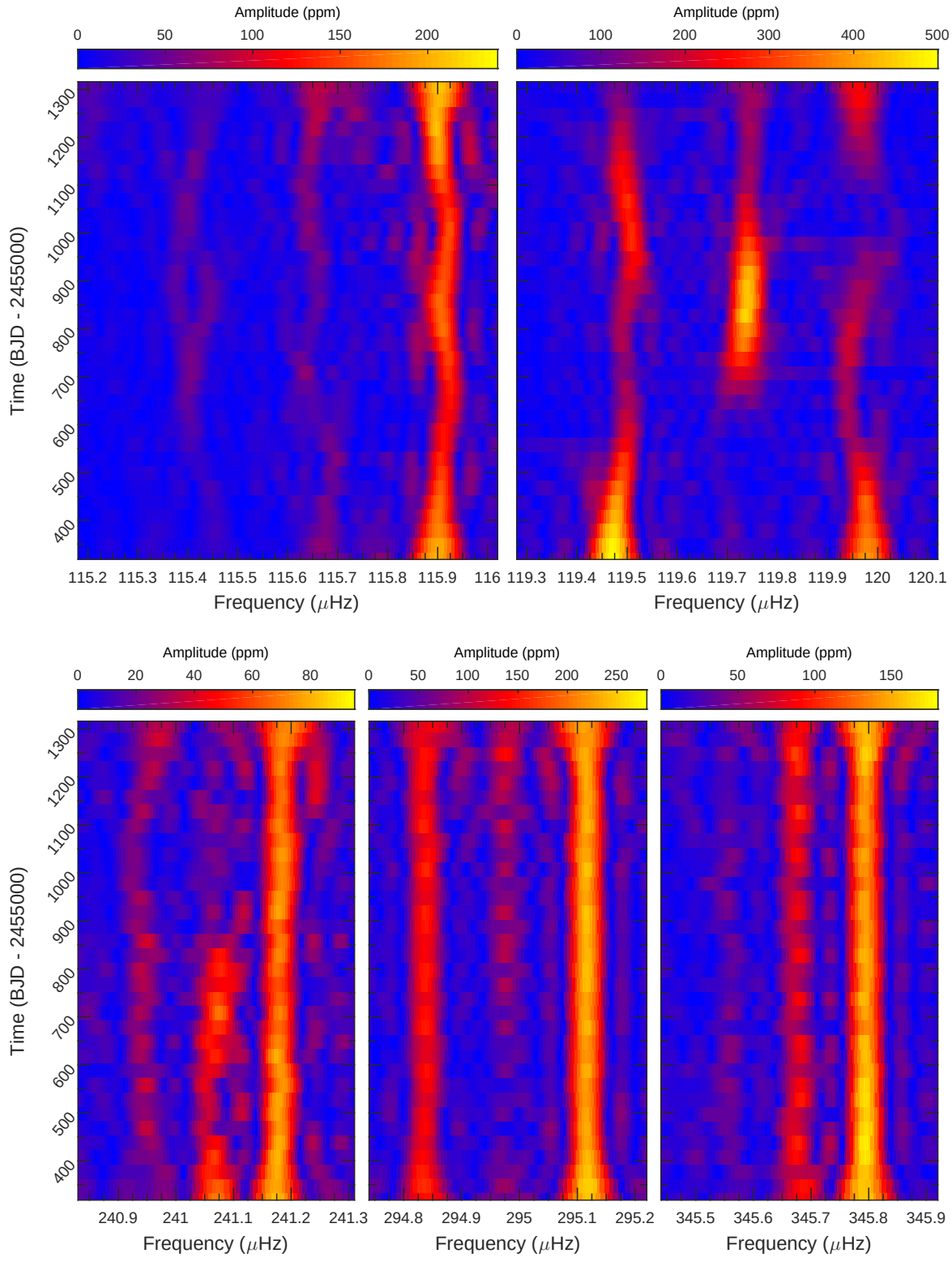

FIGURE 3.9 – Amplitude and frequency modulations of multiplet modes in the pulsating sdB star KIC 07668647. The filtering window of sLSP is chosen with a width of 270 d and time steps of 30 d. *Top panels* : two incomplete quintuplets near 116 μHz and 120 μHz. *Bottom panels* : three triplets near 241 μHz, 295 μHz and 346 μHz. The color scale represents the amplitude of the LSPs. The colorbars are different from each others and are shifted to the top of each panels.

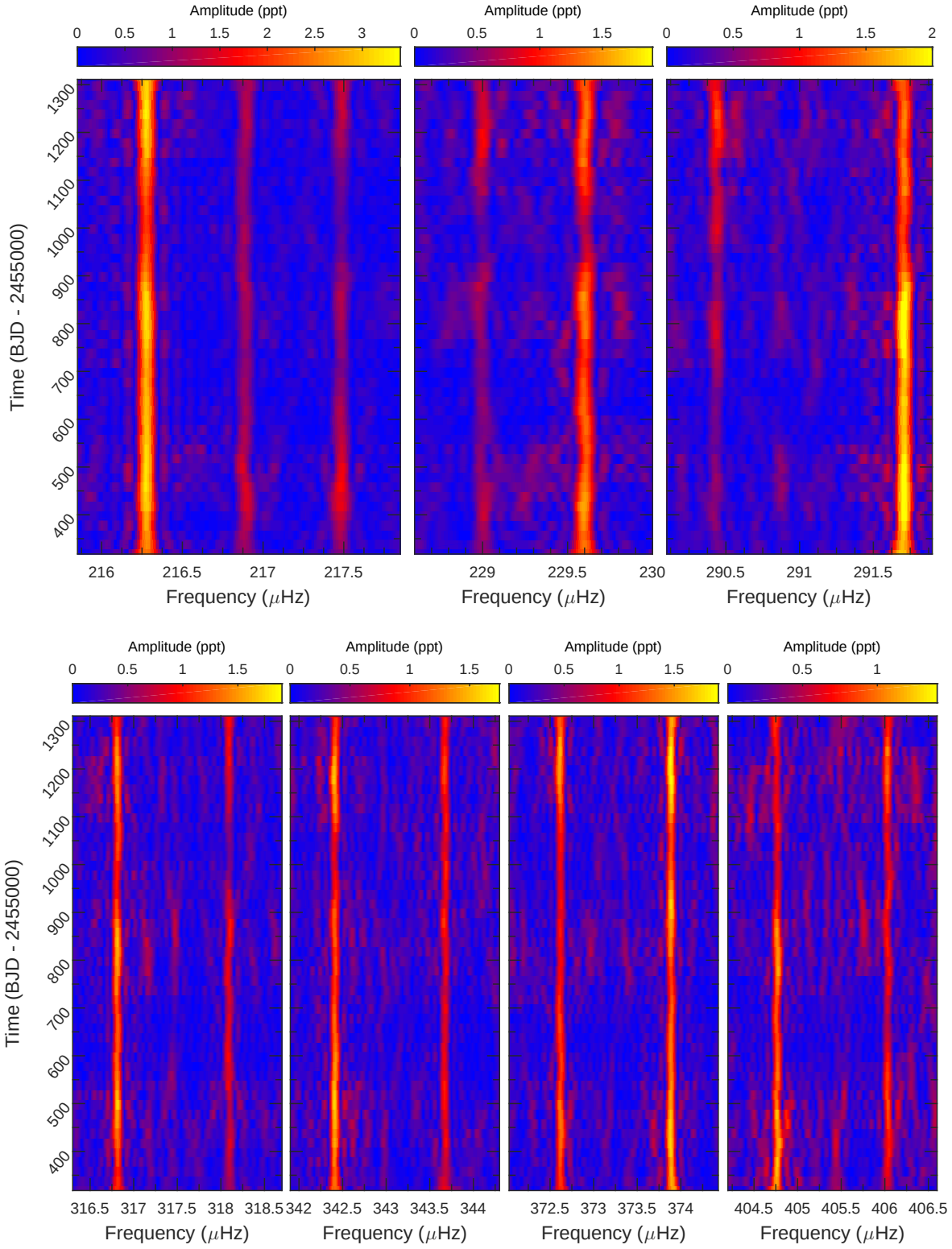

FIGURE 3.10 – Same as Figure 3.9 but for KIC 02438324. The filtering window of sLSP is chosen with a width of 200 d and time steps of 20 d. *Top panels* : one triplet near 217 μHz, and two doublets near 229.5 μHz and 291 μHz. *Bottom panels* : four doublets at 317.5 μHz, 343 μHz, 373 μHz and 405.5 μHz.

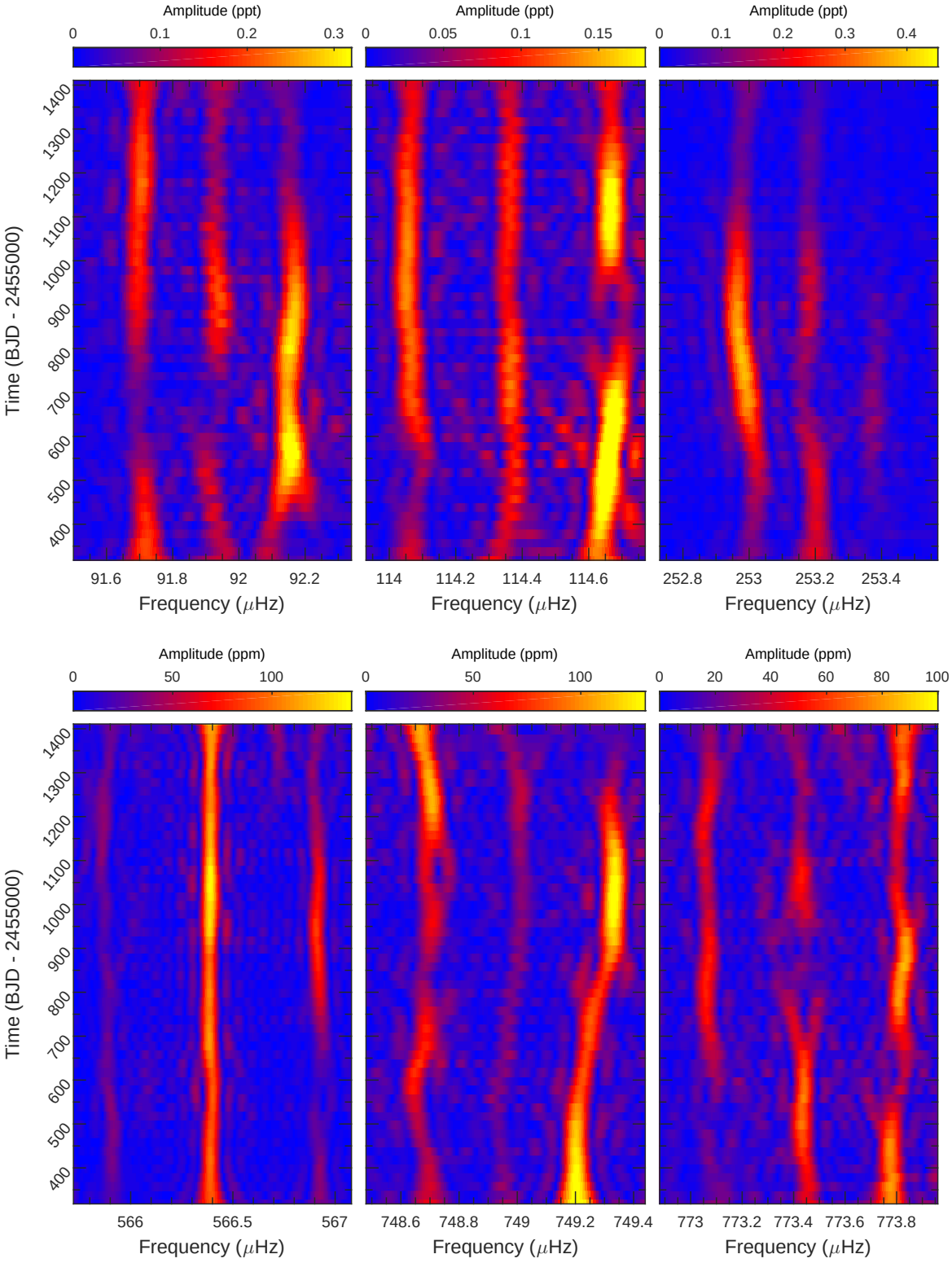

FIGURE 3.11 – Same as Figure 3.9 but for seven KIC 03527751. The filtering window of sLSP is chosen with a width of 200 d and time steps of 20 d. *Top panels* : three (possibly) incomplete quintuplets near 92 μHz, 114.4 μHz and 253.2 μHz. *Bottom panels* : another three (possibly) incomplete quintuplets near 566.5 μHz, 749 μHz and 773.4 μHz.

in each panel, respectively. At this scale, we can clearly distinguish that the mode behaviors, remain stable or show variations, from the sLSP with the optimal filtering window (here width of 270 d and time steps of 30 d). The incomplete quintuplet near 116 μHz, with two components missing, show amplitude and frequency modulations, in particularly for the mode at 115.9 μHz, whose modulations may be periodic, with a period of $\sim$ 500 d. However, we cannot give the precise period for the 115.9 μHz mode modulations since we have not extracted frequencies by parts of the entire assembled light curve. Amplitude and frequency variations also found in the 200 μHz incomplete quintuplet whose three components show coherent modulations, the amplitude of 119.7 μHz mode increases when amplitudes of the two other mode at 119.45 μHz and 119.98 μHz decreases and vice versa, and the frequencies at 119.45 μHz and 119.98 μHz sometime approach and sometime move away from the mode at 119.7 μHz. The modulations has a period around two years from inspecting the sLSP. We note that the amplitude of the 119.7 μHz mode is very low (disappears in the noise) during the first year of observation. Two of three components forming the triplet near 241 μHz show amplitude and frequency variations, while, the prograde mode looks relatively stable. From the sLSP near 295 μHz, the triplet modes remain stable both in amplitude and frequency during the 3-year observations. Note the central component has a low amplitude but still can be clearly distinguished from the noise (blue background). The triplet near 346 μHz has the same behavior as seen in the 295 μHz triplet, stable amplitudes and frequencies. Again, amplitude of the prograde mode is low but can be well recognized from the noise. Therefore, we observe different behaviors occurring between the components of the five multiplets in KIC 07668647.

Figure 3.10 shows the amplitude and frequency modulations observed in seven triplets (only one has a complete structure of three components) in KIC 02438324. The optimal filtering window is chosen with a width of 200 d and time steps of 20 d that is well suitable to resolve the 10 d rotational triplets and give a high time resolution. At this scale, we can definitely discriminate the mode behaviors, whether their amplitude are stable or vary with time. The amplitudes look stable for most of the time in the triplet at 217 μHz, while, the amplitudes of $m = \pm 1$ decrease and increase in a short time around time BJD=2 455 1000. Amplitude variations are also found in the six doublets, as revealed by the color variations in the other six panels. We find that probably periodic amplitude modulations occur in the doublets near 229.5 μHz, 317.5 μHz, 343 μHz and 373.5 μHz. In these four doublets, one could clearly see the cyclical color variations of the high amplitude components. However, at this stage, we can not distinguish the frequency variations due to the frequency resolution. Therefore the extraction of frequencies base on pieces of the entire light curve is particularly needed, in order to discover the frequency variations in these multiplets.

Figure 3.11 shows amplitude and frequency variations in six multiplets (or, possibly quintuplets) in the sdB star KIC 03527751. The optimal window is chosen to be the same as for KIC 02438324. With the given sLSPs, we find clear signatures of amplitude and frequency modulations in these six quintuplets : frequency variations of a few percents of μHz for most of the components. We discuss these interesting findings case by case. The amplitudes of the components forming the incomplete quintuplet at 92 μHz show coherent amplitude and frequency modulations. When the amplitude of the prograde mode reaches its maximum, amplitudes of the other two decreases to their minimum. We also find that the frequencies between the three components converge and diverge during the $\sim$ 1000-d observations. The incomplete quintuplet at 114.4 μHz exhibit amplitude and frequency variations. The amplitude of the 114.6 μHz component experienced two maximums in the observations. The amplitude of the component near 114 μHz decreases to its minimum when the 114.6 μHz component reaches the first maximum amplitude. The incomplete quintuplet near 253 μHz shows an interesting frequency modulation where a systematic variations happened in the 253 and 253.2 μHz component and we obser-

ved about one cycle of the frequency variations. We note that the low amplitude component near 253.4 μHz became visible from BJD=2 455 0600 to 900 when the amplitude of the 253 μHz component is relatively large. The incomplete quintuplet near 566.5 μHz misses two $m \pm 1$ components as suggested by the $\sim$ 0.5 μHz frequency spacing. This quintuplet shows amplitude and frequency variations of the three components, while, the frequencies vary in the smallest range among the six considered multiplets. The incomplete quintuplet near 749 μHz also shows systematic frequency variations in the three components. During the entire observations, the frequencies change on the order of a few tenth μHz. The amplitude of 749.2 μHz completed at least one period if the modulation is indeed periodic. The amplitude of the 749 μHz component is relatively stable although the frequency variations can be clearly distinguished. The amplitude and frequency variations of the incomplete quintuplet near 773.4 μHz are on a timescale of $\sim$ 500 days. The amplitude of 773.8 μHz component exhibits three maximums and two minimums. We therefore find that the six incomplete quintuplets all show amplitude and frequency variations in KIC 03527751 which is different from that of the triplets, e.g., in KIC 07668647.

We note that the sLSP can not provide precise values for the amplitudes and frequencies of the considered modes. It merely gives us an overall view to accelerate the search for interesting mode modulations. To get more precise information on the mode variations, one need to extract frequencies from parts of the entire light curves. This technique will be used in Chapter 4 and Chapter 5, for the modes studied in KIC 08626021 and KIC 10139564, respectively.

3.5 Conclusion

In this Chapter, we first described the details of the *Kepler* spacecraft, its FOV, and the properties of the high-quality photometric data gathered by this telescope. There are 18 sdB stars and 6 white dwarf stars that have been detected with pulsations among more than 100 candidates, including two V 361 Hya, sixteen V 1093 Her stars, one DBV and five DAV stars. Most of the sdB stars (15 of 18) and one WD star has been observed for two years and more by *Kepler* in short-cadence mode. Eight of the 18 ($\sim$ 45%) sdB stars are found in the close binary systems which is consistent with the binary fraction in Maxted et al. (2001). We use a dedicated software FELIX, which is based on the standard prewhithening and nonlinear squares fitting methods, to extract frequencies from the light curves of these compact stars. As the spaceborne photometric data are very different from that from ground-based observations, we discussed two statistical tests that aimed at calculating the appropriate detection threshold and estimating the robustness of the error determinations before we proceed with prewhitening frequencies. We used the corrected data, and first, detrended the light curves and clipped the outlier data points. Then we provided our procedures to analyze the *Kepler* photometric data with examples from several sdB stars. The Lomb-Scargle Periodogram (LSP) for a given star, KIC 07664467, clearly show an extremely sharp frequency resolution and low noise level, which enable us to detect many pulsations and slow rotation in sdB stars. After prewhitening the frequencies in another star, KIC 02991403, there are still some outstanding peaks near some prewhitened main frequencies in the residuals, indicating that these prewhitened frequencies possibly exhibit amplitude and frequency variations. The sdB stars typically rotate slowly with periods from 6 to 90 days, except for three stars that may have very long rotation periods. Rotation in three white dwarfs are derived from the *Kepler* data and the periods are of the order of a day. An interesting observation in rotational multiplets is that the same frequency mismatch of $\sim$ 0.02 μHz is detected in four triplets of KIC 11179657. The sliding LSP is used to study the amplitude and frequency variations of the concerned frequencies. This method needs an optimal filtering window to obtain a good compromise between frequency resolution, time resolution and signal-to-noise.

We selected eight stars from the whole 24 stars as first priority targets based on their observational durations, number of multiplets and periods of rotation. The preliminary results on amplitude and frequencies of the multiplet modes in three stars are provided in this chapter, KIC 07668647, KIC 02438324 and KIC 03527751. The first target show modulated amplitude and frequencies in two incomplete quintuplets and one triplet, and two triplets remain stable. The second one show amplitude variations in its seven (incomplete) triplets, while, the frequency variations may be in a small range that cannot be uncovered just by sLSP. All the six multiplets in KIC 03527751 experienced large amplitude and frequency variations. The frequency variations of some modes could be as large as a few tenth μHz. In order to obtain precise values of amplitude and frequency, one needs to prewhiten the frequencies from pieces of the entire light curves. This technique will be applied to two targets, KIC 08626021, a DBV star, and KIC 10139564, a short-period sdB star. The analysis of these two stars is presented in the next two chapters.

Chapter 4

The pulsating DB white dwarf star KIC 08626021

In this chapter, we discuss the pulsating DB white dwarf star KIC 08626021 in which two-triplet and one-doublet modes show clear amplitude and frequency modulations [1]. This is the first evidence of nonlinear mode interactions that could be attributed to a resonant mode coupling mechanism in a white dwarf star. We give a brief description of each sections in that article, and one can see details in the following attached paper. KIC 08626021 is the only DBV star observed by *Kepler*. The former studies on this star, in particular on its frequency content and seismic modeling based on the *Kepler* data, in the literature are discussed in details in Section 3.2 and also in the attached paper.

4.1 The frequency content revisited

We analyzed the nearly two years ($\sim$ 684 days) data gathered on KIC 08626021 continuously observed by *Kepler*, starting from BJD 2 455 740 and ending on BJD 2 456 424. Following the analysis procedures provided in Section 3.3, we detected 13 independent frequencies and two other linear combination (not independent) frequencies that come out well above the 5.6σ detection threshold. Additionally two suspected frequencies are identified with S/N between 5σ and 5.6σ. Our results agree well with Bischoff-Kim et al. (2014) in general, while, we found some additional features in the frequency spectrum that somewhat differs from theirs. We conclude that one frequency is an independent mode and the other two form the incomplete triplet in the frequency region 3677–3686 μHz, instead of a triplet near 3681 μHz which was formerly identified by Bischoff-Kim et al. (2014). Furthermore, both components forming the doublet near 3681 μHz show well resolved sidelobe frequencies with the same frequency separation of 0.044 μHz. Since a rotation period of $\sim$ 1.8 d has been found, this small frequency separation indicates a modulating phenomenon occurring on a timescale of $\sim$ 263 d in these two components, which is further supported by the sliding LSPs.

4.2 Amplitude and frequency modulations

The sLSPs's filtering window here is chosen to be 180-d wide with time steps of 7-d, which is the best compromise found for the case of KIC 08626021. To obtain a precise value for the

1. The results have been published on *Astronomy & Astrophysics* , 585, A22, 2016 : Amplitude and frequency variations of oscillation modes in the pulsating DB white dwarf star KIC 08626021. The likely signature of nonlinear resonant mode coupling ; Zong, W. ; Charpinet, S. ; Vauclair, G. ; Giammichele, N. ; Van Grootel, V.

amplitudes and frequencies, we also extracted frequencies in various parts of the entire light curve, i.e., the 23-month data was divided into 20 time intervals, each including 6-month of data except for the last three ones at the end of the observations. The results based on these two procedures are shown in Fig. 7, 10, 11 and 12 in the attached article.

The three components forming the triplet f_1 near 4310 μHz show signatures of quasi-periodic amplitude and frequency modulations with an averaged timescale of $\sim$ 600 days (Fig. 7). The best fitting of a sine wave function suggests a period of 580 ± 23, 680 ± 10 and 610 ± 43 days for the retrograde ($m = -1$), central ($m = 0$) and prograde ($m = +1$) component, respectively. In addition, we note that the amplitude and frequency variations show clear correlations, as both evolve in phase with the same period ($\sim$ 600 d and zero phase $\mathrm{Ph}_0 \sim 0.84$), for the side components, and are antiphased ($\mathrm{Ph}_0 = 0.34$) with the central component. The other triplet f_2 near 5073 μHz show clear amplitude variations, while, their frequencies appear to be stable (Fig. 10). The amplitude modulations of the two side components seem to evolve in phase with a quasi-periodic behavior of $\sim$ 700 days. However, the amplitude of the central mode exhibits a more complex behavior and may follow a modulating pattern on a longer timescale. The two components forming the doublet f_3 near 3681 μHz show signatures of correlated variations both in amplitude and frequency (Fig. 11). The period of amplitude variations of both modes is roughly 280 days as well as for the frequency modulations of the central mode, while, the frequency modulations for the prograde is almost twice ($\sim$ 550 d) to that of $f_{3,0}$. Therefore, the frequency separation of 0.044 μHz provide a precise estimate of the modulating period, i.e., $\sim$ 263 d. Note that the mode f_7 near 3678 μHz shows a constant amplitude and frequency behavior, which further supports that f_7 does not belong to the incomplete triplet f_3.

For completeness, we also illustrate the intriguing behavior of three frequencies through a linear combination, $f_8 \sim f_{1,-} + f_4$ (see Table 1 in the attached paper). These three components follow nearly the same trends in both frequency and amplitude. Note that one of the three involved frequencies, $f_{1,-}$, is also one of the components forming the triplet f_1.

4.3 Connections with nonlinear resonant couplings

These observed modulations cannot be related to any evolutionary effects in white dwarfs, the timescale is much longer than the observed modulations, to the presence of orbiting objects, systematic frequency variations occur in all modes, and to the magnetic activities on the stellar surface, all the modes appear to be globally affected following the same trends to various extent. Instead, the nonlinear mode interactions could address the various observed modulations because resonant mode coupling mechanisms predict that various behaviors of modulations can occur in different resonant modes : exhibiting variations in amplitude and frequency or remaining stable (see details in Section 1.4.2).

The periodic modulations in the f_1 triplet suggest that f_1 is in the intermediate regime of the triplet resonance. The theoretical calculations on the modulating period for f_1 is found to be on a timescale $P_m(\mathrm{th}) \sim 620$ d, which is consistent with the observed modulation period. The slight difference in modulating period between side components and central one might be an implication that the nonlinear mode interaction is more complex than the idealized case predicted by the theory. The retrograde mode seems to be involved into two different types of resonance as suggested by the observed modulation pattern, a case that has not been considered by the nonlinear theory yet. The doublet f_3 can be the second case of the intermediate regime of triplet resonance. The theoretical modulation period is $P_m(\mathrm{th}) \sim 518$ d, which is comparable but not strictly identical to the observed ones. The f_2 triplet is in the configuration different from the above two triplets, showing modulated amplitudes and locked frequencies. This configuration could be associated with the narrow transitory hysteresis regime (Section 1.4.3).

As the importance of the linear growth rates in these resonant mechanisms (a key factor appears in the amplitude equations, e.g., equation 1.67 in Section 1.4.2), we also provide some results of linear nonadiabatic pulsation calculations from a seismic model best representing the star (Giammichele et al., in prep.). The computations on the theoretical linear growth rates were done by using two different nonadiabatic pulsation codes, one still working in the frozen convection (FC) approximation (Brassard et al. 1992b; Fontaine et al. 1994; Brassard & Fontaine 1997) and the other implementing a time-dependent convection (TDC) treatment (Dupret 2001; Grigahcène et al. 2005). The modes of interest f_2, f_1 and f_3 have growth rates that are in the ranges $2\times10^{-13}-7\times10^{-12}$, $2\times10^{-12}-4\times10^{-11}$, and $1\times10^{-11}-2\times10^{-10}\,\mathrm{ss}^{-1}$, respectively. With these values, we obtain the parameter D (a key parameter that measures how far away are the modes from the resonance center, Section 1.4.3) which lies in the range $3\times10^{3}-6\times10^{4}$, $1\times10^{4}-5\times10^{5}$ and $7\times10^{2}-1\times10^{4}$ for the mode triplet f_1, f_2 and f_3, respectively. These values are significantly larger than those estimated by Goupil et al. (1998) and need further investigations. Nevertheless, it suggests that the nonlinear coefficients could play an important role in the determination of which regime the resonance will be in.

4.4 Summary and conclusion

We found amplitude and frequency modulations of oscillation modes in three splitting triplets that are detected in the DBV star KIC 08626021, thanks to the opportunity offered by *Kepler* high-quality and long-duration data. These interesting modulations show signatures pointing toward nonlinear resonant coupling mechanisms which occur between the triplet modes. This is the first time that such evidence is identified so clearly in a white dwarf star.

We analyzed the nearly two years *Kepler* data on KIC 08626021, following the procedures provided in Section 3.3. Our frequency content agrees well with that of Bischoff-Kim et al. (2014) in general, but with some slight difference, as we find eight independent modes (seven in theirs) and small frequency separation in the doublet f_3. The observed modulations whose periods are consistent with the prediction by resonant coupling mechanisms. However, we found a difference between the observed and theoretical D parameters in terms of the value of different regimes. This particularly needs further investigations, e.g., to obtain the nonlinear coefficients in AEs for the involved modes. Moreover, some of the involved modes seem to be able to participate in different types of resonance, which is more complex than the theoretical treatment, i.e., considering the resonant modes as an isolate system (Section 1.4).

The uncovered frequency modulations can potentially impair any attempt to measure reliably the evolutionary effects of the white dwarf on the pulsation periods. Therefore one should be extremely careful of potential contamination of such nonlinear effects when conduct the project of measure the changing rates of pulsation periods. We finally emphasize that the observed periodic modulations occurring in the intermediate regime of triplet resonance may allow for new asteroseismic diagnostics, providing in particular a way to measure for the first time linear growth rates of pulsation modes in white dwarf stars. This prospect should motivate further theoretical work on nonlinear resonant mode coupling physics and revive interest in nonlinear stellar pulsation theory in general.

A&A 585, A22 (2016)
DOI: 10.1051/0004-6361/201526300

Astronomy & Astrophysics

Amplitude and frequency variations of oscillation modes in the pulsating DB white dwarf star KIC 08626021

The likely signature of nonlinear resonant mode coupling

W. Zong[1,2], S. Charpinet[1,2], G. Vauclair[1,2], N. Giammichele[3], and V. Van Grootel[4]

[1] Université de Toulouse, UPS-OMP, IRAP, 31400 Toulouse, France
e-mail: weikai.zong@irap.omp.eu
[2] CNRS, IRAP, 14 avenue Édouard Belin, 31400 Toulouse, France
[3] Département de Physique, Université de Montréal, CP 6128, Succursale Centre-Ville, Montréal, QC H3C 3J7, Canada
[4] Institut d'Astrophysique et de Géophysique, Quartier Agora, Allée du 6 Août 19c, 4000 Liège, Belgium

Received 12 April 2015 / Accepted 22 October 2015

ABSTRACT

Context. The signatures of nonlinear effects affecting stellar oscillations are difficult to observe from ground observatories because of the lack of continuous high-precision photometric data spanning extended enough time baselines. The unprecedented photometric quality and coverage provided by the ***Kepler*** spacecraft offers new opportunities to search for these phenomena.
Aims. We use the ***Kepler*** data accumulated on the pulsating DB white dwarf KIC 08626021 to explore in detail the stability of its oscillation modes, searching, in particular, for evidence of nonlinear behaviors.
Methods. We analyze nearly two years of uninterrupted short-cadence data, concentrating on identified triplets that are caused by stellar rotation and that show intriguing behaviors during the course of the observations.
Results. We find clear signatures of nonlinear effects that could be attributed to resonant mode coupling mechanisms. These couplings occur between the components of the triplets and can induce different types of behaviors. We first notice that a structure at 3681 μHz, identified as a triplet in previous published studies, is in fact forming a doublet, with the third component being an independent mode. We find that a triplet at 4310 μHz and this doublet at 3681 μHz (most likely the two visible components of an incomplete triplet) have clear periodic frequency and amplitude modulations, which are typical of the so-called intermediate regime of the resonance, with timescales consistent with theoretical expectations. Another triplet at 5073 μHz is likely in a narrow transitory regime in which the amplitudes are modulated while the frequencies are locked. Using nonadiabatic pulsation calculations, based on a model representative of KIC 08626021 to evaluate the linear growth rates of the modes in the triplets, we also provide quantitative information that could be useful for future comparisons with numerical solutions of the amplitude equations.
Conclusions. The observed modulations are the clearest hints of nonlinear resonant couplings occurring in white dwarf stars identified so far. These should resonate as a warning to projects that aim at measuring the evolutionary cooling rate of KIC 08626021, and of white dwarf stars in general. Nonlinear modulations of the frequencies can potentially jeopardize any attempt to measure such rates reliably, unless they can be corrected beforehand. These results should motivate further theoretical work to develop the nonlinear stellar pulsation theory.

Key words. white dwarfs – stars: individual: KIC 08626021 – techniques: photometric

1. Introduction

The temporal variations of the amplitude and frequency of oscillation modes often seen, or suspected, in pulsating stars cannot be explained by the linear nonradial stellar oscillation theory (Unno et al. 1989) and must be interpreted in the framework of a nonlinear theory. It is believed that nonlinear mechanisms, such as resonant mode couplings, could generate such modulations, as, e.g., in the helium dominated atmosphere (DB) white dwarf star GD 358 (Goupil et al. 1998). Resonant couplings are, for instance, predicted to occur when slow stellar rotation produces triplet structures whose component frequencies satisfy the relation $\nu_+ + \nu_- \sim 2\nu_0$, where ν_0 is the frequency of the central $\boldsymbol{m} = 0$ mode. The theoretical exploration of these mechanisms was extensively developed in Buchler et al. (1995, 1997), but was almost interrupted more than a decade ago because of the lack of clear observational evidence of such phenomena, as a result of the difficulty in capturing amplitude or frequency variations that occur on timescales of months to years from ground-based observatories. Nevertheless, the presence of resonant couplings within rotationally split mode triplets was proposed for the first time as the explanation for the frequency and amplitude of long-term variations observed in the ***GW Vir*** pulsator PG 0122+200 (Vauclair et al. 2011) from successive campaigns on this object. This suggests that pulsating white dwarfs could be among the best candidates to detect and test the nonlinear resonant coupling theory.

White dwarfs constitute the ultimate evolutionary fate expected for ~98% of the stars in our Galaxy. While cooling down, they cross several instability strips in which they develop observable nonradial g-mode oscillations. Among these, the helium atmosphere DB white dwarfs which represent ~20% of all white dwarfs, are found to pulsate in the effective temperature range of 21 000 K to 28 000 K (Beauchamp et al. 1999; Fontaine & Brassard 2008; Winget & Kepler 2008). All classes of pulsating white dwarfs are particularly valuable for probing their interior

with asteroseismology, but it has also been proposed that hot DB pulsators with apparently stable modes could be used to measure their cooling rate, which is dominated by neutrino emission (Winget et al. 2004). The secular rates of change for the pulsation periods in hot DB pulsators is expected to be $\sim 10^{-13}$ ss^{-1}, corresponding to a timescale of 3×10^5 years. However, this possibility could be seriously impaired by other phenomena affecting the pulsation frequencies on shorter timescales. Such variations in amplitude and frequency have indeed been suspected in several white dwarf stars (e.g., PG 0122+200, Vauclair et al. 2011; WD 0111+0018, Hermes et al. 2013; HS 0507+0434B, Fu et al. 2013), as stellar evolution theory cannot explain the variations with estimated timescales at least two orders of magnitude shorter than the expected cooling rates. Nonlinear effects on stellar pulsations, including resonant mode coupling mechanisms could induce such modulations and need to be considered carefully (Vauclair 2013).

In this context, observations from space of a multitude of pulsating stars, including white dwarfs, has open up new horizons. The ***Kepler*** spacecraft monitored a 105 deg^2 field in the Cygnus-Lyrae region for nearly four years without interruption, obtaining unprecedented high quality photometric data for asteroseismology (Gilliland et al. 2010). These uninterrupted data are particularly suited to searching for long-term temporal frequency and amplitude modulations of the oscillation modes.

Among the six pulsating white dwarfs discovered in the ***Kepler*** field, KIC 08626021 (aka WD J1929+4447 or GALEX J192904.6+444708) is the only identified DB pulsator (Østensen et al. 2011). Based on the first month of short cadence (SC) ***Kepler*** data, Østensen et al. (2011) estimated that this star has an average rotation period $\boldsymbol{P}_{\rm rot} \sim 1.7$ days, derived from the observed frequency spacings of three groups of g-modes that has been interpreted as triplets due to rotation. Subsequent independent efforts to isolate a seismic model for KIC 08626021 from Bischoff-Kim & Østensen (2011) and Córsico et al. (2012) both suggest that the effective temperature of the star is significantly hotter than the value determined from the survey spectroscopy. However, the masses determined from these two models are not consistent with each other. More recently, a new asteroseismic analysis based on the full ***Kepler*** data set provided by Bischoff-Kim et al. (2014), confirmed the former results found by Bischoff-Kim & Østensen (2011). We point out that a new asteroseismic analysis of KIC 08626021 is discussed in Giammichele et al. (in prep.).

KIC 08626021 has been observed by ***Kepler*** for nearly two years in short cadence mode without interruption since the quarter Q10. Thus, it is a suitable candidate to investigate the long-term amplitude and frequency modulations of the oscillation modes occurring in this star. In this paper, we present a new thorough analysis of the ***Kepler*** light curve obtained on the DB pulsator KIC 08626021, that emphasizes, in particular, the time dependence of the amplitudes and frequencies of the modes associated with rotationally split triplets (Sect. 2). We provide arguments that link the uncovered amplitude and frequency modulations with the nonlinear mode coupling mechanisms (Sect. 3), before summarizing and concluding (Sect. 4).

2. The frequency content of KIC 08626021 revisited

The pulsating white dwarf star KIC 08626021 has been continuously observed by ***Kepler*** in short cadence (SC) mode from quarter Q10.1 to Q17.2 (when the second inertial wheel of the satellite failed). A light curve from Q7.2, well disconnected from the main campaign, is also available for that star. Some analysis of these data have already been reported in the literature (Østensen et al. 2011; Córsico et al. 2012), including most recently the asteroseismic study of Bischoff-Kim et al. (2014, hereafter BK14) which was based on the full Q10.1 – Q17.2 data set. We initially considered using these published results as the starting point of our present study, but we realized that important details were lacking for our specific purposes. Consequently, we detail below, as a necessary step, our own thorough analysis of the frequency content of KIC 08626021.

2.1. The Kepler photometry

All the data gathered by ***Kepler*** for that star are now in the public domain. We obtained the light curves from the Mikulski Archive for Space Telescopes (MAST)[1]. As is standard, these data were processed through the ***Kepler*** Science Processing Pipeline (Jenkins et al 2010). In the following, we concentrate on the consecutive data that covers Q10.1 to Q17.2, without considering Q7.2 that would introduce a large time gap in the assembled light curve. With this restriction, we are left with a mere 23 months of high precision photometric data starting from BJD 2 455 740 and ending on BJD 2 456 424 (~684 days) with a duty cycle of ~87%.

We constructed the full light curve from each quarter corrected light curves, which most notably include a correction for the amplitude due to the contamination of the star by a closeby object (this correction consider that only ~47.3% of the light comes from the DB white dwarf). Tests indicate that the main differences between these corrected data and the raw data set used by BK14 occur in the measured amplitudes of the light variations, but has otherwise no noticeable incidence on the extracted frequencies. Each quarter light curve was then individually corrected to remove long-term residual trends (using sixth-order polynomial fits) and data points that differ significantly from the local standard deviation of the light curve were removed by applying a running 3σ clipping filter. The later operation just very slightly decreases the overall noise level.

The resulting ligth curve is shown in Fig. 1 and the corresponding Lomb-Scargle periodogram (LSP; Scargle 1982) is given in Fig. 2. The low-amplitude multi-periodic modulations are clearly seen with dominant periodicities of the order of a few minutes, typical of g-mode oscillations observed in pulsating DB white dwarfs. The formal frequency resolution in the LSP (defined as the inverse of the total time base line of the observations) reaches ~0.017 μHz.

2.2. Defining a secure detection threshold

Before proceeding with the extraction of the frequencies, a brief discussion of the criterion that is used to define the confidence level of the detections is necessary. With ground-based observations of pulsating compact stars, a widely used rule of thumb was to consider the limit of 4σ (4 times the average local noise in the Fourier Transform) as the threshold above which a signal could safely be considered as real. However, with space observations, in particular with ***Kepler***, it became increasingly clear that this rule underestimates the risks of false detections resulting from statistical noise fluctuations. The reason lies most probably in the very large number of data points collected during months (or years) of observations with a sampling time of only 58 s in SC mode. In particular, more than half a million frequency bins are necessary to represent the LSP of the 684 days ***Kepler***

[1] https://archive.stsci.edu/

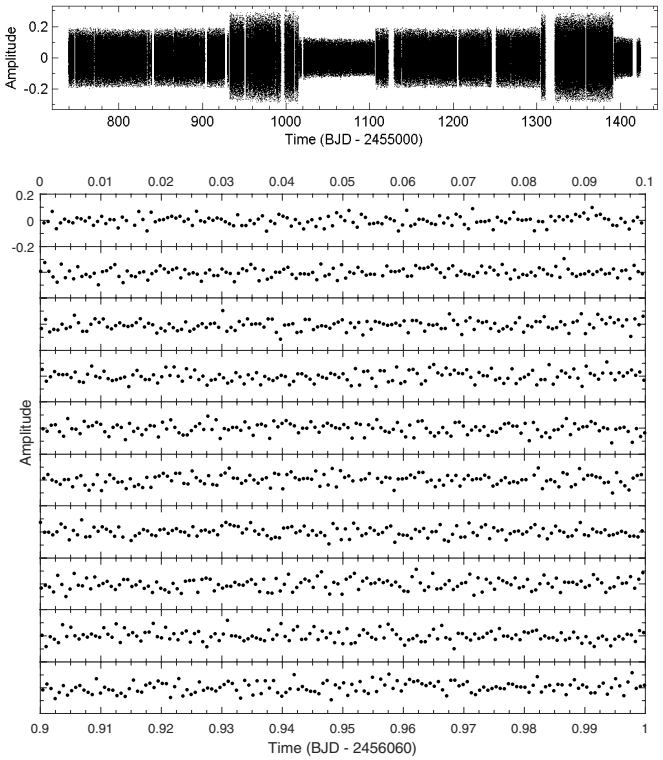

Fig. 1. ***Top panel***: condensed representation of the full ***Kepler*** light curve (Amplitude is the residual relative to the mean brightness intensity of the star vs. time in Barycentric Julian Date) covering from Q10.1 to Q17.2 (~684 days) of KIC 08626021. Between quarters, scatter sometime changes due to different levels of noise in the data (all quarters are not equivalent in photometric quality). ***Bottom panel***: close-up view showing one day of the ***Kepler*** light curve by slices of 0.1 days. At this scale, the oscillations are clearly apparent.

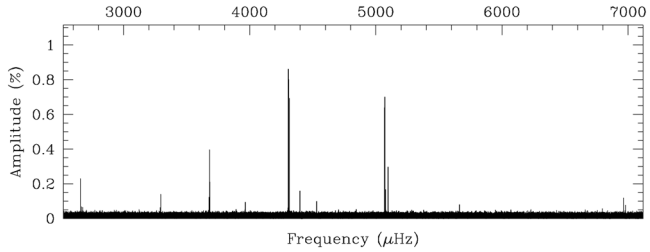

Fig. 2. Lomb-Scargle periodogram (LSP; amplitude in % of the mean brightness vs. frequency in μHz) of the ***Kepler*** light curve. The represented range covers the frequency region where the pulsation modes are detected (no significant signal is found outside these limits). Note that some well known ***Kepler*** instrumental artefacts are within this frequency range but can easily be recognized.

photometric data of KIC 08626021 and noise fluctuations are very likely to occur at least one time (and more) above a standard 4σ threshold. For this reason, the trend has been to increase the threshold to higher signal-to-noise (S/N) values in somewhat arbitrary ways to avoid false detections (e.g., BK14 just assumes that the acceptable limit is 5σ).

Instead of adopting an arbitrary value, we quantitatively estimate what should be an acceptable threshold with the following procedure. Using the same time sampling as the observations, we randomly build 10 000 artificial light curves just containing white gaussian noise (a random normal deviate is calculated at each time point). The LSPs of these artificial light curves are then calculated, as well as the median values of the noise in each

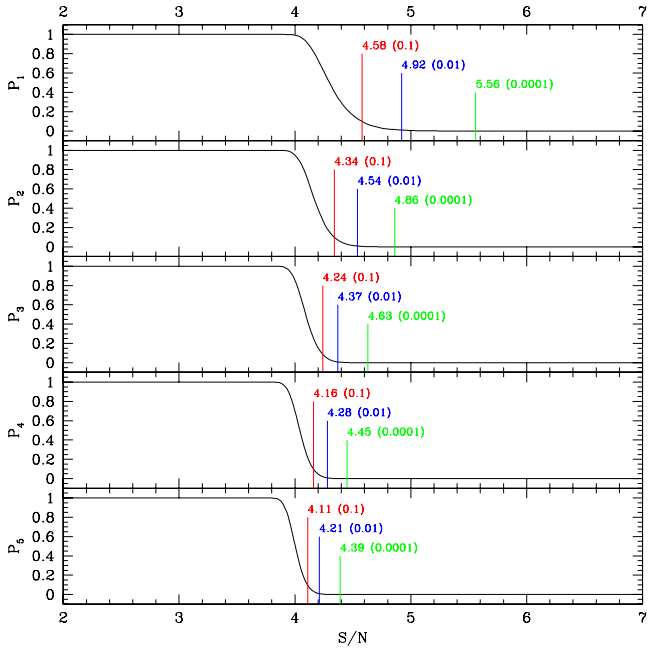

Fig. 3. False alarm probability $\boldsymbol{P_n}$ of having at least $\boldsymbol{n}$ peaks caused by noise above a given S/N threshold in the LSP of KIC 08626021 (see text for details). In each panel, the three vertical lines indicate, from left to right, the S/N value corresponding to $\boldsymbol{P_n}$ = 0.1, 0.01, and 0.0001, respectively. The limit $\boldsymbol{P_1}$ = 0.0001, meaning that the risk of having a false detection above that threshold is reduced to less than 1 chance over 10 000, defines our adopted criterion. It corresponds to the limit of 5.6σ.

resulting LSPs. For any given S/N threshold ($\boldsymbol{x}\sigma$ defined as $\boldsymbol{x}$ times the median noise level) we then find the number of times that at least $\boldsymbol{n}$ peaks in the LSP (which by definition are just noise structures) happen to be above the chosen limit. Then, dividing by the number of tests (10 000 here), we obtain the false alarm probability $\boldsymbol{P_n}(\boldsymbol{x})$ that at least $\boldsymbol{n}$ peaks above a given S/N threshold of $\boldsymbol{x}\sigma$ is due to noise.

Figure 3 shows the results of this procedure for the probabilities $\boldsymbol{P_1}$ to $\boldsymbol{P_5}$ as functions of the S/N threshold. The most interesting case is $\boldsymbol{P_1}$ (the probability that at least 1 peak due to noise is above the threshold). We clearly see here that at the usual 4σ limit, the probability to have at least one false detection is close to 1 (and ~0.5 to have at least 5 false detections according to $\boldsymbol{P_5}$), confirming that this threshold is particularly unsafe in our case. However, $\boldsymbol{P_1}$ eventually decreases with increasing S/N to reach 0.1 (10% chance) at $\boldsymbol{S/N}$ ~ 4.58, 0.01 (1% chance) at $\boldsymbol{S/N}$ ~ 4.92 (approximately the detection threshold chosen by BK14), and less than 1 chance out of 10 000 at $\boldsymbol{S/N}$ = 5.56 (this is the limit above which not a single peak due to noise has been found among the 10 000 randomly generated light curves).

Based on these calculations, we adopt, in the following, the conservative 5.6σ threshold as our limit of detection.

2.3. Extraction of the frequencies

We used a dedicated software, FELIX (Frequency Extraction for LIghtcurve eXploitation) that was developed by one of us (S.C.), to first extract the frequency content of KIC 08626021 down to our adopted detection threshold of 5.6σ (we, in practice, pushed down the limit to ~5σ; see below). The method used is based on the standard prewhithening and nonlinear least square fitting techniques (Deeming 1975) that works with no difficulty in the

Table 1. List of frequencies detected in KIC 08626021.

Id.	Frequency (μHz)	σ_f (μHz)	Period (s)	σ_P (s)	Amplitude (%)	σ_A (%)	Phase	σ_{Ph}	S/N	Comment
$f_{1,-}$	4306.52304	0.00013	232.205886	0.000007	0.867	0.012	0.7987	0.0037	73.4	$f_{1,-}$ in BK14
$f_{1,0}$	4309.91490	0.00014	232.023143	0.000007	0.804	0.012	0.5264	0.0040	68.1	$f_{1,0}$ in BK14
$f_{1,+}$	4313.30642	0.00016	231.840705	0.000008	0.701	0.012	0.7885	0.0046	59.3	$f_{1,+}$ in BK14
$f_{2,-}$	5070.03081	0.00017	197.237460	0.000007	0.641	0.012	0.1521	0.0050	54.3	$f_{2,-}$ in BK14
$f_{2,0}$	5073.23411	0.00016	197.112922	0.000006	0.705	0.012	0.0394	0.0046	59.8	$f_{2,0}$ in BK14
$f_{2,+}$	5076.44385	0.00066	196.988291	0.000026	0.167	0.012	0.1462	0.0192	14.1	$f_{2,+}$ in BK14
$f_{3,0}$ [†]	3681.80286	0.00028	271.606068	0.000020	0.397	0.012	0.1347	0.0082	33.6	$f_{3,0}$ in BK14
$f_{3,+}$ [†]	3685.00937	0.00052	271.369731	0.000038	0.212	0.012	0.4066	0.0153	18.0	$f_{3,+}$ in BK14
f_4	2658.77740	0.00047	376.112721	0.000067	0.233	0.012	0.6147	0.0140	19.7	f_5 in BK14
f_5	4398.37230	0.00068	227.356834	0.000035	0.161	0.012	0.7598	0.0200	13.6	f_7 in BK14
f_6	3294.36928	0.00079	303.548241	0.000073	0.139	0.012	0.0934	0.0234	11.8	$f_{4,0}$ in BK14
f_7	3677.99373	0.00088	271.887358	0.000065	0.125	0.012	0.6773	0.0260	10.6	$f_{3,-}$ in BK14
f_9	6981.26129	0.00139	143.240592	0.000028	0.079	0.012	0.0105	0.0404	6.7	f_{11} in BK14
Linear combination frequencies										
f_8	6965.30234	0.00090	143.568786	0.000019	0.121	0.012	0.8358	0.0264	10.3	$f_{1,-} + f_4$; f_6 in O13[a]
f_{10}	2667.95462	0.00164	374.818969	0.000230	0.067	0.012	0.7489	0.0484	5.7	$f_9 - f_{1,+}$
Frequencies above 5σ detection										
f_{11} [⋆]	2676.38212	0.00170	373.638725	0.000236	0.065	0.012	0.1443	0.0501	5.5	
f_{12} [⋆]	3290.24565	0.00176	303.928675	0.000163	0.063	0.012	0.0752	0.0519	5.3	$f_{4,-}$ in BK14

Notes. [(†)] The azimuthal order (m) identification proposed for the doublet comes from a model fit seismic solution (see Giammichele et al., in prep.); [(⋆)] these frequencies are below 5.6σ (although still higher than 5σ) and could be spurious; [(a)] Østensen (2013).

present case. The code FELIX greatly eases and accelerates the application of this procedure, especially for long and consecutive time series photometry obtained from spacecrafts like CoRoT and ***Kepler*** (Charpinet et al. 2010, 2011).

The list of extracted periodic signals is provided in Table 1 which gives their fitted attributes (frequency in μHz, period in seconds, amplitude in % of the mean brightness, phase relative to a reference t_0 time, and S/N above the local median noise level) along with their respective error estimates (σ_f, σ_P, σ_A, and σ_{Ph}). Figures 4–6 show zoomed-in views of all the identified peaks in the LSP.

We find 13 very clear independent frequencies that come out well above the detection threshold. Two additional lower amplitude peaks (f_8 and f_{10}) appear as significant but are linked to other frequencies through linear combinations and are therefore likely not independent pulsation modes. Two more frequencies (f_{11} and f_{12}) can be identified above 5σ but below 5.6σ which we mention for completeness, but that cannot be considered as secured detections. A comparison with the completely independent analysis of BK14 shows that we agree on all the relevant, well secured frequencies (i.e, with a sufficiently high S/N). We point out, however, that some additional features of the frequency spectrum are not discussed in BK14 and we differ in how to interpret some of the mode associations (see below).

As reported in BK14, six of the extracted frequencies (f_1 and f_2) form two very well defined, nearly symmetric triplets with a frequency spacing of ~3.392 μHz and ~3.206 μHz (Fig. 4). These are readily interpreted as rotationally split triplets, thus giving an average rotation period of ~1.75 days for the star. However, we argue that the three frequencies shown in Fig. 5 cannot correspond to the components of a triplet, as BK14 suggest. These frequencies form a clearly asymmetric structure with the left component (f_7) being significantly more distant

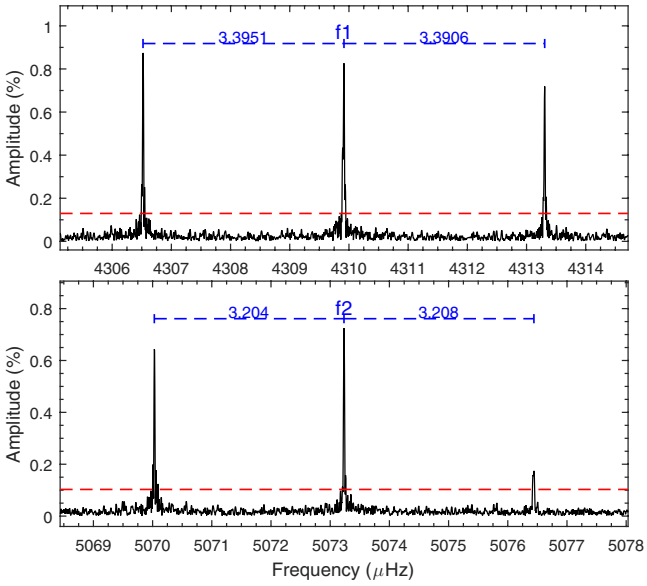

Fig. 4. Lomb-Scargle periodogram of the triplets at 4310 μHz (***top panel***) and 5073 μHz (***bottom panel***) after nearly two years of ***Kepler*** photometry gathered on KIC 08626021. The nearly equal frequency spacings are marked in the two panels. The dashed red horizontal line refers to the 5.6σ detection threshold of local noise level.

than the right component ($f_{3,+}$) from the central peak ($f_{3,0}$). We note in this context that the frequency separation between $f_{3,0}$ and $f_{3,+}$ (3.208 μHz) is similar or very close to the frequency splitting characterizing the f_2 and f_1 triplets. Our interpretation is therefore that the middle ($f_{3,0}$) and right ($f_{3,+}$) peaks are two components of a triplet whose third component is undetected,

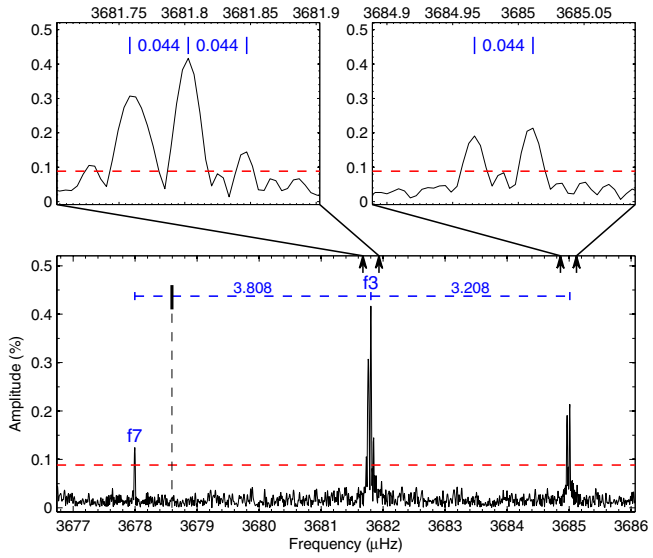

Fig. 5. Lomb-Scargle periodogram in the 3677−3686 μHz frequency range where a doublet and an independent frequency are above the 5.6σ detection threshold of local noise level. The bold black vertical segment and vertical dashed line indicate the position of one possible third component for the doublet, as shown in the bottom panel. The two ***top panels*** are the expanded view of the two components as indicated by the vertical arrows in the ***bottom panel***. Both the fine structures of the two components show well-resolved closed peaks and have the same frequency separation of 0.044 μHz.

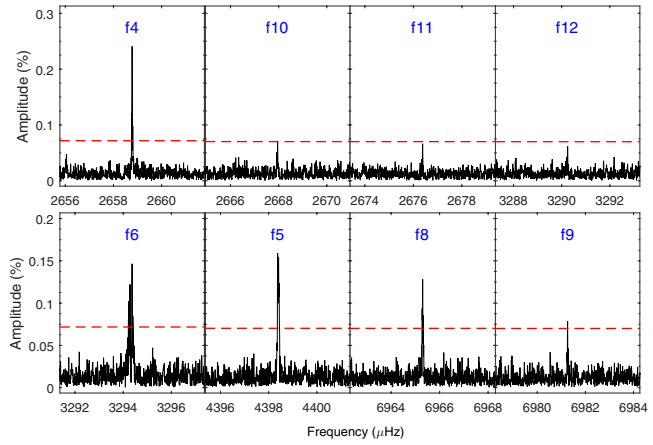

Fig. 6. Lomb-Scargle periodogram of 8 frequencies after nearly two years of ***Kepler*** photometry gathered on KIC 08626021. The two frequencies f_{11} and f_{12} are with 5.0−5.5σ of local noise level. Frequency f_8 and f_{10} are linear combination frequencies.

while the left peak (f_7) is a completely independent mode. This has some implications in finding an asteroseismic solution for KIC 08626021 as attempted by BK14, since eight independent periods should be considered and not seven (see Giammichele et al., in prep.).

Furthermore, not reported in BK14, we show in Fig. 5 that the two components of the incomplete triplet are in fact surrounded by additional structures (not tabulated in Table 1). The central peak ($f_{3,0}$) appears to have two resolved symmetric sidelobes that are located 0.044 μHz away, while the right peak ($f_{3,+}$) shows a sidelobe also separated by 0.044 μHz. These intriguing hyperfine structures cannot be associated with rotation since a much larger rotational splitting signature has already been found. Moreover, the very small frequency separation involved would indicate a modulating phenomenon that occurs on a very long timescale of ~263 days.

This finding brings us to the main subject of the present paper, which is to show that this hyperfine structure, along with other behaviors that we discuss below, can be linked to long-term amplitude and frequency modulations that are generated by nonlinear resonant coupling mechanisms between the components of rotationally split triplets.

2.4. Amplitude and frequency modulations

From now on, we mainly focus our discussions on the two well defined triplets f_1 and f_2, and on the doublet f_3 (i.e., the two visible components of an incomplete triplet). In order to analyze the temporal variability of these modes and their relationship, we used our software FELIX to compute the sliding Lomb-Scargle periodogram (sLSP) of the data set. This technique consists of building time-frequency diagrams by filtering in only parts of the data as a function of time. In the present case, we chose a filter window that is 180-day wide sled along the entire light curve by time steps of 7 days. This ensures a good compromise, for our purposes, between time resolution, frequency resolution (to resolve close structures in each LSP), and S/N. The sLSP gives an overall view of the amplitude and frequency variability that could occur for a given mode (see, e.g., the top left panel of Fig. 7). We acknowledge that BK14 also provide a similar analysis, but they chose a sliding window that is only 14-day wide, hence providing a much lower resolution in frequency. This has strong consequences on the interpretation of these data that will become obvious below. As a complementary (and more precise) method, we also extracted the frequencies (through prewithening and nonlinear least square fitting techniques) in various parts of the light curve, i.e., the 23-month light curve of KIC 08626021 was divided into 20 time intervals, each containing six months of data (for precision in the measurements) except for the last three intervals at the end of the observations. This second approach provides a measure of the (averaged) frequencies and amplitudes at a given time, along with the associated errors (see, e.g., the bottom left panel of Fig. 7).

2.4.1. The f_1 triplet

Figure 7 shows the amplitude and frequency modulations observed for the three components that form the f_1 triplet near 4310 μHz. In this plot, views of the frequency variations with time are illustrated from top to bottom-left panels. The top panel first shows the sLSP of the triplet as a whole (similar to Fig. 2 of BK14) where the signal appears, at this scale, stable in frequency but varying in amplitude for at least the central component. Then we provide increasingly expanded views (from middle-left to bottom-left panel) around the average frequency of each component. In addition, the bottom right panel shows how the amplitude of each component varies with time.

It is mentionned in BK14 that the modes, and these three components in particular, are stable in frequency over the 2-year duration of the observations. We clearly demonstrate here that this is not the case. Their statement is based on a time-frequency analysis involving a sliding Fourier Transform (sFT) that only uses a 14-day-wide window, which clearly does not permit a sufficient frequency resolution to uncover the modulations that we report here. We find that both the amplitudes and frequencies show very suggestive signatures of quasi-periodic modulations with an average timescale that we can roughly estimate to

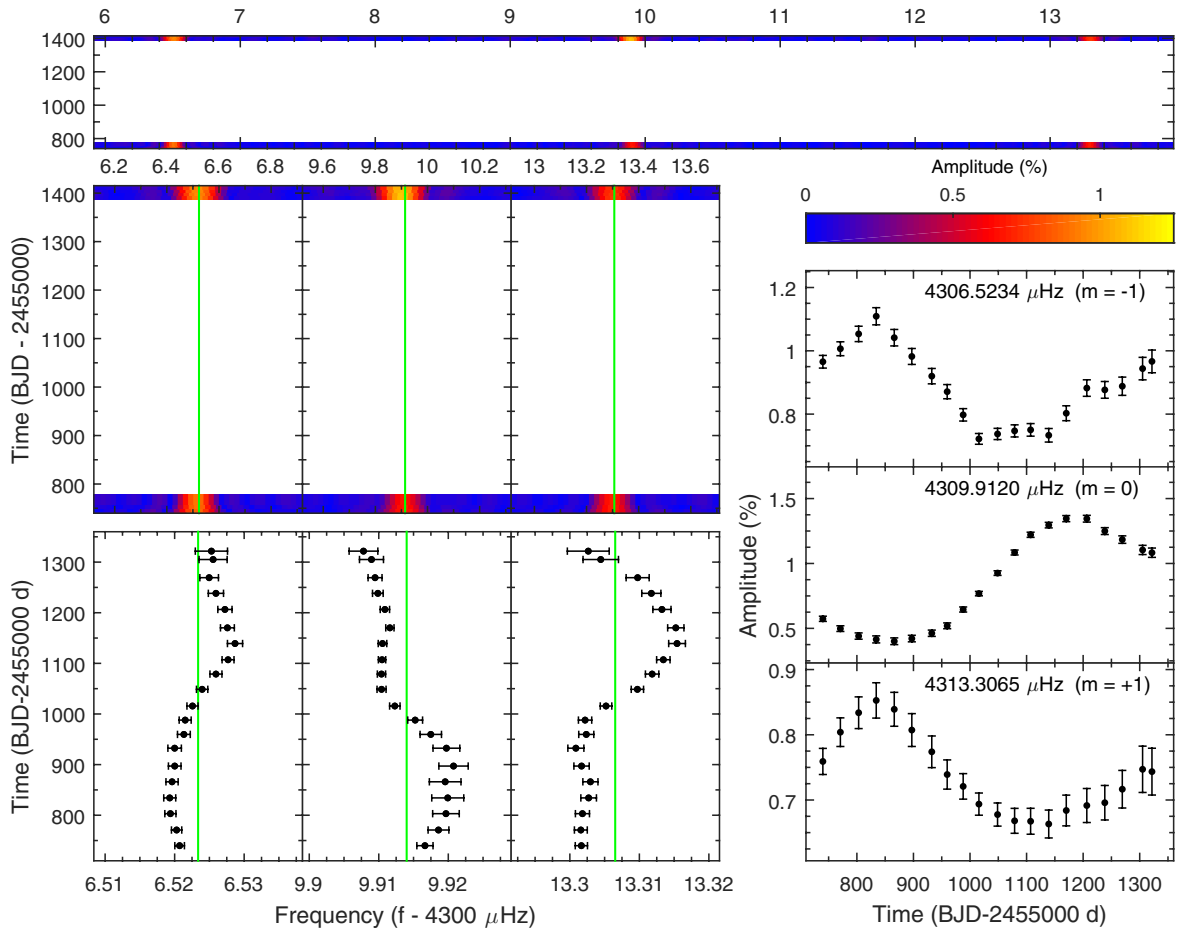

Fig. 7. Frequency and amplitude modulations in the f_1 triplet at 4310 μHz. The ***top panel*** shows the sLSP (giving the amplitude in % as a function of frequency in μHz and time in days) of the triplet as a whole. The ***middle and bottom left panels*** show increasingly expanded views around the average frequency (the solid vertical lines) of each component, with the ***bottom left panel*** obtained from prewhitening subsets of the data, thus measuring precisely the frequencies, as a function of time. The ***lower right panel*** provides the measured amplitudes as a function of time obtained for each subset of data (see text for details).

~620 days. Figures 8 and 9 illustrate further this periodicity in phase diagrams. Although very similar, we find that the modulation period associated with the side components of the triplets (~600 d) could be slightly shorter than the modulation period of the central component (~680 d). Note that the modulating periods in this triplet were obtained by searching for the best fit of a pure sine wave function to the amplitude variations. The zero phase is relative to the time of the first data point (BJD = 2 455 739.836). The same procedure was not applied to the frequency modulations since the patterns are clearly more complex than a pure sine wave function. However, since Fig. 7 suggests a cyclic behavior with roughly the same timescale, the folding periods used to construct Fig. 9 were chosen to be those derived for the amplitude modulations. This allows us to check that indeed at least two of the components (the $m = +1$ and $m = -1$ modes) accomodate rather well these periodicities, as the curves connect near phase 1[2]. For the central ($m = 0$) component, a slightly longer estimated periodicity does not permit to cover entirely the suspected modulation cycle with the data, leaving a gap between phase 0.9 and 1 where the behavior is not monitored. We cannot say in that case whether this curve would eventually connect smoothly at phase 1 or if a discontinuity exists, suggesting that either the chosen folding period is not appropriate or an additional trend is affecting the frequency of this mode.

In addition, we note that the frequency and amplitude modulations show obvious correlations, as both evolve in phase with the same period (with period of ~600 days and zero phase of ~0.84), for the side components, and are somewhat antiphased with the central component (with zero phase of 0.34), as shown in Figs. 8 and 9. We quantitatively checked this fact by computing the correlation coefficients between, e.g., the amplitudes of the $m = +1$ and $m = -1$ components ($\rho_{A_+,A_-} = +0.93$; i.e., indicative of a strong correlation) and the amplitudes of the $m = +1$ and $m = 0$ components ($\rho_{A_+,A_0} = -0.82$; i.e., indicative of a strong anti-correlation). Such correlated behavior suggests that the modes involved are somehow connected, either through a common cause that affects their amplitudes and frequencies similarly or through direct interactions that occur between the components of the triplet. This will be discussed further in Sect. 3.

2.4.2. The f_2 triplet

Figure 10 shows the modulations observed in the other triplet, f_2, at 5073 μHz. The frequencies in this triplet appear to be stable

[2] Note that the two last data points with larger error bars are less secure measurements due to the fact that the sliding Fourier transform reaches the end of the data set and incorporates shorter portions of the light curve. This affects the frequency resolution and consequently the precision of the measurements.

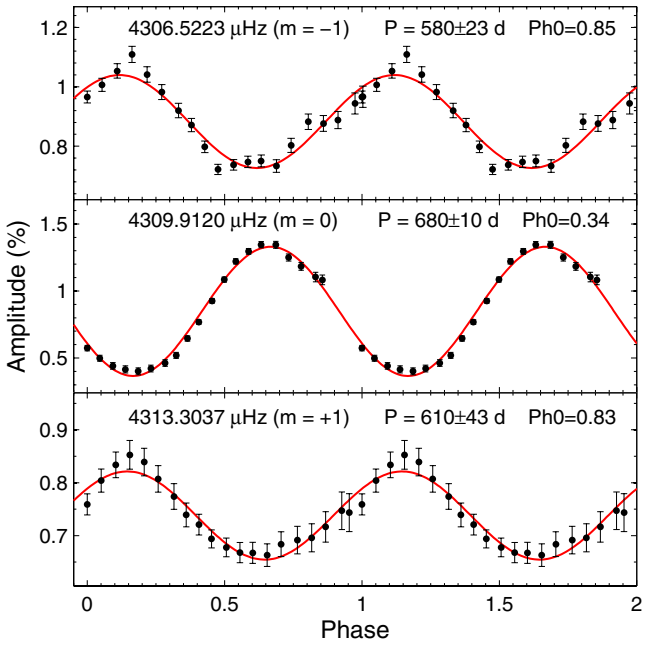

Fig. 8. Amplitude modulations observed in the f_1 triplet presented in phase diagrams with a folding period of 580 and 610 days for the two side components, and 680 days for the central component. These periods, and their associated formal errors, were estimated by fitting a sine wave (red curve) to the amplitude variations.

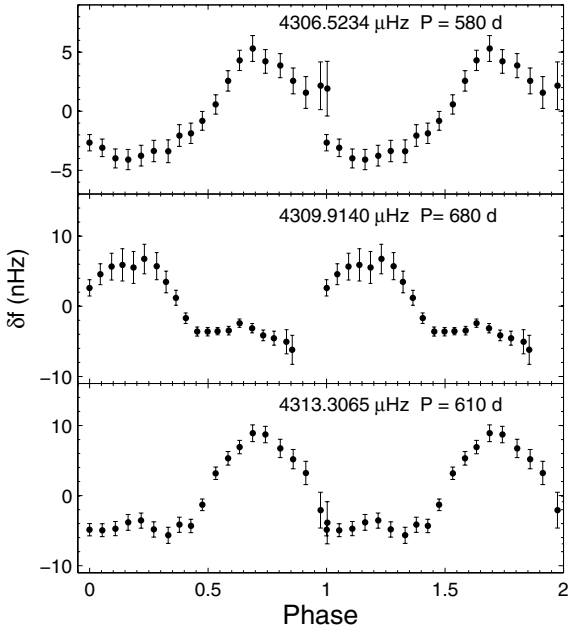

Fig. 9. Same as Fig. 8 but for the frequency modulations observed in the f_1 triplet. Note that the adopted folding periods are the values derived for the corresponding amplitude modulations.

during the nearly two years of ***Kepler*** observations, while the amplitudes show clear modulations. Note that the amplitude of the $m = +1$ component went down at some point below a signal-to-noise ratio of 4σ and was essentially lost in the noise during a portion of the last half of the observations. Four measurements could not be obtained because of this and when it was still possible to spot this component, the errors remained large.

Again in this case, the amplitudes of the two side components seem to evolve nearly in phase with a quasi-periodic behavior on a timescale that is probably slightly larger than the duration of the observations and close to a timescale of ~700 days. However, contrary to the previous case, a connection with the central component is less clear. The later seems to follow a variation pattern possibly occurring on a longer timescale. Therefore, f_2 behaves somewhat differently from f_1, a feature that we will discuss more in the next section.

2.4.3. The f_3 doublet

The 3677−3686 μHz frequency range is shown in Fig. 11 and contains the independent frequency (f_7) and the two visible components of the incomplete triplet f_3 (thus forming a doublet).

Each component of this doublet shows clear signatures of correlated variations for both amplitudes and frequencies. We note in particular a periodic modulation that occurs on a somewhat shorter timescale than for the two previous cases. A very quick look at Fig. 11 indicates a period of roughly 280 days for the amplitude variations of both modes as well as for the frequency modulation of $f_{3,0}$, which in fact can readily be connected to the hyperfine-structure sidelobes discussed in Sect. 2.3 and illustrated in Fig. 5. The frequency of $f_{3,+}$, for its part, seems to also follow a periodic trend but, quite interestingly, on a timescale that could be around twice (~550 days) the period of the other components.

It appears now clearly that a periodic frequency and amplitude modulation process is responsible for the equidistant peaks surrounding $f_{3,0}$ and $f_{3,+}$. In this context, the frequency separation of 0.044 μHz should provide a more precise estimate of the period of this modulation, which is ~263 days. Note that the other two triplets discussed previously do not show similar hyperfine splitting structures around their components simply because the period of their modulations appear to be slightly longer than the observational time baseline and those structures cannot be resolved. In the case of f_3, the observations are long enough to resolve the modulation. We further note that the amplitudes of the two components of f_3 evolves in antiphase while the frequencies are in phase during the first half of the run but then evolve in antiphase during the last part of the observations, which reflects the fact that the frequency variation of $f_{3,+}$ has approximately twice the period of the modulation seen in the frequency of $f_{3,0}$.

In contrast, the mode f_7 shows a totally different behavior as both its frequency and amplitude appear stable throughout the observing run. This could further support, if need be, the interpretation that f_7 and the f_3 complex are not part of a same triplet structure (as assumed by BK14). We indeed note that the theoretical framework in which these modulations can possibly be understood (nonlinear resonant couplings, as discussed in Sect. 3) forbids the possibility that the components of a triplet behave in different regimes.

2.4.4. Other correlated modulations

For completeness, we also illustrate the interesting behavior of three frequencies that are related by a linear combination. Figure 12 shows the amplitude and frequency modulations of $f_{1,-}$, f_4 and f_8, that satisfy almost exactly (within 2σ of the formal measurement errors) the relation $f_8 = f_{1,-} + f_4$ (see Table 1).

It is striking to see how the three components follow nearly exactly the same trends in both frequency and amplitude. These modulations could be related to the so-called parents/child mode nonlinear interactions discussed by

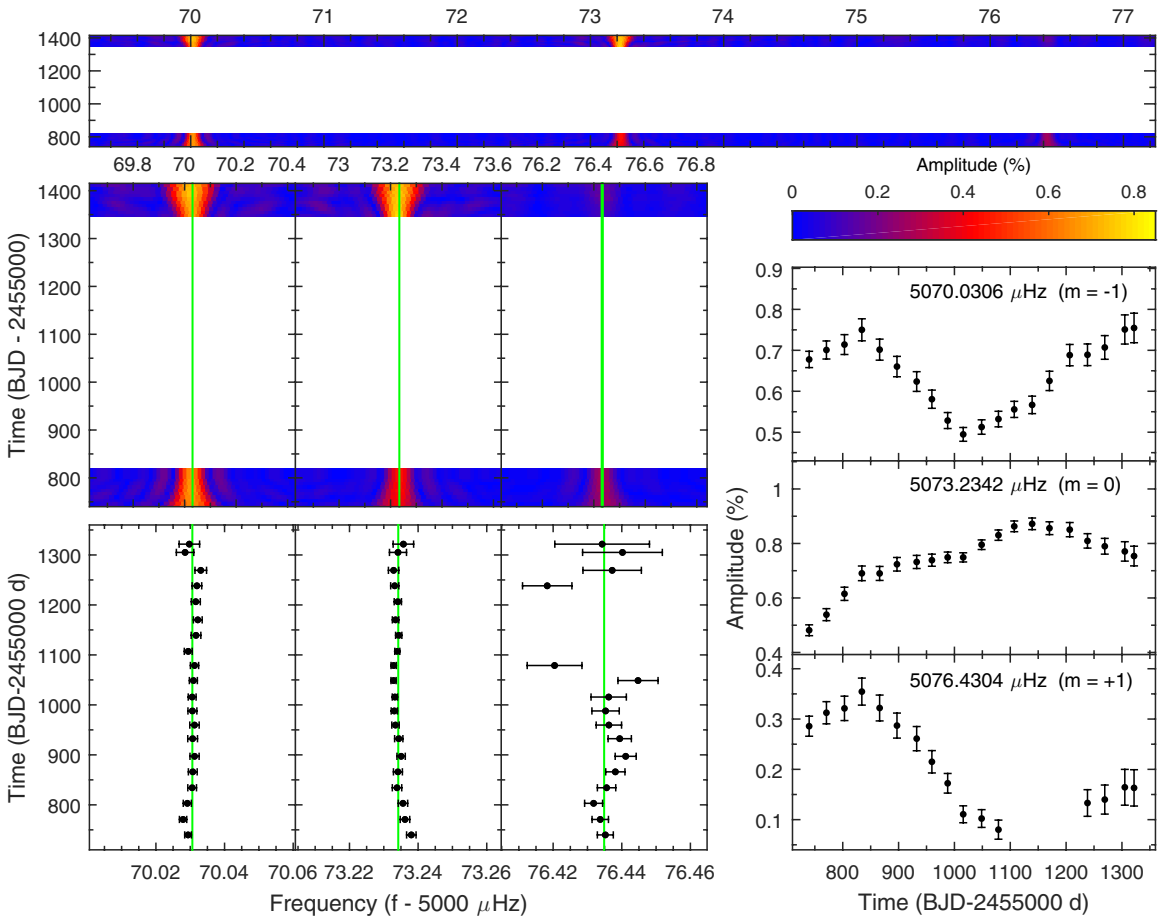

Fig. 10. Same as Fig. 7 but for the f_2 triplet at 5073 μHz. Note that the component at 5076 μHz has a very low amplitude and plunges below the 4σ detection threshold during the second half of the observations, making it difficult to follow (hence the 4 missing data points).

Breger & Montgomery (2014) or to other nonlinearities encountered in white dwarfs (e.g., Brassard et al. 1995; Wu 2001). In this context, we note, again according to the values given in Table 1, that the mean relative amplitude of f_8 (A_8 = 0.00121) is ~60 times larger than the product of the relative amplitudes of $f_{1,-}$ ($A_{1,-}$ = 0.00867) and f_4 (A_4 = 0.00233) whose value is 0.000020. Figure 13 shows that these relationships also hold (within 2σ), both for frequencies and amplitudes, for each individual measurement done as a function of time illustrated in Fig. 12. Interestingly, if this combination were to be related to the mechanism of Wu (2001), the factor of 60 connecting A_8 to $A_{1,-} \cdot A_4$ would possibly imply that the inclination angle of the star should be $50° < i < 60°$ (following Eq. (20) in Wu 2001). Alternately, f_8 could result from a resonant mode coupling phenomenon where f_8 is a true eigenmode of the star (possibly of higher degree ℓ) whose amplitude is boosted above the detection limit by the resonance following Eq. (5) of Breger & Montgomery (2014, see also Dziembowski 1982). We indeed find that our results, instead of using phase (we here use frequency), are similar to the linear combination frequency families that are described in Breger & Montgomery (2014, e.g., comparing their Figs. 4, 5 to our Fig. 13). However, at this stage, we cannot decipher which of these potential mechanisms could explain the details of this combination of frequencies because of the lack of further independent constraints (such as the inclination angle of KIC 08626021). Finally, we point out that one of the frequencies involved in this relation, $f_{1,-}$, is also involved as one of the components of the f_1 triplet discussed in Sect. 2.4.1 (and illustrated in Fig. 7).

Another similar linear combination has also been identified, involving $f_{1,+}$, f_9 and f_{10}, but the low amplitudes of f_9 and f_{10} have prevented us from analyzing its frequency and amplitude modulations. In the following, we concentrate on a possible theoretical interpretation of the frequency and amplitude modulations observed in the triplets, and we do not discuss further the properties of linear combination frequencies.

3. Links with nonlinear resonant couplings

The frequency and amplitude modulations that are observed in the two triplets and the doublet of KIC 08626021 cannot be related to any evolutionary effect, such as neutrino cooling, because the timescale involved is several orders of magnitude shorter than the cooling rate of DB white dwarfs (Winget et al. 2004). The signature of orbiting companions around the star is also ruled out by the fact that the variations occurring in different frequencies are not correlated in phase and do not have the same amplitude modulations (Silvotti et al. 2007). We also considered possibilities that instrumental modulations could occur, e.g., on a per quarter basis, such as a slightly varying contamination from the nearby star that could modulate the amplitude of the modes, but then all modes should be affected similarly, which is not what is observed. Finally, the possibility was raised that changes in the background state of the star, such as those induced by magnetic cycles or through an hypothetical angular momentum redistribution mechanism, could be responsible for the observed modulations. It is indeed well known that magnetic cycles have an impact on the frequencies of the ***p***-modes

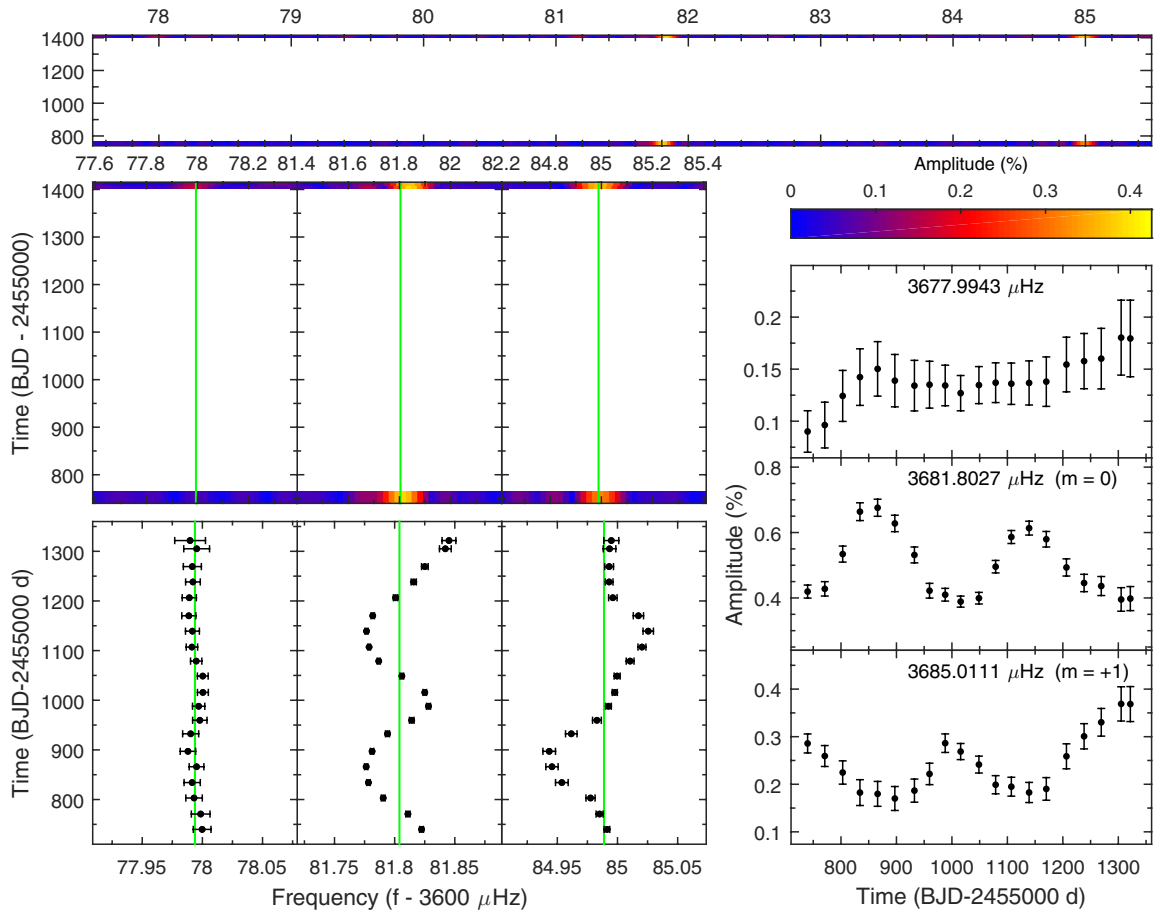

Fig. 11. Same as Fig. 7 but for the doublet f_3 at 3682 μHz and the nearby independent frequency f_7 at 3678 μHz.

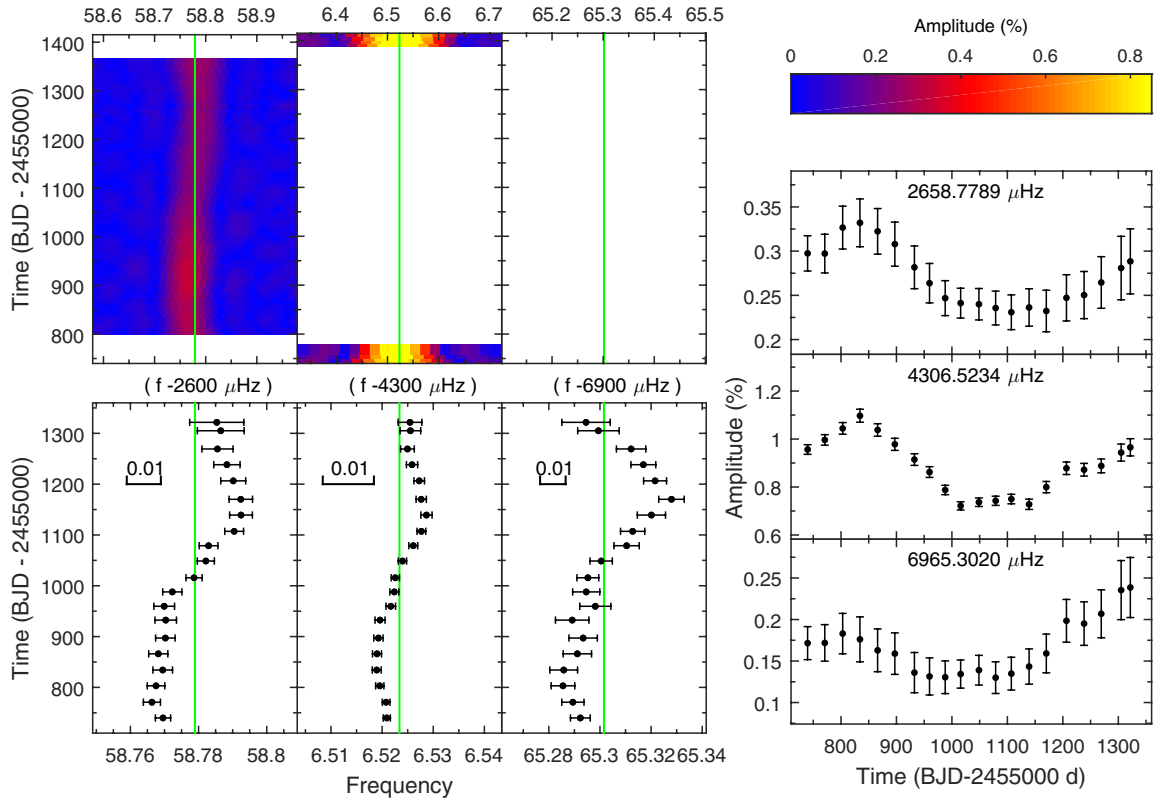

Fig. 12. Frequency and amplitude modulations of the components that form the linear combination $f_{1,-} + f_4 = f_8$. The panels are similar to those described in Fig. 7. The three components show clear periodic modulations evolving in phase. In each ***bottom left subpanels***, a segment indicates the 0.01 μHz scale.

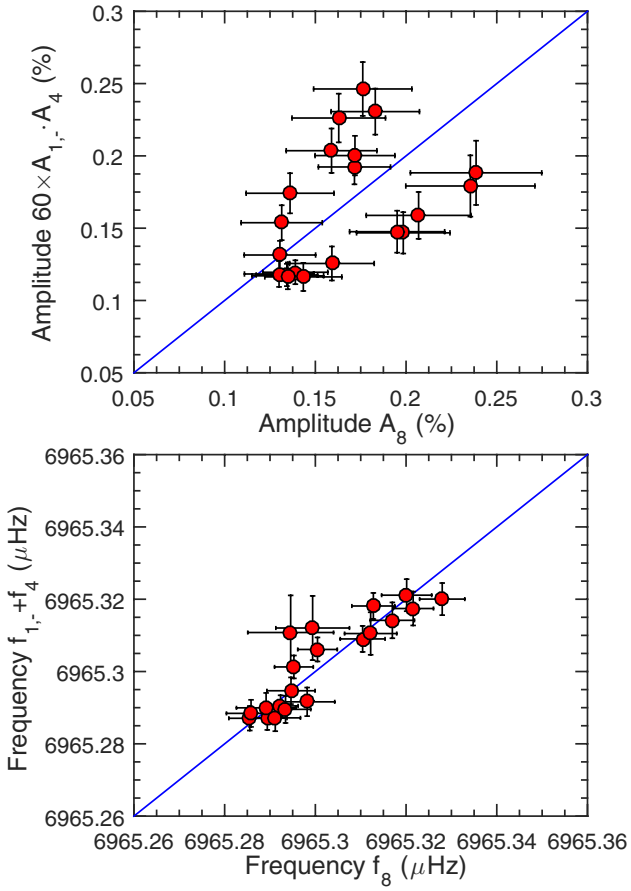

Fig. 13. ***Top panel***: comparison between the measured amplitude $\boldsymbol{A}_8$ of $\boldsymbol{f}_8$ and $60 \times \boldsymbol{A}_{1,-} \cdot \boldsymbol{A}_4$ (where $\boldsymbol{A}_{1,-}$ and $\boldsymbol{A}_4$ are the amplitudes of $\boldsymbol{f}_{1,-}$ and $\boldsymbol{f}_4$, respectively) at each time segment (see text). ***Bottom panel***: same as top panel but for a comparison between the measured frequency $\boldsymbol{f}_8$ and sum of the frequencies $\boldsymbol{f}_{1,-} + \boldsymbol{f}_4$. In both cases, the relationship is exactly statisfied along the plain diagonal line. All the measurements are found to be within 2σ of this line.

observed in the Sun, which lead to small frequency drifts that correlate well in time with tracers of the solar surface activity (see, e.g., Salabert et al. 2015 and references therein). One could imagine that such mechanisms may exist in white dwarfs as well. We think, however, that such effects would be hardly compatible with how the modes in KIC 08626021 are found to vary. In the Sun, all the modes appear to be globally affected following the same trends to some various extent, while in our case we see, for instance, a triplet $\boldsymbol{f}_1$ that shows correlated changes in frequency, and at the same time another triplet $\boldsymbol{f}_2$ whose frequencies appear to be constant. We find a mode $\boldsymbol{f}_7$ that also does not change while the two visible components of the doublet $\boldsymbol{f}_3$ nearby show correlated variations in frequency. This makes it difficult to connect these behaviors to a common global cause (i.e., small changes of the stellar structure). A cyclic redistribution of angular momentum, for its part, would affect the frequencies of the $\boldsymbol{m} = +1$ and $\boldsymbol{m} = -1$ components with an anti-correlation, while the central $\boldsymbol{m} = 0$ component should not be affected (and it is found to vary in $\boldsymbol{f}_1$). All triplets should be affected nearly the same way, but $\boldsymbol{f}_2$, showing constant frequencies, clearly is not and somewhat rules out this possibility.

Instead, we prefer to fall back to a simpler possibility. We develop in this section arguments that nonlinear resonant mode coupling mechanisms, by which both the amplitudes and frequencies of oscillation modes can be modulated on timescales of weeks, months, and even years, appears as a natural explanation for some of the observed behaviors.

3.1. The amplitude equations formalism

The amplitude equations (AEs) formalism is, to our knowledge, the only existing theoretical tool to investigate mode couplings for nonradial oscillation modes in pulsating stars. AEs in the stellar context have been extensively studied since the 1980's for different types of couplings (Dziembowski 1982; Buchler & Goupil 1984; Moskalik 1985; Dziembowski & Goode 1992; Goupil & Buchler 1994; van Hoolst 1994; Buchler et al. 1995; Goupil et al. 1998; Wu 2001; Wu & Goldreich 2001).

In the present context, we limit ourselves to the type of resonances that is discussed in Buchler et al. (1995, 1997) and Goupil et al. (1998), which involves linear frequency combinations such that $\nu_1 + \nu_2 \sim 2\,\nu_0$, and, more specifically, a particular case in which a $\ell = 1$ mode is split by slow rotation and form a nearly symmetric triplet. This choice is obviously driven by the specific configuration of the modes studied in KIC 08626021, which, we recall, are all identified as $\ell = 1$ rotationally split g-mode triplets.

To clarify this further, we do not consider here other potential coupling mechanisms described, e.g., in Wu & Goldreich (2001) because they address a different problem, namely the problem of mode amplitude saturation through a proposed mechanism that indeed involves a nonlinear resonant mode coupling, but with one parent mode that is overstable (thus gaining energy) and two independent child modes that are damped (thus dissipating the energy). In our case, we observe and focus on a different nonlinear resonant coupling that occurs within triplets of $\ell = 1$ g-modes which result from the slow rotation of the star. The three modes in the triplets are overstable and nonlinearly interact with each other because slow rotation induces a near resonance relation between their frequencies (see below). Wu & Goldreich (2001), Wu (2001), Montgomery (2005), and other related studies do not treat this case and therefore cannot be helpful to describe and interpret what is occurring inside a rotationally split triplet. The only available framework for this is the Buchler et al. (1995, 1997) and Goupil et al. (1998) papers that explicitely developed a theory to describe this kind of interaction and that should not be confused with various other works on nonlinear interactions between modes. We point out that it does not mean that the Wu & Goldreich (2001) mechanism cannot also occur in KIC 08626021, but considering the linear growth rates expected for the observed modes (see Sect. 3.3 and Table 2), eventual limit cycles that lead to cyclic amplitude variations would have timescales much longer (~1000 yrs) than what is seen. This could hardly be connected to the observed features and would most likely not be noticeable in the available data that only cover a time baseline of two years.

Going back to the configuration of interest involving rotationally split triplets, rotation when treated to first order approximation would lead to a strictly symmetric triplet that exactly satisfies the above mentionned relationship. However, terms of higher order are never exactly zero and a small asymmetry, dominated by the second order term, always exists. This asymmetry is, in fact, essential for driving the various resonant coupling behaviors. The second order effect of rotational splitting, $\delta\nu_{\rm t}$, that matters can be estimated following the equation given in Goupil et al. (1998):

$$\delta\nu_{\rm t} = 4\boldsymbol{C}_{k\ell}\frac{\Omega^2}{\nu_0}, \tag{1}$$

Table 2. Mode identification and linear nonadiabatic growth rates, κ_0, from the best seismic model of KIC 08626021.

Id.	Frequency (μHz)	ℓ	k	$C_{k\ell}$	$\kappa_0^{\dagger}$	$\delta\nu_t$ (μHz)	P_m(th) (day)	$\delta\nu_o$ (μHz)	P_m(obs) (day)	D	Comment
$f_{2,0}$	5073.23411	1	3	0.426	2×10^{-13}–7×10^{-12}	0.0148	780	0.0064	~700	1×10^{4}–5×10^{5}	Hysteresis regime*
$f_{1,0}$	4309.91490	1	4	0.456	2×10^{-12}–4×10^{-11}	0.0187	620	0.00034	~620	3×10^{3}–6×10^{4}	Intermediate regime
$f_{3,0}$	3681.80287	1	5	0.469	1×10^{-11}–2×10^{-10}	0.0223	518	...	263	7×10^{2}–1×10^{4}	Intermediate regime
f_6	3294.36928	1	6	0.467	2×10^{-11}–4×10^{-10}	...	...	...	...	...	
f_9	6981.26129	2	4	0.121	7×10^{-12}–7×10^{-11}	...	...	...	...	...	
f_5	4398.37230	2	8	0.152	4×10^{-10}–5×10^{-9}	...	...	...	...	...	
f_7	3677.99373	2	10	0.154	2×10^{-9}–4×10^{-8}	...	...	...	...	...	
f_4	2658.77740	2	15	0.161	1×10^{-7}–6×10^{-7}	...	...	...	...	...	

Notes. $^{(\dagger)}$ A range of values is given for the growth rate, reflecting calculations using various treatments and hypotheses on the efficiency of convection (see text); $^{(\star)}$ the frequencies are locked but the amplitudes are still modulated.

where $C_{k\ell}$ is the first order Ledoux constant (~0.5 for dipole g-modes) and $\Omega = 1/P_{\rm rot}$ is the rotation frequency of the star. $P_{\rm rot}$ is estimated from the first order average separation, $\Delta\nu$, between the components of the triplets and its value is ~1.75 days for KIC 08626021 (see Sect. 2). An asymmetry can also be evaluated directly from the measured frequencies of each triplet component, simply from the relation

$$\delta\nu_{\rm o} = \nu_- + \nu_+ - 2\nu_0. \tag{2}$$

According to the resonant AEs from Buchler et al. (1995) in which they ignored the slight interactions between modes with different ℓ and k, for the components in the $\ell = 1$ triplet with frequencies ν_-, ν_0 and ν_+, the corresponding amplitudes A_-, A_0 and A_+ and phases ϕ_-, ϕ_0 and ϕ_+ should obey the following relations

$$\frac{dA_-}{dt} = \kappa_- A_- + R_- A_0^2 A_+ \cos(\Phi - \delta_-) - A_-\left(q_{11}A_-^2 + q_{12}A_0^2 + q_{13}A_+^2\right) \tag{3a}$$

$$\frac{dA_0}{dt} = \kappa_0 A_0 + R_0 A_0 A_+ A_- \cos(\Phi + \delta_0) - A_0\left(q_{21}A_-^2 + q_{22}A_0^2 + q_{23}A_+^2\right) \tag{3b}$$

$$\frac{dA_+}{dt} = \kappa_+ A_+ + R_+ A_0^2 A_- \cos(\Phi - \delta_+) - A_+\left(q_{31}A_-^2 + q_{32}A_0^2 + q_{33}A_+^2\right) \tag{3c}$$

$$\frac{d\Phi}{dt} = \delta\nu - 2R_0 A_- A_+ \sin(\Phi + \delta_0) + A_0\left(R_- \frac{A_+}{A_-}\sin(\Phi - \delta_-) + R_+ \frac{A_-}{A_+}\sin(\Phi - \delta_+)\right), \tag{3d}$$

where $R_{-,0,+}$ and $q_{[(1,2,3)(1,2,3)]}$ are the nonlinear coupling coefficients associated with each component. Their values depend on complex integrals of the eigenfunctions of the modes involved in the coupling. The quantities κ_-, κ_0, and κ_+ are the linear growth rates of the $m = -1, 0, +1$ components, respectively.

The numerical solutions of the AEs associated with this resonance identify three distinct regimes (see the example provided in Buchler et al. 1997). In order of magnitude, the occurrence of these three regimes can be roughly quantified by a parameter, D, defined as

$$D \equiv \frac{2\pi\delta\nu}{\kappa_0}. \tag{4}$$

But the ranges for this parameter that defines the boundaries of the various regimes depends somewhat on the values of the nonlinear coefficients in the real star.

The first predicted situation is the nonlinear frequency lock regime in which the observed frequencies appear in exact resonance ($\delta\nu = 0$) and the amplitudes are constant. In the case of the DB white dwarf star GD 358, numerical solutions of the AEs indicated that the range of the D parameter that corresponds to this regime was between 0 and 20 (Goupil et al. 1998). However, these values are probably not universal and depend on the specific properties of the mode being considered, in particular on the value of the linear growth rate, κ_0, of the central component of the considered triplet.

When the triplet components move away from the resonance center ($\delta\nu \neq 0$), they enter the so-called intermediate regime where their amplitudes and frequencies are no longer stable and modulations can appear in the pulsations. In this regime, periodic variations can be expected with a timescale of

$$P_{\rm mod} \sim \frac{1}{\delta\nu} \simeq \frac{2\pi}{\kappa_0}\frac{1}{D}, \tag{5}$$

i.e., roughly the timescale that is derived from the inverse of the frequency asymmetry of the triplet (dominated by the second order effect of stellar rotation), which is connected to the inverse of the growth rate of the pulsating mode by the D parameter (Goupil et al. 1998).

Far from the resonance condition, the modes recover the regime of steady pulsations with nonresonant frequencies. In the nonresonant regime, the nonlinear frequency shifts become very small and the frequencies are close to the linear ones.

We finally point out that, in addition to the above three regimes, there exits a narrow hysteresis (transitory) regime between the frequency lock and intermediate regimes where the frequencies can be locked while the amplitudes still follow a modulated behavior.

3.2. Connection with the observed triplets

In light of the theoretical framework summarized above, we point out that some of the behaviors observed in the two triplets f_1 and f_2 and in the doublet f_3 (an incomplete triplet) can be quite clearly connected to nonlinear resonant couplings that occur in different regimes. We discuss each case below, but since the linear growth rate of the modes is an important ingredient to these resonance mechanism, we provide first some results of

linear nonadiabatic pulsation calculations specifically tuned for a model representing best the DBV star KIC 08626021.

3.2.1. Nonadiabatic properties of the observed modes

Following our re-analysis of the data obtained for KIC 08626021 with ***Kepler***, the recognition that eight independent periods have to be considered for a detailed asteroseismic study (and not only seven as used in BK14) coupled with our present need for a realistic seismic model representation of the star to carry out a nonadiabatic study of the mode properties led us to attempt a new asteroseismic analysis for this object. The details of this seismic study – a subject by its own that deserves a specific attention – are fully reported in Giammichele et al. (in prep.). The seismic solution that is obtained by Giammichele et al. (in prep.) for KIC 08626021 constitutes a major improvement over any of the fits proposed so far for this star, considering that it reproduces the eight independent periodicities to the actual precision of the ***Kepler*** observations. It is, therefore, an excellent reference for our purposes.

We used this specific seismic model to estimate the theoretical linear growth rates of the fitted pulsations modes. These computations were done by using two different nonadiabatic pulsation codes, one still working in the frozen convection (FC) approximation (Brassard et al. 1992; Fontaine et al. 1994; Brassard & Fontaine 1997) and the other implementing a more realistic time-dependent convection (TDC) treatement (Dupret 2001; Grigahcène et al. 2005). In DA and DB white dwarf pulsators, the superficial convection layer has an important contribution to the driving of modes (through the sometimes called convective driving mechanism). The positions of the theoretical instability strips, in particular the blue edges, are particularly sensitive to the adopted treatment (TDC vs. FC) and to the efficiency of convection itself that controls the depths of the convection zone (the α parameter in the Mixing Length Theory; see Van Grootel et al. 2012). These can also affect the growth rate of each individual mode. Unfortunately, the oscillation periods have essentially no sensitivity to the α parameter, which is therefore not constrained by seismology. In this context, we explored various combinations of α values for the two different nonadiabatic treatments of the convection perturbation to estimate the typical range of values one would expect for the growth rate of the modes.

The results of these nonadiabatic calculations are summarized in Table 2 for the triplet (and doublet) components $\boldsymbol{f}_1$, $\boldsymbol{f}_2$, $\boldsymbol{f}_3$, and, to be complete, for the other fitted frequencies as well. All these modes can effectively be driven in this star and the value of the growth rate κ_0 mostly depends on the radial order of the mode, strongly increasing when $\boldsymbol{k}$ increases. For the modes of interest, we find that κ_0 lies in the ranges 2×10^{-13}–7×10^{-12}, 2×10^{-12}–4×10^{-11}, and 1×10^{-11}–2×10^{-10} for $\boldsymbol{f}_2$, $\boldsymbol{f}_1$, $\boldsymbol{f}_3$, which, from the seismic solution of Giammichele et al. (in prep.), are successive dipole modes of radial order $\boldsymbol{k}$ = 3, 4, and 5, respectively.

3.2.2. Triplets in the intermediate regime

The periodic amplitude and frequency modulations that are observed in the triplet at 4310 μHz ($\boldsymbol{f}_1$) immediately suggest that this triplet is in the intermediate regime of the resonance (see Fig. 7 again). Both the prograde and retrograde components show a modulation of frequency and amplitude with a period of ~600 d. The central ($\boldsymbol{m}$ = 0) component of $\boldsymbol{f}_1$ has a frequency and amplitude modulation that is perhaps slightly longer (~680 d; precision is low here as this is about the same timescale as the duration of the observing campaign), but remains of the same order. For comparison purposes, we provide in Table 2 the modulation timescale $\boldsymbol{P_m}$(th) ~ $1/\delta\nu_t$ (Eq. (5)) expected from the asymmetry, $\delta\nu_t$, that is caused by the second order correction to the rotational splitting. The latter is computed with the $\boldsymbol{C_{k\ell}}$ value obtained from the reference model and the value $\boldsymbol{P}_{\rm rot}$ = 1.75 days for the rotation period of the star. With $\boldsymbol{P_m}$(th) ≃ 620 days, the value obtained is sufficiently consistent with the observed modulation period to support the idea that we have indeed uncovered the right explanation for the behavior of the components in this triplet. Interestingly, the asymmetry can also be derived directly from the measured frequencies. Using directly the values given in Table 1, the quantity $\delta\nu_o$ represents the asymmetry for the frequencies averaged over the observation time baseline. We find it to be very small, i.e., much smaller than $\delta\nu_t$, suggesting that even in this intermediate regime the nonlinear interactions may already have forced the frequencies of the triplet components to a locked position (where $\delta\nu \to 0$), on average (since the frequencies are still varying with time, oscillating around their mean value).

According to the nonlinear resonant coupling theory, all the three components in a triplet should have the same modulations, both in amplitude and frequency. The slight difference between the side components and the central component in terms of the modulation period might be that the interaction of the modes in the DBV star is more complex than the idealized case described by the theory. It might also be a suggestion that the growth rates for each component of the triplet are not similar (as is assumed in this theoretical framework). The shape of the amplitude modulations of the retrograde component $\boldsymbol{f}_{1,-}$ is not as smooth as the other two components. This might be caused by the additional coupling of the mode with $\boldsymbol{f}_4$ at 2659 μHz (see Sect. 2.4.4 and Fig. 12). Such a coupling that occurs outside the triplet is not considered by Buchler et al. (1995) who neglects other interactions with independent modes (i.e, the triplet is considered as an isolated system).

The second structure that can also be associated with the intermediate regime is the doublet $\boldsymbol{f}_3$. We recall that the best interpretation for this doublet is that it belongs to a ℓ = 1 triplet with one of the side components (the low frequency one, $\boldsymbol{f}_{3,-}$) missing, most likely because its amplitude is below the detection threshold. The two remaining components show clear periodic modulations of both frequencies and amplitudes. All variations occur on a somewhat shorter timescale of $\boldsymbol{P_m}$(obs) ~ 263 days (which means that they are fully resolved in our data set, contrary to the modulations of $\boldsymbol{f}_1$; see Sect. 2.4.3 and Fig. 11), except for the frequency of the $\boldsymbol{f}_{3,-}$ component whose modulation period appear to be approximately twice that value ($\boldsymbol{P_m}$(obs) ~ 550 days). For this $\boldsymbol{f}_3$ mode, the second order rotational splitting correction $\delta\nu_t$ also suggests a shorter modulation timescale of $\boldsymbol{P_m}$(th) ~ 518 days, which is comparable but not strictly identical. It is not possible in this case to evaluate $\delta\nu_o$ because of the missing third component.

3.2.3. A triplet in the transitory hysteresis regime

The case of the $\boldsymbol{f}_2$ triplet at 5073 μHz (see Sect. 2.4.2 and Fig. 10) is slightly different in that the frequencies are clearly stabilized while the amplitudes are modulated. This suggests that $\boldsymbol{f}_2$ is in another configuration, in between the frequency lock regime (where both amplitudes and frequencies are locked and therefore non-variable) and the intermediate regime. This configuration could be linked to the narrow transitory hysteresis regime briefly mentionned in Sect. 3.1. This finding shows that two neighbor triplets can belong to different resonant regimes (frequency lock,

narrow transition, intermediate or nonresonant), as it was also noticed for the white dwarf star GD 358 (Goupil et al. 1998).

3.3. Linear growth rates and the D parameter

Table 2 also provides the estimated values for the parameter $\boldsymbol{D}$ derived from Eq. (4) and from the values of $\delta\nu_t$ (Eq. (1)) and κ_0 (obtained from the seismic model of KIC 08626021; see Sect. 3.2.1). We find that $\boldsymbol{D}$ lies in the ranges 3×10^3–6×10^4, 1×10^4–5×10^5 and 7×10^2–1×10^4 for the triplet $\boldsymbol{f}_1$, $\boldsymbol{f}_2$ and $\boldsymbol{f}_3$, respectively. These values are at least one order of magnitude larger than the range given in Goupil et al. (1998) for the intermediate regime ($\boldsymbol{D}\sim9$–25 for the white dwarf star GD 358). This large difference is clearly caused by the linear growth rates (κ_0) adopted for the modes. Our values come from a detailed linear nonadiabatic calculation based on the seismic model. Since the three triplets are fitted to low radial order consecutive modes ($\boldsymbol{k}$ = 3, 4, and 5), their corresponding linear growth rates are generally small and differ substantially from one mode to the other (κ_0 increases rapidly with $\boldsymbol{k}$). In contrast, Goupil et al. (1998) roughly scaled the growth rate of the modes according to the relationship $\boldsymbol{A}_{\boldsymbol{k}}^2/\boldsymbol{A}_{\boldsymbol{k}'}^2 \sim \kappa_{\boldsymbol{k}}/\kappa'_{\boldsymbol{k}}$, assuming that all the coupling coefficients $\boldsymbol{q}^{\boldsymbol{R}}$ are of the same order of magnitude, leading to estimated values of $\kappa_0\sim10^{-8}$. Values comparable to Goupil et al. (1998) for the growth rate could be obtained only if the three triplets were assigned to higher radial orders ($\boldsymbol{k}$ between 10 and 15 instead of 3 to 5). This would require a huge shift compared to the current seismic solution which is clearly not permitted on the seismic modeling side.

In the AEs formalism of Buchler et al. (1997), the solutions admit three distinct regimes and one narrow transitory regime. Those regimes are related to the distance from the resonance center (i.e., $\delta\nu = 0$). The parameter $\boldsymbol{D}$ in this transitory regime should be slightly smaller than in the intermediate regime, as this transitory regime is closer to the resonance center. This means that $\boldsymbol{D}$ should be smaller for $\boldsymbol{f}_2$, which is in this transitory regime, compared to $\boldsymbol{f}_1$ and $\boldsymbol{f}_3$ that are in the intermediate regime. The ranges given for the $\boldsymbol{D}$ values in Table 2 still permit this constraint to be roughly satisfied, but the overall larger $\boldsymbol{D}$ values for $\boldsymbol{f}_2$ could also lead to a contradiction here.

We think, at this stage, that further quantitative comparisons between theoretical considerations and the observed properties of the modulations would require to solve the amplitude equations specifically for this case. This is however beyond the scope of this paper, as no specific modeling tools for these nonlinear effects is available to us at present. We emphasize that with a detailed numerical solution of the nonlinear amplitude equations, the unknown coupling coefficients could, in principle, be determined from fitting the observed frequency and amplitude modulations. These coefficients, if known, would then allow us to derive the $\boldsymbol{D}$ parameter which is strongly related to the different regimes of the nonlinear resonances. With the determination of this parameter, a measurement of the growth rate of the oscillation modes would then possibly follow, leading for the first time to an independent estimation of the linear nonadiabatic growth rates of the modes and a direct test of the nonadiabatic pulsation calculations.

4. Summary and conclusion

Frequency and amplitude modulations of oscillation modes have been found in several rotationally split triplets that are detected in the DB pulsator KIC 08626021, thanks to the high-quality and long-duration photometric data obtained with the ***Kepler*** spacecraft. These modulations show signatures that point toward nonlinear resonant coupling mechanisms which occur between the triplet components. This is the first time that such signatures are identified so clearly in white dwarf pulsating stars, although hints of such effects had already been found from ground-based campaigns in the past (e.g., Vauclair et al. 2011).

Reanalysing in detail the nearly two years of ***Kepler*** photometry obtained for this star, we have detected 13 very clear independent frequencies above our estimated secure detection threshold (5.6σ; see Sect. 2.2 and Table 1), two frequencies that appear to be linear combinations of other independent modes, and two additional, but significantly less secured, frequencies emerging just above 5σ the mean noise level. Overall, we find that our secured frequencies are consistent with those reported in BK14, but we somewhat differ in the interpretation of some structures in the frequency spectrum.

Most notably, we find that three frequencies in the 3677–3686 μHz range, formerly identified as the components of a single triplet by BK14, cannot be interpreted like this. We conclude instead that one of the frequencies ($\boldsymbol{f}_7$ in Table 1) is an independent mode while the other two ($\boldsymbol{f}_{3,0}$ and $\boldsymbol{f}_{3,+}$) form the visible components of an incomplete triplet whose third component is not seen. This has some implications for the seismic modeling which should in fact include eight independent frequencies and not only seven as in BK14. A new detailed seismic analysis of KIC 08626021 based on these eight modes is provided by Giammichele et al. (in prep.). The frequency spacings (observed between the two components of $\boldsymbol{f}_3$ and the components of other two well identified triplets, $\boldsymbol{f}_1$ and $\boldsymbol{f}_2$) indicate an average rotation period of ∼1.75 days for KIC 08626021, i.e., in agreement with the value given by BK14.

Also differing from BK14, we find that the two components of the $\boldsymbol{f}_3$ doublet have a hyperfine structure with sidelobes separated by 0.044 μHz, which indicates a modulating phenomenon that occurs on a long timescale of ∼263 days. In addition, the components that form triplets show long-term and quasi-periodic frequency and/or amplitude modulations which appear to be correlated, as they evolve either in phase or antiphase. The triplet at 4310 μHz ($\boldsymbol{f}_1$) show signs of periodic modulation of both the frequencies and amplitudes with a timescale of roughly 600 days with the side components evolving in phase, while the central mode is in antiphase. The timescale appears somewhat shorter (263 days) for the $\boldsymbol{f}_3$ doublet while the triplet $\boldsymbol{f}_2$ shows only modulations in amplitudes (the frequencies appear stable during the observations) with a probable timescale of ∼700 days.

We show that these behaviors can be related to the so-called nonlinear resonant coupling mechanisms that is expected to occur within rotationnally split triplets. The amplitude equations (Buchler et al. 1997; Goupil et al. 1998) predict three main regimes in which the triplet components may behave differently. It appears that $\boldsymbol{f}_1$ and $\boldsymbol{f}_3$ can be linked to the so-called intermediate regime of the resonance where both the amplitude and frequency of the modes should experience a periodic modulation. We find that the timescales expected from the theory are quite consistent with the observed periodicities of the modulations. The triplet $\boldsymbol{f}_2$ shows a different behavior that can be associated with a narrow transitory hysteresis regime between the intermediate regime and the frequency locked regime in which locked frequencies and modulated amplitude solutions can coexist.

We also found correlated frequency and amplitude modulations in a linear combination of frequencies which involves the modes $\boldsymbol{f}_{1,-}$ and $\boldsymbol{f}_4$, and the frequency $\boldsymbol{f}_8$. This configuration may be related to parents/child mode interactions in pulsating stars, $\boldsymbol{f}_8$ being either a combination frequency resulting from strong

nonlinearities or, because the amplitude ratio is large, an eigenmode whose amplitude has been significantly enhanced by a resonant coupling phenomenon (see Breger & Montgomery 2014). Further investigations need to be carried out to evaluate which explanation is the most plausible.

As an additional step toward comparing more quantitatively observations to the theoretical expectations, we estimated theoretical linear growth rates (see Table 2) of the triplet central components using the seismic model provided by Giammichele et al. (in prep.). We used two different nonadiabatic pulsation codes for these computations: one working in the frozen convection approximation (Brassard et al. 1992; Fontaine et al. 1994; Brassard & Fontaine 1997) and the other implementing a time-dependent convection treatement (Dupret 2001; Grigahcène et al. 2005). The modes of interest $\boldsymbol{f}_2$, $\boldsymbol{f}_1$ and $\boldsymbol{f}_3$ have growth rates that are in the ranges 2×10^{-13}–7×10^{-12}, 2×10^{-12}–4×10^{-11}, and 1×10^{-11}–2×10^{-10}, respectively. With these values, we finally estimate the parameter $\boldsymbol{D}$ (a key parameter that measures how far away is the mode from the resonance center) which is found in the range 3×10^{3}–6×10^{4}, 1×10^{4}–5×10^{5} and 7×10^{2}–1×10^{4} for the mode triplet $\boldsymbol{f}_1$, $\boldsymbol{f}_2$ and $\boldsymbol{f}_3$, respectively. These values are significantly larger than those estimated in Goupil et al. (1998) and need further investigation, but going beyond this would require to solve the amplitude equations for the specific case of KIC 08626021, which is currently not possible.

We also want to emphasize the fact that the uncovered frequency modulations, which are related to nonlinear coupling mechanisms and that occur on timesscales long enough to be difficult to detect but short compared to the secular evolution timescale, can potentially impair any attempt to measure reliably the effects of the cooling of the white dwarf on the pulsation periods. Measuring the changing rate of the pulsation periods in white dwarf stars could indeed offer an opportunity to constrain the neutrino emission physics (Winget et al. 2004; Sullivan et al. 2008). However, one should be extremely careful of the potential contamination of nonlinear effects, which may need to be corrected first. Some independent modes in KIC 08626021 that seem to be stable in frequency over much longer timescales and that do not apparently couple with other modes could be good candidates for measuring period rates of change. But nonlinear interactions could still be affecting them on longer timescales that we cannot detect with ***Kepler***.

Finally, the observed periodic frequency and amplitude modulations that occur in the intermediate regime of the resonance may allow for new asteroseismic diagnostics, providing in particular a way to measure for the first time linear growth rates of pulsation modes in white dwarf stars. This prospect should motivate further theoretical work on nonlinear resonant mode coupling physics and revive interest in nonlinear stellar pulsation theory in general.

Acknowledgements. Funding for the ***Kepler*** mission is provided by NASA's Science Mission Directorate. We greatfully acknowledge the ***Kepler*** Science Team and all those who have contributed to making the ***Kepler*** mission possible. W.K.Z. acknowledges the financial support from the China Scholarship Council. V. Van Grootel is an F.R.S-FNRS Research Associate. This work was supported in part by the Programme National de Physique Stellaire (PNPS, CNRS/INSU, France) and the Centre National d'Études Spatiales (CNES, France).

References

Beauchamp, A., Wesemael, F., Bergeron, P., et al. 1999, ApJ, 516, 887
Bischoff-Kim, A., & Østensen, R. H. 2011, ApJ, 742, L16
Bischoff-Kim, A., Østensen, R. H., Hermes, J. J., & Provencal, J. 2014, ApJ, 794, 39
Brassard, P., & Fontaine, G. 1997, White dwarfs, 214, 451
Brassard, P., Pelletier, C., Fontaine, G., & Wesemael, F. 1992, ApJS, 80, 725
Brassard, P., Fontaine, G., & Wesemael, F. 1995, ApJS, 96, 545
Breger, M., & Montgomery, M. H. 2014, ApJ, 783, 89
Buchler, J. R., & Goupil, M.-J. 1984, ApJ, 279, 394
Buchler, J. R., Goupil, M.-J., & Serre, T. 1995, A&A, 296, 405
Buchler, J. R., Goupil, M.-J., & Hansen, C. J. 1997, A&A, 321, 159
Charpinet, S., Green, E. M., Baglin, A., et al. 2010, A&A, 516, L6
Charpinet, S., Van Grootel, V., Fontaine, G., et al. 2011, A&A, 530, A3
Córsico, A. H, Althaus, L. G., Miller Bertolami, M. M., & Bischoff-Kim, A. 2012, A&A, 541, A42
Deeming, T. J. 1975, Ap&SS, 36, 137
Dupret, M. A. 2001, A&A, 366, 166
Dziembowski, W. A. 1982, Acta Astron., 32, 147
Dziembowski, W. A., & Goode, P. R. 1992, ApJ, 394, 670
Fontaine, G., & Brassard, P. 2008, PASP, 120, 1043
Fontaine, G., Brassard, P., Wesemael, F., & Tassoul, M. 1994, ApJ, 428, L61
Fu, J.-N., Dolez, N., Vauclair, G., et al. 2013, MNRAS, 429, 1585
Gilliland, R. L., Timothy, M., Christensen-Dalsgaard, J., et al. 2010, PASP, 122, 131
Goupil, M.-J., & Buchler, J. R. 1994, ApJ, 279, 394
Goupil, M. J., Dziembowski, W. A., & Fontaine, G. 1998, Balt. Astron., 7, 21
Grigahcène, A., Dupret, M.-A., Gabriel, M., Garrido, R., & Scuflaire, R. 2005, A&A, 434, 1055
Hermes, J. J., Montgomery, M. H., Mullally, F., et al. 2013, ApJ, 766, 42
Jenkins, J. M., Caldwell, D. A., Chandrasekaran, H., et al. 2010, ApJ, 713, L87
Montgomery, M. H. 2005, ApJ, 633, 1152
Moskalik, P. 1985, Acta Astron., 35, 229
Østensen, R. H. 2013, ASP Conf. Ser., 469, 3
Østensen, R. H., Bloemen, S., Vučković, M., et al. 2011, ApJ, 736, L39
Salabert, D., García, R. A., & Turck-Chièze, S. 2015, A&A, 578, A137
Scargle, J. D. 1982, ApJ, 263, 835
Silvotti, R., Schuh, S., Janulis, R., et al. 2007, Nature, 449, 189
Sullivan, D. J., Metcalfe, T. S., O'Donoghue, D., et al. 2008, MNRAS, 387, 137
Unno, W., Osaki, Y., Ando, H., Saio, H., & Shibahashi, H. 1989, Nonradial oscillations of stars (Tokyo: University of Tokyo Press), 2nd edn.
Van Hoolst, T. 1994, A&A, 292, 183
Van Grootel, V., Dupret, M.-A., Fontaine, G., et al. 2012, A&A, 539, A87
Vauclair, G. 2013, ASP Conf. Ser., 479, 223
Vauclair, G., Fu, J.-N., Solheim, J.-E., et al. 2011, A&A, 528, A5
Winget, D. E., & Kepler, S. O. 2008, ARA&A, 46, 157
Winget, D. E., Sullivan, D. J., Metcalfe, T. S., et al. 2004, ApJ, 602, L109
Wu, Y. 2001, MNRAS, 323, 248
Wu, Y., & Goldreich, P. 2001, ApJ, 546, 469

Chapter 5

The pulsating hot B subdwarf star KIC 10139564

This chapter is dedicated to the pulsating hot B sudwarf star KIC 10139564 whose multiplet modes show clear amplitude and frequency variations [1]. Those mode modulations could be the evidence of nonlinear mode interactions associated with resonant mode coupling mechanisms. We give a brief summary of the content in that article, and one can see details in the following attached paper. KIC 10139564 is the only p-mode dominated hybrid sdB star observed by *Kepler*. The former studies on this star in the literature are discussed in details in Section 3.2 and also in the attached paper, in particular on its frequency content based on the *Kepler* data.

5.1 The frequency content revisited

We analyzed the 38-month ($\sim 1\,147.5$ days) data gathered on KIC 10139564 continuously observed by *Kepler*, starting from BJD 2 455 276.5 and ending on BJD 2 456 424, with a duty cycle of $\sim 89\%$. Following the analysis procedures provided in Section 3.3, the Lomb-Scargle periodogram (LSP) shows two distinct regions with significant signal corresponding to p-modes at high frequencies (highest amplitude is around 1%) and g-modes at low frequencies (highest amplitude is around 500 ppm). We have detected 60 independent frequencies that come out above the 5.6σ detection threshold. Twenty nine of these frequencies form three triplets, one doublet, one quintuplet and two incomplete ($\ell > 2$) multiplets. We also detected another three frequencies that appear as significant but are related to other frequencies through linear combinations. Five additional "forests" of frequencies are detected in the 5400–6400 μHz region, each contains many close peaks in a very narrow frequency range (the formal frequency resolution is $\sim 0.01\,\mu$Hz). Another 14 frequencies were also prewhitened from the light curve, with amplitudes between 5.0σ and 5.6σ, which, we suspect, are real pulsations. Our well-secured extracted frequencies agree well with the independent analysis of Baran & Østensen (2013), but we detected a few more low-amplitude frequencies because the data that we considered here span over about one more year. The complicated structures of five "forests" of frequencies were not further investigated here, but were discussed in Baran et al. (2012). We point out that our extracted frequencies may differ in amplitude compared with the work of Baran & Østensen (2013) because some of these frequencies have variable amplitudes, as indicated by the broaden structures of the frequencies in the LSP.

1. The results have been published on *Astronomy & Astrophysics*, 594, A46, 2016 : Signatures of nonlinear mode interactions in the pulsating hot B subdwarf star KIC 10139564 ; Zong, W. ; Charpinet, S. ; Vauclair, G.

5.2 Amplitude and frequency modulations

We concentrate on the six multiplets that include three triplets T_1, T_2 and T_3, one doublet D_1, one quintuplet Q_1 and a likely $\ell = 4$ multiplet M_1 (see Table 2 in the attached paper). Interestingly, three of these multiplets (Q_1, M_1, and T_1) are p-modes, while the others (T_2, D_1, and T_3) involve g-modes. We also examine three linear combination frequencies (C_1) and their large amplitude ratios. The sLSPs's filtering window here is chosen to be 200-d wide with a time step of 20 days, which is optimal for the case of KIC 10139564. The entire light curve was divided into 32 time intervals, each containing 9-month of data except for the last three intervals at the end of the observations. This allows us to obtain precise values for the averaged amplitudes and frequencies in each interval.

The triplet T_1 near 5760 μHz shows clear amplitude and frequency variations (Fig. 4). We find that the two side components in T_1 show quasi-periodic modulations in frequency and evolve in antiphase. Moreover, their frequencies gradually approach toward each other, as well as toward to the central component. After extracting the long-term trend of the frequency variations, we determined quasi-sinusoidal variations of the remaining modulations with a similar period of $\sim$ 570 days for the three components (Fig. 5). The frequencies appear to be stable in the triplet T_2 near 316 μHz, while, two components display amplitude variations (Fig. 6), particularly for the largest amplitude ($m = +1$) component whose amplitude increases from $\sim$ 400 ppm to $\sim$ 600 ppm. The components forming the triplet T_3 near 519 μHz have stable frequencies and amplitudes (Fig. 7), which is further illustrated in Fig. 8. The doublet D_1 near 394 μHz is very similar to the T_2 triplet, stable frequencies and variable amplitudes (Fig. 9). We determined a period of $\sim$ 1100 days for the amplitude modulations of the two components, as illustrated by the best-fitting sinusoidal functions to the data. Moreover, the amplitude of the two components evolve almost in antiphase. The quintuplet Q_1 near 5287 μHz whose components show different kinds of amplitude and frequency variations (Fig. 10). The ($m = 0, \pm 2$) components show significant frequency variations, while, the other modes have rather stable frequencies. In contrast, the amplitudes of all the five modes vary with patterns that cannot clearly be connected to periodic modulations. We note that the frequency variations of the $m = -2$ and $m = +2$ components and the amplitude modulations of the $m = -2$ and $m = -1$ components are roughly in antiphase. The five components in the incomplete multiplet M_1 near 5413 μHz show significant frequency and amplitude variations (Fig. 11). We find that a long-term drifted trend occurs between the two side components, which may be comparable to that observed in T_1.

In addition to the above multiplets, we also focus on the interesting narrow frequency region near 6076 μHz where three structures (f_{23}, f_{35} and f_{74}) show amplitude and frequency modulations (Fig. 12). These frequencies are in fact related to components of the T_1 and T_2 triplets through linear combinations, $f_{23} \sim f_1 + f_{11}$, $f_{35} \sim f_3 + f_{21}$, and $f_{74} \sim f_3 + f_{11}$. Interestingly, we note that the frequency and amplitude variation pattern of f_{23} is similar to the variations observed for the mode f_1. This similarities also exist between the frequencies f_{35} and f_2. The peak f_{74}, for its part, shows a rather large frequency variation covering up to $\sim 0.1\,\mu$Hz.

5.3 Connections with nonlinear resonant couplings

These observed modulations obviously cannot be related to any instrumental effects, the evolutionary effects in sdB stars, the presence of orbiting companions, and the magnetic activities on the stellar surface, as mentioned in Section 4.3. Instead, we propose that nonlinear mode interactions can account for the various observed modulations. The nonlinear theory has been thoroughly discussed in Section 1.4.

The periodic modulations in the T_1 triplet suggest that T_1 is in the intermediate regime of the triplet resonance. We recall that the periods ~ 550 days and ~ 600 days for the remained short-term frequency variations of the side components and the central one, respectively, correspond to a frequency mismatch of $\delta\omega \sim 0.02\,\mu$Hz in this triplet, which is comparable to the maximum extent of the observed frequency asymmetry (from 33 measurements independently). The quintuplet Q_1 also shows amplitude and frequency variations that may be associated with the intermediate regime. However, we cannot estimate timescales for the complex modulations (possibly irregular patterns) in this multiplet. We also note that the connection of Q_1 with the intermediate regime is based on the assumption that nonlinear five-mode interactions has mainly three distinct regimes, since no theoretical exploration has been done for this five-mode case, yet. Another case may be connected with the intermediate regime : the multiplet M_1 which also shows complex amplitude and frequency variations. The timescale cannot be determined in this multiplet. This multiplet M_1 could be the siege of even more complex resonant coupling interactions than the quintuplet Q_1, since there are six detected components, with at least three components missing. The triplet T_2 shows modulated amplitude and constant frequencies that is the configuration linked to the narrow transitory hysteresis regime that is between the intermediate regime and frequency locked regime. The doublet D_1 may also be in this regime as it shows a configuration similar to T_2. The case of T_3, definitely different from the above multiplets, shows stable frequencies and amplitudes, which suggests T_3 is in the frequency locked regime where frequencies should also be equidistant. Indeed, we find that the observed frequency asymmetry, $\delta\omega = 0.0008\,\mu$Hz, that is less than the measured error $0.0011\,\mu$Hz, is consistent with no asymmetry (exact resonance). In brief summary, we have found various mode behaviors occurring in the multiplets in KIC 10139564. Those behaviors can be related to different regimes expected from amplitude equations of triplet resonance.

The amplitude and frequency variations of C_1 have strong correlations with that of the T_1 components. The large frequency variations suggest that C_1 may correspond to resonant mode coupling rather than simple linear combination frequencies. Moreover, the amplitude ratios are 37 and 85 for $f_{23} \sim f_1 + f_{11}$ and $f_{35} \sim f_3 + f_{21}$, respectively, that is significantly higher than the normal ratios in sdB stars. We note that the low amplitude frequency, f_{74}, varies on a range of $\sim 0.01\,\mu$Hz. This is possibly a real mode, with a frequency around $6076.58 - 6076.69\,\mu$Hz, which first interacts with the frequency sum $f_2 + f_{39} \sim 6076.59\,\mu$Hz, then with the frequency sum $f_3 + f_{11} \sim 6076.66\,\mu$Hz. We note that all the involved frequencies are the components of triplets T_1 and $T2$, expected to be overstable modes. Therefore, the amplitude and frequency modulations of C_1 are the results of nonlinear direct three-mode resonance. This finding suggests that the components forming a triplet can also interact with the other mode outside the triplet and the triplet resonant system cannot be simply treated as an isolated system, thus leading to a more complex pattern of mode behaviors.

The D parameter is near zero for the locked triplet T_3, as expected from the AEs (Section 1.4.3). However, we find that the D-value for the other triplets T_1 and T_2 may reflects more their linear growth rates. These two triplets have two different growth rates because that rate for p- and g-modes is substantially different (Charpinet 1999; Fontaine et al. 2003). The observed D-values for these two triplets differ somewhat from the prediction by the nonlinear AEs exploration. We recall that this difference in D-values are also observed in the DBV star KIC 08626021 (Chapter 4). This further suggests that the nonlinear behaviors not only depend on the magnitude of D, but also on the specific coupling coefficients for each specific mode (Buchler et al. 1995). The coupling coefficients, in principle, could be extracted from the observed amplitude and frequency modulations (Buchler et al. 1995), which eventually provide a way to measure the linear growth rates of these pulsation modes.

5.4 Summary and conclusion

The sdB star KIC 10139564 is the second compact target that was thoroughly investigated from the *Kepler* photometry within our project, aiming at uncovering the mechanisms responsible for amplitude and frequency modulations of the oscillation modes. In this star, six multiplets show various characters of mode behaviors that suggests nonlinear mode interactions occurring between the involved modes under resonant conditions. The observed modulations whose periods are consistent with the predictions for resonant coupling mechanisms. However, we found a difference between the observed and theoretical D parameters in terms of the value corresponding different regimes. This particularly needs further investigations, e.g., to obtain the nonlinear coefficients in AEs for the involved modes. Furthermore, some of the involved modes seem to be able to participate in different types of resonance, which may lead to more complex mode behaviors.

The observed frequency modulations likely induced by nonlinear mode interactions could challenge any future attempts to measure the evolutionary effects on the pulsation periods in pulsating sdB stars. To obtain a robust measurement of the rate of period change, the nonlinear effects should be eliminated beforehand. We finally emphasize that the observed periodic modulations occurring in the intermediate regime of the triplet resonance may allow for new asteroseismic diagnostics, providing in particular a way to measure for the first time linear growth rates of pulsation modes in hot B sudwarf stars. This prospect should motivate further theoretical work on nonlinear resonant mode coupling physics and revive interest in nonlinear stellar pulsation theory in general.

A&A 594, A46 (2016)
DOI: 10.1051/0004-6361/201629132

Astronomy & Astrophysics

Signatures of nonlinear mode interactions in the pulsating hot B subdwarf star KIC 10139564

W. Zong[1,2], S. Charpinet[1,2], and G. Vauclair[1,2]

[1] Université de Toulouse, UPS-OMP, IRAP 31400 Toulouse, France
e-mail: [weikai.zong;stephane.charpinet;gerard.vauclair]@irap.omp.eu
[2] CNRS, IRAP, 14 avenue Edouard Belin, 31400 Toulouse, France

Received 16 June 2016 / Accepted 18 July 2016

ABSTRACT

Context. The unprecedented photometric quality and time coverage offered by the *Kepler* spacecraft has opened up new opportunities to search for signatures of nonlinear effects that affect oscillation modes in pulsating stars.
Aims. The data accumulated on the pulsating hot B subdwarf KIC 10139564 are used to explore in detail the stability of its oscillation modes, focusing in particular on evidences of nonlinear behaviors.
Methods. We analyzed 38 months of contiguous short-cadence data, concentrating on mode multiplets induced by the star rotation and on frequencies forming linear combinations that show intriguing behaviors during the course of the observations.
Results. We find clear signatures that point toward nonlinear effects predicted by resonant mode coupling mechanisms. These couplings can induce various mode behaviors for the components of multiplets and for frequencies related by linear relationships. We find that a triplet at 5760 μHz, a quintuplet at 5287 μHz and a ($\ell > 2$) multiplet at 5412 μHz, all induced by rotation, show clear frequency and amplitude modulations which are typical of the so-called intermediate regime of a resonance between the components. One triplet at 316 μHz and a doublet at 394 μHz show modulated amplitude and constant frequency which can be associated with a narrow transitory regime of the resonance. Another triplet at 519 μHz appears to be in a frequency-locked regime where both frequency and amplitude are constant. Additionally, three linear combinations of frequencies near 6076 μHz also show amplitude and frequency modulations, which are likely related to a three-mode direct resonance of the type $\nu_0 \sim \nu_1 + \nu_2$.
Conclusions. The identified frequency and amplitude modulations are the first clear-cut signatures of nonlinear resonant couplings occurring in pulsating hot B subdwarf stars. However, the observed behaviors suggest that the resonances occurring in these stars usually follow more complicated patterns than the simple predictions from current nonlinear theoretical frameworks. These results should therefore motivate further work to develop the theory of nonlinear stellar pulsations, considering that stars such as KIC 10139564 now offer remarkable testbeds to do so.

Key words. techniques: photometric – stars: variables: general – stars: individual: KIC 10139564

1. Introduction

Hot B subdwarf (sdB) stars are helium core burning objects that populate the so-called extreme horizontal branch (EHB). They are expected to have a mass around 0.47 $M_\odot$ and are characterized by a very thin hydrogen-rich residual envelope containing at most ~0.02 $M_\odot$. For this reason, they remain hot and compact throughout all their helium core burning evolution, with effective temperatures, $T_{\rm eff}$, and surface gravities, $\log g$, ranging from 22 000 K to 40 000 K and from 5.2 to 6.2, respectively (Heber 2009; Fontaine et al. 2012).

The presence of pulsations in some sdB stars make them good candidates for probing their interior with the technique of asteroseismology. A first group of nonradial sdB pulsators with periods of a few minutes was theoretically predicted by Charpinet et al. (1996) and effectively discovered by Kilkenny et al. (1997). These pulsators, now referred to as the V361 Hya stars, show low-order, low-degree pressure (p-)modes that are driven by a κ-mechanism induced by the partial ionization of iron-group elements occurring in the "Z-bump" region and powered-up by radiative levitation (Charpinet et al. 1996, 1997). Long period oscillations of ~1−4 h were later discovered by Green et al. (2003), forming another group of sdB pulsators known as the V1093 Her stars. The latter show mid-order gravity (g-)modes driven by the same mechanism (Fontaine et al. 2003). Hybrid pulsators that show both p- and g-mode oscillations simultaneously have also been reported (e.g., Schuh et al. 2006). Tight seismic constraints have indeed been obtained from the measured frequencies using both types of sdB pulsators, in particular based on high-quality photometric data gathered from spaceborne telescopes (e.g., Charpinet et al. 2011; van Grootel et al. 2010). However, the reason behind the apparent variability of some oscillation modes in sdB stars, already noticed from repeated ground based campaigns (e.g., Kilkenny et al. 2007), has remained poorly understood.

The temporal variation of oscillation modes in pulsating sdB stars is beyond the scope of the standard linear nonradial stellar oscillation theory in which eigenmodes have a stable frequency and amplitude (Unno et al. 1989). These behaviors must be studied within a nonlinear framework to interpret the modulations. In particular nonlinear resonant mode coupling effects are expected to affect some oscillation modes, as noted, for example, in the helium dominated atmosphere white dwarf variable (DBV) star GD 358 (Goupil et al. 1998). Different types of resonant coupling have been investigated within the framework of the amplitude equation (AE) formalism since the 1980's

(e.g., Buchler & Goupil 1984), among them the $\nu_0 \sim \nu_1 + \nu_2$ resonance (Dziembowski 1982; Moskalik 1985) and the 2:1 resonance in Cepheid stars (Buchler & Kovacs 1986). The AE formalism was then extended to nonadiabatic nonradial pulsations in Eulerian and Lagrangian formulations by Goupil & Buchler (1994) and van Hoolst (1994), respectively. A theoretical exploration of specific cases of nonradial resonances was developed in Buchler et al. (1995, 1997), including notably the resonance occurring in a mode triplet that is caused by slow stellar rotation and which satisfies the relationship $\nu_+ + \nu_- \sim 2\nu_0$, where ν_0 is the frequency of the central $m = 0$ component. However, these theoretical developments based on AEs have since considerably slowed down, in part due to the lack of clear observational data to rely on.

The launch of instruments for ultra high precision photometry from space has changed the situation, making it now possible to capture amplitude and/or frequency modulations occurring on timescales of months or even years that were difficult to identify from ground-based observatories. It is however from ground based data that Vauclair et al. (2011) proposed for the first time that resonant couplings within triplets could explain the long-term variations, both in amplitude and frequency, seen in several oscillation modes monitored in the GW Virginis pulsator PG 0122+200, through successive campaigns.

The observation of a multitude of pulsating stars, including sdB and white dwarf stars, by the *Kepler* spacecraft has open up new opportunities to identify and characterize the mechanisms that could modulate the oscillation modes. *Kepler* monitored a 105 deg^2 field in the Cygnus-Lyrae region for around four years without interruption, thus obtaining unprecedented high quality photometric data for asteroseismology (Gilliland et al. 2010). These uninterrupted data are particularly suited for searching long-term temporal amplitude and frequency modulations. In the context of white dwarf pulsators, for instance, Zong et al. (2016, hereafter Z16) found that the DBV star KIC 08626021 shows clear signatures of nonlinear effects attributed to resonant mode couplings. In this star, three rotational multiplets show various types of behaviors that can be related to different regimes of the nonlinear resonant mode coupling mechanism. In particular some amplitude and frequency modulation timescales are found to be consistent with theoretical expectations. This finding suggests that the variations of some oscillation modes in sdB stars may also be related to nonlinear resonance effects. It is in this context that we decided to search clues of similar nonlinear phenomena involving mode interactions in pulsating sdB stars.

Eighteen sdB pulsators have been monitored with *Kepler* (see Østensen et al. 2014 and references therein). In this paper, we focus on one of them, the star KIC 10139564, which was discovered in quarter Q2.1 and then continuously observed from Q5.1 to Q17.2. A preliminary analysis based on one month of short cadence data originally showed that KIC 10139564 is a V361-Hya type (rapid, p-mode) sdB pulsator featuring also a low-amplitude g-mode oscillation (Kawaler et al. 2010). With extended data, Baran et al. (2012) detected up to 57 periodicities including several multiplets attributed to the rotation of the star. These multiplets are characterized by common frequency spacings, both for the p- and g-modes, indicating that KIC 10139564 has a rotation period of 25.6 ± 1.8 d. These authors did not find any radial-velocity variations from their dedicated spectroscopy and derived the atmospheric parameter values $T_{\rm eff}$ = 31 859 K and $\log g = 5.673$ for this star. An interesting finding concerning KIC 10139564 is that two of the identified multiplets may have degrees ℓ greater than two, a possibility further investigated by Baran & Østensen (2013). The detection of several multiplets in this star continuously monitored for more than three years makes it a target of choice for studying eventual nonlinear resonant mode couplings in sdB stars.

In this study, we show that several multiplets in KIC 10139564 have indeed amplitude and frequency modulations suggesting nonlinear resonant mode couplings, which constitutes the first clear-cut case reported for sdB pulsators, so far. In Sect. 2, we present the thorough analysis of the frequency content of the *Kepler* photometry available on KIC 10139564, including our analysis of the frequency and amplitude modulations identified in several multiplets and linear combination frequencies. In Sect. 3, we recall some theoretical background related to nonlinear resonant mode couplings, focusing mainly on two types of resonances. The interpretation of the observed modulations which may relate to nonlinear resonant mode couplings is discussed in Sect. 4. The summary and conclusion are then given in Sect. 5.

2. The frequency content of KIC 10139564 revisited

2.1. The Kepler photometry

The pulsating sdB star KIC 10139564 was observed by *Kepler* in short-cadence (hereafter SC) mode during quarter Q2.1 and from Q5.1 to Q17.2 (i.e., until the spacecraft finally lost its second inertia reaction wheel and stopped its operations). Results based on parts of these data have already been published in the literature (e.g., Baran et al. 2012; Baran & Østensen 2013). we obtained the light curves through the *Kepler* Asteroseismic Science Consortium (KASC)[1]. These data were processed through the standard *Kepler* Science Processing Pipeline (Jenkins et al. 2010). For our purposes, we do not further consider the "short" (one month) light curve of Q2.1 which is well disconnected from the main campaign and would introduce a large and detrimental gap for our upcoming analysis. This leaves us with a nearly contiguous 38-month light curve starting from BJD 2 455 276.5 and ending on BJD 2 456 424 (which spans ~1147.5 days), with a duty circle of ~89%.

The full light curve was constructed from each quarter "corrected" light curves, which most notably include a correction of the amplitudes taking into account contamination by nearby objects (this correction estimates that ~83.2% of the light comes from KIC 10139564). Each quarter light curve was individually detrended to correct for residual drifts by performing a sixth-order polynomial fit. Then, data points that differ significantly from the local standard deviation of the light curve were removed by applying a running 3σ clipping filter. Note that the latter operation decreases slightly the overall noise level in Fourier space, but has no incidence on the measured frequencies.

The fully assembled light curve of KIC 10139564 is shown in the top panel of Fig. 1 while the bottom panel expands a 0.8-day portion of the data. Low-amplitude multi-periodic oscillations dominated by periodicities of a few minutes are clearly visible. Their presence is confirmed in the corresponding Lomb-Scargle periodogram (LSP, Fig. 2; Scargle 1982). The LSP shows two distinct regions with significant signal corresponding to p-modes at high frequencies and g-modes at low frequencies. This identifies KIC 10139564 as a hybrid pulsating sdB star (Schuh et al. 2006) whose oscillations are however largely dominated by p-modes. The formal frequency resolution achieved with these data is ~0.010 μHz.

[1] http://astro.phys.au.dk/KASC

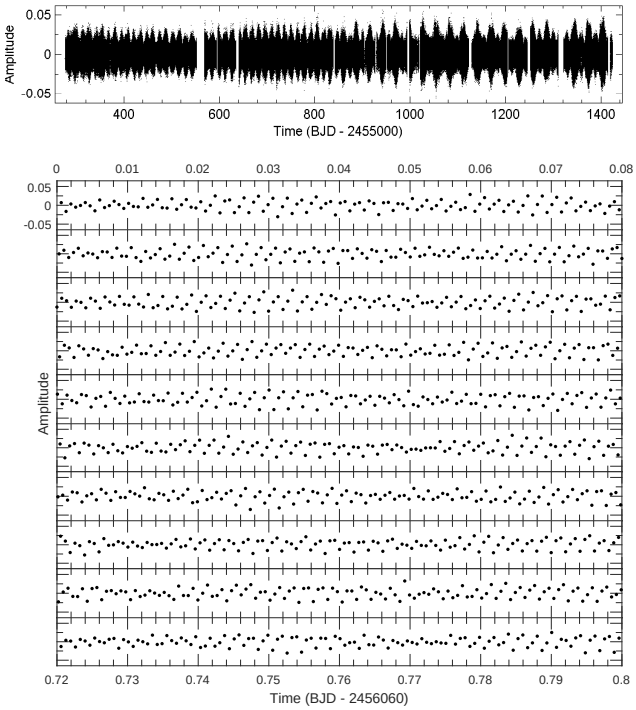

Fig. 1. *Top panel*: condensed representation of the full *Kepler* light curve of KIC 10139564 (Amplitude as the residual relative to the mean brightness intensity of the star vs time in Barycentric Julian Date) covering from Q5.1 to Q17.2 (∼1147.5 days). *Bottom panel*: close-up view showing 0.8 days of the *Kepler* light curve by slices of 0.08 days. At this scale the oscillations are clearly apparent.

2.2. Frequency extraction

A dedicated software, FELIX (Frequency Extraction for LIghtcurve eXploitation) developed by one of us (S.C.), was used to first extract the frequency content of KIC 10139564 down to a chosen detection threshold. The latter was established following the same method as in Z16 (see their Sect. 2.2), leading also in the present case to a conservative 5.6σ criterion (in practice, we searched down to $\sim 5\sigma$ if a frequency is suspected to be part of a multiplet; see below).

The extraction method is a standard prewhithening and nonlinear least square fitting technique (Deeming 1975), which works with no difficulty in the present case. The code FELIX greatly accelerates and eases the application of this procedure, especially for treating very long time-series obtained from space such as CoRoT and *Kepler* (Charpinet et al. 2010, 2011).

We provide in Table A.1 (see Appendix) a list of all the extracted frequencies with their fitted attributes (frequency in μHz, period in second, amplitude in percent of the mean brightness, phase relative to a reference time t_0, and signal-to-noise ratio) and their respective error estimates (σ_f, σ_P, σ_A, and σ_{Ph}). For convenience, because in this study we focus on a particular subset of the observed frequencies, we repeat some of these information in Table 1 for the relevant modes. The "Id." column in both tables uniquely identify a detected frequency with the number indicating the rank by order of decreasing amplitude.

We have detected 60 clear independent frequencies that comes out well above the 5.6σ detection threshold (Table A.1), of which 29 frequencies consist of three triplets, one doublet, one quintuplet and two incomplete multiplets with $\ell > 2$ (Table 1). We also detect another three frequencies that appear as significant but are linked to other frequencies through linear combinations. Five additional "forests" of frequencies, each containing many close peaks in a very narrow frequency range, are detected in the 5400−6400 μHz region. We also prewhitened 14 frequencies whose amplitudes are above 5.0σ but below 5.6σ which, we suspect, are real pulsations. Our well-secured extracted frequencies agree well with the independent analysis of Baran & Østensen (2013), but we detect a few more low-amplitude frequencies because the data that we consider here cover about one more year. We do not investigate further these "forests" of frequencies (G1–G5, see Table A.1) that show very complicated structures. These were discussed in Baran et al. (2012). We point out that our extracted frequencies may differ in amplitude compared with the work of Baran & Østensen (2013) because some of these frequencies have variable amplitudes.

2.3. Error estimates on frequencies and amplitudes

Before proceeding further in our analysis, we briefly discuss our quantitative evaluation of the uncertainties associated with the measured frequencies and amplitudes given in Tables 1 and A.1. The reliability of these error estimates is particularly important when it comes to discuss amplitude and frequency variations with time, in particular to assess if these are significant or not.

With FELIX, errors are estimated following the formalism proposed by Montgomery & Odonoghue (1999), with the particularity, however, that σ_A, the error on the amplitude of a mode, is measured directly in the Lomb-Scargle periodogram. A window around each frequency is chosen and the median value of the amplitudes in that frequency range defines σ_A. The relations given in Montgomery & Odonoghue (1999) are then used to compute the other errors, in particular σ_f, the error on the measured frequency. In order to test that this procedure is correct and does not largely under or overestimate the true errors, we conduct two Monte Carlo experiments.

We first construct an artificial light curve covering about 200 days (similar to the time baseline of each light curve pieces considered in the next subsection) with the same SC-mode sampling provided by *Kepler* in which we add white random gaussian noise. We further inject in this light curve 1000 sinusoidal signals with the same amplitude ($S/N \sim 160$) but of frequency increasing by steps of $\sim 8.2\,\mu$Hz per signal. In practice, a random frequency shift of a few tenth μHz is performed on each injected frequency in order to reduce the number of harmonics and linear combinations. The generated time series is then analyzed with our code FELIX that extracts and measures each signal and evaluates the uncertainties associated to the measured frequencies and amplitudes (σ_A and σ_f). Since the true values of these quantities are perfectly known from the signals we injected, the real distribution of the deviations between measured (prewhitenned) values and true values can be evaluated. For that purpose, we define the frequency and amplitude deviations normalized by their 1σ errors (as estimated with the code FELIX from the procedure described above), $\Delta f = (f_{pre} - f_{inj})/\sigma_f$ and $\Delta A = (A_{pre} - A_{inj})/\sigma_A$, where the subscripts indicate the prewhitened value and the injected one, respectively. A variant of this test is also performed by again injecting 1000 sinusoidal signals, but this time with random amplitudes (instead of constant ones) chosen in the $S/N \in (5, 60)$ range. This second test allows us to check also the reliability of our error estimates as a function of amplitude, considering that σ_f in particular depends on the mode S/N (σ_f increases when S/N decreases).

Figure 3 shows the results obtained in both cases. The 2D distributions of the frequency and amplitude deviations are well confined within 3σ. Moreover, the associated

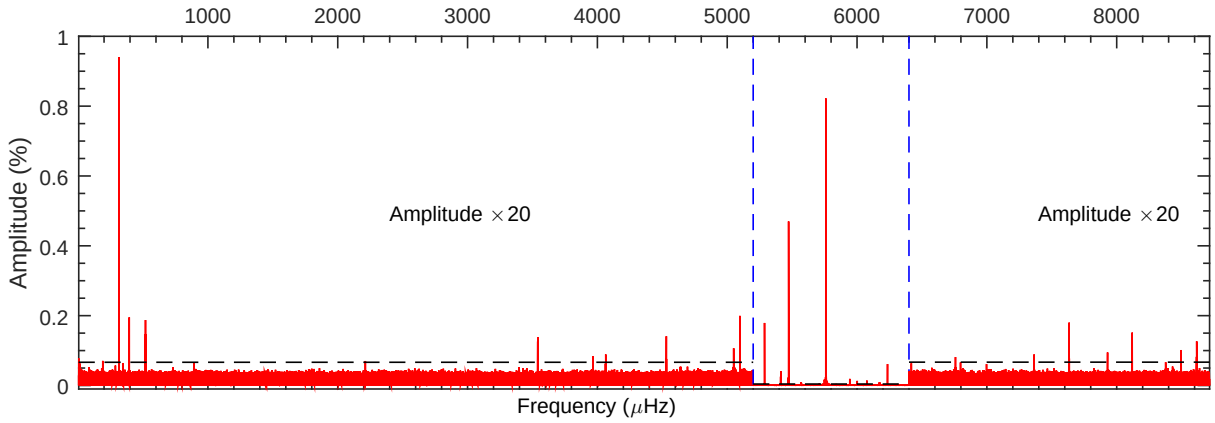

Fig. 2. Lomb-Scargle periodogram (LSP; amplitude in % of the mean brightness vs frequency in μHz) of the *Kepler* light curve for KIC 10139564. The represented range, up to the Nyquist frequency, covers the long-period *g*-mode and the short-period *p*-mode frequency domains. The region between the two dashed vertical lines at 5200 and 6400 μHz is where peaks have the largest amplitudes. However, weaker peaks outside of this particular region are present and are made visible by scaling up amplitudes by a factor of 20. The dashed horizontal line represents the 5.6σ detection threshold (see text). Some well-known *Kepler* instrumental artefacts are present, but can easily be recognized.

Table 1. List of frequencies detected in KIC 10139564 on which we focus our analysis.

Id.	Frequency (μHz)	σ_f (μHz)	Period (s)	σ_P (s)	Amplitude (%)	σ_A (%)	Phase	σ_{Ph}	S/N	† Comment
Multiplet frequencies:										
f_{39}	315.579243	0.000566	3168.776214	0.005687	0.005851	0.000596	0.2492	0.0516	9.8	$T_{2,-1}$
f_{21}	315.820996	0.000219	3166.350599	0.002193	0.015155	0.000596	0.6107	0.0199	25.4	$T_{2,0}$
f_{11}	316.066440	0.000070	3163.891744	0.000702	0.047276	0.000596	0.2063	0.0064	79.3	$T_{2,+1}$
f_{27}	394.027385	0.000342	2537.894669	0.002202	0.009667	0.000594	0.2589	0.0312	16.3	$D_{1,0}$
f_{32}	394.289823	0.000397	2536.205455	0.002555	0.008323	0.000594	0.5123	0.0363	14.0	$D_{1,+1}$
f_{34}	518.900359	0.000437	1927.152262	0.001624	0.007526	0.000592	0.6648	0.0401	12.7	$T_{3,-1}$
f_{28}	519.151796	0.000352	1926.218898	0.001305	0.009351	0.000592	0.9059	0.0323	15.8	$T_{3,0}$
f_{31}	519.402391	0.000367	1925.289559	0.001360	0.008964	0.000592	0.5369	0.0337	15.2	$T_{3,+1}$
f_{08}	5286.149823	0.000053	189.173601	0.000002	0.064784	0.000614	0.6712	0.0047	105.4	$Q_{1,-2}$
f_{10}	5286.561766	0.000060	189.158861	0.000002	0.057105	0.000614	0.4356	0.0053	92.9	$Q_{1,-1}$
f_{07}	5286.976232	0.000038	189.144032	0.000001	0.088857	0.000614	0.1202	0.0034	144.6	$Q_{1,0}$
f_{05}	5287.391879	0.000019	189.129163	0.000001	0.179339	0.000615	0.3374	0.0017	291.8	$Q_{1,+1}$
f_{06}	5287.805883	0.000029	189.114355	0.000001	0.119329	0.000615	0.7941	0.0025	194.2	$Q_{1,+2}$
f_{22}	5410.701146	0.000234	184.818931	0.000008	0.014871	0.000627	0.9524	0.0203	23.7	$M_{1,0}$
f_{67}	5411.143448	0.000958	184.803824	0.000033	0.003637	0.000627	0.4591	0.0830	5.8	$M_{1,0}$
f_{13}	5411.597301	0.000136	184.788325	0.000005	0.025636	0.000627	0.6770	0.0118	40.9	$M_{1,0}$
f_{15}	5412.516444	0.000185	184.756944	0.000006	0.018812	0.000627	0.8925	0.0160	30.0	$M_{1,0}$
f_{12}	5413.389096	0.000084	184.727161	0.000003	0.041339	0.000627	0.4037	0.0073	65.9	$M_{1,0}$
f_{19}	5413.814342	0.000222	184.712651	0.000008	0.015718	0.000627	0.7225	0.0192	25.1	$M_{1,0}$
f_{01}	5760.167840	0.000005	173.606052	...	0.825132	0.000761	0.0744	0.0004	1084.9	$T_{1,-1}$
f_{03}	5760.586965	0.000008	173.593421	...	0.554646	0.000761	0.6388	0.0005	729.3	$T_{1,0}$
f_{02}	5761.008652	0.000007	173.580715	...	0.567034	0.000761	0.5845	0.0005	745.5	$T_{1,+1}$
Linear combination frequencies C_1:										
f_{23}	6076.234996	0.000252	164.575597	0.000007	0.014360	0.000650	0.7906	0.0210	22.1	$f_{11} + f_{01}$
f_{35}	6076.408232	0.000510	164.570905	0.000014	0.007091	0.000650	0.7821	0.0426	10.9	$f_{21} + f_{03}$
f_{74}	6076.650684	0.001120	164.564338	0.000030	0.003225	0.000650	0.5520	0.0937	5.0	$f_{11} + f_{03}$

Notes. (†) The first subscript is the identity of the multiplet and the second one indicates the value of m. The m-values for the $\ell > 2$ multiplet M_1 are not provided, as the degree ℓ is not known.

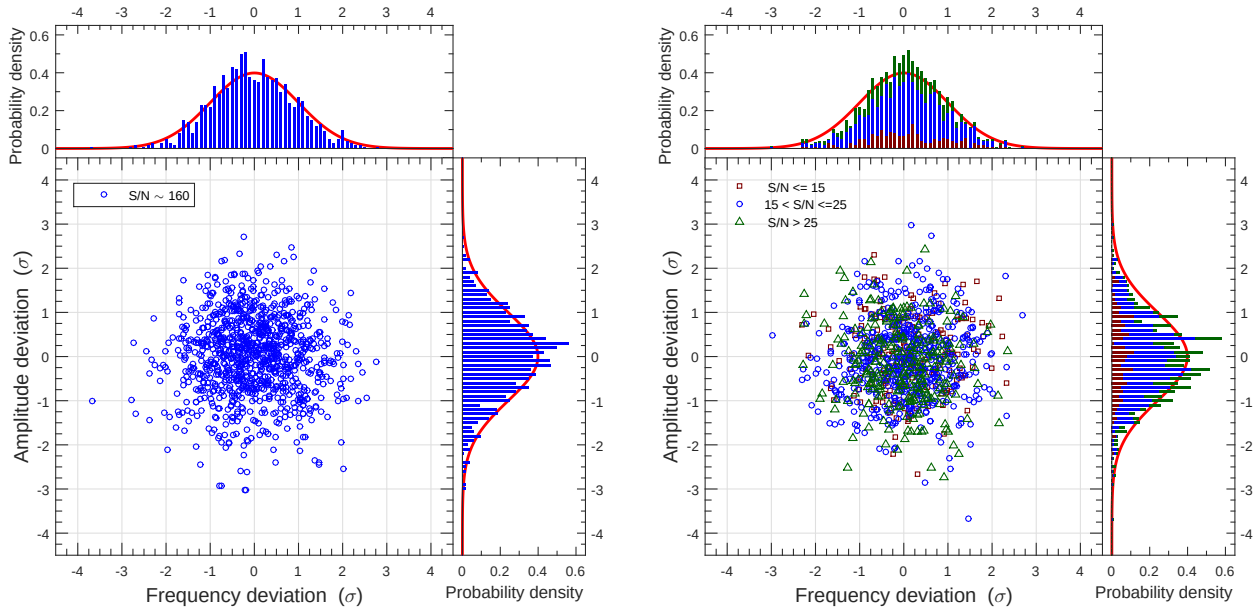

Fig. 3. *Left panel*: 2D distribution of the frequency and amplitude deviations between the prewhitened and the injected values for 1000 artificial modes of constant amplitude. S/N denotes the signal-to-noise ratio of the injected signals and the deviations have been normalized by the 1σ error, σ_A and σ_f, derived from the prewhitening procedure implemented in the code FELIX. The 2D distribution is also projected into 1D histograms (frequency and amplitude) to be compared with the Normal Distribution, $\mathcal{N}(0,1)$ plotted as a red solid curve. *Right panel*: same as above but for 1000 modes with random amplitudes. The injected modes are divided into three groups of S/N in the ranges $[5,15]$, $(15,25]$, and $(25,60]$, respectively (represented by three different colors and symbols).

1D histograms show that for both quantities, the measured deviations closely follow the Normal Distribution, $\mathcal{N}(0,1)$, plotted as a red solid curve. Only a few data points fall outside the $[-3\sigma,+3\sigma]$ range (within which 99.73% of the measurements should be for the normal distribution, $\mathcal{N}(0,1)$). This is the behavior we expect for an accurate determination of the error estimates, σ_A and σ_f, with the code FELIX. Hence, these tests demonstrate that error values derived in our frequency analysis are robust.

2.4. Amplitude and frequency modulations

From now on, we concentrate our discussion on the six multiplets, which include three triplets T_1, T_2 and T_3, one doublet D_1, one quintuplet Q_1 and a likely $\ell = 4$ multiplet M_1 (see again Table A.1). Interestingly, three of these multiplets (T_2, D_1, and T_3) involve g-modes, while the others (Q_1, M_1, and T_1) are p-modes. We also examine three linear combination frequencies (C_1). The fine structures of the multiplets are shown in the left top panels of Figs. 4, 6, 7 and 9–11. The average frequency spacing between the components of these well-defined, nearly symmetric multiplets is $\sim$0.25 μHz for the g-modes and 0.423 μHz for the p-modes, thus suggesting that the g-modes are dipoles ($\ell = 1$) in a star rotating rigidly with a period of $\sim$26 days.

In order to investigate the time variability of these oscillation modes and their relationships, we used our software FELIX to compute sliding Lomb-Scargle periodograms (sLSP) of the data set. This method constructs time-frequency diagrams by filtering in only parts of the data set as a function of time. We chose a filter window of 200-day width moved along the entire light curve by time steps of 20 days. This ensures a good compromise, for our purposes, between the frequency resolution (to resolve close structures of peaks in each LSP), time resolution, and signal-to-noise. The sLSP offers an overall view of the amplitude and frequency variations that may occur for a given mode (see, e.g., the middle left panel of Fig. 4). As a complementary (and more precise) technique, we also extracted the frequencies (through prewhitening and nonlinear least square fitting) in various parts of the light curve. The 38-month light curve of KIC 10139564 was divided into 32 time intervals, each containing nine months of *Kepler* data (for the purposes of precision in the measurements) except for the last three intervals at the end of the observations. This second approach provides a measure of the (averaged) frequencies and amplitudes at a given time, along with the associated errors (see, e.g., the right and bottom left panels of Fig. 4).

Figure 4 shows the amplitude and frequency modulations for the three components forming the triplet T_1 near 5760 μHz. As mentioned already, the top-left panel shows the triplet as revealed by the full data set with components nearly equally spaced in frequency. We note, however, that this spacing is not strictly symmetric, with a difference (or "frequency mismatch") of 0.0026 μHz. Frequency variations with time are illustrated by the sLSP diagram in the middle-left panel where the color scale represents the amplitude of the modes. An expanded view centered on the average frequency of each component is then provided in the bottom-left panel while the amplitude behavior with time for each component is shown in the right panel. The latter two are obtained from prewhitening parts of the light curve as described above.

From the sLSP diagram, we find that both the amplitudes and frequencies have varied during the *Kepler* observations. These variations are more clearly seen in the bottom-left and right panels. The side components both show suggestions of a quasi-periodic modulation in frequency and evolve in antiphase. We also note a long timescale trend as the frequencies of the two side components gradually approach toward each other, as well as toward the central component. In order to filter out these trends, we applied a parabolic fit to each component, leaving the remaining

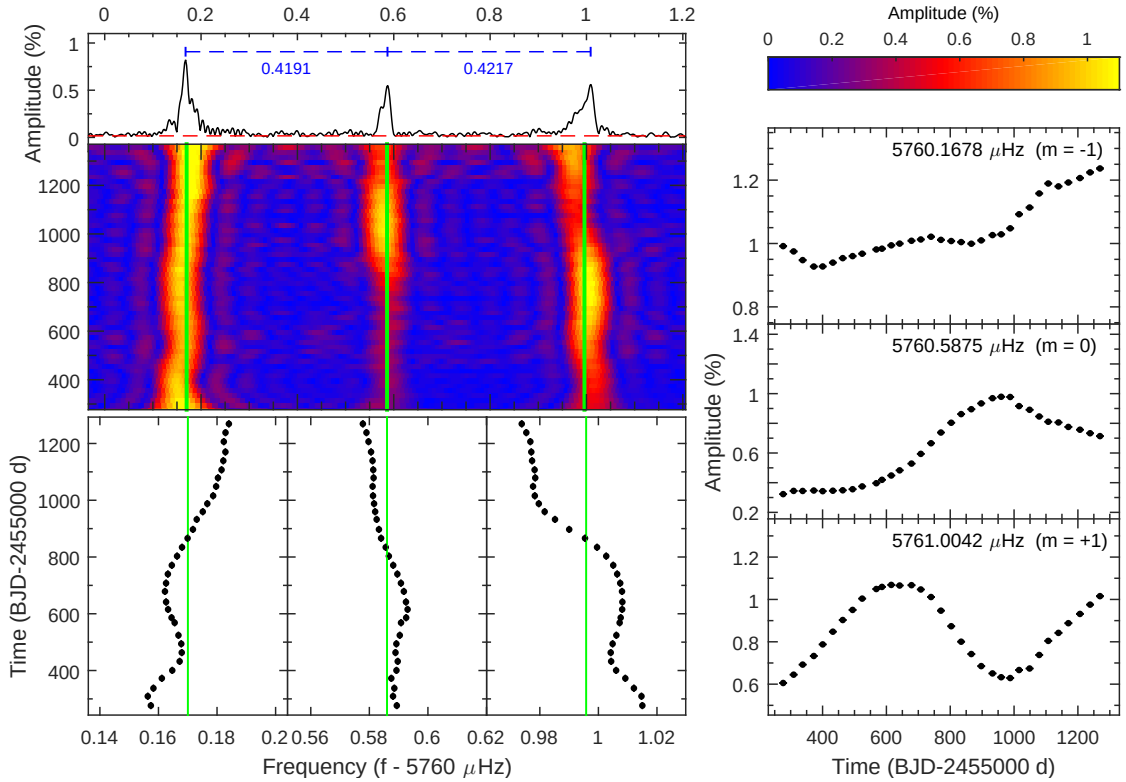

Fig. 4. Frequency and amplitude modulations in the T_1 p-mode triplet near 5760 μHz. *Top-left panel* presents the fine structures of the well defined triplet with near symmetric frequency spacings. The dashed horizontal line in red represents the 5.6 σ detection threshold. *Middle-left panel* shows the sliding Lomb-Scargle periodogram (sLSP giving the amplitude in % as a function of frequency in μHz and time in days) of the triplet as a whole. *Bottom-left panel* shows expanded views around the average frequency (the solid vertical lines, also in the *middle left panel*) of each component, obtained from prewhitening subsets of the data, thus measuring precisely the frequencies, as a function of time. *Right panel* provides the measured amplitudes as a function of time obtained for each subset of data (see text for details). Note that the errors for each measurement is smaller than the symbol itself.

signature of the quasi-periodic modulation of the frequencies (see Fig. 5). In the process, we find that the two side components had frequencies about 0.06 μHz closer to each other at the end of the run compared to the beginning of the observations. Figure 5 shows that the data almost cover two cycles of the quasi-periodic frequency variations. While clearly not strictly sinusoidal, although not very far from it, if we fit the closest pure sine wave to each curve, we find that all have a very similar (quasi-)period of ~570 days. The variations for the side components (retrograde and prograde modes) are clearly in antiphase. For the amplitude variations, we also find suggestions of a quasi-periodic modulation for the central and prograde components. The retrograde mode for its part has a more regular amplitude evolution (increase) during the course of the observations.

Figure 6 illustrates the amplitude and frequency modulations for the g-mode triplet T_2 near 316 μHz using the same presentation as in Fig. 4. In this case, the triplet shows a very small (but significant) asymmetry of 0.0036 μHz. The frequencies appear to be stable over the 38-month *Kepler* observations. The amplitude is essentially constant for the retrograde ($m = -1$) mode while the other two components display some variations. The central one may show a small oscillatory behavior, but more precise measurements would be needed to really confirm that trend. The prograde ($m = 1$) mode has its amplitude rising continuously throughout the observations, from 400 ppm up to about 600 ppm.

The amplitude and frequency variations of the g-mode triplet T_3 near 519 μHz are shown in Fig. 7. In this triplet, which

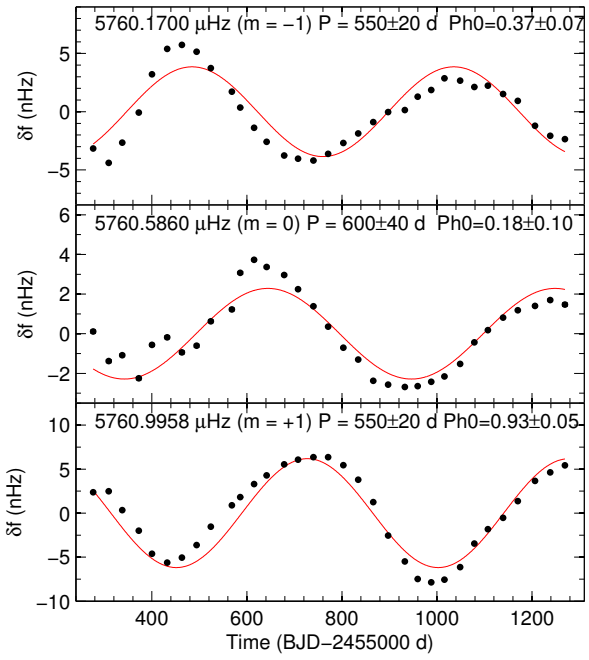

Fig. 5. Frequency modulations after removing the long-term trend in the T_1 triplet by applying a second-order polynomial fit. The solid curves represent the best fits of one pure sine wave to the frequency modulations. The associated formal errors for the periods and phases are also estimated.

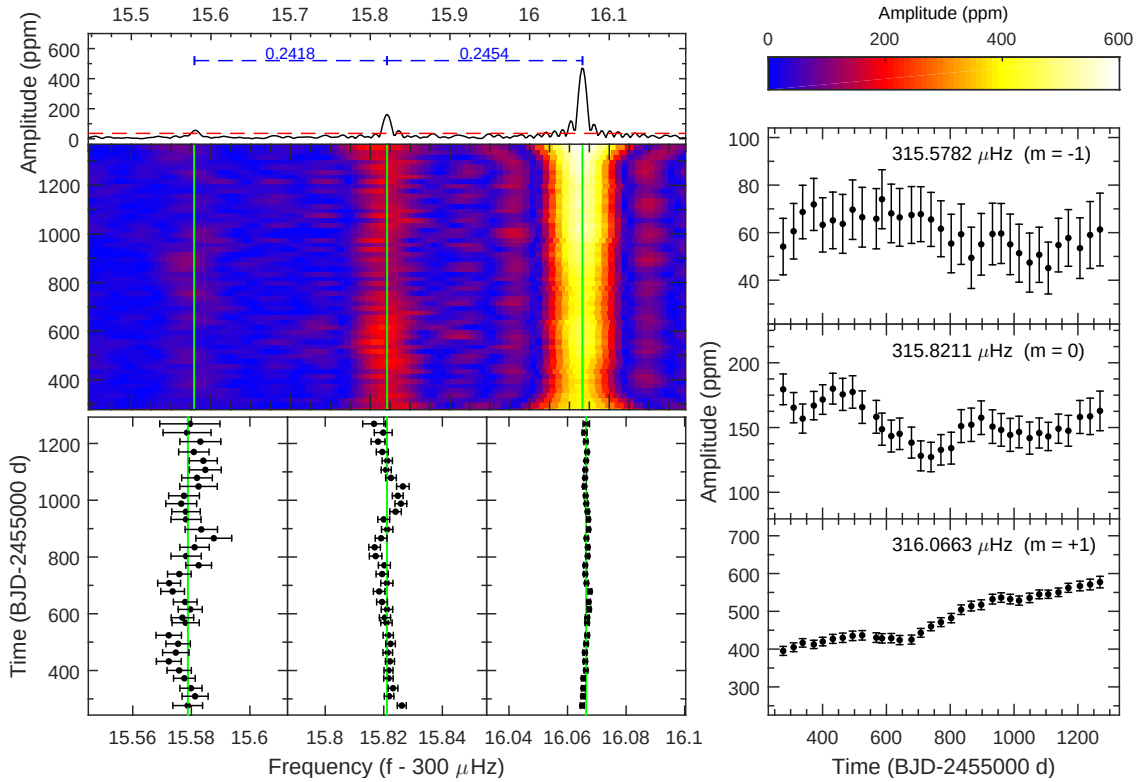

Fig. 6. Same as Fig. 4 but for the T_2 g-mode triplet near 316 μHz.

is almost perfectly symmetric, the three components have stable frequencies and amplitudes within the quoted uncertainties. This stability is further illustrated with Fig. 8 that shows the scattering of the measured frequencies and amplitudes for these modes from all the data chunks considered throughout the entire light curve. Almost all measurements are indeed confined within 2σ around their average values (and all are within 3σ). It is interesting to note that the triplet T_3 therefore has different characteristics compared to the two triplets T_1 and T_2.

Figure 9 shows the amplitude and frequency modulations for the g-mode doublet D_1 near 394 μHz. The frequencies of each component forming the doublet appear to be stable over the 38-month *Kepler* observations, while the amplitudes show very suggestive indications of quasi-periodic variations. We find that the amplitude modulations of the two components have very similar periods, about 1100 days, as illustrated by the best-fit sine waves to the data (the red solid curves in right panel of Fig. 9). Hence the available *Kepler* data just cover about one cycle of this variation, but it is remarkable that almost all the amplitude measurements match very closely the fitted sine curves. This estimated period is almost twice the period of modulations occurring in the main triplet T_1. Moreover, we clearly see that the amplitudes of the two components evolve almost in antiphase during the observing run.

Figure 10 shows the amplitude and frequency modulations for the p-mode quintuplet Q_1 near 5287 μHz. In this complete quintuplet, the $m = \pm 2$ modes and possibly the $m = 0$ central component show significant frequency variations. The other modes, with $m = \pm 1$, have frequencies which are rather stable (with only marginal fluctuations) over the entire observation run. In contrast, the amplitudes for all the modes in the quintuplet vary with patterns that cannot clearly be connected to periodic modulations, based on the available data. Of course, quasi periodic modulations with a timescale longer than twice the present *Kepler* observation cannot be ruled out. We also note that the frequency variations of the $m = -2$ and $m = +2$ components and the amplitude modulations of the $m = -2$ and $m = -1$ components are roughly in antiphase during the observation.

Figure 11 shows the amplitude and frequency modulations for the $\ell > 2$ p-mode multiplet M_1 near 5413 μHz. The ℓ-value for this group of modes is not clearly assessed yet, but a plausible interpretation is that it corresponds to an $\ell = 4$ nonuplet (Baran et al. 2012) with three undetected components and one component barely visible in the LSP of the full data set (see top-left panel of Fig. 11) but which is too low in amplitude to be studied in subsets of the light curve. Some of the frequencies and amplitudes of the five clearly visible modes in this multiplet show significant variations during the 38 months of *Kepler* observation. In particular, the frequencies of the side components drifted toward each other by ~0.032 μHz from the beginning to the end of the run. This trend may be comparable to that observed in the side components of the T_1 triplet (see Fig. 4). Moreover, the same phenomenon also occurs for some modes observed in the long-period-dominated sdB pulsator KIC 2697388 (M.D. Reed, priv. comm.).

In addition to the six multiplets discussed above, we identified other possible multiplets in the data, such as six modes near 5571 μHz (see Table A.1), in which however most of the components have amplitudes too low to be well studied in a time-frequency analysis or by prewhitening shorter parts of the light curve. We therefore do not consider them further in this work.

Beyond the multiplets generated by the rotation of the star, we also focus on the interesting narrow frequency region near 6076 μHz where three structures (f_{23}, f_{35} and f_{74}) show amplitude and frequency modulations as illustrated in Fig. 12. These frequencies are in fact related to components of the T_1 and T_2 triplets through linear combinations. We find that $f_{23} \sim f_1 + f_{11}$, $f_{35} \sim f_3 + f_{21}$, and $f_{74} \sim f_3 + f_{11}$. Interestingly, we note that

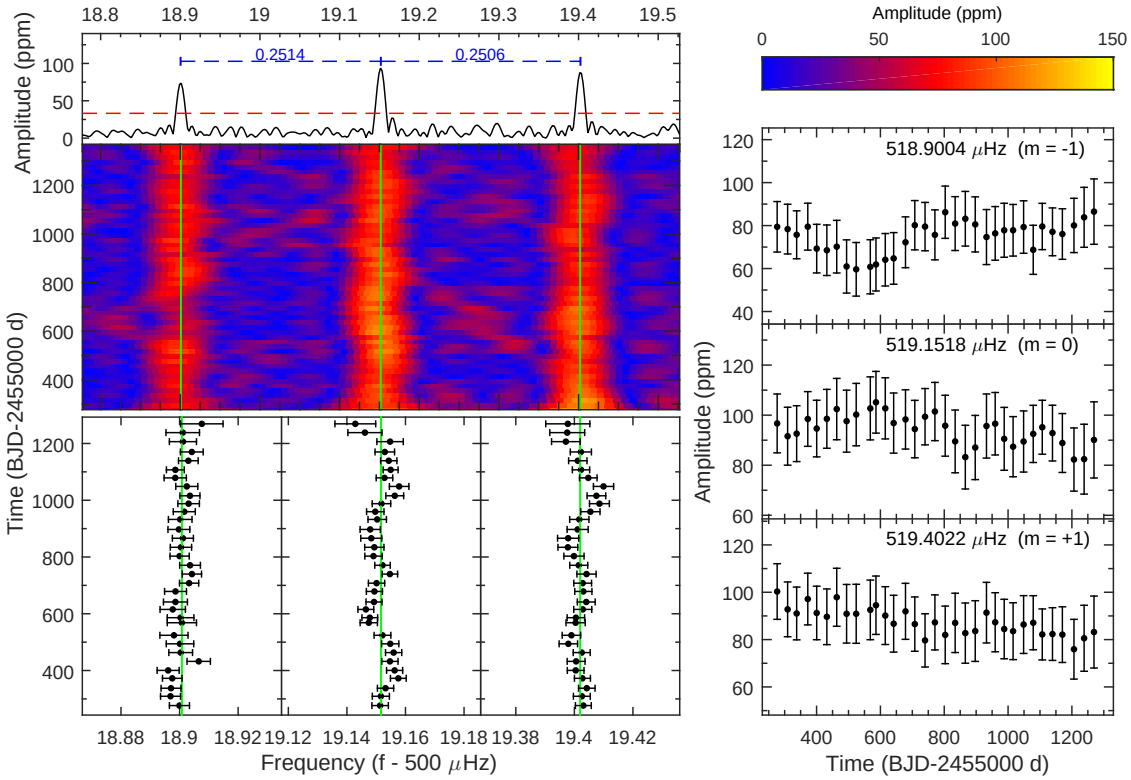

Fig. 7. Same as Fig. 4 but for the T_3 g-mode triplet near 519 μHz.

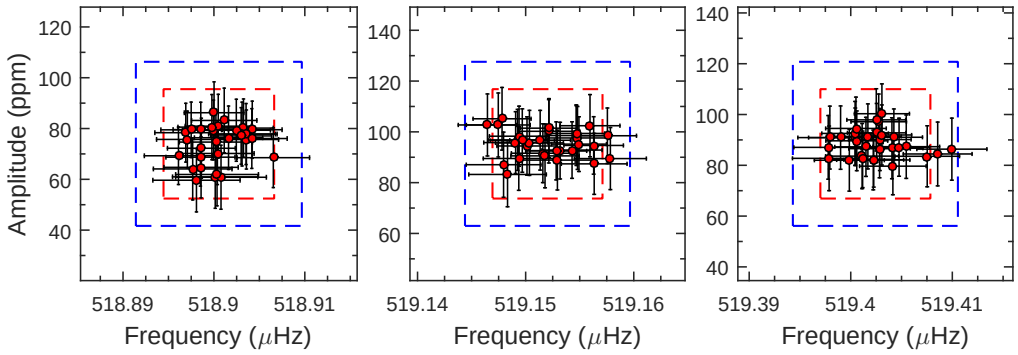

Fig. 8. Frequency and amplitude scattering for the three components forming the g-mode triplet T_3 around their averaged values. The red and blue dashed rectangles indicate the 2σ and 3σ error boxes, respectively. All the data points are within 3σ.

the frequency and amplitude variation pattern of f_{23} is similar to the variations observed for the mode f_1. Similarities also exist between the variations observed in f_{35} and f_2. The peak f_{74}, for its part, shows a rather large frequency variation covering up to ~0.1 μHz (the scales of these frequency variations are indicated by the green shadowed region in the top panel of Fig. 12).

After this description of the various behaviors encountered, we concentrate, in the following sections, on plausible theoretical interpretations for the observed amplitude and frequency modulations.

3. Resonant mode coupling and amplitude equations

In this section, we recall the most natural theoretical background to understand the behavior of the modes forming the six multiplets induced by stellar rotation. These are indeed prone to develop nonlinear interactions through resonant mode couplings, which is the mechanism that we ultimately support from our present analysis. But before moving forward in discussing details on the nonlinear resonant coupling mechanism, we first rule out several other possibilities as the cause of the observed modulations, such as instrumental effects, binarity, stochastically driven pulsations, or stellar "weather".

Instrumental modulations can possibly occur, for example, on a per quarter basis, such as a slightly varying contamination from nearby stars that could affect the amplitude of the modes. Such effects would however affect all frequencies similarly, which is not what is observed with KIC 10139564 where the modes show different types of behavior. Another effect related to the instrument that could induce frequency and amplitude modulations is the slight shift of the Nyquist frequency associated with the movement of the *Kepler* spacecraft in the Solar System barycentric reference frame. Fortunately, the multiplets that we consider (with frequencies below 5761 μHz), are far away from the Nyquist frequency limit (~8496 μHz). Moreover, such

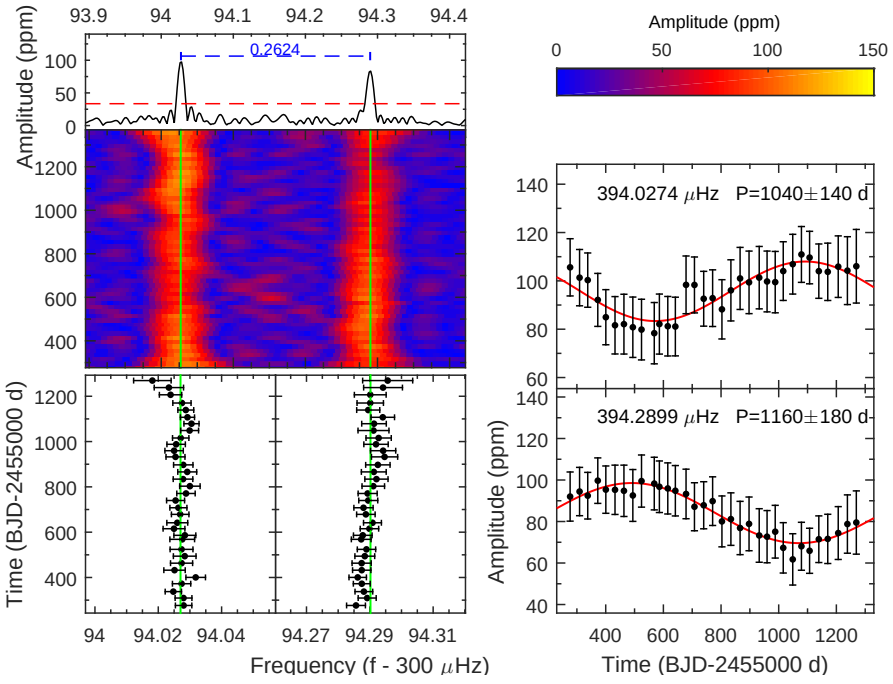

Fig. 9. Same as Fig. 4 but for the D_1 g-mode doublet near 394 μHz. The solid curves in right panel show the best fit of a pure sine wave to the amplitude modulations.

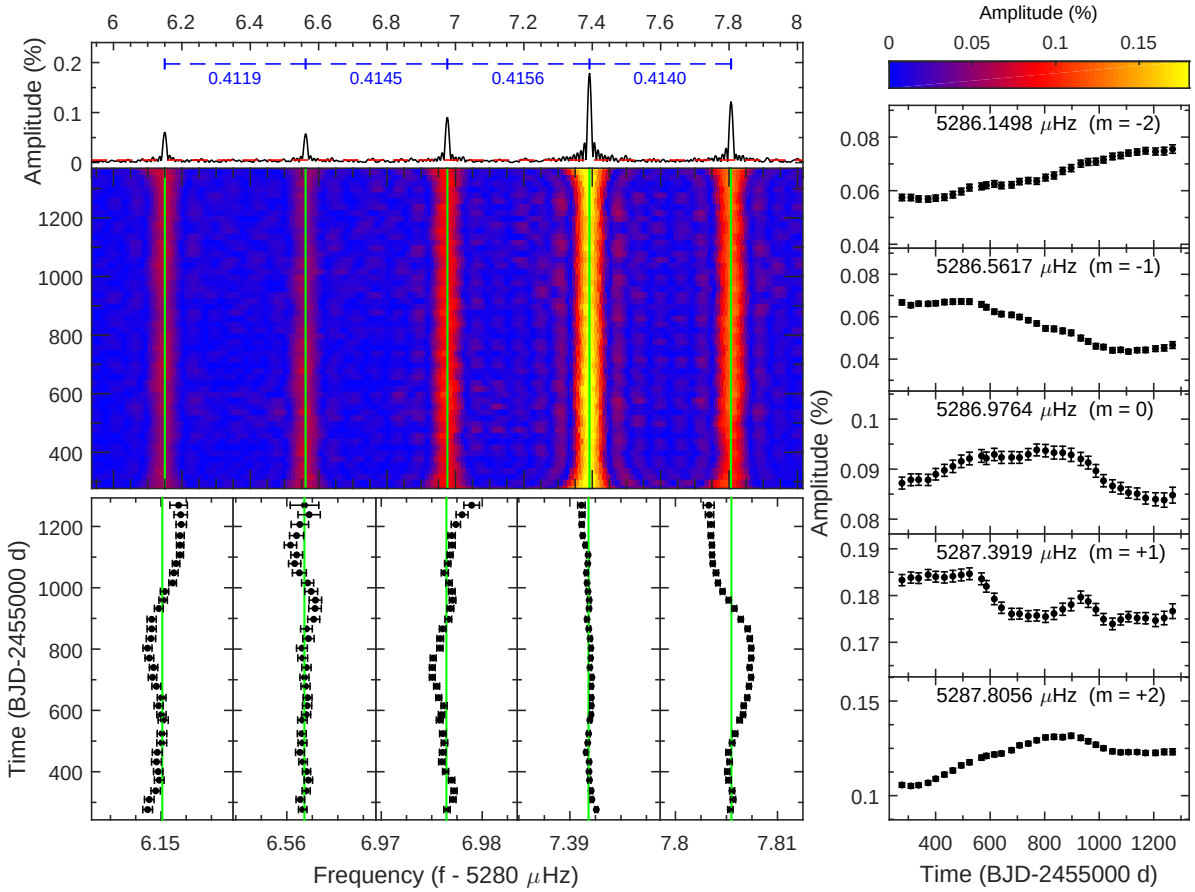

Fig. 10. Same as Fig. 4 but for the Q_1 p-mode quintuplet near 5287 μHz.

well-structured nearly equally spaced multiplets can obviously not be the mirror reflected frequencies of signals occurring above the Nyquist limit (Baran et al. 2012).

The presence of orbiting companions around compact stars could also induce frequency variations. However, these should occur in all frequencies and be correlated in phase, such as in the sdB pulsator V391 Peg (Silvotti et al. 2007). The variations that we find in several frequencies of KIC 10139564 are clearly not correlated in phase. In addition, radial velocity measurements from spectroscopy do not show any significant variation, thus

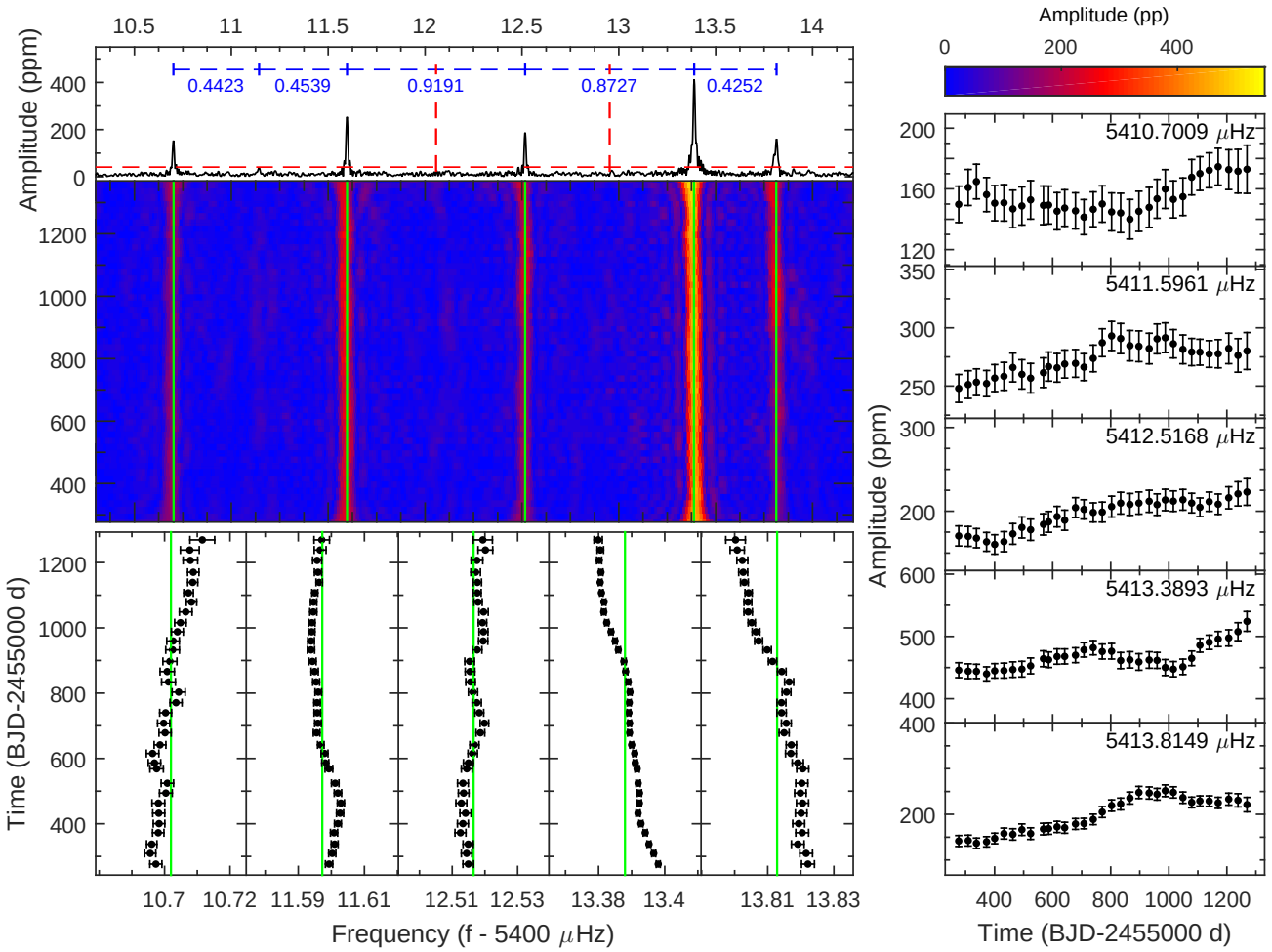

Fig. 11. Same as Fig. 4 but for the $\ell > 2$ p-mode multiplet M_1 near 5413 μHz. Note that at least three components are missing in this multiplet and the red vertical dashed lines indicate the expected position for two of them.

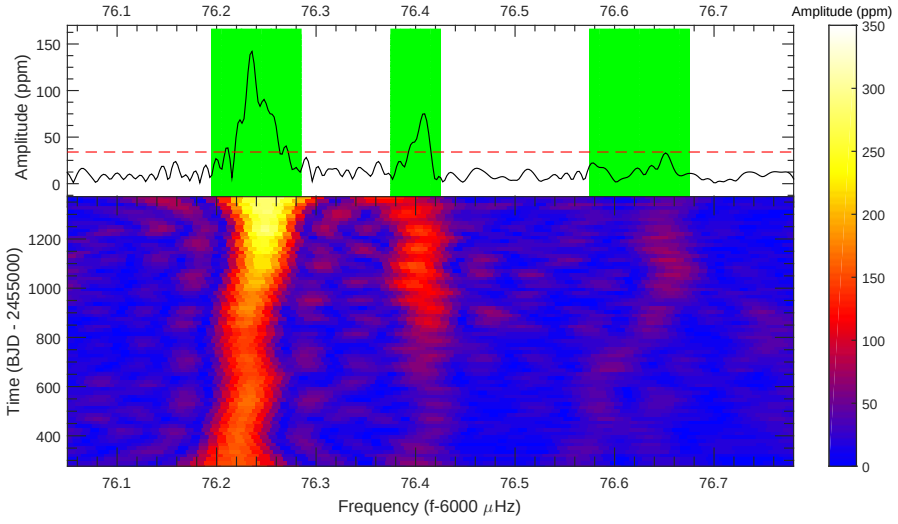

Fig. 12. Frequency and amplitude modulations of a group of linear combination frequencies C_1 near 6076 μHz. The red dashed line indicates the 5.6σ detection threshold. The green shadowed areas in *top panel* represent the scales of variation of these frequencies (see text for details).

ruling out the presence of a stellar companion (Baran et al. 2012, but for substellar objects, a higher precision would be needed to exclude this possibility).

Stochastically driven pulsations by envelope convection have long been observed in the Sun and solar-like stars. It has been claimed in the past that stochastic oscillations could also occur in some sdB pulsators, based on the observation that mode amplitudes could vary from season to season (Kilkenny et al. 2010; Reed et al. 2007). Østensen et al. (2014) recently announced that stochastic pulsations were found in the sdB star KIC 2991276, in which the amplitude and phase of the modes vary substantially and irregularly on a timescale of a month.

However, the mechanism responsible for the oscillations in sdB stars, a well identified κ-effect involving iron-group elements (Charpinet et al. 1997; Fontaine et al. 2003), is very different in nature from the stochastic driving occurring in the convective envelope of solar-like stars. Such a mechanism would indeed hardly be efficient in sdB stars that have radiative envelopes, except may be for a very narrow convective layer generated by the accumulation of iron in the Z-bump region (the latter being however extremely weak). Beyond these theoretical considerations, we find in the case of KIC 10139564 that several mode behaviors, for example, the frequencies in the triplet T_1 and the amplitudes in the doublet D_1, show correlations that would be difficult to account for with a stochastic driving mechanism and that essentially rule out this interpretation.

Changes in the background physical state of the star such as possibly induced by magnetic cycles could also be invoked for explaining amplitude and frequency modulations. Magnetic cycles indeed have an impact on the frequencies of p-modes observed in the Sun and lead to small frequency drifts that correlate in time with tracers of the solar surface activity (see, e.g., Salabert et al. 2015, and references therein). However, there is no clear observational evidence of stellar activity on the surface of sdB stars which, again, have very stable radiative envelopes and are not known to be magnetic. Cycles comparable to those observed in solar-like stars are therefore unlikely to be found in sdB stars. Moreover, such a mechanism, or more generally a phenomenon modifying the physical state of the star on a timescale of months could hardly account for the observed modulations in KIC 10139564 that show very different modulation behaviors from mode to mode, while a global change in the star would affect all modes similarly. Consequently, we also rule out this possibility in the present case.

3.1. Triplet resonance induced by slow stellar rotation

We hereafter propose that nonlinear resonant coupling mechanisms could be a natural explanation for the observed modulations in KIC 10139564. Resonant interactions between modes may indeed result in amplitude and frequency variations occurring on timescales of weeks, months, and even years.

In the present context, we limit ourselves to the type of resonances described in Buchler et al. (1995, 1997) involving linear frequency combinations $\nu_1 + \nu_2 \sim 2\,\nu_0$. More specifically, we focus on a particular case where dipole ($\ell = 1$) modes are split by slow rotation and form a nearly symmetric triplet (thus following the above relationship between the frequencies of the components). We also consider the three-mode couplings of the form $\nu_1 + \nu_2 \sim \nu_0$, which corresponds to the so-called direct resonances or parametric instabilities (Dziembowski 1982; Wu & Goldreich 2001).

We first recall some basic theoretical background relative to resonances in mode triplets created by stellar rotation. We emphasize that our focus on this particular mechanism is obviously motivated by the specific configuration of the modes observed in KIC 10139564, most of which are identified as $\ell = 1$ rotationally split triplets. We also point out that this type of nonlinear resonance has recently been strongly suggested to explain the modulations of the g-modes triplets in the DB white dwarf KIC 08626021 (Z16). It is therefore the most natural effect that one could think of in the present case. The AEs formalism could also, in principle, be extended to multiplets of degree $\ell > 1$ at the expense of solving a larger set of coupled amplitude equations (Buchler et al. 1995). However, such development has yet to be done, which is beyond the scope of our present paper. The latter would be needed for KIC 10139564 in order to fully interpret the several multiplets with $\ell > 1$ that show variations. The behavior for more complex $\ell > 1$ multiplets may indeed differ from the simpler (better documented) $\ell = 1$ triplet case, although we expect some similarities in general.

Details on the theory of nonlinear resonant couplings for three-mode interactions, such as in $\ell = 1$ triplet, can be found in (Buchler et al. 1995, 1997, Z16). We summarize below the most relevant aspects (for our purposes) of the theory. In particular, The quantity $\delta\nu$ (which we thereafter call the frequency asymmetry), measuring the departure from exact resonance (that would occur if, e.g., triplets were perfectly symmetric), is in fact essential for driving the various resonant mode coupling behaviors. Contributions to the frequency asymmetry in a given triplet generally involves higher order effects of stellar rotation on the pulsation frequencies (Dziembowski & Goode 1992; Jones et al. 1989), but could also have additional origins, such as the presence of a weak magnetic field[2]. We do not however consider further that possibility since no evidence of significant magnetism exists for sdB stars (Petit et al. 2012; Landstreet et al. 2012).

The rotationally split frequencies up to the second order, which should be the main contribution to the frequency asymmetry, are given by the formula

$$\nu_m - \nu_0 = (1 - C_{k\ell})m\Omega + D_{k\ell}\frac{m^2\Omega^2}{\nu_0}, \tag{1}$$

where the $C_{k\ell}$ coefficient is the well-known first order Ledoux constant, $D_{k\ell}$ involves a complex integration of the eigenfunctions of the modes, and $\Omega = 1/P_{\rm rot}$ is the rotation frequency of the star (expressed in Hertz). The value of $C_{k\ell}$ is typically ~0.5 for dipole g-modes when approaching the asymptotic regime, while it is usually very small ($C_{k\ell} \ll 1$) for p-modes. The second order coefficient $D_{k\ell}$ is roughly $4C_{k\ell}$ for dipole g-modes (Dziembowski & Goode 1992; Goupil et al. 1998) but can vary significantly from one p-mode to another (Dziembowski & Goode 1992; Saio 1981). The rotation period of KIC 10139564, $P_{\rm rot}$, can be estimated from the average of the frequency separations between the components of the multiplets using the first order approximation $\Delta\nu = (1 - C_{k\ell})\Omega$. We find $P_{\rm rot} \sim 26$ days for KIC 10139564 (see Sect. 2). An "observed" frequency asymmetry can also be evaluated directly from the measured frequency of each triplet component, simply from the relation

$$\delta\nu_{\rm o} = \nu_- + \nu_+ - 2\nu_0. \tag{2}$$

We note at this stage that $\delta\nu_{\rm o}$ may actually differ from asymmetries expected from linear developments (such as discussed above) because nonlinear effects can modify the frequencies of the modes.

The numerical solutions of the AEs for mode interactions in triplets mainly reveal three distinct regimes of resonances (see, e.g., Buchler et al. 1997, and in Z16). The first state is the "frequency lock" regime where all the components in the triplet have constant frequencies and amplitudes and the asymmetry tend to be zero (triplets become perfectly symmetric). The opposite configuration is the nonresonant regime where the triplet

[2] The asymmetry would be proportional to the strength of magnetic field $|\boldsymbol{B}|^2$ and the frequency of each component of the triplet (except the central, $m = 0$, one) would be shifted in the same direction (Jones et al. 1989).

configuration is likely predicted by the linear theory of stellar oscillations. Between the two, there is an intermediate regime in which all the modes in the triplet show modulated frequencies and amplitudes which can be periodic, irregular, or even chaotic.

In order of magnitude, the occurrence of these three regimes is roughly linked to a parameter D defined as (see Goupil et al. 1998)

$$D \equiv \frac{2\pi\delta\nu}{\kappa_0}, \tag{3}$$

where κ_0 is the linear growth rate of the $m = 0$ mode in the triplet (a nonadiabatic quantity). However, the ranges of values for this parameter which define the different regimes depend somewhat on the values of the nonlinear coefficients in the real star. D is also a quantitative indicator that measures how far the triplet modes are away from the exact resonance center ($D = 0$). We nonetheless summarize some of the properties encountered in previous studies as a function of D:

- In the frequency-locked regime ($\delta\nu \to 0$), the D-parameter roughly corresponds to values in the range ∼0−1 according to the AEs formalism. However, in the case of the white dwarf star GD 358, Goupil et al. (1998) found that D could be up to 20 and still correspond to a frequency-locked situation. These ranges, therefore, are somewhat dependent on the specific properties of the mode being considered, in particular on the scale of their linear growth rate, κ_0.
- The intermediate regime occurs when the triplet components move away from the resonance center ($\delta\nu \neq 0$). In this situation, if periodic variations indeed affect the considered modes, these can be expected to have a modulation timescale of

$$P_{\rm mod} \sim \frac{1}{\delta\nu} \simeq \frac{2\pi}{\kappa_0}\frac{1}{D}, \tag{4}$$

  that is, roughly the timescale derived from the inverse of the linear (i.e., unperturbed) frequency asymmetry of the triplet dominated by the second order effect of stellar rotation (following Eq. (2)). This timescale is also connected to the inverse of the growth rate of the oscillation mode through the D parameter (Goupil et al. 1998).
- The modes recover a configuration of steady pulsations with the nonresonant regime when the involved frequencies are such that the modes are now far from the resonance condition ($D \gg 1$). In this regime, the nonlinear interaction between modes is very weak and nonlinear frequency shifts become very small. Consequently, the mode frequencies are close to the linear ones.

We finally point out that in addition to the above mentioned three main regimes, a narrow hysteresis (transitory) regime exists between the frequency-locked and intermediate regimes in which the frequencies can be locked (i.e., constant), while the amplitudes still have a modulated behavior (Buchler et al. 1997).

3.2. Three mode resonance of the type $\nu_0 \sim \nu_1 + \nu_2$

In this section, we recall some properties of nonlinear interactions between oscillations modes not within triplets but whose frequencies are close to a resonance condition such that $\nu_0 \sim \nu_1 + \nu_2$. Frequencies with such a relationship could also result from simple linear combination frequencies, that is, exact sum or difference of frequencies (where the "child" frequency is not a true eigenmode), which may be related to nonlinearities in the mixing process affecting the depth of a convective zone in the outer layer of a pulsating star (Wu 2001), or to nonlinearities in the flux response induced by the surface geometrical and temperature distortions triggered by the propagating waves (Brassard et al. 1995).

A useful quantity, R, connecting the observed amplitude of the combination frequency and the amplitudes of its "parent" modes, has been defined as (van Kerkwijk et al. 2000; Wu 2001)

$$R = \frac{A_0}{A_1 \cdot A_2}, \tag{5}$$

where the A_0, A_1, and A_2 are the amplitudes of the frequencies ν_0, ν_1, and ν_2, respectively. This ratio R is typically less than ten for simple linear combinations related, such as, to nonlinearities in the flux response. Consequently, in pulsating sdB stars, the "child" frequency resulting from this effect usually has a very low amplitude compared to its "parent" frequencies. In the large amplitude and brightest known pulsating sdB star, Balloon 090100001, where such linear combination frequencies have been unambiguously observed, the amplitude ratios are 3.9, 3.7, 3.0 and 5.5 for the linear combination frequencies of four p-modes and one g-mode $f_1 + f_2$, $f_1 + f_3$, $f_1 + f_4$ and $f_1 - f_B$ in B-band photometry (Baran et al. 2008), respectively. In the present work, we however find that the identified linear combination frequencies C_1 have amplitude ratios in the 10−100 range, that is, one order of magnitude larger than typical linear combination frequencies observed so far. One possible interpretation for the high amplitude ratios is that the frequency sum/difference is near the resonance condition of $\nu_0 \sim \nu_1+\nu_2$ and its amplitude is boosted significantly by the resonance (e.g., Dziembowski 1982; Breger & Montgomery 2014).

The AEs formalism treating the $\nu_0 \sim \nu_1 + \nu_2$ type of resonance, including the parametric instability and the direct resonance (see below), is similar to the case of a triplet resonance (e.g., see the amplitude equations in Buchler et al. 1997, Z16). According to Dziembowski (1982), the three-mode interactions can be described by the following coupled system

$$\frac{{\rm d}\boldsymbol{A_0}}{{\rm d}t} = \kappa_0 \boldsymbol{A_0} + {\rm i}\frac{q}{2\nu_0 I_0}\boldsymbol{A_1 A_2}\exp(-{\rm i}\delta\nu t), \tag{6a}$$

$$\frac{{\rm d}A_1}{{\rm d}t} = \kappa_1 \boldsymbol{A_1} + {\rm i}\frac{q}{2\nu_1 I_1}\boldsymbol{A_0 A_2^*}\exp(-{\rm i}\delta\nu t), \tag{6b}$$

$$\frac{{\rm d}\boldsymbol{A_2}}{{\rm d}t} = \kappa_2 \boldsymbol{A_2} + {\rm i}\frac{q}{2\nu_2 I_2}\boldsymbol{A_0 A_1^*}\exp(-{\rm i}\delta\nu t). \tag{6c}$$

Where $\boldsymbol{A_j^*}$ is the complex conjugate of the amplitude $\boldsymbol{A_j}$ ($\boldsymbol{A_j} = A_j e^{{\rm i}\phi_j}$), I_j is the mode inertia, and κ_j is the linear growth rate for the three involved frequencies. The quantity q is a nonlinear coupling coefficient, and $\delta\nu$ is the frequency mismatch relative to pure resonance defined by the relationship $\delta\nu = \nu_0 - \nu_1 - \nu_2$.

The nonlinear Eqs. (6a), (6b) and (6c) cannot be solved by analytical methods, but solutions for the equilibrium state (all time derivatives set to zero) can be obtained. In particular, the equilibrium solution leads to an amplitude ratio

$$R = \frac{q}{2\nu_0\kappa_0 I_0} \equiv \frac{A_0}{A_1 \cdot A_2}. \tag{7}$$

The stability of the equilibrium-state depends on the growth (damping) rates and the frequency mismatch (e.g., Dziembowski 1982).

In a three-mode direct resonance, the child mode is damped and has a frequency very close to the sum of frequencies of its two parent modes which are linearly driven (unstable). The child mode amplitude is very sensitive to its mode inertia, linear growth rate, and to the nonlinear coupling coefficient (see Eq. (7)). This near resonance mode can grow up to a very large amplitude if the quantity $q/\kappa_0 I_0$ is sufficiently large. The coupling coefficient q follows from a complex integration of the coupled mode eigenvectors and its explicit form can be found in Dziembowski (1982). It may be possible, in principle, to calculate this coefficient provided that the mode eigenfunctions are known. However, this would require that a precise seismic solution is found for KIC 10139564, which still has to be obtained. To test the theory of a three-mode direct resonance, we would also need to know the linear damping (growth) rate and the inertia of the damped mode, eventually corrected by the effect of slow stellar rotation (e.g, see Carroll & Hansen 1982). However, the situation could be simplified in the case of unstable equilibrium state where the amplitude and frequency of the child mode should exactly follow those of its parent modes, even if the growth rates and coupling coefficients are unknown. Fortunately, the equilibrium state of three-mode direct resonances seems always unstable because the growth (damping) rates cannot satisfy the stability criteria of the Hurwitz theorem (Dziembowski 1982). Therefore, each frequency and amplitude measurement could be used as one independent test of these particular nonlinear couplings. Furthermore, this also provides a method to separate the child mode from their parent modes according to the amplitude and frequency relationships (e.g., Breger & Montgomery 2014).

The parametric instability is another form of three-mode resonant coupling that could destabilize a pair of stable daughter modes from an overstable (driven) parent mode (Wu & Goldreich 2001). In this mechanism, the overstable parent mode gains energy through the driving engine (a κ-mechanism in our case) and the two independent damped child modes dissipate energy. This configuration would lead the system to reach limit cycles under certain conditions (e.g., if $\delta\nu < \kappa_1$ or κ_2, Wu & Goldreich 2001; Moskalik 1985). During such limit cycles, the amplitude of the parent mode first increases slowly on a timescale of κ_0^{-1}, then decreases rapidly on a timescale of $\kappa_{1,2}^{-1}$. A the same time, the amplitude of the daughter modes follow the opposite behavior. In sdB stars, we point out that the linear growth rate of the parent mode κ_0 would be usually far smaller than the damping rate of the daughter modes $\kappa_{1,2}$. We further mention that the nonlinear interactions between the parent/child modes would also affect their periods as a result of phase variations. The nonlinear frequency shift could be of the order of a few μHz in some extreme conditions (Wu & Goldreich 2001; Moskalik 1985). We point out that a parametric instability can also occur in multiplets. In such circumstances, different m components that forms the multiplet may share some common damped daughter modes. Having common daughter modes involved in different parametric resonances, that is, involving different parent overstable components, will obviously induce more complex dynamic modulations than simple periodic variations that could be expected from pure three-mode only interactions. We indeed point out that both the triplet resonance that was explored by Buchler et al. (1995, 1997) and the three-mode $\nu_0 \sim \nu_1 + \nu_2$ resonances that were investigated by Dziembowski (1982), Moskalik (1985) and Wu & Goldreich (2001) are treated as isolated systems, i.e., assuming only interactions between the three involved modes and ignoring the possible influence of other modes. Modes with the highest amplitudes are more likely to efficiently couple with different resonances, such as in a multiplet resonance and in a $\nu_0 \sim \nu_1 + \nu_2$ resonance.

4. Connections with mode behaviors seen in KIC 10139564

In light of the theoretical background summarized in the last section, we tentatively interpret some of the behaviors described in Sect. 2 for the frequencies listed in Table 1. These indeed show striking similarities with patterns expected for nonlinear resonant mode interactions that occur in various regimes.

4.1. Multiplets in the intermediate regime

The first connection is for the modes belonging to multiplets that show quasi-periodic amplitude and frequency modulations. In particular, the p-mode triplet near 5760 μHz (T_1) shows indication that it could be evolving within the so-called intermediate regime of a triplet resonance. We recall (see Sect. 2; Fig.5) that the frequencies of the two side components in this triplet, besides showing a long term drift, vary quasi-periodically in antiphase with a timescale of ~550 days. The central component of T_1, for its part, has a frequency modulation which also vary, possibly with a slightly longer period of ~600 days. For comparison purposes, the modulation timescale is expected to be related to the inverse of the linear (i.e., unperturbed) frequency asymmetry in the triplet (see Eq. (4)), which therefore should be $\delta\nu \sim 0.02$ μHz. Assuming that this frequency asymmetry originally comes from the second order effect of slow rotation, and given the average rotation frequency of the star (~0.42 μHz, corresponding to ~26 days), the $D_{k\ell}$ coefficient in Eq. (1) can be estimated to ~200 for that mode. This value is plausible because the $D_{k\ell}$ coefficient is found to vary over a large range for dipole p-modes (Dziembowski & Goode 1992; Saio 1981). However, to compute D_{kl} in this specific case and compare with this value, a precise seismic solution for KIC 1013956 has to be worked out, but is not available yet. It has to be noted that the frequency asymmetry measured from the averaged frequencies given in Table 1 is only 0.0026 μHz that is one order of magnitude lower than the value derived from the modulation frequency (~0.02 μHz). We note, however, since the frequencies are varying with time, that the maximum extent of the observed frequency asymmetry is ~0.02 μHz when considering the 33 measurements independently (see Fig. 4). We point out that these observed values (0.0026 μHz on average and ~0.02 μHz for the maximum asymmetry) are similar to those observed in the main triplet of the DBV star KIC 08626021, which is also in the intermediate regime (Z16). Nonlinear resonant interactions are bound to perturb the linear frequencies of the modes, forcing them in some cases to shift toward the exact resonance (obtained when the system is locked). It is therefore not surprising to observe a frequency asymmetry that can be significantly smaller than the theoretical shift expected in the linear theory context.

In terms of amplitude modulations, the situation is bit less clear as only the prograde component in T_1 shows a quasi-periodic modulation, with a timescale of ~800 days, while, for the other two components, particularly for the retrograde mode, their amplitude variations appear somewhat irregular.

In addition to the frequency variations of T_1 discussed above, we note that the three components that form this triplet feature a regular drift toward each other which, if nothing change, would lead them to merge into one frequency on a timescale of ~10 yr.

Such a merging is of course not conceivable and what we observe is more likely a small fraction of a variation cycle occurring on a timescale much longer than the duration of the *Kepler* observations. This suggests that the triplet resonance is probably not the only mechanism that affects the stability of T_1. This added complexity may also explain the more erratic behavior of the amplitude variations in this triplet. Quite notably, we indeed find that all the components of T_1 can be linked to other frequencies forming linear combinations satisfying the conditions for a three-mode resonance $\nu_0 \sim \nu_1 + \nu_2$. This will be further discussed in Sect. 4.4.

The quintuplet Q_1 also shows components with amplitude and frequency variations (see Fig. 10) that may be associated to the intermediate regime. In this case, however, we cannot estimate timescales for the modulations which appear to have a more complex behavior than the modulations detected in the T_1 triplet or, if we compare to other cases, in the triplets of the pulsating DB star KIC 08626021 (Z16). The averaged frequency mismatch, $\delta\nu_o$, for Q_1 is about 0.0018 μHz. This could either be the result of the nonlinear coupling mechanism locking the modulated components close to the exact resonance, even if they are in the intermediate regime (see the case of T_1, as well as the triplets in the DBV star KIC 08626021), or it could indicate that the modulation timescale for Q_1 is ~17.6 yr (the inverse to $\delta\nu_o$, if their amplitudes have a periodic behavior). As there has been no theoretical exploration of the nonlinear five-mode interaction yet, the connection of Q_1 with the intermediate regime is based on the assumption that nonlinear five-mode interactions has also mainly three distinct regimes. The coupled amplitude equations for the five-mode resonance involve more terms in each AE and the numerical solutions are more difficult to search for.

Another case may be connected with the intermediate regime: the multiplet M_1 which shows amplitude and frequency variations (see Fig. 11). But, again, we cannot determine any timescale for the complex modulations occurring in this multiplet. In that case, there is also a slow trend leading frequencies, particularly for the most side components, to seemingly converge. This trend is very similar to the slow variation observed in the T_1 triplet. It could possibly be a fraction of a variation cycle with a much longer timescale than the duration of the observations, but more observations would be needed to confirm this hypothesis. This multiplet M_1 should be the siege of even more complex resonant coupling interactions than the quintuplet Q_1, since there are six detected components, with at least three components missing.

4.2. Triplets in the transitory regime

Another type of behavior encountered in our data can be linked to the narrow transitory hysteresis regime which is between the frequency lock and intermediate regimes. This state is characterized by stable frequencies but varying amplitudes. This is notably observed in the g-mode triplet T_2 (see Fig. 6). For this triplet, the observed frequency mismatch is about 0.0036 μHz, that is, very similar to the value measured for the T_1 triplet (see left-top panel of Figs. 4 and 6). We also point out that T_2 may couple with the p-mode triplet T_1 through a three-mode resonance $\nu_0 \sim \nu_1 + \nu_2$, as discussed in Sect. 4.4.

The incomplete triplet D_1 may also be associated to this transitory regime as it shows quasi-periodic amplitude modulations and stable frequencies. Due to the missing component, we cannot measure the frequency mismatch for this doublet. We note that the AEs for the triplet resonance indicate that the modes cannot be stable, i.e, there is no fixed-point solution, if one of the visible modes forming the incomplete triplet is the central ($m = 0$) component (Buchler et al. 1995). Thus, at this stage, we may just fail to detect either the third component of the triplet whose amplitude may be lower than the detection threshold (meaning that the triplet is indeed in the narrow transitory regime), or the nonlinear modulation of the frequencies, which may be smaller in amplitude than our current precision (meaning a doublet in the intermediate regime, as predicted by the AEs).

4.3. A triplet in the frequency-locked regime

The last case occurring in a different regime is the g-mode triplet T_3, which shows stable amplitudes and frequencies (see Figs. 7 and 8). This suggests that T_3 is in the configuration of the frequency-locked regime where the triplet approaches the resonance center, i.e., $\delta\nu \to 0$ and both the frequencies and amplitudes are constant. Indeed, we find that the observed frequency asymmetry, $\delta\nu_o$, is 0.0008 μHz (Fig. 7) for T_3, which is less than the measured error 0.0011 μHz. The triplet T_3 is therefore exactly (within measurement errors) at the resonance center, contrary to T_1 and also T_2 which has constant frequencies but a small non-zero frequency mismatch.

In summary, the various behaviors encountered in the multiplets detected in KIC 10139564 seem to cover all the different regimes expected in a context of resonant mode coupling in multiplets. This mechanism is therefore quite likely responsible, at least in part, for the observed phenomena. In the following section, we discuss another type of resonance, the $\nu_0 \sim \nu_1 + \nu_2$ nonlinear interaction.

4.4. Three-mode resonance

In this section, we discuss the variations of a group of frequencies C_1, including f_{23}, f_{35} and f_{74}, that are involved in a relationship $\nu_0 \sim \nu_1 + \nu_2$. We find that the variations of these frequencies have strong correlations with the variations of the components in the triplet T_1 (see Figs. 4 and 12). The large frequency variations first suggest that the C_1 frequencies correspond to three-mode resonances rather than simple linear combination frequencies. The result of prewhitening the frequencies f_{23} and f_{35} (using the same method as for the multiplets) is shown in Figs. 13 and 14, respectively. Most of the amplitude and frequency measurements for f_{23} and f_{35} are exactly following the variation of amplitude and frequency of the sums $f_1 + f_{11}$ and $f_3 + f_{21}$ within 1σ, respectively (see in particular the middle and bottom panels of Figs. 13 and 14).

The amplitude ratio R is 37 and 85 for $f_{23} \sim f_1 + f_{11}$ and $f_{35} \sim f_3 + f_{21}$, respectively. These values are significantly higher than those observed for normal linear combination frequencies in sdB stars (see the example given in Sect. 3.2). There is also a possible true linear combination frequency in KIC 10139564 with the frequency $f_{79} \sim f_1 - f_4$ (see Table 2) which indeed has a very low amplitude (signal-to-noise ratio of 5.1) and an amplitude ratio R less than one. Thus, we propose that there should be real pulsation modes near the position of the linear combination frequencies $f_1 + f_{11}$ and $f_3 + f_{21}$ and these modes had their amplitudes boosted through a resonance. In the $\nu_0 \sim \nu_1 + \nu_2$ resonance, the child mode indeed follows the behavior of its parent modes (see, again, Figs. 13 and 14 and examples provided by Breger & Montgomery 2014).

We note that another frequency, f_{74}, is also in the region near 6076 μHz, but has an amplitude too low to be monitored over time using the prewhitening technique on subsets of the

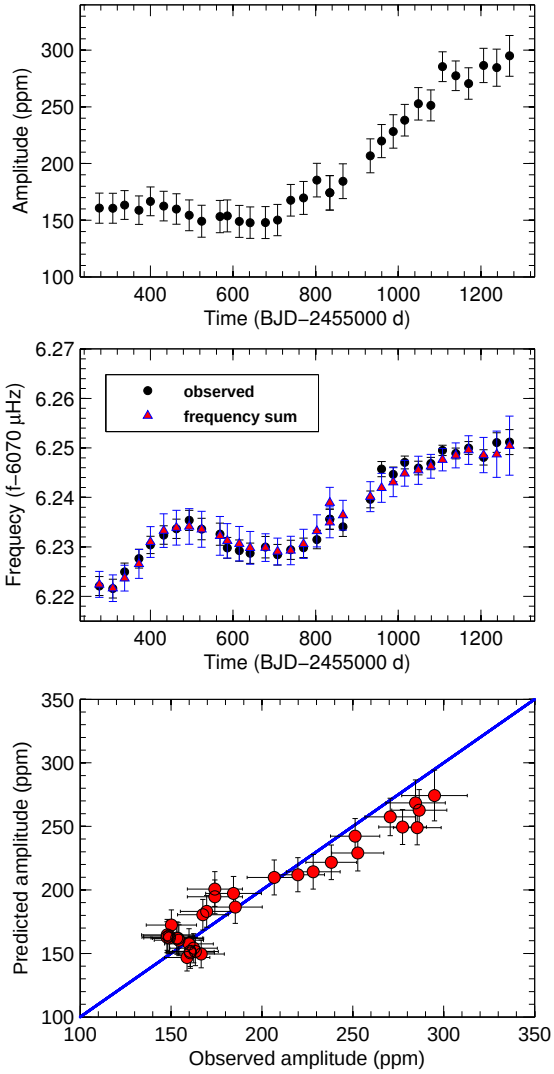

Fig. 13. Amplitude and frequency variations of the linear combination frequency $f_{23} = f_1 + f_{11}$. *Top panel*: measured amplitudes as a function of time obtained from each data subset (using the same method as for multiplets). *Middle panel*: measured frequencies from each data subset compared with the frequency sum $f_1 + f_{11}$, both as a function of time. *Bottom panel*: observed amplitudes of f_{23} vs predicted amplitudes of $R\times$ the product of f_1 and f_{11} amplitudes (see Eq. (6) for the definition of R). In both cases (frequency and amplitude comparisons), the measurements are found to be within 1σ.

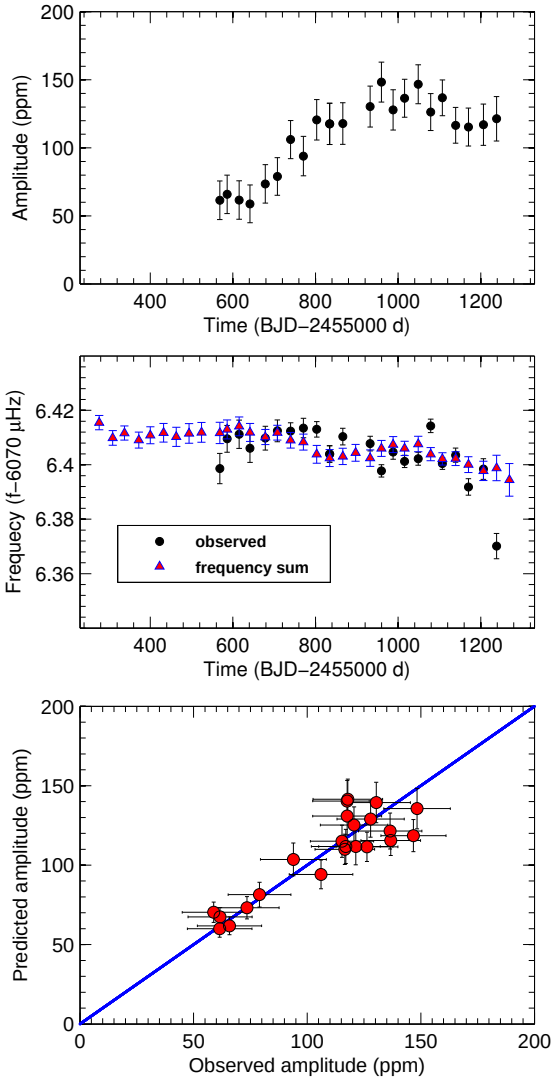

Fig. 14. Same as Fig. 13 but for the linear combination frequency $f_{35} = f_3 + f_{21}$. Note that there are ten missing measurements for f_{21}, including the first nine data points, because the amplitudes were lower than 4σ. The last data point is also not shown because of a large associated error, this measurement being at the end of the data set.

data. However, Fig. 12 still clearly shows that this frequency is varying smoothly during the observation, from ~6076.58 μHz (the first half part of the run) to ~6076.68 μHz (the second half part). We speculate that there is possibly a real mode, with a frequency around 6076.58−6076.69 μHz, which first interacts with the frequency sum $f_2 + f_{39} \sim 6076.59\,\mu$Hz, then with the frequency sum $f_3 + f_{11} \sim 6076.66\,\mu$Hz, because the influence from the latter modes become stronger than the former ones during the last half of the observation run, due to the amplitude of f_3 increasing significantly in the second half of the *Kepler* time series. This, again, suggests that the C_1 frequencies are really part of $\nu_0 \sim \nu_1 + \nu_2$ resonances instead of being simple linear combination frequencies.

All of the involved frequencies, $f_{1,2,3,11,21,39}$, are the components of the triplets T_1 and T_2. They are expected to be overstable (driven) modes, thus meaning that they are involved in a three-mode direct resonance and not a parametric resonance which involves one overstable parent mode and two damped unstable daughter modes.

At this stage, it becomes natural to interpret the complex variations observed in the components of T_1 and T_2 to be linked with the fact that these modes are simultaneously involved in two different types of resonances, that is, a triplet resonance and $\nu_0 \sim \nu_1 + \nu_2$ direct resonances. In this situation, the triplet resonance may be the dominating nonlinear interaction occurring in the triplet, while the nonlinear coupling with the modes outside the triplet could strongly perturb the periodic amplitude and frequency modulations expected if the triplets were pure isolated systems. This shows that nonlinear mode interactions in real stars are certainly more complex configurations than those treated by current simplified theoretical approaches. Moreover, since the T_2 triplet is in the transitory regime, with frequencies locked by the nonlinear coupling within the triplet, the nonlinear interactions outside this triplet are therefore unable to destroy this frequency locking, resulting in no long-term frequency variation as can be seen in the T_1 triplet. Interestingly, the resonant mode coupling theory predicts that a limit cycle (steady equilibrium state) may not be reached in the case of three-mode direct

resonance (which is likely at work here as discussed above). The evolution of this long-term frequency variation in T_1, whether the mode frequencies will further converge or eventually diverge, and the evolution of T_2, whether frequencies will remain constant or the locked regime will eventually be broken, will need further observation either from ground or by future space instruments currently in preparation such as TESS and PLATO (Rauer et al. 2014; Ricker et al. 2014).

4.5. The D-parameter and further insight on the modulations

The value of the D-parameter, that defines how far the modes are from the resonance center, is usually connected to the kind of regime a multiplet is in when undergoing resonant mode interactions. This D-value is in particular sensitive to the linear growth rate of the oscillation modes (see again Sect. 3).

For the frequency-locked regime that is observed in KIC 10139564 with the T_3 triplet, D is near or exactly zero, as predicted by the AEs (Buchler et al. 1995; Goupil et al. 1998). The D-value for the other triplets T_1 ($\delta\nu_o \sim 0.0026\,\mu$Hz) and T_2 ($\delta\nu_o \sim 0.0036\,\mu$Hz) may reflects more their linear growth rates since, with very similar frequency mismatches, the two triplets are found to be in different regimes. The growth rate values are indeed substantially different between p- and g-modes (Charpinet 1999; Fontaine et al. 2003). Assuming the growth rate for p-modes is of the order of $10^{-6}\,s^{-1}$ (Charpinet 1999), the corresponding D value for the T_1 triplet would be far less than one, indicating that T_1 should be in the frequency-locked regime (Buchler et al. 1997; Goupil et al. 1998), but we find it to be in the intermediate regime. We note however that this estimate for the value of D is based on the measured frequency mismatch which may not be representative of the unperturbed frequency asymmetry that enters in the definition of D. The latter is likely much larger (see Sect. 4.1), leading to a somewhat larger D-value more in line with the observed regime of the resonance for T_1. The D-value for the g-mode triplet T_2, for its part, could be much larger than that of T_1, considering the much smaller growth rates of the $\ell = 1$ g-modes (Fontaine et al. 2003). Extended ranges for D were also found in the DBV star KIC 08626021 (Z16), where the D-values for the triplets are at least two orders of magnitude larger than those suggested in Goupil et al. (1998). This suggests that the nonlinear behaviors not only depend on the magnitude of D, but also on the specific coupling coefficients for each specific mode (Buchler et al. 1995).

Further quantitative comparisons between the observed modulations and the theoretical framework would require to solve the amplitude equations for the specific case of KIC 10139564. This would require to calculate the coupling coefficients in the AEs, which, in principle, could be extracted from the observed amplitude and frequency modulations (Buchler et al. 1995). With these known coupling coefficients, one could then determine the ranges of D-values related to each different regime of the nonlinear resonance. A measurement of the growth rates of the oscillation modes would then possibly follow with the determination of this parameter, which may lead for the first time to an independent estimation of the linear nonadiabatic growth rates of the modes and a direct test of nonadiabatic pulsation calculations in sdB stars.

5. Summary and conclusion

While studying the high-quality and long-duration photometric data provided by the *Kepler* spacecraft on the pulsating sdB star KIC 10139564, we have identified different patterns in the frequency and amplitude modulations of the oscillation modes belonging to several rotationally split multiplets or linear combination frequencies. These modulations show signatures that can be associated to nonlinear resonant mode coupling mechanisms that could occur between the multiplet components themselves and with other modes under certain conditions, that is, satisfying a $\nu_0 \sim \nu_1 + \nu_2$ resonance relationship. This is the first time that such signatures are quite clearly identified in pulsating hot B subdwarf stars, and the second case reported so far for a compact pulsator monitored with *Kepler* photometry (see Z16).

We first reanalyzed the 38-month of *Kepler* photometry obtained for KIC 10139564, leading to the detection of 60 independent frequencies above a secured detection threshold (5.6σ; see Table A.1). Among these, 29 frequencies consist of three triplets, one doublet, one quintuplet and two incomplete multiplets with $\ell > 2$ (see Table 1). Another three detected frequencies are linked to other frequencies through linear combinations. Five additional groups of frequencies are found in the region between 5400 and 6400 μHz, which have very complicated structures. Finaly, we also find 14 independent frequencies and two frequencies satisfying linear combination relationships that could be real as their amplitudes are between 5σ and 5.6σ above the noise. In general, our well secured frequencies are in good agreement with the former analysis from Baran et al. (2012). In this paper, we particularly concentrated our study on six multiplets and three linear combination frequencies observed near 6076 μHz.

We found different types of mode behaviors occurring in the above mentioned frequencies. A "short timescale" quasi-periodic amplitude and frequency modulations along with a slow trend of the frequencies to convergence toward each other occur in the dominant p-mode triplet near 5760 μHz (T_1). The ~570-day quasi-periodic frequency modulation evolve in antiphase between the two side components in this triplet. Modulated frequencies and amplitudes are also found in a quintuplet near 5287 μHz (Q_1) and a ($\ell > 2$) multiplet near 5412 μHz (M_1), but the modulations do not show a clear periodicity. One triplet near 316 μHz (T_2) has a distinct behavior from the above mentioned multiplets, as it shows stable frequencies but varying amplitudes. A similar phenomenon occurs in a doublet near 394 μHz (D_1) which shows constant frequencies and an ~1100 days periodic amplitude modulations. Another triplet at 518 μHz (T_3) completely differs from all the above multiplets, with constant amplitudes and frequencies throughout the whole observation run. In addition, we also discovered amplitude and frequency variations in three frequencies near 6076 μHz (C_1) that are linked to other independent frequencies through linear combinations.

After ruling out various possible causes for the modulations, we showed that these mode behaviors could be related to the different types of nonlinear resonances that should occur according to the amplitude equation formalism. In particular, nonlinear resonant couplings within a multiplet can lead to three main regimes, all of which are possibly occurring in KIC 10139564. The multiplets T_1, Q_1 and M_1 can be associated with the intermediate regime of the resonance where the involved modes have modulated amplitudes and frequencies. The triplet T_2 and doublet D_1 have a different behavior that could be associated to a narrow transitory regime in which the frequencies of the modes can be locked (constant) while the amplitudes experience modulations. The behavior of the triplet T_3 is the unique case found in this star that can be associated to the frequency lock regime of the resonance, where both amplitudes and frequencies are stable. In addition, the large amplitude ratios between the C_1

frequencies and their main parent modes, together with the large variation of amplitude and frequency observed for these peaks, suggest that C_1 correspond to three-mode direct resonances. We indeed found that the frequencies of C_1 exactly follow the evolution of their main parent modes. Moreover, as the parent modes of C_1 are also the components of T_1 and T_2, we suggest part of the complexity of the mode behaviors could be related to these cross interactions between the various modes. In particular, the slow variations occurring in T_1 may be related to the $\nu_0 \sim \nu_1 + \nu_2$ resonance superimposed to the triplet resonance occurring between the components.

We emphasize that the observed frequency modulations likely induced by nonlinear mode interactions could challenge future attempts to measure the evolutionary effects on the oscillation mode periods in pulsating sdB stars. Compared to the resonant variations taking place on timescales of years, the rate of period change of the pulsations due to stellar evolution in sdB stars is much longer, typically occurring on a timescale of $\sim 10^6$ yr (Charpinet et al. 2002). Nonlinear modulations of the frequencies can potentially jeopardize any attempt to measure reliably such rates, unless they can be corrected beforehand. These nonlinear modulations could also complicate the detection of exoplanets or stellar companions around sdB stars using the technique of measuring phase changes in the pulsations (Silvotti et al. 2007). It should be possible however to distinguish between the two effects, considering that nonlinear couplings may induce different behaviors on different modes, while external causes such as an orbiting body should affect all modes similarly.

Finally, we note that our analysis suggests that resonances occurring in real stars, in which modes could be involved in two or more types of different couplings, lead to more complicated patterns than those predicted by current theoretical frameworks which treat the modes only as isolated systems within one type of resonance and ignore the nonlinear interactions that could occur simultaneously outside of the system. This should motivate further theoretical work to develop nonlinear stellar pulsation theory for more precise predictions of the mode behaviors in pulsating stars in general.

Acknowledgements. Funding for the *Kepler* mission is provided by NASA's Science Mission Directorate. We greatfully acknowledge the *Kepler* Science Team and all those who have contributed to making the *Kepler* mission possible. WKZ acknowledges the financial support from the China Scholarship Council. This work was supported in part by the Programme National de Physique Stellaire (PNPS, CNRS/INSU, France) and the Centre National d'Études Spatiales (CNES, France).

References

Baran A. S., & Østensen R. H. 2013, Acta Astron., 63, 79
Baran, A., Pigulski, A., O'Toole, S. J. 2008, MNRAS, 385, 255
Baran A. S. Reed, M. D., Stello, D., et al. 2012, MNRAS, 424, 2686
Brassard, P., Fontaine, G., & Wesemael, F. 1995, ApJS, 96, 545
Breger, M., & Montgomery, M. H. 2014, ApJ, 783, 89
Buchler, J. R., & Goupil, M. J. 1984, ApJ, 279, 384
Buchler, J. R., & Kovacs, G. 1986, ApJ, 303, 794
Buchler, J. R., Goupil, M.-J., & Serre, T. 1995, A&A, 296, 405
Buchler, J. R., Goupil, M.-J., & Hansen, C. J. 1997, A&A, 321, 159
Carroll, B. W., & Hansen, C. J. 1982, ApJ, 279, 394
Charpinet, S. 1999, Ph.D. Thesis, Univ. Montréal
Charpinet, S., Fontaine, G., Brassard, P., & Dorman, B. 1996, ApJ, 471, L103
Charpinet, S., Fontaine, G., Brassard, P., et al. 1997, ApJ, 483, L123
Charpinet, S., Fontaine, G., Brassard, P., & Dorman, B. 2002, ApJS, 140, 469
Charpinet, S., Green, E. M., Baglin, A., et al. 2010, A&A, 516, L6
Charpinet, S., Van Grootel, V., Fontaine, G., et al. 2011, A&A, 530, A3
Deeming, T. J. 1975, Ap&SS, 36, 137
Dziembowski, W. A. 1982, Acta Astron., 32, 147
Dziembowski, W. A., & Goode, P. R. 1992, ApJ, 394, 670
Fontaine, G., Brassard, P., Charpinet, S., et al. 2003, ApJ, 597, 518
Fontaine, G., Brassard, P., Charpinet, S., et al. 2012, A&A, 539, A12
Gilliland, R. L., Timothy, M., Christensen-Dalsgaard, J., et al. 2010, PASP, 122, 131
Green, E. M., Fontaine, G., Reed, M. D., et al. 2003, ApJ, 583, L31
Goupil, M. J., & Buchler, J. R. 1994, A&A, 291, 484
Goupil, M. J., Dziembowski, W. A., & Fontaine, G. 1998, Balt. Astron., 7, 21
Heber, U. 2009, ARA&A, 47, 211
Jenkins, J. M., Caldwell, D. A., Chandrasekaran, H., et al. 2010, ApJ, 713, L87
Jones, P. W., Hansen, C. J., Pesnell, W. D., & Kawaler, S. D. 1989, ApJ, 336, 403
Kawaler, S. D., Reed, M. D., Quint, A. C., et al. 2010, MNRAS, 409, 1487
Kilkenny, D. 2007, Commun. Asteroseismol., 150, 234
Kilkenny, D. 2010, Ap&SS, 329, 175
Kilkenny, D., Koen, C., O'Donoghue, D., & Stobie, R. S. 1997, MNRAS, 285, 640
Landstreet, J. D., Bagnulo, S., Fossati, L., Jordan, S., & O'Toole, S. J. 2012, A&A, 541, A100
Montgomery, M. H., & Odonoghue, D. 1999, Delta Scuti Star Newsletter, 13, 28
Moskalik, P. 1985, Acta Astron., 35, 229
Østensen, R. H., Reed, M. D., Baran, A. S., & Telting, J. H. 2014, A&A, 564, L14
Petit, P., Van Grootel, V., Bagnulo, S., et al. 2012, in Fifth Meeting on Hot Subdwarf Stars and Related Objects, ASP Conf. Ser., 452, 87
Rauer, H., Catala, C., Aerts, C., et al. 2014, Exp. Astron., 38, 249
Reed, M. D., O'Toole, S. J., Terndrup, D. M., et al. 2007, ApJ, 664, 518
Ricker, G. R., Winn, J. N., Vanderspek, R., et al. 2014, SPIE, 9143E, 20
Saio, H. 1981, ApJ, 244, 299
Salabert, D., García, R. A., & Turck-Chièze, S. 2015, A&A, 578, A137
Scargle, J. D. 1982, ApJ, 263, 835
Schuh, S., Hubber, J., Dreizler, S., et al. 2006, A&A, 445, 131
Silvotti, R., Schuh, S., Janulis, R., et al. 2007, Nature, 449, 189
Unno, W., Osaki, Y., Ando, H., Saio, H., & Shibahashi, H. 1989, Nonradial oscillations of stars, 2nd edn. (Tokyo: University of Tokyo Press)
van Grootel, V., Charpinet, S., Fontaine, G., et al. 2010, ApJ, 718, L97
Van Hoolst, T. 1994, A&A, 292, 183
van Kerkwijk, M. H., Clemens, J. C., & Wu, Y. 2000, MNRAS, 314, 209
Vauclair, G., Fu, J.-N., Solheim, J. E., et al. 2011, A&A, 528, A5
Wu, Y. 2001, MNRAS, 323, 248
Wu, Y., & Goldreich, P. 2001, ApJ, 546, 469
Zong, W., Charpinet, S., Vauclair, G., et al. 2016, A&A, 585, A22 (Z16)

Appendix A: Additional table

Table A.1. List of frequencies detected in KIC 10139564.

Id.	Frequency (μHz)	σ_f (μHz)	Period (s)	σ_P (s)	Amplitude (%)	σ_A (%)	Phase	σ_{Ph}	S/N	† Comment
Multiplet frequencies:										
f_{39}	315.579243	0.000566	3168.776214	0.005687	0.005851	0.000596	0.2492	0.0516	9.8	$T_{2,-1}$
f_{21}	315.820996	0.000219	3166.350599	0.002193	0.015155	0.000596	0.6107	0.0199	25.4	$T_{2,0}$
f_{11}	316.066440	0.000070	3163.891744	0.000702	0.047276	0.000596	0.2063	0.0064	79.3	$T_{2,+1}$
f_{27}	394.027385	0.000342	2537.894669	0.002202	0.009667	0.000594	0.2589	0.0312	16.3	$D_{1,0}$
f_{32}	394.289823	0.000397	2536.205455	0.002555	0.008323	0.000594	0.5123	0.0363	14.0	$D_{1,+1}$
f_{34}	518.900359	0.000437	1927.152262	0.001624	0.007526	0.000592	0.6648	0.0401	12.7	$T_{3,-1}$
f_{28}	519.151796	0.000352	1926.218898	0.001305	0.009351	0.000592	0.9059	0.0323	15.8	$T_{3,0}$
f_{31}	519.402391	0.000367	1925.289559	0.001360	0.008964	0.000592	0.5369	0.0337	15.2	$T_{3,+1}$
f_{08}	5286.149823	0.000053	189.173601	0.000002	0.064784	0.000614	0.6712	0.0047	105.4	$Q_{1,-2}$
f_{10}	5286.561766	0.000060	189.158861	0.000002	0.057105	0.000614	0.4356	0.0053	92.9	$Q_{1,-1}$
f_{07}	5286.976232	0.000038	189.144032	0.000001	0.088857	0.000614	0.1202	0.0034	144.6	$Q_{1,0}$
f_{05}	5287.391879	0.000019	189.129163	0.000001	0.179339	0.000615	0.3374	0.0017	291.8	$Q_{1,+1}$
f_{06}	5287.805883	0.000029	189.114355	0.000001	0.119329	0.000615	0.7941	0.0025	194.2	$Q_{1,+2}$
f_{22}	5410.701146	0.000234	184.818931	0.000008	0.014871	0.000627	0.9524	0.0203	23.7	$M_{1,0}$
f_{67}	5411.143448	0.000958	184.803824	0.000033	0.003637	0.000627	0.4591	0.0830	5.8	$M_{1,0}$
f_{13}	5411.597301	0.000136	184.788325	0.000005	0.025636	0.000627	0.6770	0.0118	40.9	$M_{1,0}$
f_{15}	5412.516444	0.000185	184.756944	0.000006	0.018812	0.000627	0.8925	0.0160	30.0	$M_{1,0}$
f_{12}	5413.389096	0.000084	184.727161	0.000003	0.041339	0.000627	0.4037	0.0073	65.9	$M_{1,0}$
f_{19}	5413.814342	0.000222	184.712651	0.000008	0.015718	0.000627	0.7225	0.0192	25.1	$M_{1,0}$
f_{25}	5570.030091	0.000389	179.532244	0.000013	0.010056	0.000703	0.5938	0.0300	14.3	$M_{2,0}$
f_{56}	5570.484768	0.000964	179.517590	0.000031	0.004058	0.000703	0.8087	0.0744	5.8	$M_{2,0}$
f_{61}	5570.937140	0.001001	179.503013	0.000032	0.003913	0.000704	0.8254	0.0772	5.6	$M_{2,0}$
f_{29}	5571.393930	0.000421	179.488295	0.000014	0.009297	0.000705	0.5332	0.0325	13.2	$M_{2,0}$
f_{43}	5572.293674	0.000760	179.459314	0.000024	0.005168	0.000706	0.5854	0.0584	7.3	$M_{2,0}$
f_{50}	5572.728096	0.000902	179.445324	0.000029	0.004356	0.000707	0.5037	0.0693	6.2	$M_{2,0}$
f_{45}	5708.908076	0.000897	175.164845	0.000028	0.004648	0.000749	0.0571	0.0650	6.2	$M_{2,0}$
f_{01}	5760.167840	0.000005	173.606052	...	0.825132	0.000761	0.0744	0.0004	1084.9	$T_{1,-1}$
f_{03}	5760.586965	0.000008	173.593421	...	0.554646	0.000761	0.6388	0.0005	729.3	$T_{1,0}$
f_{02}	5761.008652	0.000007	173.580715	...	0.567034	0.000761	0.5845	0.0005	745.5	$T_{1,+1}$
Independent frequencies:										
f_{72}	892.042910	0.000986	1121.022305	0.001239	0.003319	0.000588	0.6058	0.0909	5.6	
f_{70}	2212.606534	0.000942	451.955639	0.000192	0.003462	0.000586	0.0639	0.0872	5.9	
f_{37}	3540.459896	0.000514	282.449182	0.000041	0.006309	0.000583	0.3837	0.0478	10.8	
f_{36}	3541.431179	0.000477	282.371716	0.000038	0.006796	0.000583	0.4013	0.0444	11.7	
f_{47}	4064.355754	0.000719	246.041454	0.000044	0.004526	0.000585	0.4296	0.0667	7.7	
f_{46}	5048.744283	0.000729	198.069053	0.000029	0.004548	0.000596	0.9108	0.0664	7.6	
f_{41}	5049.709963	0.000610	198.031176	0.000024	0.005432	0.000596	0.6548	0.0556	9.1	
f_{63}	5052.604965	0.000879	197.917709	0.000034	0.003771	0.000596	0.5451	0.0800	6.3	
f_{04}	5472.861431	0.000007	182.719773	...	0.476915	0.000638	0.2824	0.0006	747.9	
f_{42}	5709.026672	0.000793	175.161207	0.000024	0.005254	0.000749	0.0777	0.0575	7.0	
f_{53}	5740.666960	0.001002	174.195787	0.000030	0.004168	0.000751	0.8817	0.0724	5.6	
f_{49}	5740.807435	0.000946	174.191525	0.000029	0.004411	0.000751	0.0263	0.0684	5.9	
f_{50}	5746.615392	0.000612	174.015474	0.000019	0.006881	0.000757	0.0989	0.0439	9.1	
f_{18}	5747.099099	0.000261	174.000828	0.000008	0.016157	0.000757	0.8738	0.0187	21.3	
f_{17}	5748.065581	0.000257	173.971571	0.000008	0.016414	0.000758	0.5427	0.0184	21.7	
f_{16}	5749.067189	0.000256	173.941262	0.000008	0.016476	0.000758	0.1319	0.0183	21.7	

Notes. (†) The first subscript is the identity of the multiplet and the second one indicates the value of m. The m-values for two $\ell > 2$ multiplets, M_1 and M_2, are not provided as the degree ℓ is not known.

Table A.1. continued.

Id.	Frequency (μHz)	σ_f (μHz)	Period (s)	σ_P (s)	Amplitude (%)	σ_A (%)	Phase	σ_{Ph}	S/N	† Comment
f_{44}	5840.820662	0.000903	171.208818	0.000026	0.004685	0.000761	0.7872	0.0645	6.2	
f_{65}	6057.645946	0.000970	165.080629	0.000026	0.003740	0.000652	0.2785	0.0815	5.7	
f_{55}	6057.688799	0.000876	165.079461	0.000024	0.004142	0.000652	0.9775	0.0736	6.3	
f_{66}	6106.662077	0.000977	163.755582	0.000026	0.003675	0.000646	0.6890	0.0822	5.7	
f_{60}	6757.710494	0.000838	147.979112	0.000018	0.003938	0.000594	0.1752	0.0767	6.6	
f_{59}	6758.215141	0.000835	147.968062	0.000018	0.003954	0.000594	0.1869	0.0764	6.7	
f_{30}	7633.720521	0.000360	130.997722	0.000006	0.009090	0.000589	0.1759	0.0332	15.4	
f_{40}	7634.190048	0.000592	130.989665	0.000010	0.005536	0.000589	0.3321	0.0546	9.4	
f_{64}	7634.677476	0.000873	130.981302	0.000015	0.003753	0.000589	0.1106	0.0805	6.4	
f_{52}	8118.752590	0.000768	123.171631	0.000012	0.004284	0.000591	0.3497	0.0705	7.2	
f_{33}	8119.248304	0.000436	123.164111	0.000007	0.007538	0.000591	0.4515	0.0400	12.7	
f_{48}	8496.107048	0.000733	117.700965	0.000010	0.004503	0.000594	0.8648	0.0744	7.6	
f_{71}	8496.293646	0.000973	117.698380	0.000013	0.003395	0.000594	0.0896	0.0934	5.7	
f_{54}	8615.236287	0.000795	116.073427	0.000011	0.004159	0.000594	0.5932	0.0727	7.0	
f_{38}	8616.169582	0.000539	116.060854	0.000007	0.006128	0.000594	0.7833	0.0498	10.3	
Linear combination frequencies:										
f_{23}	6076.234996	0.000252	164.575597	0.000007	0.014360	0.000650	0.7906	0.0210	22.1	$f_{11} + f_{01}$
f_{35}	6076.408232	0.000510	164.570905	0.000014	0.007091	0.000650	0.7821	0.0426	10.9	$f_{21} + f_{03}$
f_{74}	6076.650684	0.001120	164.564338	0.000030	0.003225	0.000650	0.5520	0.0937	5.0	$f_{11} + f_{03}$
f_{68}	190.138219	0.000959	5259.331906	0.026527	0.003563	0.000614	0.2639	0.0847	5.8	$f_{01} - f_{25}$
f_{79}	287.306296	0.001081	3480.605932	0.013093	0.003075	0.000598	0.9190	0.0982	5.1	$f_{01} - f_{04}$
Group frequencies:										
f_{20}	5471.730865	0.000230	182.757527	0.000008	0.015410	0.000637	0.9397	0.0196	24.2	G1
f_{14}	5944.170986	0.000209	168.232038	0.000006	0.019127	0.000720	0.1222	0.0158	26.6	G2
f_{24}	6001.472409	0.000273	166.625776	0.000008	0.013532	0.000664	0.2224	0.0223	20.4	G3
f_{26}	6172.852132	0.000353	161.999669	0.000009	0.009980	0.000633	0.6961	0.0302	15.8	G4
f_{09}	6234.713029	0.000058	160.392306	0.000001	0.062028	0.000648	0.9590	0.0072	95.7	G5
f_{51}	6315.214679	0.000798	158.347744	0.000020	0.004312	0.000619	0.3510	0.0700	7.0	G6
Suspected frequencies:										
f_{77}	4061.893709	0.001051	246.190588	0.000064	0.003097	0.000585	0.9507	0.0974	5.3	
f_{57}	5838.962703	0.001063	171.263296	0.000031	0.003980	0.000761	0.6543	0.0758	5.2	
f_{62}	5841.187712	0.001114	171.198059	0.000033	0.003796	0.000761	0.7222	0.0796	5.0	
f_{58}	5841.581605	0.001068	171.186516	0.000031	0.003960	0.000761	0.1969	0.0762	5.2	
f_{83}	345.231189	0.001151	2896.609673	0.009656	0.002878	0.000596	0.8214	0.1050	4.8	
f_{84}	345.597339	0.001193	2893.540798	0.009988	0.002777	0.000596	0.3501	0.1088	4.7	
f_{78}	345.976695	0.001077	2890.368090	0.008999	0.003076	0.000596	0.4839	0.0982	5.2	
f_{69}	6106.245918	0.001014	163.766742	0.000027	0.003544	0.000646	0.6171	0.0852	5.5	
f_{75}	6418.164502	0.001068	155.807786	0.000026	0.003178	0.000610	0.7474	0.0950	5.2	
f_{76}	6758.687089	0.001049	147.957730	0.000023	0.003148	0.000594	0.5124	0.0959	5.3	
f_{80}	6997.352981	0.001084	142.911184	0.000022	0.003003	0.000586	0.5103	0.1005	5.1	
f_{73}	7633.957044	0.001007	130.993663	0.000017	0.003251	0.000589	0.2483	0.0930	5.5	
f_{81}	8117.287298	0.001114	123.193866	0.000017	0.002953	0.000591	0.7915	0.1022	5.0	
f_{82}	8377.175646	0.001119	119.371975	0.000016	0.002937	0.000591	0.8589	0.1040	5.0	

Conclusions and Perspectives

This thesis reports on a detailed investigation of the mode behaviors in compact pulsators based on the unprecedented high-quality and contiguous photometric data from the *Kepler* spacecraft. We identify the first clear-cut (quasi-) periodic amplitude and frequency modulations in sdB and white dwarf pulsators. These cases are the first clear evidence of nonlinear resonant mode couplings in compact pulsators that was proposed more than three decades ago (Vauclair & Bonazzola 1981). The observed modulations provide new insight on nonlinear asteroseismology, as well as new methods to process the signals of variable modes from the observed light curves. We foresee that increasing attention will focus on amplitude and frequency modulations observed from space in the near future, motivating further development of nonlinear oscillation theory in general.

Summary of the results

Kepler monitored 24 compact pulsators in short-cadence exposure mode, including six white dwarfs and 18 hot B subdwarfs. Most of them have been contiguously observed for more than two years. The frequency contents suggest that those sdB pulsators are typically slow rotating objects with periods from ~ 6 to ~ 90 days and white dwarf pulsators rotate with a period of the order of days. We use a prevalent method—the sliding Lomb-Scargle periodogram—to search for temporal mode behaviors in these compact pulsators. We find that it is a common phenomenon that oscillation modes in compact pulsators show amplitude and/or frequency variations. The most interesting results are found in two stars, KIC 08626021 and KIC 10139564.

KIC 08626021, the only DB white dwarf star in *Kepler* field, has been continuously observed by *Kepler* for nearly two years. We mainly concentrate on the rotational splitting triplets as well as on frequencies through linear combinations. These frequencies show intriguing amplitude and frequency behaviors during the *Kepler* observations, which are clear signatures of nonlinear effects that could be attributed to resonant mode coupling mechanisms. We first notice that a structure at 3681 μHz, identified as a triplet in previous published studies, is in fact forming a doublet, with the third component being an independent mode. This doublet (an incomplete triplet) and a triplet at 4310 μHz have clear periodic frequency and amplitude modulations, which are in the typically so-called intermediate regime of the triplet resonance, with timescales consistent with theoretical expectations. Another triplet at 5073 μHz is likely in a narrow transitory regime in which the amplitudes are modulated simultaneously with constant frequencies. Using nonadiabatic pulsation calculations, based on a model representative of KIC 08626021 to evaluate the linear growth rates of the modes in the triplets, we also provide quantitative information that could be useful for future comparisons with numerical solutions of the amplitude equations. The observed modulations are the clearest hints of nonlinear resonant mode couplings occurring in white dwarf stars identified so far.

KIC 10139564, the only short-period dominated hybrid pulsating sdB star in the *Kepler* field, has been observed contiguously by *Kepler* for 38 months. This star present many rotational

multiplets as revealed from its frequency content. We, again, mainly focus on mode multiplets and on frequencies forming linear combinations to investigate the intriguing amplitude and frequency behaviors during the course of the observations. We find clear signatures that point toward nonlinear effects predicted by resonant mode coupling mechanisms. We find that a triplet at 5760 μHz, a quintuplet at 5287 μHz and a ($\ell > 2$) multiplet at 5412 μHz show clear frequency and amplitude modulations which are in the typically so-called intermediate regime of a resonance between the multiplet components. One triplet at 316 μHz and a doublet at 394 μHz show modulated amplitudes and constant frequencies which can be associated with a narrow transitory regime of the resonance. We find that another triplet at 519 μHz appears to be in a frequency lock regime where both frequency and amplitude are constant. Additionally, three linear combination of frequencies near 6076 μHz also show amplitude and frequency modulations, which are likely related to a three-mode direct resonance of the type $\nu_0 \sim \nu_1 + \nu_2$. The identified amplitude and frequency modulations are the first clear-cut signatures of nonlinear resonant couplings occurring in pulsating hot B subdwarf stars

However, we find that the observed behaviors in both cases (KIC 08626021 and KIC 10139564) suggest that the resonances occurring in these stars usually follow more complicated patterns than the simple predictions from current nonlinear theoretical frameworks. Theoretically, the resonant modes are only treated as isolated systems within one type of resonance and ignore the nonlinear interactions (very slight) that could occur simultaneously outside of the system. Observationally, we find that the triplet resonance modes can also be involved in other types of resonance, e.g., three-mode resonance $\nu_0 \sim \nu_1 + \nu_2$. We also mention that the observed values of the key parameter D in the triplet resonance somewhat differ from the values predicted by the nonlinear theory. This suggests that the nonlinear behaviors not only depend on the magnitude of D, but also on the specific coupling coefficients for each specific mode (Buchler et al. 1995).

We finally emphasize that the observed frequency modulations likely induced by nonlinear mode interactions could challenge any attempt to measure the evolutionary effects on oscillation mode periods in pulsating sdB and white dwarf stars. The rates of period change of pulsations due to stellar evolution in compact stars are much longer than that of the nonlinear effects, e.g., a timescales of $\sim 10^5$ years in DBV stars (Winget et al. 2004) and $\sim 10^6$ years in sdB star (Charpinet et al. 2002b), respectively. Measuring the changing rate of the pulsation periods in pulsating stars can indeed offer some constraints on basic physics, e.g., in white dwarfs, it could offer an opportunity to constrain the neutrino emission physics (Winget et al. 2004). However, one should be extremely careful of the potential contamination from nonlinear effects when one attempts to measure reliably such rates, which may need to be corrected beforehand. These nonlinear modulations could also complicate the detection of exoplanets or stellar companions around compact stars using the technique of measuring phase changes in the pulsations (e.g., Silvotti et al. 2007). Nevertheless, it should be possible to distinguish between the two effects, considering that nonlinear couplings may induce different behaviors on different modes, while external causes such as an orbiting body should affect all modes similarly.

Further perspectives

These intriguing observed amplitude and frequency modulations, induced by nonlinear mode interactions, should bring significant constraints for further development of the nonlinear stellar pulsation theory, for the development of new methods and techniques to prewhiten observed light curves, for the application of nonlinear resonance to other types of pulsating stars, and for the study resonant mode behaviors observed from future space missions as well as ground-based telescopes.

The differences, between our observed modulations and the theoretical expectations, should

motivate further theoretical work to develop nonlinear stellar pulsation theory for more precise predictions of the mode behaviors in pulsating stars in general. We indeed observed that the modes outside the isolated triplet resonance can be strong enough to interact with the triplet modes. This and multiplet modes ($\ell > 1$) both involve more than three mode interactions, which has not been currently explored theoretically. As more modes are involved, the amplitude and frequency modulations may seem more complicated than those of three mode interactions. The observed modulations may pave the way to extract nonlinear coupling coefficients in real stars for the first time (Buchler et al. 1995), from which one then could determine the values of the key parameter D, in different regimes of the triplet resonance, in real stars. The periodic modulations, associated with the intermediate regime in the triplet resonance, may also provide a way to measure the linear growth rates of oscillation modes, as the modulation timescales have a very tight relationship with the inverse of the growth rates.

The modulations due to nonlinear effects induce hyperfine structures or very complex broaden structures in the Lomb-Scargle periodograms. Such signals cannot be well extracted from light curves by the current standard prewhitening method which uses pure sinusoidal fittings. After removing a high amplitude peak, there may be many other significant peaks around the frequency position of that peak. We therefore propose a new method to prewhiten variable frequencies considering that the sidelobes or complex broaden structures contain important information on the amplitude and frequency variations in these variable signals. Many of statistical tests and simulations need to be conducted to check the reliability of the proposed method in the near future. It will be incorporated in our current program FELIX after testing its feasibility. With this new method at hand, it will greatly accelerate the speed and improve the efficiency to characterize the mode behaviors in pulsating stars, particularly for the stars observed by *Kepler* with a duration of ~ 4 years.

We indeed also find interesting amplitude and frequency variations in other compact pulsators from the *Kepler* photometry. More work is needed to investigate the amplitude and frequency behaviors thoroughly in these stars. As coupling coefficients may differ from each resonant mode in each star, the resonant modes may have a variety of amplitude and frequency behaviors. We think that a library of mode behaviors from the *Kepler* compact pulsators needs to be constructed in which different kinds of mode behaviors could be conveniently found. Mathematically, nonlinear amplitude equations are ubiquitously applicable to any type of pulsating stars. It is particularly interesting to observe amplitude and frequency variations in other types of pulsators in the *Kepler* field. Recently, Bowman et al. (2016) have studied a comprehensive set of ~ 1000 δ Scuti stars observed by *Kepler* with a duration of ~ 4 years, mainly concentrating on amplitude behaviors of oscillation modes.

We end up this thesis with the prospectives that oscillation mode behaviors can also be observed from future space missions, e.g., TESS, since some bright compact pulsators exhibit amplitude variations from ground-based observations. A full cycle of modulations with timescales of weeks or months may be discovered in these bright compact stars from the near future missions. In many respects, nonlinear stellar oscillation theory can now develop on a new observational background, which may revive interest in these physical phenomena.

Conclusion et perspectives

Cette thèse présente une investigation détaillée du comportement des modes dans les pulsateurs compacts basée sur les données continues et d'une qualité sans précédent fournies par le satellite *Kepler*. Nous identifions clairement des modulations quasi-périodiques d'amplitude et de fréquence dans les pulsateurs sdB et naines blanches. Les cas étudiés mettent en évidence pour la première fois sans ambiguïté l'existence de couplages résonants nonlinéaires entre modes dans ces pulsateurs compacts, des effets suspectés dans ces étoiles voilà plus de trois décennies (Vauclair & Bonazzola 1981). Les modulations observées permettent un regard nouveau sur l'astérosismologie nonlinéaire, et nécessitent de nouvelles méthodes pour analyser le signal de ces modes variables dans les courbes de lumière. Nous estimons que dans les années à venir, un intérêt grandissant pour l'étude des modulations d'amplitude et de fréquence à l'aide des données spatiales permettra des développements nouveaux en théorie nonlinéaire des oscillations nonradiales.

Résumé des resultats

Le satellite *Kepler* a observé 24 pulsateurs compacts en mode cadence courte, incluant six naines blanches et 18 sdB. La plupart ont été suivies continuellement pendant plus de deux ans. Le contenu en fréquences suggère que ces étoiles sont typiquement des rotateurs lents avec des périodes entre ~ 6 et ~ 90 jours, alors que la période de rotation pour les naines blanches sont de l'ordre de la journée. Nous utilisons des périodogrammes de Lomb-Scargle à fenêtre glissante pour identifier des variations temporelles des modes dans ces pulsateurs compacts. Nous trouvons que les modes d'oscillation dans ces étoiles montrent communément des modulations d'amplitude et de fréquence. Les résultats les plus intéressants concernent deux étoiles : KIC 08626021 et KIC 10139564.

KIC 08626021, la seule naine blanche pulsante de type DB observée dans le champs *Kepler*, a été continuellement suivie par le satellite pendant près de deux ans. Nous nous sommes principalement concentrés sur les triplets engendrés par la rotation stellaire ainsi que sur les fréquences liées au travers d'une relation de combinaison linéaire. Ces fréquences montrent des modulations d'amplitude et de fréquence durant les observations *Kepler* que l'on peut clairement associer à des effets non linéaires, en particulier de couplage résonnant entre modes. Nous avons tout d'abord remarqué qu'une structure à $3681\,\mu$Hz, identifiée comme un triplet dans une analyse préalablement publiée sur KIC 08626021, est en fait un doublet et un mode indépendant. Ce doublet (un triplet incomplet) et un triplet à $4310\,\mu$Hz montrent clairement une modulation périodique de l'amplitude et de la fréquence de chacune des composantes. Ce comportement est typique du régime intermédiaire des couplages résonants entre modes et le temps caractéristique des modulations est conforme avec les attentes théoriques. Un autre triplet à $5073\,\mu$Hz est probablement dans un régime transitoire de la résonance dans lequel les amplitudes sont modulées simultanément alors que les fréquences sont constantes. Sur la base de calculs non adiabatiques appliqués sur un modèle sismique représentatif de KIC 08626021

pour évaluer les taux de croissance linéaires des modes formant les triplets, nous apportons également des informations quantitatives qui pourront être utiles pour des comparaisons avec de futurs calculs numériques détaillés résolvant les équations d'amplitude. Les modulations observées dans KIC 08626021 sont le plus clair indice d'effets non linéaires liés à des couplages résonnants entre modes identifiés à ce jour dans les naines blanches.

KIC 10139564, la seule étoile sdB pulsante hybride dominée par les modes p découverte dans le champ *Kepler*, a été observée continuellement par le satellite pendant 38 mois. Cette étoile présente de nombreux multiplets liés à la rotation comme le montre l'analyse des fréquences. Encore une fois, nous nous sommes focalisé sur les multiplets de modes et sur les fréquences formant des combinaisons linéaires pour étudier les intriguantes variations d'amplitude et de fréquence observées durant ces observations. Nous trouvons à nouveau des signatures claires qui pointent vers des effets non linéaires semblable à ceux prédits dans le cadre des mécanismes de couplages résonnants. Nous trouvons qu'un triplet à 5760 μHz, un quintuplet à 5287 μHz et un multiplet ($\ell > 2$) à 5412 μHz montrent des modulations d'amplitude et de fréquence typiques du régime intermédiaire d'une résonance entre les composantes. Un triplet à 316 μHz et un doublet à 394 μHz montre des amplitudes modulées mais des fréquences constantes, une configuration qui peut être associée à un régime transitoire de la résonance. Un autre triplet à 519 μHz semble être dans le régime vérouillé où les frequences et les amplitudes sont constantes. De plus, trois combinaisons linéaires de frequences vers 6076 μHz montrent également des modulations d'amplitude et de frequence qui sont probablement reliées à une résonance directe à trois modes du type $\nu_0 \sim \nu_1 + \nu_2$. Les modulations d'amplitude et de fréquence identifiées dans KIC 10139564 représentent le premier cas clairement établi de couplages non linéaires résonnants entre modes dans une étoile sdB pulsante.

Néanmoins, nous trouvons dans les deux cas (KIC 08626021 et KIC 10139564) que les comportements observés pour les résonnances se produisant dans ces étoiles suivent des schémas plus complexes qui ceux prédits par les modèles théoriques nonlinéaires actuels. En effet, les résonnances entre modes sont généralement traitées comme des systèmes isolés dans ces modèles simplifiés et les interactions non linéaires (même faibles) pouvant se produire simultanément en dehors du système sont ignorées. Or ces interactions multiples existes, lorsque l'on observe notamment que les modes en résonance dans un triplet peuvent également être impliqués dans un autre type de résonnance, par exemple une resonance à trois modes indépendants de type $\nu_0 \sim \nu_1 + \nu_2$. Nous trouvons par ailleurs que les valeurs estimées pour le paramètre D dans la résonance entre composantes d'un triplet diffèrent sensiblement des valeurs prédites par la théorie non linéaire. Ceci suggère que les comportements non linéaires ne dépendent pas seulement de la valeur de D, mais aussi des coefficients de couplage spécifiques à chaque mode (Buchler et al. 1995).

Finalement, nous insistons sur le fait que les modulations de fréquence observées induites par les interactions non linéaires peuvent ruiner toute tentative de mesurer les effets évolutifs sur les périodes des modes d'oscillation dans les étoiles sdB et naines blanches pulsantes. Les temps caractéristiques de changement des périodes dus à l'évolution stellaire, e.g., $\sim 10^5$ années pour les étoiles DBV (Winget et al. 2004) et $\sim 10^6$ années pour les étoiles sdB (Charpinet et al. 2002b), sont beaucoup plus longs que les temps caractéristiques des effets non linéaires. Mesurer le taux de changement des périodes de pulsation peut en effet apporter des contraintes sur la physique interne. Par exemple dans les naines blanches, cela offre l'opportunité de contraindre le taux d'émission des neutrinos (Winget et al. 2004). Toutefois, nos résultats montrent qu'il faut rester extrêmement prudent sur la contamination possible par des effets non linéaires, qu'il faut préalablement corriger, si l'on veut mesurer ces taux de façon fiable. Ces modulations non linéaires compliquent également la détection d'exoplanètes ou de compagnons stellaires autour des étoiles compactes selon la technique des variations de phase des modes de pulsation (e.g.,

Silvotti et al. 2007). Néanmoins, il demeure possible de distinguer entre ces deux effets puisque les couplages non linéaires induisent généralement des comportements différents d'un mode à l'autre alors que des causes externes, comme la présence d'un corps en orbite, affectent tous les modes de la même façon.

Perspectives

Les modulations d'amplitude et de fréquence observées, induites par des interactions non linéaires entre modes, devraient apporter des contraintes significatives au développement de la théorie non linéaire des pulsations stellaires. Elles doivent inciter également le développement de nouvelles méthodes d'analyse des données photométriques, notamment au niveau des techniques de "prewhitenning". L'identification de résonnances non linéaires similaires dans d'autres types d'étoiles pulsantes est une autre extension de cette thèse, ce qui permettra d'étudier plus avant le comportement des modes dans ces régimes non linéaires, notamment grâce aux futures missions spatiales et à des campagnes au sol dédiées.

Les divergences entre les modulations mises en évidence dans cette thèse et les calculs théoriques doivent motiver des études plus poussées sur la théorie non linéaire des oscillations stellaire pour des prédictions plus précises du comportement des modes dans les étoiles pulsantes en général. Nous avons en effet observé que des résonnances externes aux résonnances se produisant dans un triplet de modes peuvent être suffisamment fortes pour influencer le comportement global des modes. Ces cas, ainsi que les multiplets de modes ($\ell > 1$), impliquent des interactions à plus de trois modes pour lesquelles il n'existe aucun modèle théorique pleinement adapté actuellement. Comme plus de modes sont impliqués, les modulations d'amplitude et de fréquence sont certainement plus complexes que dans le cas simple d'interactions à trois modes. Les modulations observées pourraient permettre pour la première fois d'extraire les coefficients de couplage non linéaires dans les étoiles (Buchler et al. 1995). De ces coefficients, il serait alors possible de déterminer les valeurs du paramètre D dans différents régimes de résonnance. Les modulations périodiques associées au régime intermédiaire pourraient aussi permettre d'évaluer le taux de croissance linéaire des modes d'oscillation, puisque le temps caractéristique des modulations est intimement lié à ce taux.

Les modulations dues aux effets non linéaires induisent des structures hyperfines ou des structures élargies dans les diagrammes de Lomb-Scargle. Ces signaux ne peuvent pas être extraits proprement des courbes de lumière avec les techniques standard de "prewhitenning" qui supposent des modulations purement sinusoïdales. Après l'extraction du pic principal de plus grande amplitude, il reste alors des pics résiduels d'amplitude significative au voisinage de la fréquence enlevée. Nous proposons de développer une nouvelle méthode pour extraire des fréquences modulées, utilisant le fait que les lobes secondaires ou les structures élargies contiennent des informations importantes sur les variations d'amplitude et de fréquence des modes. Des tests statistiques et des simulations permettront de vérifier la fiability des méthodes proposées dans un avenir proche. Nous planifions d'incorporer ces approches dans le programme FELIX. Ces nouvelles méthodes permettront d'améliorer l'efficacité de l'extraction des propriétés des modes d'oscillation dans les étoiles pulsantes, particulièrement pour les étoiles observées par *Kepler* pendant ~ 4 years.

Nous trouvons en effet des variations d'amplitude et de fréquence intéressantes dans d'autres pulsateurs compacts parmi l'échantillon *Kepler*. Plus de travail est nécessaire pour étudier en détail le comportement des modes dans ces étoiles. Comme les coefficients de couplage diffèrent d'un mode à l'autre et d'une étoile à l'autre, les modes résonnants peuvent développer une multitude d'effets. Nous pensons qu'une bibliothèque recensant les différents comportements de chaque mode identifié dans chaque pulsateur compact observé par *Kepler* sera utile pour

classifier les différents effets. Mathématiquement, les équations d'amplitude sont applicables à tout type d'étoile pulsante. Il sera alors particulièrement intéressant d'observer les modulations d'amplitude et de fréquence dans d'autres types de pulsateurs du champ *Kepler*. Ainsi, récemment, Bowman et al. (2016) ont étudié un ensemble de ~ 1000 étoiles δ Scuti suivies par *Kepler* pendant ~ 4 ans, en se concentrant principalement sur les modulations d'amplitude des modes d'ocillation.

Nous terminons cette thèse avec la perspective que le comportement à long terme des modes d'oscillation puisse être observé avec les futures missions spatiales, comme avec TESS puisque des pulsateurs compacts brillants connus pour montrer des changements d'amplitude des modes seront parmi les cibles de cette mission. La couverture de cycles entiers de modulations d'amplitude et de fréquence sur des échelles de temps de semaines ou mois pourraient ainsi être révélés dans ces étoiles. Sur plusieurs aspects, la théorie non linéaire des oscillations stellaires peut à présent se développer sur de nouvelles contraintes observationnelles, ce qui ne manquera pas de raviver l'intérêt pour la physique de ces phénomènes.

Appendix A

Physical terms in stellar oscillation theory

A.1 Low-order associated Legendre functions

We list the first several associated Legendre functions $P_\ell^m(\mu)$ with low degree $\ell \leqslant 2$ as follows :

$$P_0^0(\mu) = 1, \tag{A.1}$$

$$P_1^0(\mu) = \mu, \tag{A.2}$$

$$P_1^1(\mu) = -(1-\mu^2)^{1/2}, \tag{A.3}$$

$$P_2^0(\mu) = \frac{1}{2}(3\mu^2 - 1), \tag{A.4}$$

$$P_2^1(\mu) = -3\mu(1-\mu^2)^{1/2}, \tag{A.5}$$

$$P_2^2(\mu) = -3(1-\mu^2)^{1/2}, \tag{A.6}$$

and for the negative one with the relationship of

$$P_\ell^{-m}(\mu) = (-1)^m \frac{(\ell-m)!}{(\ell+m)!} P_\ell^m(\mu), \tag{A.7}$$

and the spherical harmonic function $Y_\ell^m(\theta,\phi)$ with low degree $\ell \leqslant 2$,

$$Y_\ell^m(\theta,\phi) = (-1)^{(m+|m|)/2} \Big[\frac{2\ell+1}{2\pi}\frac{(\ell-|m|)!}{(\ell+|m|)!}\Big]^{1/2} P_\ell^m(\mu) e^{im\phi}. \tag{A.8}$$

$$Y_0^0(\theta,\phi) = \frac{1}{2}\frac{1}{\sqrt{\pi}}, \tag{A.9}$$

$$Y_1^0(\theta,\phi) = \frac{1}{2}\sqrt{\frac{3}{\pi}}\cos\theta, \tag{A.10}$$

$$Y_1^{\pm1}(\theta,\phi) = \mp\frac{1}{2}\sqrt{\frac{3}{2\pi}}\sin\theta\, e^{\pm i\phi}, \tag{A.11}$$

$$Y_2^0(\theta,\phi) = \frac{1}{4}\sqrt{\frac{5}{\pi}}(3\cos^2\theta - 1), \tag{A.12}$$

$$Y_2^{\pm1}(\theta,\phi) = \mp\frac{1}{2}\sqrt{\frac{15}{2\pi}}\sin\theta\cos\theta\, e^{\pm i\phi}, \tag{A.13}$$

$$Y_2^{\pm2}(\theta,\phi) = \frac{1}{4}\sqrt{\frac{15}{2\pi}}\sin^2\theta\, e^{\pm 2i\phi}. \tag{A.14}$$

A.2 The linear and nonlinear adiabatic operators

The linear operator for adiabatic nonradial oscillations is expressed as

$$\mathscr{L}(\boldsymbol{\xi}) \equiv \frac{1}{\rho^2}(\nabla p)\nabla\cdot(\rho\boldsymbol{\xi}) - \frac{1}{\rho}\nabla(\boldsymbol{\xi}\cdot\nabla p) - \frac{1}{\rho}\nabla(p\Gamma_1)\nabla\cdot\boldsymbol{\xi}) + \nabla\Big\{G\int_V \frac{\nabla_{\mathbf{x}}\cdot[\rho(\mathbf{x})\boldsymbol{\xi}(\mathbf{x})]d^3\mathbf{x}}{|\mathbf{x}-\mathbf{r}|}\Big\}, \quad \text{(A.15)}$$

where the last term is the partial differential of the gravitational potential,

$$\frac{\partial\Phi'}{\partial t} = G\int_V \frac{\nabla_{\mathbf{x}}\cdot[\rho(\mathbf{x})\boldsymbol{\xi}(\mathbf{x})]d^3\mathbf{x}}{|\mathbf{x}-\mathbf{r}|}. \quad \text{(A.16)}$$

The quadratic operator one is given by (Dziembowski 1982),

$$\begin{aligned}\mathscr{N}(\mathbf{v}) =& \frac{\partial}{\partial t}\Big[\nabla(\frac{\mathbf{v}^2}{2}) - \mathbf{v}\times(\nabla\times\mathbf{v}) - \frac{\rho'}{\rho^2}\nabla p' + \frac{1}{2\rho^3}(\rho')^2\nabla p\Big] \\ &+ \frac{\nabla p}{\rho}\mathbf{v}\cdot\nabla(\frac{\rho'}{\rho}) + \frac{1}{\rho}\nabla\{\nabla\cdot\mathbf{v}[\boldsymbol{\xi}\cdot\nabla(p\Gamma_1)] + p\Gamma_1\chi\nabla\cdot\boldsymbol{\xi}] - \mathbf{v}\cdot\nabla p'\} \\ &+ G\nabla\Big(\int_V \frac{\nabla_{\mathbf{x}}\cdot[\rho'(\mathbf{x})\mathbf{v}(\mathbf{x})]d^3\mathbf{x}}{|\mathbf{x}-\mathbf{r}|}\Big).\end{aligned} \quad \text{(A.17)}$$

where $\chi = \Gamma_1 + (\partial\Gamma_1/\partial\ln p)_{ad}$.

A.3 The rotational Kernel function

$$\begin{aligned}K_{n\ell m}(r,\theta) =& \rho r^2\Big[(-\xi_r^2 + 2\xi_h\xi_r)(P_\ell^m)^2 + \xi_h^2\Big(2P_\ell^m\frac{dP_\ell^m}{d\theta}\frac{\cos\theta}{\sin\theta} - (\frac{dP_\ell^m}{d\theta})^2 - \frac{m^2}{\sin^2\theta}(dP_\ell^m)^2\Big)\Big] \\ &\times\Big[\frac{2}{2\ell+1}\frac{(\ell+|m|)!}{(\ell-|m|)!}\int_0^R \rho r^2[\xi_r^2 + \ell(\ell+1)\xi_h^2]dr\Big]^{-1}\end{aligned} \quad \text{(A.18)}$$

A.4 The stable criteria for parametric resonance

$$\begin{aligned}\mathscr{D} =& 3\{(\zeta_2+\zeta_3-1)[(\zeta_2-\zeta_3)^2 + 2(\zeta_2+\zeta_3)^2 + 1] - 6\zeta_2\zeta_3\}(\delta\omega/\overline{\kappa})^4 + \\ &\{(\zeta_2+\zeta_3-1)[(\zeta_2-\zeta_3)^2 + (\zeta_2+\zeta_3)^2 + 2] - 12\zeta_2\zeta_3\}(\delta\omega/\overline{\kappa})^2 + \\ &\{(\zeta_2+\zeta_3-1)^3 - 2\zeta_2\zeta_3 > 0,\end{aligned} \quad \text{(A.19)}$$

where $\zeta_{2,3} = -\kappa_{2,3}/\kappa_1 > 0$ in the case of parametric resonance.

A.5 Geometric factors for linear combination frequencies

The transformation between the spherical coordinate system (Θ,Φ) defined by the stellar rotation axis and (θ,ϕ) that defined by the line of observing sight is as,

$$\cos\Theta = -\sin\Theta_0\sin\theta\cos\phi + \cos\Theta_0\cos\theta, \quad \text{(A.20a)}$$

$$\sin\Theta\cos\Phi = \cos\Theta_0\sin\theta\cos\phi + \sin\Theta_0\cos\theta, \quad \text{(A.20b)}$$

$$\sin\Theta\sin\Phi = \sin\theta\sin\phi, \quad \text{(A.20c)}$$

where Θ_0 is the angle between the two coordinate systems. The geometric factors is defined as,

$$g_\ell^m(\Theta_0) \equiv \frac{1}{2\pi}\oint_0^{2\pi} d\phi \int_0^1 h(\mu)\mu\, d\mu\, \mathrm{Re}[Y_\ell^m(\Theta,\Phi)], \tag{A.21}$$

and the angular dependence of a linear combination frequency is described as,

$$G_{\ell_i\ell_j}^{m_i\pm m_j}(\Theta_0) \equiv \frac{1}{2\pi}\oint_0^{2\pi} d\phi \int_0^1 h(\mu)\mu\, d\mu \times P_{\ell_i}^{m_i}(\Theta)P_{\ell_j}^{m_j}(\Theta)\cos[(m_i \pm m_j)\Phi]. \tag{A.22}$$

Here $\mu = \cos\theta$, and $h(\mu)$ is the limb-darkening function. One could easily calculate the geometric ratio, $G_{\ell_i\ell_j}^{m_i\pm m_j}/g_{\ell_i}^{m_i}g_{\ell_j}^{m_j}$, for the low-degree modes without any difficulty.

Appendix B

Conference proceedings

19th European Workshop on White Dwarfs
ASP Conference Series, Vol. 493
Dufour, Bergeron, and Fontaine, eds.

Evidence of Resonant Mode Coupling in the Pulsating DB White Dwarf Star KIC 08626021

W. Zong,[1] S. Charpinet,[1] and G. Vauclair[1]

[1] *CNRS, Université de Toulouse, UPS-OMP, IRAP, Toulouse 31400, France;*
weikai.zong@irap.omp.eu , stephane.charpinet@irap.omp.eu ,
gerard.vauclair@irap.omp.eu

Abstract. The *Kepler* spacecraft provides new opportunities to search for long term frequency and amplitude modulations of oscillation modes in pulsating stars. We analyzed nearly two years of uninterrupted data obtained with this instrument on the DBV star KIC 08626021 and found clear signatures of nonlinear resonant mode coupling affecting several triplets. The behavior and timescales of these amplitude and frequency modulations show strong similarities with theoretical expectations. This may pave the way to new asteroseismic diagnostics, providing in particular ways to measure for the first time linear growth rates of pulsation modes in white dwarf stars.

1. Introduction

The *Kepler* spacecraft is a magnificent instrument to search for long term frequency and amplitude modulations of oscillation modes in pulsating stars. Among the 6 pulsating white dwarfs present in the *Kepler* field, KIC 08626021 is the unique DB pulsator. It has a rotation period $P_{rot} \sim 1.7$ days, estimated from the observed frequency spacings of 3 g-mode triplets (Østensen et al. 2011). It has been observed by *Kepler* for 23 months in short cadence (SC) mode without interruption. Thus, it is a suitable candidate to investigate the resonant mode coupling mechanisms that could induce long term amplitude and frequency modulations of the oscillation modes. Such resonant couplings are predicted to occur in triplets where the rotationally shifted components have frequencies ν_1 and ν_2 such that $\nu_1 + \nu_2 \sim 2\,\nu_0$, where ν_0 is the frequency of the central component. The theoretical exploration of those mechanisms was extensively developed long before the era of space observations (Buchler et al. 1995, 1997) but was almost interrupted more than a decade ago because of the lack of clear observational evidence of such phenomena, due to the difficulty of capturing amplitude or frequency variations that occur on months to years timescales from ground based observatories. Resonant coupling within triplets was proposed for the first time as the explanation for the frequency and amplitude long term variations observed in the GW Vir pulsator PG 0122+200 (Vauclair et al. 2011). We present the analysis of KIC 08626021 in which two triplets exhibit amplitude and frequency variations during the 23-month of observation. Such time modulations pave the way to new asteroseismic diagnostics, providing in particular ways to measure for the first time linear growth rates of pulsation modes in white dwarf stars.

2. Frequency and Amplitude Modulations

The white dwarf star KIC 08626021 has been continuously observed by *Kepler* since quarter Q10.1 up to Q17.2. The high precision photometric data cover ~ 684.2 days (23 months), with a duty circle of ~ 89 %. We used a dedicated software, FELIX, to extract frequencies (details of the program can be found in Charpinet et al. 2010). In this study, we concentrate on rotationally split triplets and investigate the variation of amplitude and frequency between components of these triplets and their relationship. We point out that the frequencies near 3682 μHz reported by Østensen et al. (2011) were in fact resolved into several close peaks with the 23-month light curve. It is therefore probably not a real triplet contrary to the other structures found at 4310 and 5073 μHz (see below). In order to study the variability with time of these modes, we constructed a filter window covering 200 days and slid the filter window along the whole light curve by time steps of 20 days, thus constructing a time-frequency diagram. We also prewhithened the frequencies "chunk by chunk", i.e., the 23-month light curve of KIC 08626021 was divided into 20 chunks, each containing 6-month of data except the last 3 chunks being at the end of the observations. The results for the two triplets are discussed below.

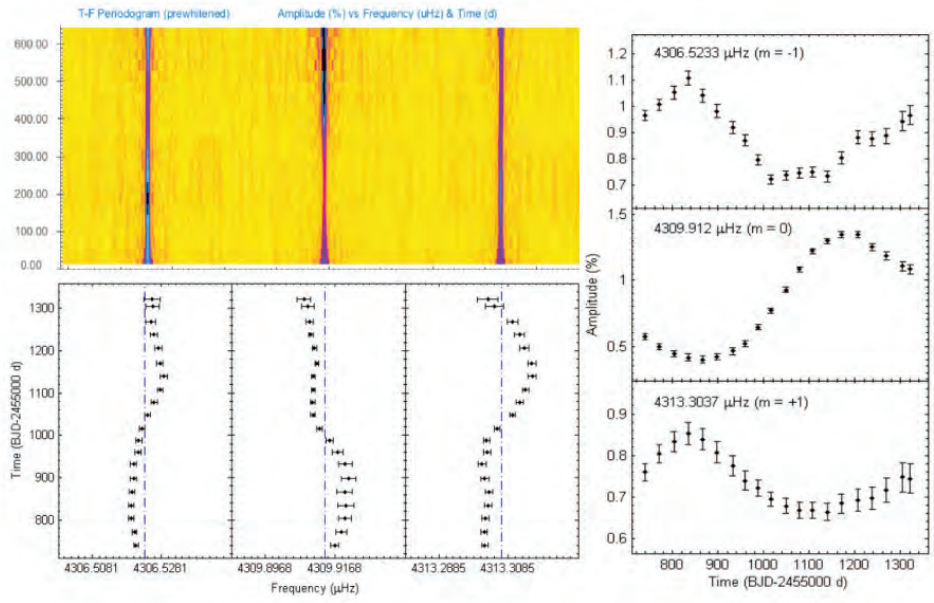

Figure 1. Frequency and amplitude modulations of the triplet at 4310 μHz. The frequencies and amplitudes of the triplet show clear signatures of periodic modulations, as shown in the left bottom panel and right panel. The grey scale in the upper left panel represents the amplitude. The dashed line in the lower right panel is the average value of the frequency (see text for details). Note that the frequency scales (x axis) in the upper and lower left panels are different.

The amplitude and frequency modulations of the triplet near 4310 μHz are shown in Figure 1 . The grey scale (or color scale for electronic version) in the upper left panel represents the amplitude. The vertical dashed line in the lower left panel is the average

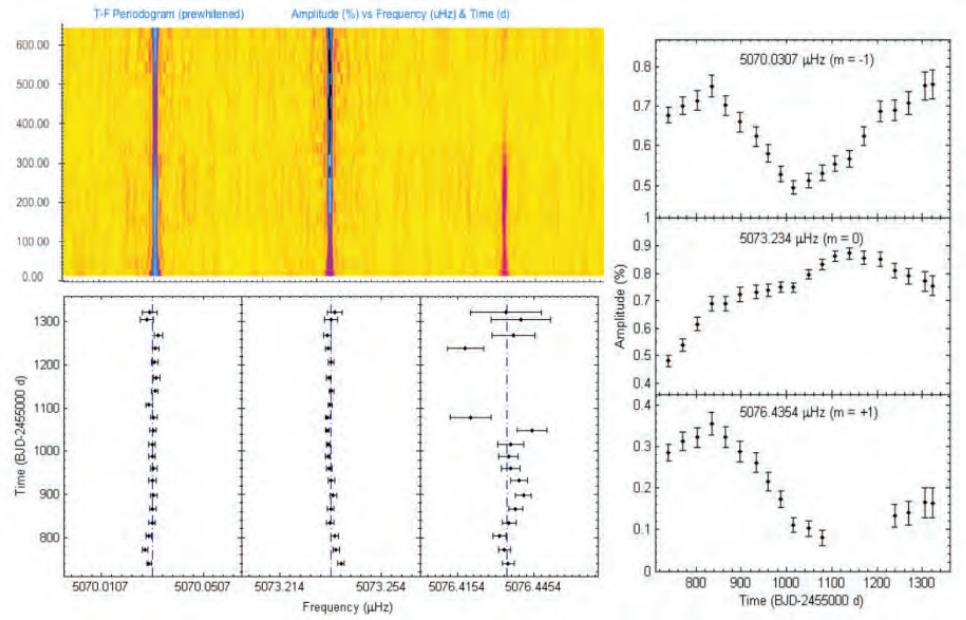

Figure 2. Frequency and amplitude modulations as shown in Figure 1 but for the triplet at 5073 μHz.The amplitudes of the triplet show clear signatures of periodic modulations, as shown in the right panel. The frequencies of the triplet are relatively stable during the observation.

value of the frequency over the entire run. The right panel shows the amplitude modulations of each component forming the triplet. Both the amplitudes and frequencies show clear signatures of quasi periodic modulations with the same timescale of ~ 750 days. The frequencies and amplitudes of the side components evolve in phase and are antiphased with the central component. Figure 2 shows the modulations observed in the other triplet at 5073 μHz. The frequencies in this triplet appear to be stable during the nearly two years of monitoring, while the amplitudes show modulations. Note that the amplitude of the m = -1 component went down below the 4σ detection threshold and was essentially lost in the noise during the last half of the observations.

3. Discussion

The frequency and amplitude modulations observed in the triplets of KIC 086226021 can be related to nonlinear resonant mode coupling mechanisms. The first triplet at 4310 μHz (Figure 1) behaves like if it is in the intermediate regime of the resonance, in which the oscillation modes undergo periodic amplitude and frequency modulations. Theory suggests that the time scale of these modulations should be roughly a few times the inverse of the growth rate of the pulsating mode (Goupil et al. 1998). Therefore this periodicity could in principle be used to measure the growth rate. In addition if we compare the second order effect of rotational splitting as estimated directly from the measured mean frequencies :

$$\delta\nu = \nu_1 + \nu_2 - 2\nu_0 \qquad (1)$$

with the estimated value following Dziembowski & Goode (1992),

$$\delta\nu = 4C\frac{\Omega^2}{\nu_0} \qquad (2)$$

where C is the first order Ledoux constant (~ 0.5 for dipole g-modes) and $\Omega = 2\pi/P_{rot}$ is the angular frequency of the stellar rotation, i.e ., $\delta\nu \sim 0.018\,\mu$Hz, both are found to be very similar. In the intermediate regime, the expected periodic modulation timescale is $P_{mod} \sim 1/\delta\nu$ (Goupil et al. 1998), which with the values given above leads to $P_{mod} \sim$ 650 days, i.e., very similar to the amplitude and frequency modulation timescale of 750 days roughly estimated from Figure 1. This further supports our interpretation that nonlinear resonant coupling is indeed at work in this star. The triplet at 5073 μHz (Figure 2) would be in a different regime, likely in the nonresonant regime. The amplitude of the components show clear modulations while the frequency are relatively stable during the observation. This means the ratio of the real part over the imaginary part of the coupling coefficients is large in that case. This ratio roughly measures nonlinear nonadiabaticities in the star. Hence our result shows that two neighbor triplets can belong to different resonant regimes (frequency lock, time dependent or nonresonant), as it was also suggested in the white dwarf star GD 358 (Goupil et al. 1998).

4. Conclusion

Frequency and amplitude modulations of oscillation modes have been found in several rotationally split multiplets detected in the DB pulsator KIC 08626021, thanks to the high quality and long duration photometric data obtained with the *Kepler* spacecraft. These modulations show signatures pointing toward nonlinear resonant coupling mechanisms occuring among the multiplet components. This is the first time that such signatures are identified so clearly in white dwarf pulsating stars. Periodic modulations of frequency and amplitude that occur in the intermediate resonant regime may allow for new asteroseismic diagnostics, providing in particular a way to measure for the first time linear growth rates of pulsation modes in white dwarf stars. Such results should motivate further theoretical work on nonlinear resonant mode coupling mechanisms and revive interest in nonlinear stellar pulsation theory in general. Finally, we mention that similar modulations are also found in hot B subdwarf stars according to *Kepler* data.

Acknowledgments. WKZ acknowledges the financial support from the China Scholarship Council. This work was supported in part by the Programme National de Physique Stellaire (PNPS, CNRS/INSU, France) and the Centre National d'Etudes Spatiales (CNES, France).

References

Buchler, J. R., Goupil, M.-J. & Hansen, C. J. 1997, A&A, 321, 159
Buchler, J. R., Goupil, M.-J. & Serre, T. 1995, A&A, 296, 405
Charpinet, S., Green, E. M., Baglin, A., et al. 2010, A&A, 516, L6
Dziembowski, W. A. & Goode, Philip R. 1992, ApJ, 394, 670
Goupil, M. J., Dziembowski, W. A. & Fontaine, G. 1998, BaltA, 7, 21
Østensen, R. H., Bloemen, S., Vučković, M., et al. 2011, ApJL, L39, 736
Vauclair, G., Fu, J.-N., Solheim, J.-E., et al. 2011, A&A, 528, 5

EPJ Web of Conferences **101**, 06069 (2015)
DOI: 10.1051/epjconf/201510106069

Evidence of Resonant Mode Coupling in the Hot B Subdwarf Star KIC 10139564

W. Zong[1,a], S. Charpinet[1] and G. Vauclair[1]

[1] CNRS, Université de Toulouse, UPS-OMP, IRAP, Toulouse 31400, France

Abstract. The *Kepler* spacecraft provides new opportinuties to observe long term frequency and amplitude modulations of oscillation modes in pulsating stars. We analyzed more than three years of uninterrupted data obtained with this instrument on the hot B subdwarf (sdB) star KIC 10139564 and found clear signatures of nonlinear resonant mode coupling affecting several multiplets. The observed periodic frequency and amplitude modulations may allow for new asteroseismic diagnostics, providing in particular ways to measure linear growth rates of pulsation modes in hot subdwarf stars for the first time.

1 Introduction

The *Kepler* spacecraft is a magnificent instrument to observe long term frequency and amplitude modulations of oscillation modes in pulsating stars. Among the 18 oscillating sdB stars monitored in the *Kepler* field, KIC 10139564 is the unique p-mode dominated (V361 Hya type) pulsator with low amplitude g-mode oscillations. It has been observed by *Kepler* for 38 months in short cadence (SC) mode without interruption. Its rotation period is ~ 26 days according to several multiplets with common frequency spacings found in both the g- and p-mode regions. Thus, it is a well suited candidate to investigate resonant mode coupling mechanisms that could affect amplitudes and frequencies of oscillation modes – in particular those in rotationally split multiplets – over long timescales. The theory for these mechanisms has been investigated long before the era of space observations but suffered from the lack of observational evidence and constraints due to the timescales involved. We present the analysis of KIC 10139564 showing that some multiplets (in particular triplets) clearly have amplitudes and frequencies varying with time in a manner that can be related to nonlinear resonant mode coupling. Some of these modes would be in the intermediate regime of a resonant coupling mechanism occuring when linear frequencies follow the relation $\nu_1 + \nu_2 \sim 2\,\nu_0$, which generally happens for frequencies split by slow stellar rotation [1]. The characterization of the induced modulations may offer new asteroseismic diagnostics, providing in particular ways to measure linear growth rates of pulsation modes in hot subdwarf stars for the first time.

2 Results and Discussion

The sdB star KIC 10139464 has been continuously observed by *Kepler* since quarter Q5.1 up to Q17.2. The high precision photometric data cover $\sim 1{,}147.5$ days (38 months), with a duty circle of $\sim 89\,\%$. We used a dedicated software, FELIX, to extract the frequencies from the lightcurve (details of this program can be found in Ref [2]). We defined a filter window covering 200 days and slid the filter window along the whole light curve by time steps of 20 days, thus constructing a time-frequency diagram. We also extracted the frequencies "chunk by chunk", i.e Â., the 38-month light curve of

[a] e-mail: weikai.zong@irap.omp.eu

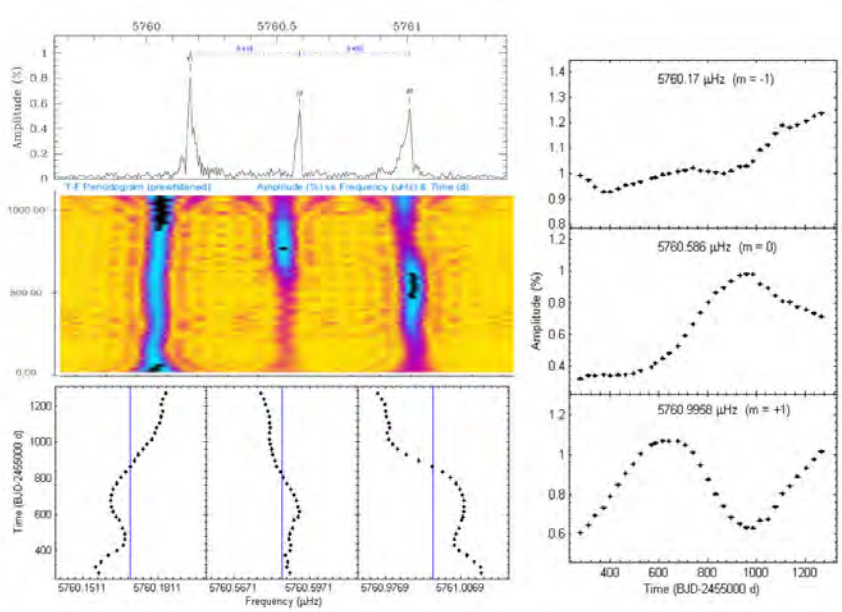

Fig. 1. Frequency and amplitude modulations of the dominant triplet near 5760 μHz.

KIC 10139564 was divided into 33 chunks. Each chunk contains 9-month of SC mode data, except the last three chunks being at the end of the *Kepler* observations.

The amplitude and frequency modulations of the dominant triplet at 5760 μHz are shown in **Fig. 1**. The right panel shows the amplitude modulations of each component forming the triplet. The frequencies in the two lower-left panels also show clear signatures of periodic modulations. These modulations can be related to nonlinear resonant mode coupling mechanisms in pulsating stars. This triplet at 5760 μHz at least qualitatively behaves like if it is in the intermediate regime of the resonance, in which the oscillation modes undergo periodic amplitude and frequency modulations with a time scale of roughly a few times the inverse of the growth rate of the pulsating mode [3]. Therefore periodic modulations as found in the illustrated triplet could in principle be used to measure the growth rate. Other multiplets detected in KIC 10139564 show similar behaviors not presented here due to space constraints.

3 Conclusion

Frequency and amplitude modulations of oscillation modes have been found in several rotationally split multiplets detected in the sdB pulsator KIC 10139564, thanks to the high quality and long duration photometric data obtained with the *Kepler* spacecraft. These modulations show signatures pointing toward nonlinear resonant coupling mechanisms occuring among the multiplet components. This is the first time that such signatures are identified in sdB pulsating stars. Periodic modulations of frequency and amplitude that occur in the intermediate resonant regime may allow for new asteroseismic diagnostics, providing in particular a way to measure for the first time linear growth rates of pulsation modes in sdB stars. These growth rates are directly linked to the mode driving engine, a κ-mechanism involving the iron bump and powered up by radiative levitation. Such results should motivate further theoritical work on nonlinear resonant mode coupling mechanisms and revive interest in nonlinear stellar pulsation theory in general.

References

1. Buchler, J. R., Goupil, M.-J. & Serre, T. A&A, **295**, (1995), 405
2. Charpinet, S., Green, E. M., Baglin, A., et al. A&A, **516**, (2010), L6
3. Goupil, M. J., Dziembowski, W. A. & Fontaine, G. BaltA, **7**, (1998), 21

Nonlinear asteroseismology: insight from amplitude and frequency modulations of oscillation modes in compact pulsators from *Kepler* photometry

Weikai Zong[1,2,⋆], *Stéphane* Charpinet[1,2,⋆], *Gérard* Vauclair[1,2,⋆], *Noemi* Giammichele[1,2,3], and *Valérie* Van Grootel[4]

[1] *CNRS, IRAP, 14 avenue Edouard Belin, F-31400 Toulouse, France*
[2] *Université de Toulouse, UPS-OMP, IRAP, Toulouse F-31400, France*
[3] *Département de Physique, Université de Montréal, CP 6128, Succursale Centre-Ville, Montréal, QC H3C 3J7, Canada*
[4] *Institut d'Astrophysique et de Géophysique, Quartier Agora, Allée du 6 Août 19c, 4000 Liège, Belgium.*

Abstract. Nonlinear mode interactions are difficult to observe from ground-based telescopes as the typical periods of the modulations induced by those nonlinear phenomena are on timescales of weeks, months, even years. The launch of space telescopes, e.g., *Kepler*, has tremendously changed the situation and shredded new light on this research field. We present results from *Kepler* photometry showing evidence that nonlinear interactions between modes occur in the two compact pulsators KIC 8626021, a DB white dwarf, and KIC 10139564, a short period hot B subdwarf. KIC 8626021 and KIC 10139564 had been monitored by *Kepler* in short-cadence for nearly two years and more than three years without interruption, respectively. By analyzing these high-quality photometric data, we found that the modes within the triplets induced by rotation clearly reveal different behaviors: their frequencies and amplitudes may exhibit either periodic or irregular modulations, or remain constant. These various behaviors of the amplitude and of the frequency modulations of the oscillation modes observed in these two stars are in good agreement with those predicted within the amplitude equation formalism in the case of the nonlinear resonant mode coupling mechanism.

1 Introduction

Evolved compact pulsators, white dwarf and hot B subdwarf (sdB) stars, have been well investigated by the technique of asteroseismology. White dwarf stars are the end fates of stellar evolution for 98% of the stars in our Galaxy. They span over quite a large region in the H-R diagram, with effective temperature of $\sim$ 10 000 − 170 000 K and surface gravity of $\sim$ 5.5 − 8.5 dex [1, 2]. SdB stars belong to the extreme horizontal branch in the H-R diagram, with a mass typically of $\sim 0.47 M_{\odot}$, effective temperature of 22 000 − 40 000 K and surface gravity of $\sim$ 5.2 − 6.1 [3]. Observations from ground-based telescopes suggest that pulsation modes in compact pulsating stars may exhibit temporal variations in their amplitudes and/or frequencies, e.g., the GW Virginis variable star PG 0122+200 [4]. However, it is difficult to observe one entire modulation cycle from ground as the modulations are typically much slower than the pulsation periods themselves [5].

The launch of space telescopes, such as *Kepler*, has tremendously changed the situations of uncovering the modulations of amplitude and frequency in pulsating stars. There are 113 candidates of compact stars that had been monitored by *Kepler* during its survey phase, aiming at searching for compact pulsators [6]. In the original *Kepler* mission, the final number of evolved compact pulsators reaches 24, including 6 pulsating white dwarf star and 18 pulsating sdB stars, see., e.g., Ref. [7]. Most of these 24 stars, in particular for sdB pulsators, have been observed by *Kepler* for more than two years without interruption. They are suitable candidates to observe the variability and stability in their oscillation modes.

In this proceeding, we assemble the results of first evidences of amplitude and frequency modulations of multiplet modes in two of these 24 compact stars, a Helium-atmosphere white dwarf, KIC 8626021, and a short-period V 361 Hya stars, KIC 10139654, pointing toward nonlinear mode interactions. These findings suggest that *Kepler* opens a new era to investigate nonlinear asteroseismology.

2 Nonlinear resonant mode couplings

The theoretical explorations of nonlinear asteroseismology, described in the framework of the amplitude equation (AE) formalism, began around 1980's. It concerned the mode resonance in the adiabatic and nonadiabatic cases [8, 9]. A specific case of nonlinear AEs had been then applied to nonradial triplet modes that are induced by stellar rotation [10].

Within nonlinear asteroseismology, the stellar oscillations can be represented by temporal amplitudes as

$$\mathbf{z} = \sum_j \frac{1}{2} A_j(t) e^{i\omega_j t} \mathbf{e}_j + C + O, \qquad (1)$$

⋆ e-mail: [weikai.zong,stephane.charpinet,gvauclair]@irap.omp.eu

where $\mathbf{e}_j$, ω_j, and $A_j(t)$ denote the linear nonadiabatic eigenvectors, eigenfrequency and the temporal amplitude of mode j, respectively, C denotes complex conjugation and O represents 'higher order terms'.

For an $\ell = 1$ triplet, the nonlinear complex nonadiabatic AEs of the three modes are rewritten as an set [10],

$$\frac{dA_-}{dt} = \kappa_- A_- + R_- A_0^2 A_+ \cos(\Phi - \delta_-) - A_-(q_{11}A_-^2 + q_{12}A_0^2 + q_{13}A_+^2), \quad (2a)$$

$$\frac{dA_0}{dt} = \kappa_0 A_0 + R_0 A_0 A_+ A_- \cos(\Phi + \delta_0) - A_0(q_{21}A_-^2 + q_{22}A_0^2 + q_{23}A_+^2), \quad (2b)$$

$$\frac{dA_+}{dt} = \kappa_+ A_+ + R_+ A_0^2 A_- \cos(\Phi - \delta_+) - A_+(q_{31}A_-^2 + q_{32}A_0^2 + q_{33}A_+^2), \quad (2c)$$

$$\frac{d\Phi}{dt} = \delta\omega - 2R_0 A_- A_+ \sin(\Phi + \delta_0) + A_0(R_- \frac{A_+}{A_-}\sin(\Phi - \delta_-) + R_+ \frac{A_-}{A_+}\sin(\Phi - \delta_+)), \quad (2d)$$

where the combination phase $\Phi = \phi_+ + \phi_- - 2\phi_0$, κ_i denote the linear growth rates, q_{ij} and R_i are the coupling coefficients, the phase shifts δ_i with the relation of $r_i = R_i \exp(i\delta_i)$, and the frequency mismatch $\delta\omega = \omega_+ + \omega_- - 2\omega_0$.

The numeric explorations of the above AEs reveal three distinct regimes of amplitude and frequency modulations of the interacting modes [10]:

a) The nonlinear frequency lock regime. The nonlinear couplings force the frequencies to be well equally spaced in the triplet modes, $\delta\omega = 0$. The amplitudes are all constant and typically asymmetric, $A_- \neq A_+$.

b) The intermediate regime. The resonance modes exhibit amplitude and frequency modulations that can be periodic, multi-periodic, irregular, or even chaotic, depending on the real parameters of the star. When the periodic modulations occur, the period of the modulations is about the inverse of the frequency mismatch, $1/\delta\omega$, or $\sim 1/\kappa$.

c) The nonresonant regime. The nonlinear coupling effects are very small and the linear frequencies are very close to the linear results.

In the case of the three-mode resonance condition where $\omega_1 \sim \omega_2 + \omega_3$, the amplitude equation within the adiabatic approximation can be written as,

$$\frac{dA_1}{dt} = \kappa_1 A_1 + \frac{iq}{\omega_1 I_1} A_2 A_3 e^{-i\delta\omega t}, \quad (3a)$$

$$\frac{dA_2}{dt} = \kappa_2 A_2 + \frac{iq}{\omega_2 I_2} A_1 A_3^* e^{-i\delta\omega t}, \quad (3b)$$

$$\frac{dA_3}{dt} = \kappa_2 A_3 + \frac{iq}{\omega_3 I_3} A_1 A_2^* e^{-i\delta\omega t}. \quad (3c)$$

where the frequency mismatch is $\delta\omega = \omega_1 - \omega_2 - \omega_3$, term I_j are the mode inertia, the nonlinear coupling coefficient q is very complicated and can be found in [8].

The numerical results suggest that the involved modes can be stable or modulate depending on the type of resonance and parameters such as their linear growth (damping) rates and the frequency mismatch [8].

3 Amplitude and frequency modulations

We have observed clear amplitude and frequency variations in two compact pulsators with photometry from the original *Kepler* mission. As space is limited, we only show here the modulations in the primary triplets in the two compact stars, KIC 8626021, a DB pulsating white dwarf, and KIC 10139564, a short-period pulsating sdB star. One can find more details and interesting mode behaviors in the two recently published papers [11, 12].

KIC 8626021 had been continuously monitored by *Kepler* in short-cadence for nearly two years, from quarter Q10.1 to Q17.2. Figure 1 shows the observed amplitude and frequency variations in the primary triplet near 4310 μHz in that star. The results suggest that both amplitude and frequency have signatures of quasi-periodic patterns which is further confirmed by the best sinusoidal fitting by one pure sine wave. The derived periods are 580 ± 23, 680 ± 10 and 610 ± 43 days for the retrograde mode, central mode and prograde mode, respectively. More interestingly, we also observed that the two side components seem to evolve nearly in phase with similar modulation period of $\sim$ 600 d and nearly in anti-phase with the central component (which exhibits a slightly longer modulation period of $\sim$ 700 d) in this triplet.

KIC 10139564 had been contiguously observed by *Kepler* in short-cadence for more than three years, from quarter Q5.1 to Q17.2. Figure 2 shows the amplitude and frequency modulations of the primary p-mode triplet near 5760 μHz in that star. We note that the hyperfine structures of the triplet components are significantly broaden which possibly indicate that the modes are unstable. This is further illustrated by the results shown in the other panels. We observed that the components show clear amplitude and frequency modulations: quasi-periodic frequency variations in all components and quasi-periodic amplitude variations in two components. It is very suggestive that the frequencies of the two side components evolve in anti-phase, which becomes more evident after removing the long-term trend of the frequency variations through quadratic fittings [12].

4 Discussions

The observed periodic behaviors of the triplets discussed here are pointing toward the intermediate regime of nonlinear mode couplings where nonlinear interacting modes may have periodic amplitude and frequency modulations. We discuss the two cases below. More details for different mode behaviors observed in these two targets can be found in Ref. [11, 12], where cases of frequency locked, regular or irregular variations are observed.

For the triplet near 4310 μHz in KIC 8626021, all the components show periodic amplitude and frequency vari-

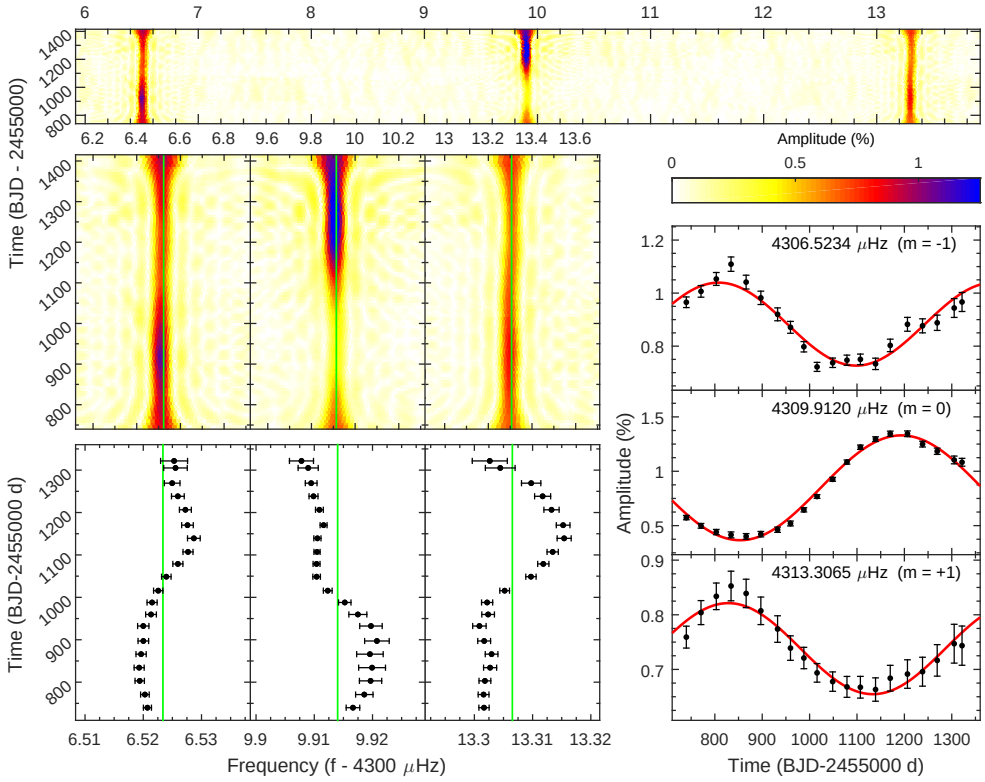

Figure 1. Amplitude and frequency modulations in the triplet near 4310 μHz in the DB white dwarf star KIC 8626021. The color panels represent the sliding Lomb-Scargle periodogram. The vertical solid lines are the averaged values of the frequencies. Each data points in the *bottom left* and *lower right* panels are obtained from prewhitening subsets of the photometric data. The red solid curves denote the best sinusoidal fittings of amplitude variations. One can see more details in Ref. [11].

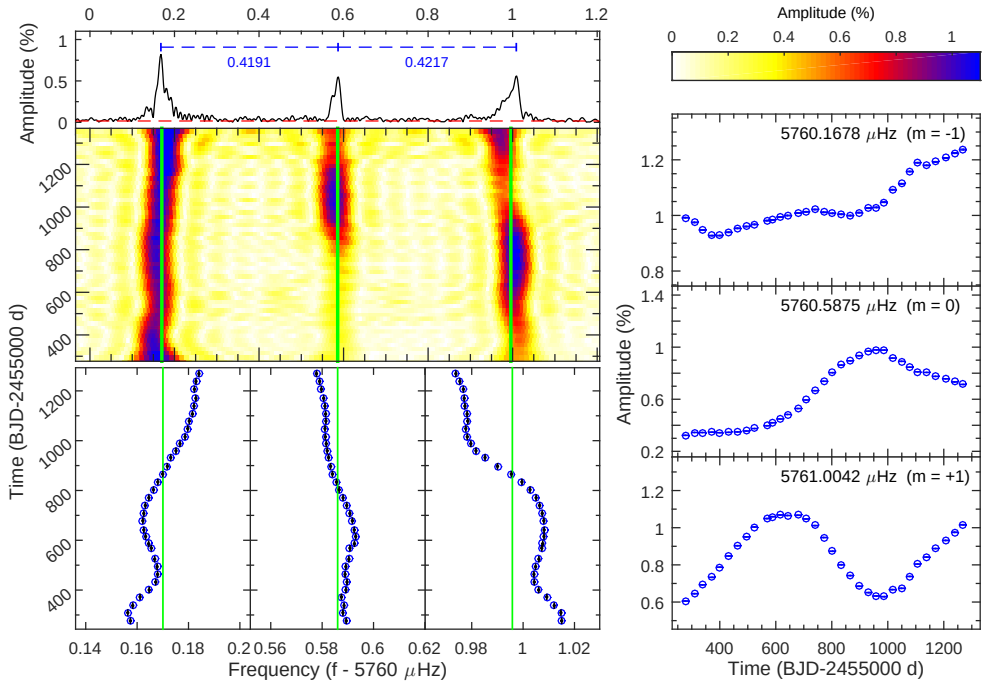

Figure 2. Similar as Fig. 1 but for the triplet modes in the short-period sdB star KIC 10139564 [12], except for the top panel. *Top-left* panel presents the hyperfine structure of the well defined triplet with near symmetric frequency spacing. We note that the error for each measurement is smaller than the symbol itself.

ations on the timescale of $\sim$ 620 d. This value is consistent with the theoretical expectation of $P_m(\mathrm{th}) \sim 1/\delta\omega_t$ = 620 d. This support the idea that we uncovered the right explanation for the mode behaviors in this triplet. However, as the coupling coefficients in the amplitude equations are unknown, we cannot conduct further quantitative comparisons between theoretical explorations and the observed modulations.

The triplet near 5760 μHz in KIC 10139564 shows quasi-periodic frequency and amplitude modulations that are also linked to the intermediate regime of nonlinear resonant mode couplings. The period of frequency variations in all the three components is about 580 d after removing the long-term trend [11]. This period should correspond to a value of $\sim 0.02\,\mu$Hz, the inverse of the frequency mismatch $\delta\omega$ in this triplet, which can be theoretically met when we consider the rotation up to second order for the p-modes [13]. The observed frequency asymmetry $\delta\omega_o$ is only 0.0026 μHz (see Fig. 2). However, we note that the maximum of the observed frequency mismatch of each subset data is about 0.02 μHz. This result suggests that the nonlinear mode interactions possibly force the frequencies to vary around the near exact resonance.

5 Conclusions

The *Kepler* spacecraft provides unprecedented high-quality and uninterrupted photometric data with a time baseline over a couple of years, which is very crucial to investigate behaviors of amplitude and frequency modulations of oscillation modes in pulsating stars. We study in depth the mode behaviors of triplet components in two compact pulsators from *Kepler* photometry, KIC 8626021, a DB white dwarf star, and KIC 10139564, a p-mode dominated hot B subdwarf star. We find clear periodic modulations of amplitude and frequency in two triplets in those two stars, that can be associated with the intermediate regime of nonlinear resonant coupling mechanism. The observed timescales of the modulations are consistent with the predictions of nonlinear amplitude equation formalism. We also observed a variety of mode behaviors in many multiplet modes in those two stars and more details can be seen in Ref. [11, 12]. These results are the first evidence of nonlinear mode interactions in pulsating compact stars.

We emphasize that the frequency variations induced by nonlinear effects could jeopardize any attempt to measure the secular rates of the pulsation period changes induced by evolutionary effect since the former one has a much larger influence on the pulsation periods than that from the latter one. To observe reliable change rates of the pulsation periods, one should be extremely careful in correctly extracting the frequencies and remove the nonlinear corrections beforehand.

These intriguing observed amplitude and frequency modulations, induced by nonlinear mode interactions, should bring significant constraints for further progress in the nonlinear stellar pulsation theory, for the development of new methods and techniques to prewhiten observed light curves, for the application of nonlinear resonance to other types of pulsating stars, and for the study of resonant mode behaviors observed from future space missions as well as ground-based telescopes, possibly, leading a new way to the "nonlinear asteroseismology".

References

[1] Fontaine, G., & Brassard, P. 2008, PASP, 120, 1043

[2] Winget, D. E., & Kepler, S. O. 2008, ARA&A, 46, 157

[3] Heber, U. 2016, PASP, 128, 082001

[4] Vauclair, G., Fu, J.-N., Solheim, J.-E., et al. 2011, A&A, 528, A5

[5] Goupil, M. J., Dziembowski, W. A., & Fontaine, G. 1998, Baltic Astronomy, 7, 21

[6] Østensen, R. H., Silvotti, R., Charpinet, S., et al. 2010, MNRAS, 409, 1470

[7] Østensen, R. H., Reed, M. D., Baran, A. S., & Telting, J. H. 2014, A&A, 564, L14

[8] Dziembowski, W. 1982, Acta Astron., 32, 147

[9] Buchler, J. R., & Goupil, M.-J. 1984, ApJ, 279, 394

[10] Buchler, J. R., Goupil, M.-J., & Hansen, C. J. 1997, A&A, 321, 159

[11] Zong, W., Charpinet, S., Vauclair, G., Giammichele, N., & Van Grootel, V. 2016a, A&A, 585, A22

[12] Zong, W., Charpinet, S., & Vauclair, G. 2016b, A&A, 594, A46

[13] Soufi, F., Goupil, M. J., & Dziembowski, W. A. 1998, A&A, 334, 911

References

Abbott, B. P., Abbott, R., Abbott, T. D., et al. 2016, Phys. Rev. Lett., 116, 061102

Aerts, C., Christensen-Dalsgaard, J., & Kurtz, D. W. 2010, Asteroseismology (Springer Science+Business Media B.V.)

Althaus, L. G., Córsico, A. H., & Miller Bertolami, M. M. 2007, A&A, 467, 1175

Althaus, L. G., Córsico, A. H., Miller Bertolami, M. M., García-Berro, E., & Kepler, S. O. 2008, ApJ, 677, L35

Baglin, A., Auvergne, M., Boisnard, L., et al. 2006, in COSPAR Meeting, Vol. 36, 36th COSPAR Scientific Assembly

Baran, A., Pigulski, A., & O'Toole, S. J. 2008, MNRAS, 385, 255

Baran, A. S. 2012, Acta Astron., 62, 179

Baran, A. S. & Østensen, R. H. 2013, Acta Astron., 63, 79

Baran, A. S., Reed, M. D., Stello, D., et al. 2012, MNRAS, 424, 2686

Baran, A. S., Telting, J. H., Németh, P., Bachulski, S., & Krzesiński, J. 2015a, A&A, 573, A52

Baran, A. S., Telting, J. H., Németh, P., et al. 2016, A&A, 585, A66

Baran, A. S. & Winans, A. 2012, Acta Astron., 62, 343

Baran, A. S., Zola, S., Blokesz, A., Østensen, R. H., & Silvotti, R. 2015b, A&A, 577, A146

Barceló Forteza, S., Michel, E., Roca Cortés, T., & García, R. A. 2015, A&A, 579, A133

Bell, K. J., Hermes, J. J., Bischoff-Kim, A., et al. 2015, ApJ, 809, 14

Bergeron, P., Fontaine, G., Billères, M., Boudreault, S., & Green, E. M. 2004, ApJ, 600, 404

Bischoff-Kim, A., Østensen, R. H., Hermes, J. J., & Provencal, J. L. 2014, ApJ, 794, 39

Blanchette, J.-P., Chayer, P., Wesemael, F., et al. 2008, ApJ, 678, 1329

Borucki, W. J., Koch, D., Basri, G., et al. 2010, Science, 327, 977

Bowman, D. M., Kurtz, D. W., Breger, M., Murphy, S. J., & Holdsworth, D. L. 2016, MNRAS, 460, 1970

Bradley, P. A. & Dziembowski, W. A. 1996, ApJ, 462, 376

Brassard, P. & Fontaine, G. 1997, in Astrophysics and Space Science Library, Vol. 214, White dwarfs, ed. J. Isern, M. Hernanz, & E. Garcia-Berro, 451

Brassard, P. & Fontaine, G. 2008, in ASP Conf. Ser., Vol. 392, Hot Subdwarf Stars and Related Objects, ed. U. Heber, C. S. Jeffery, & R. Napiwotzki, 261

Brassard, P., Fontaine, G., Billères, M., et al. 2001, ApJ, 563, 1013

Brassard, P., Fontaine, G., & Wesemael, F. 1995, ApJS, 96, 545

Brassard, P., Fontaine, G., Wesemael, F., & Tassoul, M. 1992a, ApJS, 81, 747

Brassard, P., Pelletier, C., Fontaine, G., & Wesemael, F. 1992b, ApJS, 80, 725

Breger, M. & Montgomery, M. H. 2014, ApJ, 783, 89

Breger, M., Stich, J., Garrido, R., et al. 1993, A&A, 271, 482

Brickhill, A. J. 1991, MNRAS, 251, 673

Brickhill, A. J. 1992, MNRAS, 259, 519

Brown, T. M., Latham, D. W., Everett, M. E., & Esquerdo, G. A. 2011, AJ, 142, 112

Buchler, J. R. 1993, Ap&SS, 210, 9

Buchler, J. R. 1998, in ASP Conf. Ser., Vol. 135, A Half Century of Stellar Pulsation Interpretation, ed. P. A. Bradley & J. A. Guzik, 220

Buchler, J. R. & Goupil, M.-J. 1984, ApJ, 279, 394

Buchler, J. R., Goupil, M.-J., & Hansen, C. J. 1997, A&A, 321, 159

Buchler, J. R., Goupil, M. J., & Serre, T. 1995, A&A, 296, 405

Buchler, J. R. & Kovacs, G. 1986, ApJ, 308, 661

Carroll, B. W. & Hansen, C. J. 1982, ApJ, 263, 352

Charpinet, S. 1999, PhD thesis, UNIVERSITE DE MONTREAL (CANADA)

Charpinet, S., Brassard, P., Fontaine, G., et al. 2009a, in AIP Conference Series, Vol. 1170, AIP Conf. Series, ed. J. A. Guzik & P. A. Bradley, 585–596

Charpinet, S., Fontaine, G., & Brassard, P. 2009b, A&A, 493, 595

Charpinet, S., Fontaine, G., & Brassard, P. 2009c, Nature, 461, 501

Charpinet, S., Fontaine, G., Brassard, P., et al. 1997a, ApJ, 483, L123

Charpinet, S., Fontaine, G., Brassard, P., & Dorman, B. 1996, ApJ, 471, L103

Charpinet, S., Fontaine, G., Brassard, P., & Dorman, B. 1997b, ApJ, 489, L149

Charpinet, S., Fontaine, G., Brassard, P., & Dorman, B. 2002a, ApJS, 139, 487

Charpinet, S., Fontaine, G., Brassard, P., & Dorman, B. 2002b, ApJS, 140, 469

Charpinet, S., Fontaine, G., Brassard, P., et al. 2011a, Nature, 480, 496

Charpinet, S., Green, E. M., Baglin, A., et al. 2010, A&A, 516, L6

Charpinet, S., Silvotti, R., Bonanno, A., et al. 2006, A&A, 459, 565

Charpinet, S., Van Grootel, V., Fontaine, G., et al. 2011b, A&A, 530, A3

Charpinet, S., Van Grootel, V., Reese, D., et al. 2008, A&A, 489, 377

Christensen-Dalsgaard, J. 2002, Reviews of Modern Physics, 74, 1073

Christensen-Dalsgaard, J. & Frandsen, S. 1983, Sol. Phys., 82, 165

Cohen-Tannoudji, C., Diu, B., & Laloë, F. 1977, Quantum mechanics. Volume I (New York : Wiley ; 1st edition)

Córsico, A. H., Althaus, L. G., Miller Bertolami, M. M., & Bischoff-Kim, A. 2012, A&A, 541, A42

Costa, J. E. S. & Kepler, S. O. 2008, A&A, 489, 1225

Cowling, T. G. 1941, MNRAS, 101, 367

Cox, J. P. 1980, Theory of stellar pulsation (Princeton : Princeton University Press, 1980. 393 p.)

Cuypers, J. 1980, A&A, 89, 207

Deeming, T. J. 1975, Ap&SS, 36, 137

Degroote, P., Briquet, M., Catala, C., et al. 2009, A&A, 506, 111

Dolez, N. & Vauclair, G. 1981, A&A, 102, 375

Dolez, N., Vauclair, G., Kleinman, S. J., et al. 2006, A&A, 446, 237

Dorman, B., Rood, R. T., & O'Connell, R. W. 1993, ApJ, 419, 596

Drechsel, H., Heber, U., Napiwotzki, R., et al. 2001, A&A, 379, 893

Dufour, P., Liebert, J., Fontaine, G., & Behara, N. 2007, Nature, 450, 522

Dupret, M. A. 2001, A&A, 366, 166

Dziembowski, W. 1977, Acta Astron., 27, 203

Dziembowski, W. 1982, Acta Astron., 32, 147

Dziembowski, W. & Krolikowska, M. 1985, Acta Astron., 35, 5

Dziembowski, W. A. 1993, in ASP Conf. Ser., Vol. 40, IAU Colloq. 137 : Inside the Stars, ed. W. W. Weiss & A. Baglin, 521–534

Dziembowski, W. A. & Goode, P. R. 1992, ApJ, 394, 670

Eddington, A. S. 1926, The Internal Constitution of the Stars (Cambridge : Cambridge University Press)

Fontaine, G., Bergeron, P., Brassard, P., et al. 2014, in IAU Symposium, Vol. 301, Precision Asteroseismology, ed. J. A. Guzik, W. J. Chaplin, G. Handler, & A. Pigulski, 273–280

Fontaine, G., Bergeron, P., Brassard, P., et al. 1991, ApJ, 378, L49

Fontaine, G. & Brassard, P. 2008, PASP, 120, 1043

Fontaine, G., Brassard, P., & Bergeron, P. 2001, PASP, 113, 409

Fontaine, G., Brassard, P., Charpinet, S., et al. 2003, ApJ, 597, 518

Fontaine, G., Brassard, P., Charpinet, S., et al. 2012, A&A, 539, A12

Fontaine, G., Brassard, P., & Dufour, P. 2008, A&A, 483, L1

Fontaine, G., Brassard, P., Wesemael, F., & Tassoul, M. 1994, ApJ, 428, L61

Fontaine, G., Lacombe, P., McGraw, J. T., et al. 1980, ApJ, 239, 898

Foster, H. M., Reed, M. D., Telting, J. H., Østensen, R. H., & Baran, A. S. 2015, ApJ, 805, 94

Gianninas, A., Bergeron, P., & Fontaine, G. 2005, ApJ, 631, 1100

Gilliland, R. L., Brown, T. M., Christensen-Dalsgaard, J., et al. 2010, PASP, 122, 131

Gough, D. O. & Thompson, M. J. 1990, MNRAS, 242, 25

Goupil, M.-J. & Buchler, J. R. 1994, A&A, 291, 481

Goupil, M. J., Dziembowski, W. A., & Fontaine, G. 1998, Baltic Astronomy, 7, 21

Green, E. M., Fontaine, G., Reed, M. D., et al. 2003, ApJ, 583, L31

Green, R. F., Schmidt, M., & Liebert, J. 1986, ApJS, 61, 305

Greenstein, J. L. & Sargent, A. I. 1974, ApJS, 28, 157

Greiss, S., Gänsicke, B. T., Hermes, J. J., et al. 2014, MNRAS, 438, 3086

Greiss, S., Hermes, J. J., Gänsicke, B. T., et al. 2016, MNRAS, 457, 2855

Grigahcène, A., Dupret, M.-A., Gabriel, M., Garrido, R., & Scuflaire, R. 2005, A&A, 434, 1055

Guckenheimer, J., Holmes, P., & Slemrod, M. 1984, Journal of Applied Mechanics, 51, 947

Han, Z., Podsiadlowski, P., Maxted, P. F. L., & Marsh, T. R. 2003, MNRAS, 341, 669

Han, Z., Podsiadlowski, P., Maxted, P. F. L., Marsh, T. R., & Ivanova, N. 2002, MNRAS, 336, 449

Hansen, C. J., Cox, J. P., & van Horn, H. M. 1977, ApJ, 217, 151

Heber, U. 1986, A&A, 155, 33

Heber, U. 2009, ARA&A, 47, 211

Heber, U. 2016, ArXiv e-prints

Heber, U., Hunger, K., Jonas, G., & Kudritzki, R. P. 1984, A&A, 130, 119

Hermes, J. J., Kepler, S. O., Castanheira, B. G., et al. 2013a, ApJ, 771, L2

Hermes, J. J., Montgomery, M. H., Gianninas, A., et al. 2013b, MNRAS, 436, 3573

Hermes, J. J., Montgomery, M. H., Winget, D. E., et al. 2012, ApJ, 750, L28

Hermes, J. J., Mullally, F., Østensen, R. H., et al. 2011, ApJ, 741, L16

Howell, S. B., Sobeck, C., Haas, M., et al. 2014, PASP, 126, 398

Humason, M. L. & Zwicky, F. 1947, ApJ, 105, 85

Jeffery, C. S. & Saio, H. 2006, MNRAS, 372, L48

Jenkins, J. M., Caldwell, D. A., Chandrasekaran, H., et al. 2010, ApJ, 713, L87

Jones, P. W., Hansen, C. J., Pesnell, W. D., & Kawaler, S. D. 1989, ApJ, 336, 403

Kawaler, S. D., Reed, M. D., Østensen, R. H., et al. 2010, MNRAS, 409, 1509

Kepler, S. O., Costa, J. E. S., Castanheira, B. G., et al. 2005, ApJ, 634, 1311

Kepler, S. O., Kleinman, S. J., Nitta, A., et al. 2007, MNRAS, 375, 1315

Kilkenny, D. 2010, Ap&SS, 329, 175

Kilkenny, D. 2016, MNRAS, 457, 575

Kilkenny, D., Koen, C., O'Donoghue, D., & Stobie, R. S. 1997, MNRAS, 285, 640

Kilkenny, D., O'Donoghue, D., Koen, C., Lynas-Gray, A. E., & van Wyk, F. 1998, MNRAS, 296, 329

Kim, A., Winget, D. E., & Montgomery, M. H. 2006, Mem. Soc. Astron. Italiana, 77, 460

Kleinman, S. J., Nather, R. E., Winget, D. E., et al. 1998, ApJ, 495, 424

Kovacs, G. & Buchler, J. R. 1989, ApJ, 346, 898

Krzesinski, J. 2015, A&A, 581, A7

Kurtz, D. W., Shibahashi, H., Dhillon, V. S., et al. 2013, MNRAS, 432, 1632

Landolt, A. U. 1968, ApJ, 153, 151

Lasker, B. M. & Hesser, J. E. 1969, ApJ, 158, L171

Lasker, B. M. & Hesser, J. E. 1971, ApJ, 163, L89

Ledoux, P. 1951, ApJ, 114, 373

Leighton, R. B., Noyes, R. W., & Simon, G. W. 1962, ApJ, 135, 474

Lomb, N. R. 1976, Ap&SS, 39, 447

Lynden-Bell, D. & Ostriker, J. P. 1967, MNRAS, 136, 293

Maxted, P. F. L., Heber, U., Marsh, T. R., & North, R. C. 2001, MNRAS, 326, 1391

Maxted, P. F. L., Marsh, T. R., & North, R. C. 2000, MNRAS, 317, L41

McGraw, J. T. 1979, ApJ, 229, 203

McGraw, J. T., Liebert, J., Starrfield, S. G., & Green, R. 1979, in IAU Colloq. 53 : White Dwarfs and Variable Degenerate Stars, ed. H. M. van Horn & V. Weidemann, 377–381

Montgomery, M. H. & Odonoghue, D. 1999, Delta Scuti Star Newsletter, 13, 28

Moskalik, P. 1985, Acta Astron., 35, 229

Napiwotzki, R. 1997, A&A, 322, 256

Napiwotzki, R., Karl, C. A., Lisker, T., et al. 2004, Ap&SS, 291, 321

Nather, R. E., Winget, D. E., Clemens, J. C., Hansen, C. J., & Hine, B. P. 1990, ApJ, 361, 309

Nayfeh, A. H. 1973, Perturbation methods (New York : Wiley)

Osaki, J. 1975, PASJ, 27, 237

Østensen, R. H., Bloemen, S., Vučković, M., et al. 2011a, ApJ, 736, L39

Østensen, R. H., Degroote, P., Telting, J. H., et al. 2012, ApJ, 753, L17

Østensen, R. H., Green, E. M., Bloemen, S., et al. 2010a, MNRAS, 408, L51

Østensen, R. H., Reed, M. D., Baran, A. S., & Telting, J. H. 2014a, A&A, 564, L14

Østensen, R. H., Silvotti, R., Charpinet, S., et al. 2011b, MNRAS, 414, 2860

Østensen, R. H., Silvotti, R., Charpinet, S., et al. 2010b, MNRAS, 409, 1470

Østensen, R. H., Telting, J. H., Reed, M. D., et al. 2014b, A&A, 569, A15

O'Toole, S. J. & Heber, U. 2006, A&A, 452, 579

Pablo, H., Kawaler, S. D., & Green, E. M. 2011, ApJ, 740, L47

Pablo, H., Kawaler, S. D., Reed, M. D., et al. 2012, MNRAS, 422, 1343

Pesnell, W. D. 1985, ApJ, 292, 238

Pnigouras, P. & Kokkotas, K. D. 2015, Phys. Rev. D, 92, 084018

Quirion, P.-O., Fontaine, G., & Brassard, P. 2004, ApJ, 610, 436

Quirion, P.-O., Fontaine, G., & Brassard, P. 2012, ApJ, 755, 128

Randall, S. K., Calamida, A., Fontaine, G., Bono, G., & Brassard, P. 2011, ApJ, 737, L27

Randall, S. K., Matthews, J. M., Fontaine, G., et al. 2005, ApJ, 633, 460

Rauer, H., Catala, C., Aerts, C., et al. 2014, Experimental Astronomy, 38, 249

Reed, M. D., Baran, A., Østensen, R. H., Telting, J., & O'Toole, S. J. 2012, MNRAS, 427, 1245

Reed, M. D., Baran, A., Quint, A. C., et al. 2011, MNRAS, 414, 2885

Reed, M. D., Foster, H., Telting, J. H., et al. 2014, MNRAS, 440, 3809

Reed, M. D., Kawaler, S. D., Østensen, R. H., et al. 2010, MNRAS, 409, 1496

Ricker, G. R., Winn, J. N., Vanderspek, R., et al. 2014, in Proc. SPIE, Vol. 9143, Space Telescopes and Instrumentation 2014 : Optical, Infrared, and Millimeter Wave, 914320

Robinson, E. L., Kepler, S. O., & Nather, R. E. 1982, ApJ, 259, 219

Rybicki, G. B. & Lightman, A. P. 1979, Radiative processes in astrophysics (New York, Wiley-Interscience, 1979. 393 p.)

Saio, H. 1981, ApJ, 244, 299

Saio, H. & Cox, J. P. 1980, ApJ, 236, 549

Scargle, J. D. 1982, ApJ, 263, 835

Schuh, S., Huber, J., Dreizler, S., et al. 2006, A&A, 445, L31

Silvotti, R., Bonanno, A., Bernabei, S., et al. 2006, A&A, 459, 557

Silvotti, R., Charpinet, S., Green, E., et al. 2014a, A&A, 570, A130

Silvotti, R., Fontaine, G., Pavlov, M., et al. 2011, A&A, 525, A64

Silvotti, R., Östensen, R., Telting, J., & Lovis, C. 2014b, in ASP Conf. Ser., Vol. 481, 6th Meeting on Hot Subdwarf Stars and Related Objects, ed. V. van Grootel, E. Green, G. Fontaine, & S. Charpinet, 13

Silvotti, R., Schuh, S., Janulis, R., et al. 2007, Nature, 449, 189

Soufi, F., Goupil, M. J., & Dziembowski, W. A. 1998, A&A, 334, 911

Starrfield, S. G., Cox, A. N., Hodson, S. W., & Pesnell, W. D. 1983, ApJ, 268, L27

Telting, J. H., Baran, A. S., Nemeth, P., et al. 2014, A&A, 570, A129

Telting, J. H., Østensen, R. H., Baran, A. S., et al. 2012, A&A, 544, A1

Théado, S., Vauclair, S., Alecian, G., & LeBlanc, F. 2009, ApJ, 704, 1262

Unno, W., Osaki, Y., Ando, H., Saio, H., & Shibahashi, H. 1989, Nonradial oscillations of stars (Tokyo : University of Tokyo Press, 1989, 2nd ed.)

Van Grootel, V., Charpinet, S., Brassard, P., Fontaine, G., & Green, E. M. 2013a, A&A, 553, A97

Van Grootel, V., Charpinet, S., Fontaine, G., et al. 2010a, ApJ, 718, L97

Van Grootel, V., Charpinet, S., Fontaine, G., Green, E. M., & Brassard, P. 2010b, A&A, 524, A63

Van Grootel, V., Dupret, M.-A., Fontaine, G., et al. 2012, A&A, 539, A87

Van Grootel, V., Fontaine, G., Brassard, P., & Dupret, M.-A. 2013b, ApJ, 762, 57

Van Hoolst, T. 1994a, A&A, 292, 471

Van Hoolst, T. 1994b, A&A, 286, 879

van Kerkwijk, M. H., Clemens, J. C., & Wu, Y. 2000, MNRAS, 314, 209

Vanderburg, A., Johnson, J. A., Rappaport, S., et al. 2015, Nature, 526, 546

Vauclair, G. 1971, in IAU Symposium, Vol. 42, White Dwarfs, ed. W. J. Luyten, 145

Vauclair, G. 2013, in ASP Conf. Ser., Vol. 479, Progress in Physics of the Sun and Stars : A New Era in Helio- and Asteroseismology, ed. H. Shibahashi & A. E. Lynas-Gray, 223

Vauclair, G. & Bonazzola, S. 1981, ApJ, 246, 947

Vauclair, G., Fu, J.-N., Solheim, J.-E., et al. 2011, A&A, 528, A5

Vauclair, G., Goupil, M. J., Baglin, A., Auvergne, M. ., & Chevreton, M. 1989, A&A, 215, L17

Vauclair, G., Moskalik, P., Pfeiffer, B., et al. 2002, A&A, 381, 122

Vučković, M., Aerts, C., Östensen, R., et al. 2007, A&A, 471, 605

Vučković, M., Kawaler, S. D., O'Toole, S., et al. 2006, ApJ, 646, 1230

Walker, G., Matthews, J., Kuschnig, R., et al. 2003, PASP, 115, 1023

Winget, D. E., Hansen, C. J., & van Horn, H. M. 1983, Nature, 303, 781

Winget, D. E. & Kepler, S. O. 2008, ARA&A, 46, 157

Winget, D. E., Nather, R. E., Clemens, J. C., et al. 1991, ApJ, 378, 326

Winget, D. E., Nather, R. E., Clemens, J. C., et al. 1994, ApJ, 430, 839

Winget, D. E., Robinson, E. L., Nather, R. D., & Fontaine, G. 1982a, ApJ, 262, L11

Winget, D. E., Sullivan, D. J., Metcalfe, T. S., Kawaler, S. D., & Montgomery, M. H. 2004, ApJ, 602, L109

Winget, D. E., van Horn, H. M., Tassoul, M., et al. 1982b, ApJ, 252, L65

Wood, J. H., Zhang, E.-H., & Robinson, E. L. 1993, MNRAS, 261, 103

Woudt, P. A., Kilkenny, D., Zietsman, E., et al. 2006, MNRAS, 371, 1497

Wu, Y. 2001, MNRAS, 323, 248

Wu, Y. & Goldreich, P. 2001, ApJ, 546, 469

York, D. G., Adelman, J., Anderson, Jr., J. E., et al. 2000, AJ, 120, 1579

Zong, W., Charpinet, S., & Vauclair, G. 2015, in ASP Conf. Ser., Vol. 493, 19th European Workshop on White Dwarfs, ed. P. Dufour, P. Bergeron, & G. Fontaine, 261

Zong, W., Charpinet, S., Vauclair, G., Giammichele, N., & Van Grootel, V. 2016, A&A, 585, A22

Résumé

Les interactions non linéaires entre modes de pulsation, induisant des modulations d'amplitude et de fréquence, sont difficiles à mettre en évidence avec les télescopes au sol en raison des temps caractéristiques en jeu, de l'ordre de la semaine, du mois, ou même de l'année. L'avènement des télescopes spatiaux comme KEPLER (opéré par la NASA) a considérablement changé la donne en apportant de nouvelles données pour ce domaine de recherche. Dans cette thèse, nous analysons les données photométriques obtenues avec KEPLER pour 24 étoiles compactes pulsantes, incluant 18 étoiles sous-naines de type B (sdB) et 6 naines blanches. Nous établissons que les modulations d'amplitude et de fréquence des modes d'oscillation sont un phénomène courant dans ces étoiles. Nous étudions en particulier deux étoiles : KIC 0862602, une naine blanche pulsante de type DB, et KIC 10139564, une étoile sdB variable à courtes périodes. KIC 0862602 et KIC 10139564 ont été observées sans interruption par KEPLER en cadence rapide pendant deux années pour la première et plus de trois ans pour la seconde. En analysant en détail ces données photométriques de très haute précision, nous mettons en évidence différents types de comportements affectant les composantes de triplets induits par la rotation stellaire. Les fréquences et amplitudes de ces modes montrent des variations soi périodiques soi irrégulières, ou demeurent constantes. Ces comportements peuvent être connectés à ceux prédits par les équations d'amplitude dans le cas de couplages non linéaires résonants entre modes, en particulier pour les temps caractéristiques des modulations. De plus, nous montrons que les modes en résonance constituant les triplets peuvent également interagir avec des modes extérieurs par le biais d'autres formes de résonances telle que la résonance à trois modes $\nu_0 \sim \nu_1 + \nu_2$, une situation qui n'est pas prise en compte dans le cadre théorique existant. Ces études apportent pour la première fois une preuve claire de l'existence de mécanismes de couplages non linéaires entre modes d'oscillations dans les pulsateurs compacts. Cette découverte résonne comme un avertissement pour les projets visant à mesurer les taux de changement des périodes dus à l'évolution dans les étoiles compactes en général. Les modulations de fréquence d'origine non linéaire peuvent potentiellement empêcher toute mesure fiable de ces taux, à moins de corriger ces effets auparavant. Les modulations observées caractérisées dans cette thèse apportent un regard nouveau sur "l'astérosismologie non linéaire" et appellent à revisiter les méthodes d'analyse des courbes de lumière pour en extraire les modes d'amplitude et de fréquence variables. Dans un futur proche, nous anticipons davantage d'attention portée à ces phénomènes non linéaires dans différents types d'étoiles pulsantes observées depuis l'espace, ainsi qu'un regain d'intérêt pour la théorie non linéaire des oscillations stellaires en général.